INFORMATION TO USERS

This manuscript has been reproduced from the microfilm master. UMI films the text directly from the original or copy submitted. Thus, some thesis and dissertation copies are in typewriter face, while others may be from any type of computer printer.

The quality of this reproduction is dependent upon the quality of the copy submitted. Broken or indistinct print, colored or poor quality illustrations and photographs, print bleedthrough, substandard margins, and improper alignment can adversely affect reproduction.

In the unlikely event that the author did not send UMI a complete manuscript and there are missing pages, these will be noted. Also, if unauthorized copyright material had to be removed, a note will indicate the deletion.

Oversize materials (e.g., maps, drawings, charts) are reproduced by sectioning the original, beginning at the upper left-hand corner and continuing from left to right in equal sections with small overlaps. Each original is also photographed in one exposure and is included in reduced form at the back of the book.

Photographs included in the original manuscript have been reproduced xerographically in this copy. Higher quality 6" x 9" black and white photographic prints are available for any photographs or illustrations appearing in this copy for an additional charge. Contact UMI directly to order.

UMI®

Bell & Howell Information and Learning
300 North Zeeb Road, Ann Arbor, MI 48106-1346 USA
800-521-0600

NOTE TO USERS

Page(s) not included in the original manuscript are unavailable from the author or university. The manuscript was microfilmed as received.

ii

This reproduction is the best copy available.

UMI

Generic Dynamic Modelling and Model-Based Trajectory Tracking Control of Wheeled Mobile Robots (WMRs)

Karunananth G. Thanjavur

A Thesis

in

The Department of Mechanical Engineering

Presented in Partial Fulfilment of the Requirements

for the Degree of Master of Applied Science at

Concordia University

Montréal, Québec, Canada

August 1997

ABSTRACT

Generic Dynamic Modelling and Model-Based Trajectory Tracking

Control of Wheeled Mobile Robots (WMRs)

Karunananth G. Thanjavur

This thesis focusses on the dynamic modelling and on the systematic evaluation of model-based control schemes for trajectory tracking of Wheeled Mobile Robots (WMRs) for industrial applications. The research extends the theoretical and experimental work at the Centre for Industrial Control, Department of Mechanical Engineering, Concordia University on mobile robotics since 1982.

The methodology applies the Kane's approach to model WMRs. This approach uses the natural degrees of freedom and emphasises the system's non-holonomic nature, unlike schemes based on the Newton-Euler and Lagrangian methods. The novel 5-step procedure is applied to model WMRs with common wheel types and configurations for various loading and operating conditions. The dynamic loads on the wheels are obtained using 'virtual' speeds. The methodology is illustrated by deducing the dynamic equations of common WMRs.

The insight into the mobile robot's dynamic behaviour provided by the model is used for model-based trajectory tracking control. The performances of the Feed Forward and the Computed Torque schemes have been evaluated through simulations and with experiments using a differentially driven WMR.

The experimental results indicate that the inclusion of the dynamics in the closed

control loop reduces tracking errors by an order of 50% in comparison with a conventional PD controller. Results also indicate the importance of accounting for the dynamic nature of wheel loads and of dynamic model parameters in the Feed Forward controller performance.

Acknowledgements

This thesis is but one small step on an endless search for a nebulous grail; even that small step of mine represents the encouragement and the assistance of many, including those who have walked my way and broken this trail for me. It is to all of them, too numerous to be individually mentioned, that I wish to extend words of sincere gratitude.

Foremost are my teachers, past and present, (Late) Dr. A.J. Saber, who encouraged me to explore, Dr. R.M.H. Cheng, who patiently honed my efforts and Dr. R. Rajagopalan, who helped bring them to full fruition. It has been a long and, at times, difficult road but that is what makes it all the more memorable. And as a true mark of appreciation of their untiring efforts, I hope to pass on to those after me, their words, not just about the nuts and the bolts of dynamics and control but also on the rich philosophy of research.

With the same breath I wish to thank Mr. Gilles Huard, for all that he has taught me, from TTL Logic to Greek philosophy. It really has been a pleasure to work with and learn from him. In his capacity as my supervisor at work, Dr. Henry Hong, fostered my part-time studies with his encouragement and understanding. Many thanks to Mr. John Elliot, Mr. Paul Scheiwiller and Mr. Brian Cooper for the time, help and advice freely given during the machining and the assembly of the various mechanical modifications on the CONCIC III.

During the experimentation, Mr. Weichun Yu and Mr. Haifeng Lin, friends and colleagues, always found the time to assist me with the work. It is not just for their time but also for the many useful discussions, comments and suggestions that I wish to thank them. And to my friend, Mr. Jalil Monsef, who patiently helped during many a long tedious hour of editorial work on the manuscript, special thanks.

To my family, whose love and support go far beyond the confines of any one undertaking, thank you, it is wonderful to be a part of you.

To

the loving and ever fresh memory

of my dearest parents

this thesis is dedicated

May I aspire to keep your legacies alive

Table of Contents

List of Figures

List of Tables

Nomenclature

${}^{A}\alpha_{B}$	Angular acceleration[1] of rigid body B in frame A
$\dot{\gamma}$	Rotational speed of castor
δ , $\dot{\delta}$	Swivel angle and swivel rate of castor
ϵ_{θ}	Error in joint position
$\epsilon_{\dot{\theta}}$	Error in joint speed
ϵ_{s}	Error in generalised position
ϵ_{u}	Error in generalised speed
ζ , $\dot{\zeta}$	Angle and rate of swing of the suspended load
θ_{a}	Actual joint (wheel) angle
$\dot{\theta}_{a}$	Actual joint (wheel) speed
κ	Curvature of the path
τ	Drive torque
τ_{f}	Torque due to friction
τ_{s}	Steer torque
ϕ , $\dot{\phi}$	Steer angle and steer rate of steered wheel
${}^{A}\omega_{B}$	Angular velocity of rigid body B in frame A
ω_{i}^{B}	Holonomic partial angular velocity vector of body, B corresponding u_i
ϖ_{i}^{B}	Non-holonomic partial angular velocity vector of body, B, for u_i
Δ	Determinant of the Jacobian matrix
Ω	Skew symmetric angular velocity matrix
${}^{A}a_{B}$	Acceleration vector of point B in frame A

[1] in the derivations, any consitent set of units may be used; in this thesis, SI units are used where applicable.

g	Acceleration due to gravity
h	Distance from geometric centre, G, to the floor
I_d	Drive current from power amplifiers
m_B	Mass of a body, B
${}^k\boldsymbol{n}_i$	Unit vector i of the coordinate frame k
$\boldsymbol{n}_i$	Inertial frame with origin at O
${}^1\boldsymbol{n}_i$	Vehicle frame with origin at reference point G
${}^2\boldsymbol{n}_i$	Steering frame with origin at steer axis W_S
${}^A\boldsymbol{p}_B$	Position vector of point B in frame A
r	Wheel radius
r_c	castor radius
s_d , s_a	Desired and actual generalised position
u_d , u_a	Desired and actual generalised speed
$\dot{u}_d$	Desired generalised acceleration
$\underline{\dot{u}}$	Resolved generalised acceleration
u_i	Generalised speed corresponding to one degree of freedom of WMR
$\boldsymbol{v}_i^P$	Holonomic partial velocity vector of point, p corresponding to u_i
$\tilde{\boldsymbol{v}}_i^P$	Non-holonomic partial velocity vector of point, p corresponding to u_i
${}^A\boldsymbol{v}_B$	Velocity vector of point B in frame A
x_f , y_f , z_f	Coordinates of wheel frame W_F in vehicle frame
x_s , y_s	Coordinates of steer axis W_S in vehicle frame
x_w , y_w , z_w	Coordinates of wheel W in vehicle frame
A_{ij}	Elements of the Jacobian matrix
C_f , D_f	Coefficients of rolling (tire) friction model
$\mathbf{D}$	Cross coupling matrix of coriolis and centrifugal terms
$\mathbf{F}^P$	External force acting at a point, P; referred as active force

$\tilde{F}_t^P$	Generalised active force of p corresponding to u_t
$\tilde{F}_t^{*B}$	Generalised inertia force of B corresponding to u_t
$\mathbf{J}$	Jacobian matrix
K_p , K_v	Proportional and derivative controller gains
$\mathbf{M}$	Mass matrix of the WMR
$\mathbf{Q}$	Vector of wheel vertical loads and side forces
$\mathbf{R}^{*B}$	Inertia force acting on the centre of mass of a rigid body, B
$\mathbf{T}^B$	Applied torque on a body; referred as active torque
$\mathbf{T}^{*B}$	Inertia torque acting on rigid body, B
W	Centre of mass of wheel unit
W_F	Centre of mass of wheel frame
W_S	Steer axis

Chapter 1

Wheeled Mobile Robots - A Perspective

1.1 Introduction

Robots in general, and mobile robots in particular, have long been a fascinating subject to the lay person and to the scientist alike. From the pens of science fiction writers and the imagination of motion picture producers, we have seen a vast array of robots which are increasingly anthropomorphic or human like, almost in keeping with the evolving technology. In the scientific world, developing and applying a mechanism that has a certain degree of mobility and autonomy and allowing it to interact with the real world has spurred vigourous research efforts spanning a multitude of disciplines which includes mechanical engineering, electrical engineering, mathematics, computer science, economics and industrial engineering, and some new areas such as knowledge engineering and manufacturing engineering.

The word 'robot' is derived from the Czech word 'robota' which means work. It was first coined to indicate an intelligent machine by the playwright, Karel Capek in his play, 'Rossum's Universal Robots' in 1920. During the decades since then the word has been applied to mean a variety of mechanical devices such as teleoperators, underwater vehicles, autonomous land rovers and so on. Virtually anything that operates with some degree of autonomy has been termed a robot. *A robot*, as defined by the Robot Institute of America is, *a reprogrammable multifunctional device designed to move material, parts, tools or specialized devices through variable programmed motions for the performance of a variety of tasks* [1].

1.2 A Brief History of Wheeled Mobile Robots

Attempts to build mobile devices with some form of intelligence started soon after World War II. In the U.S.A., the first Wheeled Mobile Robot (WMR), or the Automated Guided Vehicle (AGV) as it is also termed in the literature, was developed in the early 1950's by the Barrett Electronics. The first AGV system was installed by them at the Mercury Motor Freight in Columbia, South Carolina, in 1954. However, serious scientific research into the area of autonomous mobile robotics started only in the early 1960's. A brief history of experimental WMRs is traced in Appendix A using material culled from the voluminous literature on the subject.

1.3 WMR research at the Centre for Industrial Control, Concordia University

At the Centre for Industrial Control (CIC), Department of Mechanical Engineering, Concordia University, Montreal, research in various areas related to Wheeled Mobile Robots has been ongoing since 1982. The analytical work has been supplemented by extensive experimental investigations using the four generations of mobile robots designed and developed at the Centre. In the following paragraphs a brief review of the pioneering work at the Centre is traced. Full details are provided in Appendix A.

Investigations by Cheng et al. [2] from 1982 to 1985 led to the development of the first experimental platform, CONCIC I, the 3-wheeled WMR with tricycle wheel configuration, shown in Fig.1.1. The WMR was designed to follow a guide path laid on the floor using camera vision with on-board image processing and path planning. The controller used parallel processing for image analysis and for motion control, both steering and driving.

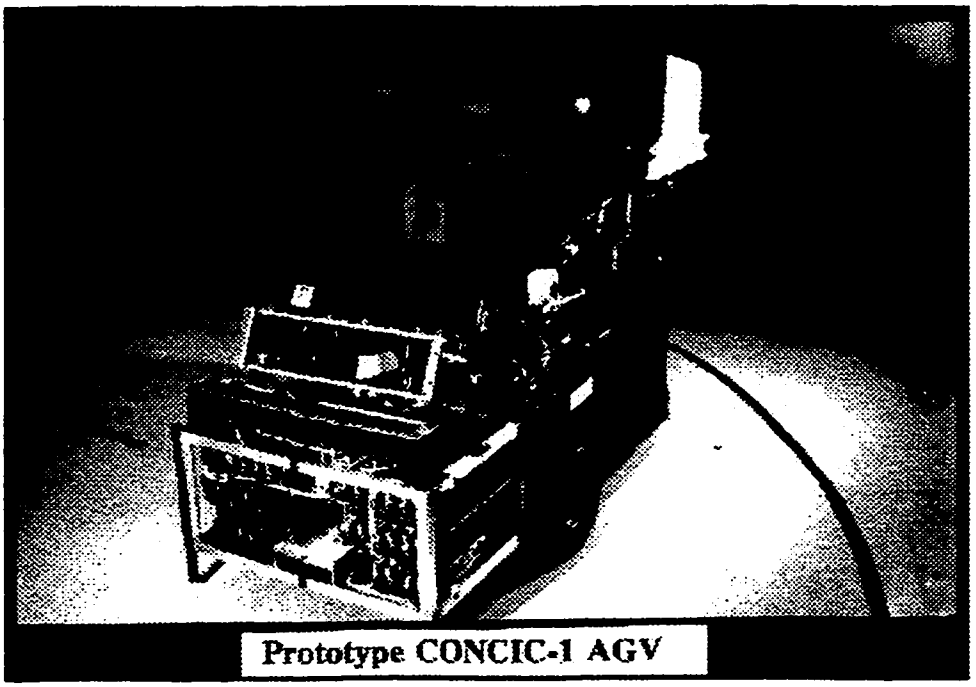

Figure 1.1 The prototype automated guided vehicle, CONCIC I, designed and developed at the Centre for Industrial Control , Concordia University, Montreal [14].

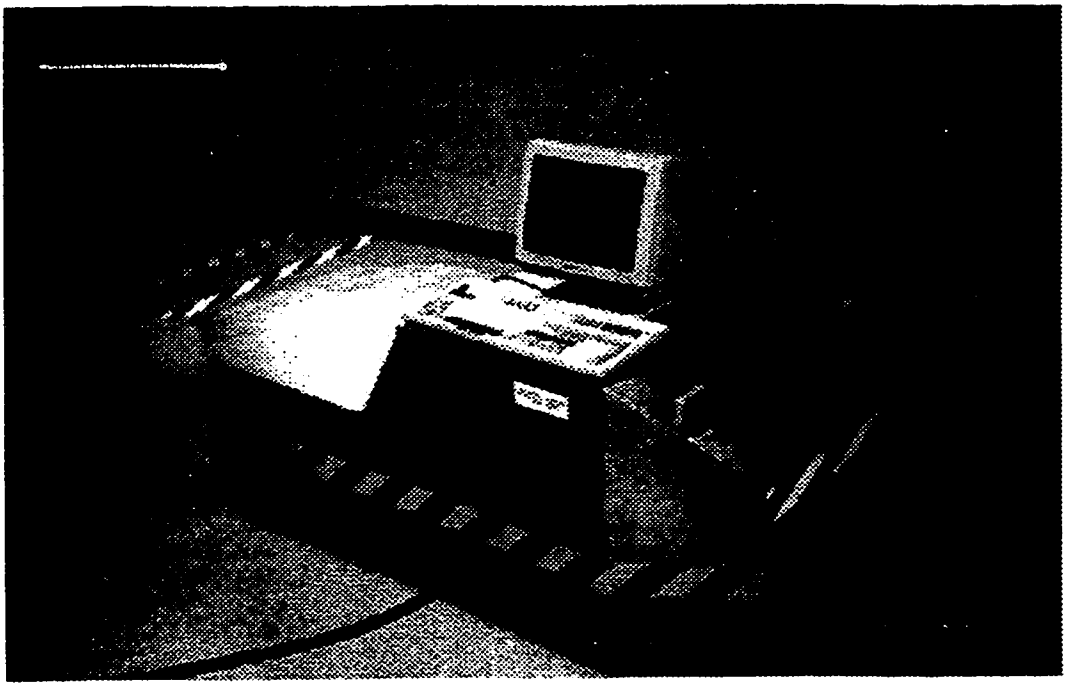

Figure 1.2 The second generation mobile robot, CONCIC II, with camera guidance designed and developed at CIC [15].

The CONCIC II, shown in Fig.1.2 the second experimental WMR designed and developed by Rajagopalan [15] at the CIC from 1988 to 1990 was designed with many new and practical features. The mobile robot utilised a binary digitizing camera with DMA data transfer for the optical guidance system adopted by Rajagopalan and Cheng [4, 5]. A diamond wheel configuration was used with two independently driven wheels located symmetrically along the transverse axis. Steering was achieved by differential drive, since the wheels were independently driven.

In order to explore dynamic modelling and control of WMRs, the third experimental platform, CONCIC III, shown in Fig.1.3, was built by Mehrabi [6] in 1993. Dynamic modelling of mobile robots was first explored by Huang [7], Huang and Cheng [8] and Huang, Cheng and Sankar [9] who developed a dynamic model of CONCIC II as part of a simulation package designed for kinematic and dynamic analysis of differentially driven mobile robots and laid the foundation for a general dynamic modelling scheme for mobile robots. Mehrabi, Cheng and Hemami [10] extended this to two and three degree of freedom non-linear dynamic models. Using feedback linearization, an optimal dynamic controller was synthesized and implemented on CONCIC III.

The first Automated Transit Vehicle (ATV), the CONCIC IV, shown in Fig.1.4, was designed and built at the Centre from 1994 to 1996 by Pharand and completed later by Perelli [11]. The WMR was much bigger in dimensions than its predecessors but the same modular mechanical design was adopted. Rajagopalan and Perelli [12] used a Charge Coupled Device (CCD) camera for road following by the ATV. A hierarchial control system was used with an Intel 486-66 MHz processor, a C-40 transputer network and four LM628 servo motion

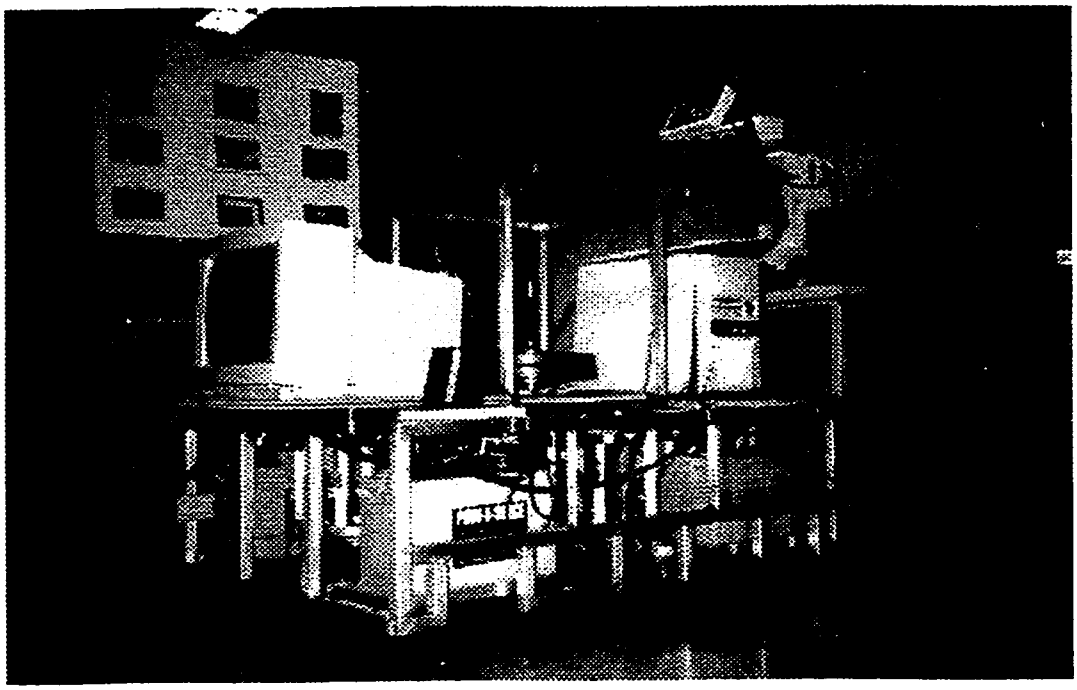

Figure 1.3 The experimental platform, CONCIC III, designed and developed at the CIC [16] carrying a suspended load for this thesis work.

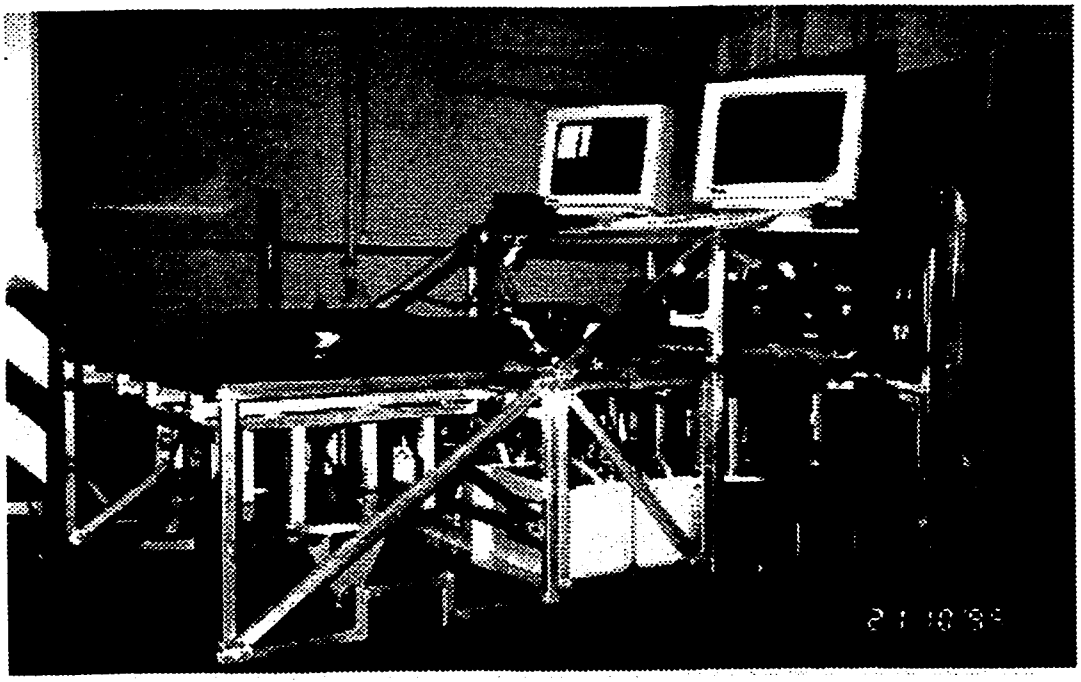

Figure 1.4 The automated vehicle, CONCIC IV, with camera vision for automated transit applications designed and developed at the CIC [18].

control chips. For high speed image processing the Texas Instruments C-40 DSP network was used.

The dynamic control of WMRs was extended to include Computed Torque Control (CTC) by Rajagopalan and Barakat [13, 14] and by Barakat [15] who successfully synthesised a novel CTC scheme for WMRs and implemented it on the CONCIC III. The performance of the proposed controller was validated by comparison with a kinematic PD controller for straight line trajectories on level ground and up a slope.

Mobile robotics research and development in the primary areas of camera guidance, control and kinematic and dynamic modelling of WMRs is ongoing at the Centre. The work presented in this thesis is based upon and draws from this rich and varied experience.

1.4 Present and Future Applications of Wheeled Mobile Robots

The literature surveyed indicates that the primary use of WMRs in the industry has been in the area of material handling especially in manufacturing, assembly or in ware house applications. In North America, the automotive industries have been the leaders in the introduction and the continued use of the mobile robot technology. For instance, the General Motors plant at Oshawa, Ontario, uses more than 500 mobile robots in its automobile assembly plant.

In manufacturing and assembly, WMRs are being used as mobile platforms programmed to carry a component through various stages of manufacturing or assembly, each stage being done at one of a series of work stations. These WMRs do not have much built-in autonomy but function as semi-intelligent mobile systems with excellent trajectory tracking

capability. Buried underground wires are the most common method used to provide path guidance with inductive type pick-ups fitted to the vehicle.

In addition to the typical industrial sectors, mobile robots are finding applications in an ever increasing number of other areas. The Navlab [16], designed and built jointly by the Department of Computer Science and the Robotics Institute, Carnegie-Mellon University, Pittsburgh is a self contained laboratory for navigational vision system research for mobile robot systems in outdoor settings. The research efforts are directed towards highway automation with navigation on roads while avoiding obstacles.

The mobility of robots need not be restricted to land based wheeled mobility only. Undersea exploration was pioneered by the Undersea Artic Research Vehicle (UARS) built at the University of Washington Applied Physics Laboratory. Such unmanned, untethered submersibles are becoming a viable tool to compliment the capabilities of manned and unmanned tethered submersibles for deep sea work such as pipeline search and inspection. Air borne mobile robots to date can be classified as 'smart missiles' only [17]. The targeting information is preprogrammed and the systems navigate autonomously using various types of active or passive sensors. Tactical missiles perform target detection and recognition with corresponding correction of their trajectory.

1.5 Summary

In this chapter a perspective on the field of robotics and, specially, mobile robotics has been provided. The origins and the current definitions of the terms *robot* and *automation* have been provided. These terms have made their way into everyday parlance due to the explosion

of science fiction or sci-fi literature and motion pictures in recent times. For the past fifteen years, the Centre for Industrial Control, Department of Mechanical Engineering, Concordia University, Montreal has been actively engaged in research activities in mobile robots, especially in the areas of camera guidance, dynamic and kinematic modelling and control. The chapter concludes with some of the applications of mobile robots in the industry as well as in non-conventional applications such as undersea exploration and nuclear facility monitoring and maintenance.

Chapter 2

Literature Survey and Problem Definition

2.1 Introduction

The research work presented in this thesis addresses issues related to modelling the dynamic behaviour and to the control of Wheeled Mobile Robots in, the predominant, industrial applications. Examples and illustrations given in this thesis are, therefore, drawn from this sector. However, it is evident from the list of applications given in Section 1.4 and in Appendix A that WMRs are being applied in a growing number of areas. The scope of the work presented in this thesis is general and the results provided may be applied to these varied areas as well.

In a typical industrial application, the mobile robot moves along a constrained path under some form of guidance scheme while carrying out one or more preprogrammed tasks autonomously at stations enroute. An example drawn from the automotive industry is shown in Fig. 2.1 in which the WMR is carrying a car engine suspended on a sling to an assembly station in an automobile production line. In a typical application such as the one used for illustration, the motion of the WMR depends on the simultaneous interactions with the payload and with the environment and this complex dynamic behaviour needs attention for effective control. If the on-board controller treats the WMR-payload system only as a kinematic system, path following may degrade to unacceptable levels. In highway applications, wheeled robots must also be capable of travelling at considerable speeds in widely varying and largely unknown environments while following a desired path. In such

Figure 2.1 A WMR carrying a suspended engine in an automotive assembly line.

industrial and highway applications, safety is a major concern as well. The need to understand the dynamic behaviour of WMRs better and to study the effectiveness of controllers which account for the dynamic nature of the mobile robot provides the impetus for this research work.

The review has been divided into sections dealing with the two primary areas of interest, dynamic modelling and model based control of WMRs, as well as one secondary section dealing with path planning and trajectory generation which is a basic necessity for the motion of the WMR. Section 2.2 is devoted to a review of the methodologies adopted in published literature for the dynamic modelling of WMRs. A review of dynamic control schemes for trajectory tracking for wheeled mobile robots follows in Section 2.3. A brief

review of model based control schemes for stationary robots relevant to the current research is given in Section 2.3.1. Section 2.3.2 reviews dynamic control schemes for WMR applications. Path planning and trajectory generation schemes available in the literature for mobile robots are discussed in Section 2.4.

The literature review leads naturally to the statement of the purpose of the investigation carried out in this thesis. Problem definition in Section 2.5 forms the second part of this chapter. A description of the organization of the thesis is also provided in that section. The chapter concludes with a summary of the important issues discussed in these sections.

2.2 Dynamic Modelling of Wheeled Mobile Robots

An important part of the design of WMRs is the analysis and the prediction of the dynamic behaviour of the mobile robot and its dynamic interaction with the payload and the environment. A dynamic model relates the motion parameters of the mobile robot to the applied forces and torques. Of interest to the engineer using model based control for a WMR are the acceleration, velocity and position of the robot and the actuator drive torque required. A forward dynamic model is used to analyze the response of the robot for a chosen control strategy using simulations. The inverse dynamic model is the heart of the controller. Using the desired and actual trajectory, the actuator torques are obtained. In such applications, the dynamic model must take into account the dynamic effects of the dead weight and payload of the robot, side forces due to operational speed and path followed, centrifugal and gyroscopic forces while negotiating curves, tire characteristics and road conditions. A good dynamic model of the plant improves the performance of dynamic model based controllers,

such as a Computed Torque Controller. In addition, the dynamic model should be computationally simple for real-time control implementation.

The dynamic analysis of mechanical systems such as the WMR may be classified under Multibody Dynamics since the mobile robot, by itself, is composed of a number of interconnected bodies, for instance the main body and the drive motor sets, constrained to move together as a single system. The dynamic model is a mathematical representation of the physical system, based on certain assumptions to provide an idealization of the nature of the system [18]. In the analysis of such multibody dynamic systems, assumptions have to be necessarily made to reduce the complexity of the system to a tractable level. The ideal dynamic model is one which is simple yet provides a good description of the essential features of the actual system. The standards by which each model is judged are not universal and are dictated by the specific area of application. WMRs often have to move at considerable speed in a constrained environment while carrying a heavy payload, which may include passengers [19]. The issue of safety to personnel in and around the WMR in such applications exacts accurate trajectory following. Hence a good understanding of the dynamic behaviour of the WMR system is essential in most applications.

The study of classical dynamics, of which multi body dynamics is a sub topic, is concerned with the interrelation between the time evolution of the motion of physical systems and the forces causing the motion [20]. The adjective classical has been specifically mentioned in this context since the physical systems are treated using macroscopic models utilising the continuum hypothesis according to which matter is continuously distributed in space occupied by a physical system and is concerned only with systems in which the speed of each body is

much less than that of light.

In addition, according to the literature surveyed, in the specific area of dynamic modelling of wheeled mobile robots, all the components are considered to be rigid bodies with negligible deformation. Flexibility in the joints and the members of the system and non-linear effects such as backlash and stiction, which are issues in stationary robots have not been addressed for mobile robots. Ostensibly, flexibility has been reduced to negligible levels by over designing the mechanical structure of the robot.

2.2.1. State-of-the-Art in Dynamic Modelling

In the study of the dynamics of vehicle systems in general and of mobile robots in particular, the two classical methods adopted are

(1) the force methods based on Newton's Laws for single particles extended for rigid bodies by Euler and commonly termed the Newton-Euler method in Robotics literature and

(2) the energy methods based on Hamilton's Principle in the form of Lagrange's equations of motion.

Muir and Newman [21] have proposed a modified Newton-Euler method which uses the transformation approach proposed by them [22] for the kinematic modelling. The Natural Orthogonal Complement method has been proposed by Saha and Angeles [23] and by Cyril, Cheng and Sankar [24] instead of the Lagrangian multipliers normally used when applying the Lagrangian equations to non-holonomic systems. In this thesis, the dynamic equations are derived using the Kane's approach [25], also termed Lagrange's form of d'Alembert's principle.

The following paragraphs discuss each method adopted in the literature. The unique advantages offered by the Kane's approach in the dynamic modelling of non-holonomic systems such as a WMR are highlighted. At this juncture, the definition of a non-holonomic system as applicable to the class of wheeled mobile robots must be made. The description for non-holonomic systems given here has been adopted from [26]. In multibody dynamics, a set of interconnected bodies are constrained to move as a single system. In the specific context of WMRs, the constituent components may be described as rigid bodies with no loss of generality. To describe the position of each body, a six dimensional vector, **r**(t), is required. Since the motion of the various constituent bodies is constrained, the position vectors for the constituent rigid bodies are not independent but are related in such a way as to satisfy the constraints. In the case of a Wheeled Mobile Robot, the constraint equations appear as non-integrable differential equations of the form

$$\sum^{i} a_i(q_k,t)\,\dot{q}_i + a_t(q_k,t) = 0 \qquad \textbf{(2.1)}$$

where q_i are generalised coordinates and the dot refers to the first differential with respect to time. The coefficients, a_i and a_t , may be functions of the generalised coordinates and time in the general case. These systems are classified as *non-holonomic* systems, or more specifically as *anholonomic* or *Pfaffian* systems. The constraint equations are also termed as motion constraint equations since they involve the first time derivatives of the generalised positional coordinates.

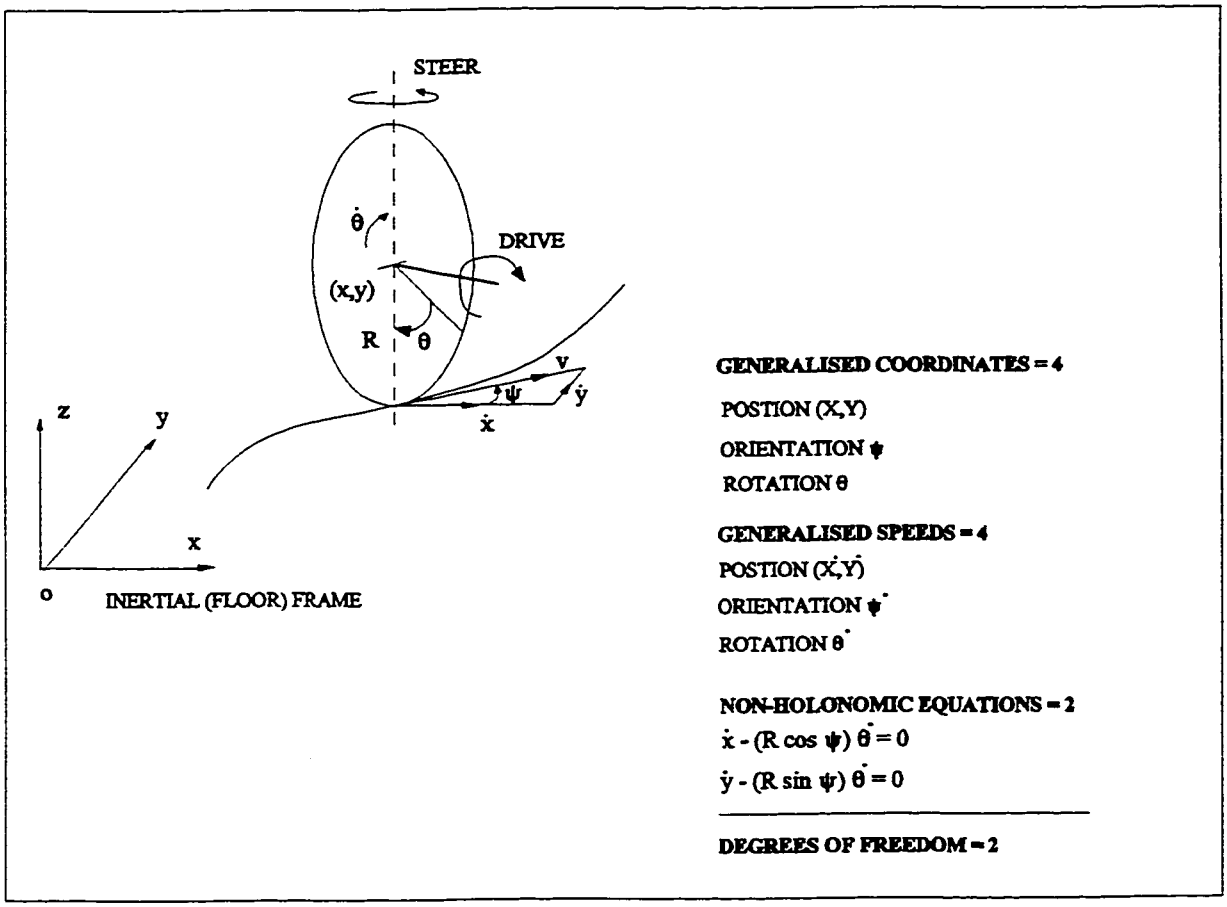

Figure 2.2 A wheel as a non-holonomic system

A wheel, shown in Fig.2.2, may be used as a simple example of a non-holonomic system. The wheel is assumed to move on a rough plane with adequate friction at the point of contact to prevent slippage. It is also assumed that the wheel is constrained to rotate in the vertical plane without tilting. Under these conditions, four time dependent variables or generalised coordinates are needed to describe the location of the wheel in the inertial coordinate system. Using cartesian coordinates, the position of the centre of the wheel is given by x and y, the orientation of thewheel by ψ and the angle of rotation by θ. However, due to the no-slip condition at the point of contact, the forward motion and the rotation of

the wheel are constrained by

$$\begin{aligned} \dot{x} - (R\cos\psi)\dot{\theta} &= 0 \\ \dot{y} - (R\sin\psi)\dot{\theta} &= 0 \end{aligned} \tag{2.2}$$

The presence of ψ indicates that these equations may not be directly integrated and the dependent generalised coordinates eliminated. Such a system is called a non-holonomic system and the constraint equations are referred to a non-holonomic equations. Hence, of the four generalised speeds only two are independent for this system. The two constraint equations indicate that the system has two degrees of freedom only.

2.2.2 Newton-Euler and Related Methods

The Newton's laws can be utilised to obtain the dynamic equations only when all the forces acting on a given body are known. In the Newton-Euler method for WMRs, the non-holonomic system is dissembled into its constituent components and the dynamic equations are derived for each component separately. In order to account for the connectivity of the system, constraint forces are introduced between any two interconnected components. These forces appear as equal and opposite applied forces in the derivation of the equations for any two contiguous components. The constraint forces are eliminated when the dynamic equations are assembled. The introduction of the constraint forces whose magnitude and direction may be obtained only by solving the dynamic equations thus increases the number of unknowns and consequently the number of equations. The internal constraint forces are of little interest from the control standpoint and their inclusion in the derivation only increases

the mathematical complexity of the problem.

Huang [7] and Cheng, Huang and Sankar [9] have adopted the Newton-Euler force balance approach to develop a simulation package for the dynamics of differentially driven WMRs using the CONCIC II described in Section 1.3 as a case study. This differentially driven WMR is modelled as a collection of interconnected bodies comprising the body, two drive wheels and two castors. The WMR is assumed to have two degrees of freedom, viz., forward translation and rotation about the vertical yaw axis. By systematically applying a force balance along the axes of freedom the dynamic equations of the WMR are obtained. The pivot angle and the rotational speed of the castors are related to those of the drive wheels through non-holonomic equations. The WMR is assumed to move at velocities up to a maximum of 1.2 $m.s^{-1}$ and hence inertial forces such as centrifugal forces during cornering and the Coriolis forces due to acceleration of the rotating wheels in the non-inertial coordinate frame attached to the body of the WMR are neglected. The vehicle moves with negligible longitudinal slip and side slip since the Coulomb frictional forces at the wheels and castors are assumed to be adequate to prevent slip during phases of acceleration. Tire frictional forces are modelled using the linear empirical relation described by Wong [27] using model parameters obtained through experimental work. However, the vertical load on each wheel and castor is assumed to be a constant and equal to one fourth of the total weight of the WMR. In reality, the vertical loads on the wheels and the castors are dynamic in nature and are dependent on the forward and angular acceleration of the vehicle. At the low operating speeds for which the dynamic model is obtained, these forces may be assumed to be constants. However, a generic dynamic model must account for the inertial transfer of wheel

vertical loads and for the variations in the tire friction due to such transfers.

Mehrabi, Cheng and Hemami [10] have applied the Newton-Euler method to derive the dynamic model of a 3-degree of freedom WMR, with forward velocity, and yaw and roll rotational velocities. The WMR is assumed to have a suspension and the roll degree of freedom represents rotation of the sprung mass about the longitudinal axis of the vehicle. Simultaneous pitch motion, though possible, has not been considered. However, it has been shown that by examining a non-dimensional number, called the '*roll number*', the non-linear dynamic model may be reduced to a two degree of freedom linear model. By so linearising the dynamic model, controller synthesis is made easier. Simulation and experimental results presented validate the optimal controller design adopted. In the derivation of the dynamic equations, the assumptions made are the same as those made by Huang [7] except for the inclusion of a fore-aft transfer of wheel loads during acceleration and deceleration as the wheel configuration is different. The derivation uses only side forces and cornering forces at the tires due to slip and does not include centrifugal nor coriolis forces arising from the inertia of the constituent bodies even though high forward and angular accelerations are considered.

The dynamic model developed by Huang [7] and by Cheng, Huang and Sankar [9] has been applied by Rajagopalan and Barakat [13, 14] and by Barakat [15] to propose a novel Computed Torque controller for CONCIC II. The dynamic model and the controller have been shown to perform satisfactorily by both simulations and experimental work at speeds up to 1 $m.s^{-1}$ and for payload changes up to 5 times the weight of the WMR. Chen [28] has extended the method proposed by Cheng, Huang and Sankar [9] to develop a systematic dynamic modelling methodology for WMRs with up to 4 degrees of freedom, viz., forward

and lateral translations and roll and yaw rotations. She addresses the conventional wheel types by using the steer-drive wheel unit as the generic model. The method is systematic and the equations obtained are in a compact form suitable for computer implementation, either for simulations or for digital controller design. However, the force balance from which the dynamic equations are derived do not account for the inertial centrifugal and Coriolis forces, nor for the dynamic shifts of the vertical loads between the wheels and the castors during motion. The WMR is also assumed to carry only deadweight payloads and hence the model is inadequate for cases where the load has its own dynamic behaviour, such as a suspended load.

Yu and Moskwa [29] have utilized the Newton-Euler method for the derivation of the dynamic equations of a four wheel omni-directional vehicle. Each wheel is independently driven and steered to provide three degrees of freedom, forward and lateral translational motion and rotation about the yaw axis. Other than the drive torques for the wheels, only tire friction forces, obtained using Dugoff's tire friction model [30], have been considered. The tire friction model needs the vertical forces acting at each wheel; the total weight of the WMR has been assumed to be equally distributed between the four wheels. The dynamic model does not account for centrifugal or Coriolis forces and no mention is made of the operating speeds of the WMR.

Matsumoto and Tomizuka [31] have adopted the Newton-Euler method to derive the dynamic model of a four wheeled WMR with two degrees of freedom. The lateral motion and the yaw rotation are controlled by using either differential drive for the front or rear wheels or by driving or steering the rear wheels. The model assumes small values of steering angle,

wheel slip angle, vehicle slip angle and yaw rate. In addition, the vehicle forward velocity has been assumed to be constant or slowly changing. Since the rate of change of both the forward velocity and the yaw rate are assumed small, inertial cross coupling terms do not appear in the dynamic equations. Tire friction forces have been obtained using the longitudinal road-tire friction coefficient obtained form the wheel slip angle using the model proposed by Abe [32]. Inertial redistribution of the vertical wheel load has been assumed to be due to centripetal forces only. Since, the angular acceleration is assumed to be small, a linear relation has been derived for the vertical loads in terms of the mass of the WMR, the radius of curvature of the path, the forward velocity and yaw rate.

Muir and Neuman [21] have used the Newton-Euler method along with a kinematic methodology for WMRs developed by them [22]. WMRs are kinematically different from non-redundant tree-like stationary robots in that they contain closed chains and both surface (lower pair) and point (higher pair) contact may be present. It is this nature of the system that makes it non-holonomic and which permits only some of the degrees of freedom to be actuated. Muir and Neuman [22] have used the transformation approach for the kinematic modelling of WMRs. In the dynamic modelling methodology presented, inertial and external applied forces at all the bodies of the system are propagated through the joints to a common point, the centre of mass coordinate system of the main body. The propagation utilises the transpose of the link Jacobian and the coupling matrix of the joint which is based on the friction present. By Newton's law, the three components each of the resultant force and the resultant torque must be instantaneously in equilibrium. Equating each component to zero yields six equations. The geometric constraint equations are then used to eliminate the extra

degrees of freedom to provide the final set of dynamic equations. Even though this method accounts for unactuated and unsensed joints and joint friction, the drawbacks of utilising Newton-Euler method are carried into this system as well. A WMR is a non-holonomic system but the method incorporates this information in the last step of the derivation only. This leads to redundant equations which tend to mask the nature of the physical system. Moreover, the vertical loads on the wheels are constraint forces applied by the ground and by eliminating them to obtain the dynamic equations, one loses a vital piece of information required to compute the frictional forces at the tires.

The Kane's approach adopted in this thesis addresses both these issues elegantly by identifying in the first step of the derivation the actual number of degrees of freedom and using only those to obtain the dynamic equations. 'Virtual' degrees of freedom are introduced, where required, in order to obtain additional equations for the constraint forces at the wheels.

2.2.3 Lagrangian and Related Methods

In the Lagrangian approach, the derivation of the Lagrangian of the system is identical for both holonomic and for non-holonomic systems using the generalised coordinates and their time derivatives, the generalised speeds. At this stage no steps are taken to incorporate the non-holonomic nature of the system due to which the number of generalised speeds is equal to or greater than the degrees of freedom. Using the Lagrangian, the dynamic equations are derived. Again it must be emphasised that there are as many equations as the number of generalised speeds, which for a non-holonomic system is generally greater than the number of degrees of freedom. For non-holonomic systems, the usual method is to introduce the

motion constraint equations into the dynamic equations using Lagrange multipliers. These multipliers are not constants and are usually functions of all the generalised coordinates and often of time as well. They represent a set of unknowns, physically representing the constraint forces, whose values may only be obtained as a part of the solution. This implies solving a set of coupled second order (or first order, if state space methods are employed) differential equations and solving a set of linear equations for the Lagrange multipliers simultaneously. The Lagrange equations of motion when applied to non-holonomic systems thus introduces redundancy.

In the Lagrangian approach, the virtual work due to the external applied forces are expressed as the generalised forces. For forces which may be derived from a potential function, the dynamic equations reduce to a simple form. Thus the Lagrangian approach is more amenable to the inclusion of friction in which the frictional force is proportional to the generalised speeds, for example, viscous friction. Such frictional forces may be derived from the Rayleigh's dissipation function [20] and may be incorporated into the Lagrangian. Other types of friction on the other hand must be accounted for only by including the generalised force terms for each of the generalised coordinates. In a system such as the WMR, where frictional forces are dominant, inclusion of the friction forces in terms of the generalised forces for the dynamic equation for each generalised speed leads to a redundant, cumbersome set of equations.

In their work on the modelling and the control of non-holonomic wheeled mobile robots, d'Andrea-Novel, Bastin and Campion [33], adopt the classical Lagrangian approach for the dynamic model for a 2-degree of freedom WMR with wheels in a tricycle

configuration. The Lagrange equations of motion include the inertial effects such as the Coriolis and the centrifugal terms ; however, inclusion of friction has not been addressed. For this vehicle, seven generalised coordinates are required to describe the configuration but the motion constraints reduce the number of independent generalised speeds to 2. Since the vehicle is assumed to move in a horizontal plane only, the Lagrangian contains only the kinetic energy. The kinetic energy is derived in terms of all the seven generalised speeds. Using the Lagrangian, seven equations, one for each generalised speed, are derived to describe the dynamics of the WMR. However, to account for the motion constraints, five Lagrangian multipliers are used which in turn leads to five more equations for the multipliers. Using conditions of pure rolling and non-slipping for all the wheels, the non-holonomic constraint equations are derived. Thus a total of twelve equations are used to describe a WMR with only 2-degrees of freedom. Friction, either at the tires or in the actuators, is not included which makes the final form of the equations an approximation of the real WMR.

Canudas de Wit and Roskam [34] use a transformation of variables to linearize the non-linear dynamic equation for the 2-dof WMR about the operating point. The linear equations are then used to construct a control scheme. Frictional forces appear in the dynamic equations but no mention is made on the nature of the frictional forces nor how they may be modelled. The dynamic equations and the control scheme are applied to a 2-dof micro robot, the micro WMR-Kitborg. In the experimental results presented, friction forces have been neglected due to the miniature size of the mobile robot.

Zhao and BeMent [35] have studied the controllability of non-holonomic robot systems utilising special synchro-drive mechanisms for six common wheel and axle

configurations with 2- or 3-degrees of freedom. The dynamic equations are derived using the Lagrange equations of motion. The body of synchro-drive robots, due to the special drive arrangement, only translate and do not rotate around the centre of mass or the origin of the local coordinate system fixed to the WMR. For this reason, centrifugal and coriolis do not appear in the dynamic equation. However, even in synchro-drive mobile robots, the payload does rotate with the drive wheel system. In addition, the drive motor sets normally have appreciable inertia. Due to these reasons, neglecting the centrifugal and coriolis forces leads to large approximations. Frictional forces are again neglected in this model.

To obviate the computational complexity of evaluating the Lagrange multipliers, other methods have been suggested which eliminate the presence of the multipliers from the dynamic equations. Saha and Angeles [23] and Cyril, Cheng and Sankar [24] suggest employing a mathematical construct called the Natural Orthogonal Complement in the proposed Newton-Euler / Euler-Lagrange hybrid formulation for a 3 wheel 2-dof WMR. Sarkar, Yun and Kumar [36] adopt a similar method to eliminate the constrained generalised speeds from the equations of motion. The method is similar to the canonical transformations [20] used in the Hamilton equations of motion for transformations between generalised speeds in the phase space of the system. Using a set of smooth, linearly independent vectors representing the degrees of freedom of the system, they construct a matrix that lies in the null space of the matrix representing the non-holonomic constraint relations. Premultiplying the Lagrange equations of motion by the transpose of this matrix eliminates the Lagrange multipliers. However, it must be stated that by doing so, ***these methods mask an essential physical attribute of the non-holonomic system***. The linearly independent generalised speeds

obtained by the canonical transformations do not represent actual generalised speeds but are purely mathematical constructs used to reduce the mathematical complexity of the problem.

2.3 Review of Control Schemes for Wheeled Mobile Robots

Wheeled mobile robots need some form of control system to provide them with the measure of autonomy with and for which they are designed. In the structured environments present in industrial applications of WMRs, the autonomy expected of the mobile robots is to track a desired trajectory using feed back from one or more sensors. This requires the fusion of three distinct areas, viz., planning, guidance and control [36]. Task level planning may include precompiled plans stored in the controllers memory by a human planner, reactive or dynamic planning and finally an integration of prior plans and information obtained during task execution. In this thesis, attention is focussed on control aspects only and pre-compiled task planning is restricted to executing a desired trajectory.

2.3.1 Guidance schemes

Guidance systems provide task or cartesian level information which is used by the controller for reactive or dynamic planning. A wide variety of guidance schemes are listed in WMR literature. The reader is referred to the exhaustive review of guidance schemes given by Rajagopalan and Cheng [5], Rajagopalan and Perelli [12], Meystel [17] and Iyengar and Elfes [37]. For the control of CONCIC III, Mehrabi, Cheng and Hemami [10] has used a dead-reckoning guidance scheme. In this method, no cartesian level sensors are used and the position and the orientation of the WMR in the world or the floor frame is estimated using

wheel motion sensors such as optical encoders. Wheel position sensors are less expensive but are prone to erroneous position indications due to accumulated errors in the devices and uncertainty in the geometric parameter values, such as the wheel span and radius, needed for the transformation from joint values to cartesian values. The focus in this thesis is on the application of dynamic model based controllers for servo control of a WMR. The performances of the controllers are judged by a performance index computed at the joint level. Hence, the dead reckoning method of guidance has been adopted in this thesis as well.

2.3.2 Control of Wheeled Mobile Robots

In this section, published literature related to control of WMRs in general and to model based control are reviewed. The control structure of the schemes for WMRs are found to have certain similarities to the control methods applied to stationary robots. In model based control, the inverse dynamic model must be modified only to include the dominant frictional forces. Gravitational effects may be neglected where WMRs are assumed to operate on a horizontal task space. Hence, a review of pertinent model based control schemes for stationary robots is given in Section 2.3.2.1. This section also summarises the work done by An, Atkeson and Hollerbach in the experimental evaluation of model based controllers for stationary manipulators since one of the objectives of this thesis is to provide a similar comparison for WMR model based controllers. A survey of control schemes for WMRs is provided in Section 2.3.2.2.

2.3.2.1 Model Based Control of Stationary Manipulators

Model based control literature related to stationary robots is vast and numerous control schemes utilising the full non-linear dynamic model or a dynamic model linearised about the operating point have been proposed and implemented. Zhao [38], constructed and tested a Computed Torque Controller based on parallel processing technology for a 6-degree of freedom PUMA 560 robot at the CIC, Concordia University, Montreal.

An, Atkeson and Hollerbach [39] undertook out a systematic experimental evaluation of the Feed Forward Controller and the Computed Torque Controller for stationary manipulators. In this thesis research, a similar experimental evaluation of dynamic model based control schemes for WMRs is undertaken. In addition the model based controllers used in this thesis use the structure proposed by them for the dynamic controllers. Their evaluation of model based controllers as well as model based learning was performed using the 3 link MIT Serial Link Direct Drive Arm (DDArm).The Computed Torque Controller used in the study was based on the Resolved Acceleration Controller proposed by Luh, Walker and Paul [40] and implemented on the Stanford Arm. The Resolved Acceleration methodology is an extension of the Resolved Motion Rate control scheme first proposed by Whitney [41] for manipulators and human prostheses. Based on the evaluation, An, Atkeson and Hollerbach have concluded that both the dynamic model based control schemes consistently outperform the kinematic PD controller. However, they have also observed that the Feed Forward Controller performed just as well as the Computed Torque Controller in all the tests.

Leahy, Valavanis and Saridis [42] have evaluated the effects of the structure of the inverse dynamic models used for robot control. In a subsequent article, they [43] have shown

that feedforward compensation of non-linear velocity dependent friction improves controller efficiency. Khosla and Kanade [44] have reported a real time implementation and evaluation of model based control schemes on the CMU DD Arm II (Carnegie Mellon University Direct Drive Arm). It has been shown that the CT scheme outperforms the PD controller as long as there is no torque saturation in the actuators.

Goldenberg, Apkarian and Smith [45] have proposed an adaptive approach for on line 'recursive' identification of unknown loading and parameter uncertainty. Uebel, Minis and Cleary [46] have extended the Computed Torque control for a robot arm with flexible, geared joint drive systems. In a comparison of performances with a PD controller, it has been observed that the latter showed smaller orientation error for no-load tests. The poor performance of the CT controller has been ascribed to inaccuracies in the friction model used for the last three joints which govern orientation of the end effector. In model based control, these results underline the importance of evaluating the relative importance of the various terms in the dynamic model and the values of the dynamic parameters used in the model.

2.3.2.2 Model Based Control of Wheeled Mobile Robots

In the area of Wheeled Mobile Robots, the literature on model based control is lacking in volume and most of the published results have been obtained by computer simulations only. Pioneering work in this area has been carried out at the CIC, Concordia University, Montreal by Cheng and Huang [8], Mehrabi, Cheng and Hemami [10], Rajagopalan and Barakat [14] and Rajagopalan and Cheng [47].

Rajagopalan and Barakat [14] proposed and implemented a novel Computed Torque

Controller on the CONCIC II, the experimental differential drive WMR described in Section 1.3. The controller uses errors in the forward and angular velocities and the desired acceleration to compute the actuator drive torques using the inverse dynamic model of the WMR. The inverse dynamic model proposed by Cheng, Huang and Sankar [9] for the CONCIC II has been simplified for the real time implementation of the controller. The performance of the CT controller has been compared with that of a conventional PID controller for straight line trajectories at a maximum speed of 1 m/s. Using simulations, the robustness of the proposed dynamic scheme has been proven by disturbance rejection for payload changes for as much as five times the mass of the WMR. Experimental results also include straight line trajectories up and down a ramp.

Mehrabi, Cheng and Hemami [10] undertook a systematic evaluation of the use of a full non-linear dynamic model and a simple linearised version for analytical studies and for the design of controllers for WMRs. His work focussed on 2- and 3-degree of freedom WMRs executing planar motion. Using sensitivity theory, a systematic parametric study has been carried out on the effects of parameter variations on the transient and steady state responses during trajectory execution. As a result of these studies, three non-dimensional numbers have been identified, viz., the Roll Number, the Yaw Number and the Velocity Constant. Small values of the Roll Number may be used to simplify 3-degree of freedom dynamic models to the simpler 2-dof models by neglecting the roll motion. The Yaw number and the Velocity Constant may be used to characterize when to use the dynamic model or a simple kinematic model to represent the motion behaviour of the WMR. The results of the analysis have been applied to the design of an optimal controller which minimises a quadratic error cost function.

The performance of the optimal controller has been studied both by simulations and by experimental work carried out on the CONCIC III described in Section 1.3. For the experimental work, a dead reckoning method of guidance scheme has been adopted to track a piece wise continuous cubic polynomial trajectory.

Reister [48] has reported a wheel motion control system for the omnidirectional HERMES III, the WMR built at the Oak Ridge National Laboratory, Tennessee, to serve as an experimental platform for research in mobile robotics [49]. The motion system consists of a controller, a driver and a reckoner. The controller takes as input the goal or the next position at which the platform is commanded to be and the current wheel state. This information is used by a QuickPlan function in the controller which uses one of seven in-built modes to calculate the wheel control signals. All seven modes use only the kinematic model of the WMR. Experimental results for this piecewise, dead reckoning method of control have been presented at forward speeds of 0.5 m. s^{-1} for a 90-degree turn and a S-profile path to validate the efficacy of the scheme.

Rajagopalan and Cheng [5] have adopted a conventional PD feedback controller for trajectory tracking with cartesian level feed back from a binary camera. The camera is focussed on an illuminated track laid on the floor and image processing is used to provide instantaneous position and orientation offsets. The guidance and control schemes have been implemented on the CONCIC II, described in Section 1.3, to validate the methodology.

Sarkar, Yun and Kumar [36] have investigated two types of control algorithms for the control of mechanical systems with rolling holonomic and non-holonomic constraints, with particular reference to WMRs. They have synthesised a non-linear feedback to cancel the non-

linearities in the dynamics of the 2-degree of freedom WMR so that the state equations are simplified. A second non-linear feedback linearises and decouples the input-output map so that the overall system is decoupled into two linear subsytems. Using pole placement for the outer linear position feedback loop, they stabilize these two subsystems and achieve the desired performance both in trajectory tracking and in path following. No experimental implementation is reported and only simulation results are provided to prove the efficacy of this control methodology.

Bétourné and Campion [50] address the problem of violation of the non-holonomic constraints in mobile robots. They identify two cases where the kinematic constraints are not satisfied, (i) between the wheel and the ground due to slippage and (ii) due to uncoordinated wheel orientation angles in redundant mobile robots with steering wheels. Using non-linear feedback, the proposed control law computes the drive torques in such a way that the dynamics of the tracking errors in the joint parameters are linear and stable. It must be noted that the control law is constructed for trajectory tracking in the joint space under the assumption that satisfactory behaviour in the joint space of the mobile robot will result in similar behaviour in the task space close to the desired values. Simulation results are provided to illustrate the methodology but no experimental results are given.

d'Andréa-Novel, Campion and Bastin [51] also use feedback linearisation techniques to solve tracking control problems in mobile robots. In an earlier publication, [33], they have shown that with static state feedback it is possible to reduce the dynamics of a 3-wheel 2-degree of freedom mobile robot to a form for which stabilising input-output linearising control is possible. As an extension to a more general class of WMRs, they show in the later

publication that for omnidirectional WMRs, trajectory tracking can be achieved by a smooth static linearizing state feedback. For WMRs with only 2-dof, termed in their work as 'car-like robots', they propose a smooth dynamic linearizing state feedback as long as the robot is moving. These non-linear controllers are applied to WMRs with five different wheel types and configurations according to the generic type classification of mobile robots [52]. Simulation results are provided to illustrate the design methodology.

Canudas de Wit and Roskam [34] have provided experimental results of a nonlinear controller which decouples, linearises and stabilises locally the non-linear dynamic model of a 2-dof mobile robot. The desired trajectory is piecewise straight line segments generated by an on-line trajectory generation scheme. The controller is applied to, the WMR Kitborg, a teaching and research purpose micro mobile robot. The robot has two driven wheels and a spherical wheel at the centre of mass for stability. In the experimental work frictional forces, which are normally dominant and difficult to model and control, have been neglected due to the size of the WMR. The controller is shown to perform satisfactorily for simple closed geometric figures, such as a square and an octagon, composed of straight line paths.

Zhao and BeMent [35] have used the Potential Field Control method for trajectory tracking of a synchro-drive WMR. The Potential Field method of control uses a vectorial sum of attractive and repulsive forces from the obstacles around the mobile robot to provide a resultant force to guide the vehicle. Simulation results on the performance of the Potential Field controller are provided to prove that limit cycles are possible in trajectory tracking. It is also demonstrated that PD controllers provide stable trajectory tracking for WMRs.

Matsumoto and Tomizuka [31] have addressed the issues of independent lateral and

yaw motion control in automatic vehicle control in highway automation. To this end, they have studied the conventional front wheel steering, front steering and rear differential drive and finally, front and rear independent steering as the three different drive-steer configurations. The dynamic model derived by them accounts for tire longitudinal friction, turning moment and front-aft wheel load transfer during acceleration and deceleration. However, the vehicle velocity has been considered to be a constant or a slowly varying parameter (low accelerations). Under this assumption, the non-linear dynamic model has been expressed in linear form. By pole placement, the two control signals, viz., the lateral velocity and the yaw rate have been obtained. Experimental results obtained using a laboratory vehicle with maximum forward speed of 3 $m.s^{-1}$ are provided. The assumption that forward and rotational accelerations are small for a vehicle used in highway automation restricts the applicability of the results.

Yu and Moskwa [29] have used the input-output linearisation technique to transform the non-linear dynamic model to a linear form. They have used for their analysis an independently driven 4-wheel WMR with coordinated front and rear steering. A sliding mode controller has been designed to modify the steering and the braking commands to provide better maneuverability and vehicle stability. Simulations results have been provided to prove that the controller performs satisfactorily in both respects.

Sørdalen and Canadus de Wit [53] have proposed a piecewise smooth feedback control law for path following for the kinematic model of a WMR. The vehicle analyzed is a 2-degree of freedom WMR with wheels in a tri-cycle configuration. The problem addressed is path following in the configuration space with the path being specified by an initial and a

final position along with a number of intermediate points. The path is assumed to consist of piece wise straight line segments and arcs. The controller is shown to provide exponential convergence to the desired path. Only simulation results are provided to prove that the kinematic controller does perform satisfactorily for path following in the cartesian frame.

Samson and Ait-Abderrahim [54] have presented a general study of the problem of feedback control of a WMR in cartesian space. The WMR used in the analysis is a 3-wheel differentially driven vehicle with a free wheeling castor in front ; the problem addressed has been restricted to kinematic control only. For trajectory tracking, they have proposed using a 'virtual' reference cart whose trajectory is predetermined and parametrised by time. Using computer simulation studies, the performances of a few linear and non-linear control schemes have been analyzed. They conclude that though it is not possible to stabilize the WMR both in position and in orientation by pure state feedback, it is possible to stabilize only two of the configuration variables. They have also shown that via the introduction of the reference cart, feedback stabilisation in both position and orientation becomes possible as long as the virtual cart is moving. Finally, they have concluded that due to the non-holonomic nature of WMR systems, control approaches developed for stationary manipulators apply only partially to mobile robots.

Wiens and Jang [55] have been, according to this survey of WMR literature, the only reported work on the effects of the dynamic interactions between a WMR and a robot arm mounted on it. A highly simplified model of the WMR consisting of only a mass and the robot arm consisting of a mass at the end of an arm have been used in the analysis. The ground has been considered to be a stiff spring-damper system. The objective of the study was to evaluate

the effectiveness of various Passive Control Systems (PCS) to reduce or to eliminate the dynamic coupling between the WMR and the robot arm. Three PCS systems, the Kelvin-Voigt spring damper system, the Maxwell spring-damper system and the standard linear spring-damper system have been studied. Simulations results are provided to prove that the utilisation of the PCS systems reduces the dynamic interaction. It has also been concluded that the Kelvin-Voigt PCS system gives the near optimal system design.

Joshi and Desrochers [56] have considered the problem of the control of a mobile robot subject to random disturbances. The mobile robot consists of a two link robotic manipulator mounted on a mobile platform and subject to disturbances around the roll, pitch and yaw axes. The control strategy used is non-linear feedback which results in linear closed loop dynamics. An integral feedback controller is used for disturbance rejection. Path segmentation has been adopted to circumvent stability problems as the integral controller adds to the order of the system. From the simulation results provided, it is concluded that the mobile robot-manipulator system was able to withstand large disturbances yet complete its task.

2.4 Path Planning and Trajectory Generation for WMRs

The list of applications or potential applications for WMRs given in Section 1.4, indicates that the environment in which the mobile robot operates may include the whole spectrum from being highly organised to totally unknown. The former setting may be found, for instance, in a production line in an automobile factory where the WMR is programmed to carry the chassis of an automobile through different stations in the assembly and finishing

processes. On the other hand, the Planetary Rover [57] must be able to sense its environment, plan and traverse a course through that environment and react appropriately to unexpected situations as they appear. This is done while the path planner is guiding the WMR towards some goal set by the human user. In the context of this thesis, path planning and trajectory generation refer to the structured industrial setting only. Furthermore, since dead reckoning method of guidance has been adopted, with no cartesian level feedback, the structure of the surroundings is assumed to be a constant. The desired trajectory is preplanned by the human user using one of the methods reviewed in this section.

Samson and Ait-Abderrahim [54] have pointed out, in their study on feedback control of mobile robots, that the path planning problem for mobile robots is closely linked to the feedback control problem. This is due to the non-holonomic nature of the system which makes it controllable but not necessarily feedback stabilisable. In the case of a WMR, starting from any initial condition, it is possible to find a set of piecewise constant inputs to reach a final configuration. However, not all these paths in the configuration space may necessarily be feedback stabilisable for a non-linear WMR system. This, according to them, provides a strong link between the path planning problem and the feedback control problem for WMRs.

Kanayama and Miyake [58] define the problem of path planning for a WMR and provide a solution in terms of piecewise continuous straight line segments connected by clothoid pairs. They define the path in the 2-dimensional cartesian world frame in terms of the quadruple, **P**, consisting of the x and y coordinates, the direction of the tangent vector and the curvature of the path. The path planning problem, as defined by them, is to find a directed curve that starts at the initial posture and terminates at a pre-defined final posture and passes

through the set of user defined intermediate postures. They then simplify the problem further with the condition of zero curvature at both the initial and the final postures. Of the many classes of curves that may be chosen, they use the class of curves called Clothoids or Cornu spirals [59]. A clothoid is a curve whose curvature is a linear function of the arc length, s. The path of the WMR is thus composed of straight lines and clothoid pairs upto a maximum of 2. Though the algorithm is fast and simple, the assumption of zero curvature at both the end postures restricts the application of the clothoid solution to straight line segments connected by clothoid pairs. It must be mentioned that Mark [60], in an unpublished work at the CIC, Concordia University, suggested the same approach to WMR path planning.

Mukherjee and Anderson [61] adopt methods from differential geometry to provide a solution for the path planning of WMRs. Starting with the general non-holonomic equations for a Pfaffian system, they prove that the configuration variables may be taken from one set of values to a final desired set of values by first driving the set of independent variables (corresponding to the degrees of freedom of the system) from the initial to the final state. The dependent variables may then be driven to the final configuration by the use of cyclic motion of the independent variables. Using Green's theorem, they have reduced the problem of path planning to finding a surface area in configuration space. For a WMR, though the proposed solution may be used to plan feasible paths, the additional time constraint normally present may make the trajectory impractical. Trajectory planning, in the case of a WMR, must necessarily be made in phase space and not in configuration space due to such time constraints present. In addition, the assumption that all of the configuration space is available for path planning is another drawback since the presence of obstacles in the path of the WMR may

make some regions of the configuration space unavailable for path planning.

Reister and Pin [62] propose a time optimal trajectory planning scheme for a differentially driven WMR. They redefine the time optimal trajectory generation problem to finding a set of inputs, the two drive wheel accelerations in the case of the differential drive, that will minimise an objective functional, which for the WMR is the transition time. Using the Pontryagin Maximum Principle from Optimisation Theory, they have shown that the optimal trajectory is a bang-bang trajectory in which the wheel accelerations (which translate to the drive torques for the actuators) are either at their positive or at their negative maximum. In addition, they have shown that, for planar motion, the WMR may be driven from an initial to a final position (orientation not defined) in three switch times; where orientation is also defined, the number of switch times required is four. They have proven the feasibility of the approach by applying it to the trajectory generation of Hermes III, the experimental WMR cited earlier [49]. In the reported test trajectory, the WMR attained a top speed of 0.4 m/s ; it is also reported that a kinematic PID controller was used in the experiment. The switching of the acceleration (and correspondingly, the drive torque) may lead to undue mechanical stress on the drive train of the WMR. In addition, due to the dynamic behaviour of the WMR-payload system, full drive torque at a certain point of the trajectory, such as in a curve, may lead to wheel slippage. Thus the time optimal solution, though theoretically attractive, may pose serious practical problems.

Wang, Linnett and Roberts [63] have addressed the problem of feasibility of a planned path when the WMR is constrained by steering angle limits. A 3-wheel WMR with a single steering wheel in front in the tricycle configuration is used in the derivation. They have shown

that a path planned for a reference point at the midpoint of the rear axle and composed of straight line and arc segments, may not be feasible when the steering wheel has limited steering angle capability. They extend their work to prove that shifting the reference point to another location may make the same global path in the floor frame feasible. The problem of collision free path planning has been addressed [64] in a companion article. They have identified rotation of the vehicle, relationship between the heading of the vehicle and the tangent vector of the path, steering angle limits and the final goal orientation as the four key points that must be addressed in path planning. In addition, a feasible path satisfying these kinematic constraints, according to them, may be considered to be the final path if and only if it is collision free. For every feasible path, they have proposed using generalised polygon obstacles, obtained by enclosing obstacles by circles, and tangent graph methods to identify collision free final paths. The piece wise straight line and arc segment approach used by them to generate the feasible path may be made geometrically smooth with coincident tangent vectors at their points of intersection. However, due to discontinuities in the curvature of an arc (equal to the inverse of the radius) and that of a straight line (equal to zero) at points of intersection of path segments, such a kinematic path leads to discontinuous angular acceleration when applied to a WMR. These discontinuities translate to step changes in the drive torques needed from the actuators.

2.5 Scope of the Study and Problem Definition

From the literature review it can be seen that the dynamic models of the non-holonomic multi-body WMR system deduced using conventional methods do not emphasize the non-holonomic nature of the system; lead to a redundant set of equations for all the generalised speeds and not just for the degrees of freedom; necessitate reformulation of the complete set of equations to include the effects of a payload (even though it does not affect the non-holonomic nature of the system); require the specification of constraint forces between contiguous bodies (Newton-Euler method only); assume low accelerations since the specification of the inertial forces are not systematic; necessitate an additional set of equations for the Lagrange multipliers (Lagrangian method); and do not provide a systematic approach to obtain the dynamic wheel loads (Lagrangian method). These drawbacks arise from the simplifyinng assumptions normally adopted while using these schemes.

With regards to model based control, the survey of the literature indicates that there has been no investigation into the trajectory tracking control of a WMR carrying an active payload such as a suspended load; and several control schemes for WMRs have been proposed in the literature but normally controller performance has been validated only by simulations, exceptions being the systematic experimental work at the CIC.

Thus this thesis focusses on two main areas for WMRs

- Dynamic modelling
- Model-based control

In dynamic modelling, the principal focus of the present study is to develop a dynamic modelling methodology for a WMR which will

- model any combination of steering / driving wheels and castors
- systematically include inertial forces such as centrifugal and coriolis forces
- address the transfer of vertical and side wheel loads due to the dynamic behaviour of the WMR
- include the dynamic interactions between the WMR and an active payload, such as a suspended load, during trajectory following and
- include the effects of gravitational forces on WMR dynamics for non-planar operation.

The principal objectives in model based control are to

- use the dynamic model to synthesize two popular model based control schemes, the Feed Forward Controller and the Computed Torque Controller
- conduct a systematic experimental comparative evaluation of the two dynamic model based control schemes with a kinematic PD controller under realistic operating and loading conditions.

2.6 Thesis Layout

The thesis is divided into three sections following the introduction to WMR technology presented in Chapter 1 and a review of pertinent published literature in the areas of dynamic modelling, model based control and path planning in the current chapter, Chapter

2. These sections are designed to address the objectives set forth in Section 2.5. Dynamic modelling and the development of a general dynamic modelling methodology for the non-holonomic WMR system with and without payload is explored in Chapter 3. Model based control of WMRs, specifically using a Feed Forward Controller and a Computed Torque Controller, is discussed in Chapter 4. These two control schemes have been adapted from the model based control schemes presented by An [39] for the stationary direct drive, MIT DDArm. Each controller is synthesised using joint level feed back and cartesian level feedback. The related topic of path planning and trajectory generation is discussed in Chapter 5. The path planning scheme is based on the scheme proposed by Nelson [65] for a lane change trajectory.

The study of the performances of the model based controllers, both by computer simulations and by experimental trials using the CONCIC III, are presented in the final section of the thesis in Chapter 6 and Chapter 8 respectively. A description of the experimental system is given in Chapter 7. The conclusions drawn from this investigation are summarised in Chapter 9. During the course of the work, a number of issues that warrant further exploration surfaced. These avenues of possible future work are also presented in this chapter.

2.7 Summary

A survey of published literature for WMRs in the areas of dynamic modelling, model based control and path planning is presented in this chapter. Each publication is discussed in detail to highlight the state of art and the current level of understanding in these areas. In these discussions, the reader's attention is drawn particularly to aspects which have been

chosen for investigation in this thesis. The objectives of this research effort are then presented with an explanation of the particular issues they address. The layout of the thesis is given so as to provide the reader with a guide through the material covered in the later chapters.

The review of published material in the area of dynamic modelling indicates that the common methodologies, viz., the Newton-Euler and the Lagrange equations of motion, used successfully for holonomic stationary manipulator systems may lead to redundant equations or may necessitate simplifications when applied to non-holonomic WMR systems.

In the dynamic control of WMRs, many control schemes have been proposed in the literature including model based control and other non-linear control schemes. The satisfactory performances of most of these control schemes have been validated in the publications by computer simulations only. At the present time few experimental investigations have been carried out for WMRs. In this thesis, the Feed Forward Controller and the Computed Torque Controller have been synthesised and applied for dynamic control of the experimental CONCIC III WMR

Chapter 3

Generalised Methodology for Modelling WMR Dynamics

3.1 Introduction

A dynamic model relates the motion parameters of the mobile robot to the applied forces and torques. In control applications, a forward dynamic model is used to analyze the response of the robot for a chosen control strategy using simulations. In model based control, the inverse dynamic model is the heart of the controller. In such a control scheme, the desired and actual trajectory parameters are used to obtain the drive torques from the actuators. In control applications, the dynamic model must take into account the dynamic effects of the dead weight and payload of the mobile robot, side forces due to operational speed and path followed, centrifugal and gyroscopic forces while negotiating curves, tire characteristics and road conditions. Hence, a good dynamic model of the WMR incorporates the essential physical nature into the design of controllers, such as a Computed Torque Controller [15, 39, 47]. In addition, the dynamic model should be computationally simple for real-time control implementation.

A generalised procedure, based on the Kane's method, to deduce the dynamic equations of WMRs has been developed as part of this thesis work and is presented in this chapter. The methodology, consisting of five steps, is developed for a mobile robot using common wheel types and configurations. This approach focusses on the degrees of freedom of the system and this eliminates redundancy. It addresses the requirements of a dynamic model enumerated in Section 2.5 by incorporating closed-chains and higher-pair joints, as well

as friction and unactuated and unsensed joints in the derivation. Explicit expressions to compute the dynamic wheel loads needed by tire friction models are developed.

The several unique advantages offered by the Kane's approach for the dynamic modelling of WMRs are highlighted in Section 3.2. The generalised dynamic modelling methodology for WMRs proposed in this thesis is described in Section 3.3. The method consists of a sequence of five steps that may be applied to all common wheel types and wheel configurations found in mobile robotic literature. The derivations carried out on each step are discussed in detail. The nomenclature and the notations pertaining to the Kane's approach [25] have been adopted and used throughout the derivations.

Using this methodology, the detailed derivations of the dynamic equations are presented in Section 3.4 using a steer-drive wheel unit as the generic wheel type. The geometrical parameters used in the derivations are general in nature so that the equations may be applied to any common WMR wheel configuration. The set of generalised speeds in the derivations has been augmented with the 'virtual' speeds in order to obtain equations for the side forces and the dynamic vertical loads experienced by the wheel during motion. This approach of using the steer-drive wheel unit has been adopted from Chen [28] since the equations for all other common wheel types, viz., the steer only wheel, the castor with swivel, the drive only wheel and the castor without swivel, may be obtained by simplifications and substitutions of the appropriate geometric and inertial parameters. For each of the wheel types listed above, the modifications to the equations and the appropriate substitutions of parameters along with any simplifications that apply are given in the Section. 3.4.2 to Section 3.4.5 respectively.

In keeping with the objective to develop a modelling methodology that will include the effects of the payload on the dynamic behaviour of the WMR, Section 3.4.6 describes the inclusion of a deadweight. A suspended load has been chosen to illustrate the methodology for an active load and the derivations are given in Section 3.4.7.

Finally, in Section 3.5, three common wheel configurations for WMRs are used as case studies to illustrate the application of the methodology. The dynamic equations for a WMR with wheels in a tri-cycle configuration are obtained in Section 3.5.1. 1. A differentially driven WMR is used as the second case study in Section 3.5.1.2. In Section 3.5.1.3, a WMR with an omni-directional wheel configuration using four independently driven steer-drive units is analyzed. Finally, the set of equations of motion of a differentially driven WMR carrying a suspended load are derived in Section 3.5.1.4. The equations obtained in the Section 3.5.1.4 are used in the subsequent chapters for designing the model based controllers for CONCIC III, the experimental WMR used for this thesis. The WMR has been modified to carry a suspended load for the experimental investigations. The chapter concludes in Section 3.6 with a summary of the important aspects of the methodology.

3.2 Advantages of Kane's Approach for WMR Modelling

In the proposed methodology, the dynamic equations of a WMR are derived using the Kane's approach [25, 65, 66], also termed Lagrange's form of d'Alembert's principle [67]. The method has been applied by Kane and by other researchers to obtain the dynamic equations of serial link manipulators [18, 68, 69] and in the study of space craft dynamics [70, 71] which are also non-holonomic systems. However, Thanjavur and Rajagopalan [72] provide

the first discussion on the advantages offered by the Kane's approach over the other classical methods to model the dynamics of a WMR. The generalised dynamic modelling methodology for WMRs developed as part of this thesis is in submission for publication [73].

Muir and Neuman [21] point out that the Lagrangian [74] and the Iterative Newton-Euler [40] methods for modelling the dynamics of stationary robots with open chain configurations are not adequate for modelling WMRs. The reasons cited are that, in the case of a WMR, closed-chains where the wheels are in contact with the environment as well as higher-pair joints with line or point contact are present (giving rise to the non-holonomic nature of the system). Other reasons given are the substantial amounts of friction at the tires and the actuators in the WMR and the presence of unsensed and unactuated joints, both of which are absent in the case of stationary robots. However, it is shown in this chapter that the Kane's method does incorporate all the requirements listed above and provides a systematic approach to derive the dynamic equations of non-holonomic systems.

For the modelling of non-holonomic systems such as a WMR, the Kane's approach offers several unique advantages over the Lagrangian and the Newton-Euler methods cited in the survey in Section 2.3. Major advantages experienced in using Kane's method are enumerated below

- In non-holonomic systems, the motion constraints demand that the power input due to the action of a force be distributed among some or all the components of the system. This contrasts with holonomic systems such as open chain robotic manipulators where the power input due to the drive torque at any joint affects only the more distal links. This nature of sharing of input power in a non-holonomic system

is incorporated into the derivation as *non-holonomic partial velocities*[1]. In the modelling of non-holonomic systems, the Kane's method thus offers a physical insight on the effect of the motion constraints on the dynamic behaviour of the system.

- The Kane's method focusses on the degrees of freedom and on the motion of the system [18]. For each degree of freedom, the method reduces to an equation of two groups of scalar quantities, namely *generalised active forces* and *generalised inertia forces*. There are only as many equations as the degrees of freedom and no redundant unknowns are introduced ;
- The Kane's method provides expressions for constraint forces when required by the model. As an illustration, explicit algebraic expressions for the lateral and the vertical loads on the wheels of the WMR are obtained. These vertical forces are then used to model rolling friction at the wheels ;
- This approach permits the inclusion of the effects of any general loading condition, be it a deadweight or an active payload, into the dynamic equations without derivation of all the equations as is necessary in both the Newton-Euler and the Lagrangian methods. The degrees of freedom of the load do not affect the motion constraints and the related degrees of freedom of the WMR. Thus, in the Kane's approach, the dynamic equations of the WMR are augmented with the payload dynamics.
- The method offers a systematic approach to the dynamic modelling of WMRs with no mathematical complexity leading to a set of equations suitable for computer simulation studies and the synthesis of control algorithms.

---

[1] terminology specific to Kane's method [25] shown italicized.

3.3. Proposed Dynamic Modelling Scheme

The dynamic modelling scheme proposed in this thesis is based on the Kane's approach as applied to a non-holonomic system. The disadvantages of modelling schemes based on either the Newton-Euler or on the Lagrangian method are summarised in Section 2.5. The objective is to develop a modelling methodology for a WMR executing planar motion under conditions of loading seen in the industry. In addition, the method should address the disadvantages of the existing schemes and possess the following features

- highlight and emphasize the non-holonomic nature of the physical system
- use only the degrees of freedom and not all the generalised speeds
- incorporate the effects of various payloads into the dynamic equations of the mobile robot without repeating the complete derivation
- provide a systematic method of obtaining the dynamic wheel loads

3.3.1 Modelling Assumptions

The primary assumptions on which the method is based on are that

- the Coulomb frictional forces at all the wheels are adequate to prevent slippage
- the WMR retains its non-holonomic nature throughout the trajectory
- the deformations in the components and mechanical vibrations are negligible and
- the components may be modelled under the lumped mass assumption as a system of interconnected rigid bodies

3.3.2 Coordinate Frame Assignments

For the present modelling, the WMR is considered to be a system, S, composed of interconnected rigid bodies, viz., the vehicle body, steer and drive wheel units and castors. In Fig. 3.1, O is the origin of the inertial coordinate system, n_i used to describe the dynamics of the WMR. The vehicle shown in this figure does not refer to any vehicle in particular. The drive, steer and castor units are shown here only to illustrate the assignment of the coordinate frames and the degrees of freedom (dof) available for these wheel units. The inertial coordinate system is also referred to as the floor coordinate system. G is the principal reference point on the WMR. G is also the origin of the local coordinate system ${}^1n_i$ fixed on the WMR. The coordinate system ${}^1n_i$ is oriented such that the ${}^1n_1$ axis lies along the longitudinal axis of the WMR in the usual forward direction of motion. The ${}^1n_3$ axis is normal to the plane of operation of the WMR and points in the upward direction. The orientation of the coordinate system ${}^1n_i$ in the inertial coordinate system is measured by the angle of yaw, ψ. The yaw angle, ψ, is the angle between the n_1 and the ${}^1n_1$ axes measured as a rotation about the n_3 axis. For steered wheel units and for castors with swivel, W_s is the point of intersection of the steering axis or the axis of swivel and the $({}^1n_1, {}^1n_2)$ plane. Inclined steering is not addressed and the steering axis is parallel to the ${}^1n_3$ axis. W_s is the origin of the coordinate system ${}^2n_i$ fixed to the wheel assembly. The coordinate system ${}^2n_i$ is fixed such that a positive rotation of the wheel or castor about the ${}^2n_2$ axis produces forward motion of the WMR. The ${}^2n_3$ axis lies along the steering axis. The orientation of the ${}^2n_i$ coordinate system in the ${}^1n_i$ coordinate system is measured by the steer angle, ϕ. The steer angle, ϕ, is the angle between the ${}^1n_1$ and the ${}^2n_1$ axes measured as a rotation about the ${}^1n_3$ axis. When

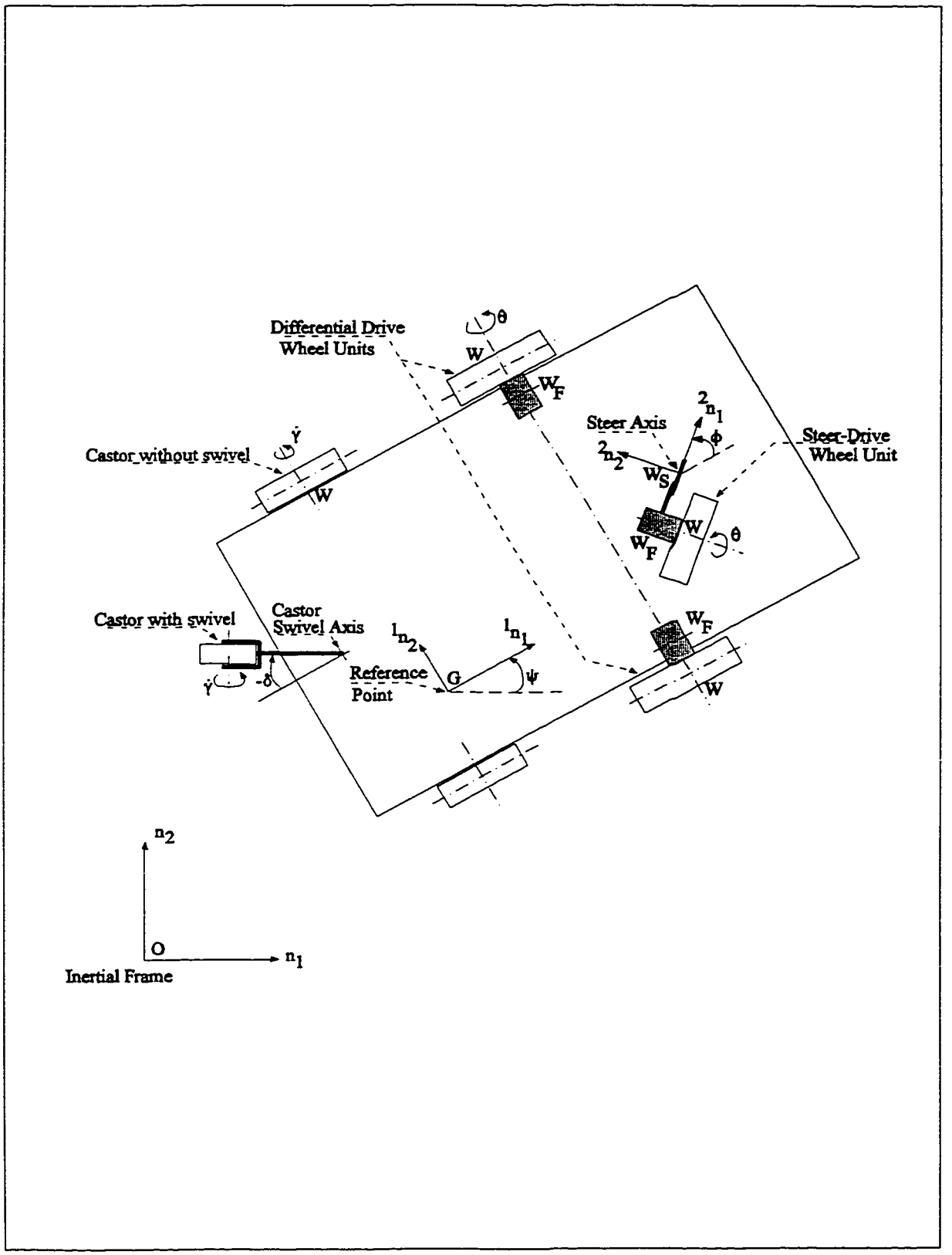

Figure 3.1 Coordinate frame assignment and principal points on a WMR.

$\phi = 0$, the vertical plane of the wheel is parallel to the ${}^{1}n_{1}$ axis. W is the centre of mass of the rotational elements of a wheel unit which typically include the wheel, the drive train components and the rotor of the drive motor. The angle of rotation of the wheel is expressed in terms of θ, measured from an arbitrary reference point. It is to be noted that θ is a cyclic coordinate and that only the wheel rotational speed or the first derivative of θ appears in the dynamical equations of the WMR; hence, no coordinate system is employed to define the rotational angle. W_f is the centre of mass of the wheel frame which includes all the components in a wheel unit excluding rotational elements. Neglecting tire deformations and area of contact of the wheel on the ground, the point, W_p, is modelled to be directly under the centre of mass, W, of the wheel.

3.3.3 Procedure Developed to Deduce the Dynamic Model

A five step procedure has been developed in this thesis for the derivation of the dynamic model of a WMR using the Kane's method and is presented below. Using this procedure, the dynamic model for a generic WMR has been developed and is presented here. Using this generic dynamic model, one could develop the equations of motion for a WMR with a specific wheel configuration.

Step 1: Derive the Non-holonomic Equations

The first step in Kane's formulation is to express the motion constraints present in the WMR system as non-holonomic equations. These motion constraints arise due to the no-slip condition assumed to exist at all the wheels. The non-holonomic equations are also used to

define the linearly independent, scalar generalised speeds, u_i , corresponding to the degrees of freedom of the system.

The number of independent generalised speeds is fixed by the number of degrees of freedom of the mobile robot. However, any suitable linear combination of the derivatives of the generalised coordinates may be used as a generalised speed. The only requirement is that the relationship be non-singular. The final form and complexity of the dynamic equations depend on the definition of the generalised speeds. With a suitable choice of the generalised speeds, the physical nature of the various terms in the dynamic equations, for example the centrifugal and the coriolis forces, may be easily identified. For planar motion of the WMR, the forward speed, u_1 the lateral speed, u_2 and the yaw rate, u_6 provide a suitable choice of generalised speeds. The speeds u_1 and u_2 are linear combinations of the Cartesian speeds, $\dot{x}$ and $\dot{y}$, in the inertial floor frame while u_6 is the rate of rotation about the z-axis. The steer rate, $\dot{\phi}$ of a wheel unit and the rate of rotation of a wheel, $\dot{\theta}$ are related to these three generalised speeds through the non-holonomic equations expressed in matrix form as

$$\begin{Bmatrix} \dot{\phi} \\ \dot{\theta} \end{Bmatrix} = \begin{bmatrix} A_{11} & A_{12} & A_{13} \\ A_{21} & A_{22} & A_{23} \end{bmatrix} \begin{Bmatrix} u_1 \\ u_2 \\ u_6 \end{Bmatrix} \qquad \textbf{(3.1)}$$

The elements of the coefficient matrix are functions of the generalised coordinates and, for a WMR, are not explicit functions of time. The nature of the coefficient matrix depends on the type of wheel units employed and their configuration in the WMR. For instance, for a differential drive, u_1 and u_6 are the independent generalised speeds and the dependent speeds, u_2 and $\dot{\theta}$ are related to them through a 2×2 coefficient matrix. The values of the elements

depend on the geometric parameters of the wheel units and the wheel configuration used.

Step 2: Obtain partial velocities and partial angular velocities

Due to the non-holonomic nature of the WMR system, the effect of a force or a torque acting on any rigid body in the system is propagated to all the other interconnected rigid bodies in the system, with an associated magnitude and direction. In the Kane's method [25] this effect is expressed by vector quantities called partial velocities and partial angular velocities.

To obtain the partial velocity of the point of action, p, of a force, the velocity, ${}^{O}v_{p}$, in the inertial floor frame is obtained in terms of the generalised speeds. Intermediate coordinate frames with suitable location and orientation are used in the derivation. For example, the choice used by Huang [7] is to place these frames such that axis of a steer or a rotational degree of freedom coincides with a principal axis of the frame. Once the velocity, ${}^{o}v_{p}$, of the point, p, is obtained in terms of only the independent generalised speeds, the coefficient of each generalised speed, u_i, in the expression is identified as the partial velocity, $\bar{v}_i^p$. For the WMR, the partial angular velocity, $\bar{\omega}_i^B$, of a rigid body, B, corresponding to each generalised speed, u_i, is obtained likewise from the angular velocity of the rigid body, ${}^{O}\omega_{B}$, in the inertial floor frame. In Kane's method, these non-holonomic partial velocities are obtained the partial differentials

$$\begin{aligned} \bar{v}_i^p &= \frac{\delta}{\delta u_i}({}^{O}v_p) \\ \bar{\omega}_i^B &= \frac{\delta}{\delta u_i}({}^{O}\omega_B) \end{aligned} \qquad \textbf{(3.2)}$$

In the case of a WMR, the linear velocity of the centre of mass of a wheel unit and the angular velocity are usually more conveniently derived in terms of the generalised speeds and also the steer rate and the wheel rotation rate. In this case the coefficients of the generalised speeds are not the partial velocities. Using the terminology coined by Kane [25], these coefficients are the *holonomic* partial velocities, v_t and ω_t. In this thesis, the term partial velocity is used to indicate non-holonomic partial velocity ; however, only in particular instances requiring clarity, the adjective non-holonomic is explicitly used.

The motion constraints present in the WMR system as given by the non-holonomic equations, Eqn.(3.1) are used to obtain the *non-holonomic* partial velocities. For example, the non-holonomic partial velocity, $\tilde{v}_1^W$, and the non-holonomic partial angular velocity, $\tilde{\omega}_t^W$, of the centre of mass, W, of a wheel, corresponding to the generalised speed, u_1, are

$$\begin{aligned} \tilde{v}_1^W &= v_1^W + A_{11} v_\phi^W + A_{21} v_\theta^W \\ \tilde{\omega}_1^W &= \omega_1^W + A_{11} \omega_\phi^W + A_{21} \omega_\theta^W \end{aligned} \qquad \textbf{(3.3)}$$

In Eqn.(3.3), the holonomic partial velocities v_1, v_ϕ, v_θ are the coefficients of the corresponding speeds, $u_1, \dot{\phi}, \dot{\theta}$ in the expression for the velocity, ${}^O v_W$, of W in the inertial floor frame. The coefficients, A_{j1} are provided by the non-holonomic equation, Eqn.(3.1). Similar expressions apply to the generalised speeds, u_2 and u_6 using the appropriate matrix elements from Eqn.(3.1). The same procedure is applied to obtain the partial angular velocities as well.

For a WMR, the points for which partial velocities are required are (i) the mass centres of all the bodies with non-negligible inertial properties and (ii) the points of action of frictional forces, usually the tire friction in the case of a WMR. The partial angular

velocities are required for all rigid bodies with non-negligible inertia such as the body of the WMR and the steered and driven wheels. It must be noted that, in a WMR, the steer and the drive actuators are located on the vehicle, hence the action and the reaction of these torques on adjacent rigid bodies of the system must be taken into account.

Step 3: Compute Generalised Active Forces

In the case of the WMR, the active forces are the gravitational forces acting at the centres of mass of bodies with non-negligible mass and the tire frictional forces acting at the points of contact of the wheels on the ground. The active torques are the steering torques and the drive torques. If the rigid body, B, in the WMR system is acted upon by a set of active forces and torques, the set is reduced to a single equivalent force, F, acting at the point, p and a single equivalent torque, T. For each body, B, using the equivalent force and torque and the partial velocities obtained in step 2, the scalar Generalised Active Force, $\tilde{F}_i^B$, for each generalised speed, u_i, is obtained as

$$\tilde{F}_i^B = \bar{\omega}_i^B \cdot T + \bar{v}_i^p \cdot F \qquad (3.4)$$

The generalised active force for each generalised speed is the sum of the inner products of all active forces acting on the WMR and the partial velocities of the points of action and the torques and the corresponding partial angular velocities. In the derivation of the dynamic equations, the generalised active force is obtained for each generalised speed.

Step 4: Compute the Generalised Inertia Forces

The inertia force and torque contributions to the dynamics of the WMR arise only from bodies with non-negligible inertial properties. For each such body, B, the acceleration, ${}^{O}a_{p}$ of the centre of mass, p, and the angular acceleration, ${}^{O}\alpha_{B}$, of the body in the inertial floor frame are first obtained. Using these accelerations and the known inertial properties of the body, the inertia force, $\mathbf{R}^{*}$, and the inertia torque, $\mathbf{T}^{*}$ are obtained as

$$\begin{aligned} R^{*} &= -m\,{}^{O}a_{p} \\ T^{*} &= -{}^{O}\alpha_{B}\cdot I - {}^{O}\omega_{B}\times I\cdot {}^{O}\omega_{B} \end{aligned} \tag{3.5}$$

where m and **I** are the mass and the central inertia dyadic of the body. For the body B, the scalar generalised inertia force, $\tilde{F}_{i}^{*B}$, for each generalised speed is then obtained as

$$\tilde{F}_{i}^{*B} = \bar{\omega}_{i}^{B}.T^{*} + \bar{v}_{i}^{p}.F^{*} \tag{3.6}$$

Step 5: Assembly of Dynamic Equations

Kane's dynamic equations for each of the generalised speeds, u_i representing the degrees of freedom of the non-holonomic WMR system are

$$\sum_{j=1}^{k}\left(\tilde{F}_{i}^{j} + \tilde{F}_{i}^{*j}\right) = 0 \qquad i = 1..n \tag{3.7}$$

where k represents the number of rigid bodies in the WMR and n is the number of degrees of freedom. Using the generalised active forces from Step 3 for the wheels and the body of the WMR and the generalised inertia forces obtained in Step 4, the dynamic equations are

assembled. The terms containing the rotational and the steer speeds and accelerations are replaced by those containing only the generalised speeds using the non-holonomic equations. This stage of the derivation is illustrated thoroughly in the case studies.

3.3.4 Constraint forces and friction forces

The vertical and lateral loads carried by the wheels of the WMR arise from the forces of constraint exerted by the ground on the wheel. These are the forces required to constrain the WMR to planar motion. For the non-holonomic conditions to apply, the Coulomb frictional forces at the contact patches, which depend on the coefficient of friction and on the vertical wheel load, must be high enough to provide the no-slip condition at all the wheels. These constraint forces also affect the dissipative tire friction forces, classified as rolling friction and turning friction, which in turn play a part in the overall dynamic behaviour of the WMR.

The constraint forces are non-working forces and hence will not normally appear in the dynamic equations. However, to compute the frictional forces at the wheels, which must be included in the dynamic model, the Kane's method [25] offers a scheme to obtain the constraint forces while deriving the dynamic equations. This is done by introducing 'virtual' generalised speeds that produce virtual displacements along the lines of action of the constraint forces. These *'virtual' generalised speeds* are used to compute the velocities and the partial velocities in Step 2. Since these speeds are virtual in nature, they appear neither in the derivation of the accelerations nor in the inertia forces and torques. However, the generalised inertia forces are obtained for the 'virtual' speeds in the same manner as for the

'real' generalised speeds in Step 4. When the dynamic equations for the 'virtual' speeds are assembled, a set of linear equations relating the constraint forces are obtained.

The constraint forces are dynamic in nature. So, in simulation studies of the dynamic behaviour of the WMR, these linear equations for the constraint forces have to be solved simultaneously while integrating the dynamic equations. The constraint forces are normally statically indeterminate; the symmetric distribution of the wheel units about the longitudinal and lateral axes of the WMR is used along with the equations obtained above to solve for the constraint forces.

Once the constraint forces are known, the tire friction forces may be computed using any of the friction models available. Using the longitudinal rolling friction model by Wong [27], the frictional force, F_f, acting on a wheel is

$$F_f = sign(\dot{\theta}) C_f (1 + D_f r\dot{\theta}) Q_3^w \qquad \textbf{(3.8)}$$

where C_f, D_f are model constants, $\dot{\theta}$ is the speed of wheel rotation, r is wheel radius and Q_3^w is the vertical load carried by the wheel. The longitudinal frictional force acting on a castor is obtained using the same model with suitable substitutions of geometric parameters.

It must be emphasised that the dynamic redistribution of the tire loads and the effect on the frictional force at each wheel must be explicitly computed in real-time control of WMRs. In previous work [7, 15, 28] on modelling WMRs, the problem of constraint force calculation is not addressed and the vertical loads are assumed to be constant and equal to the static loads. However, in the dynamic control of WMRs using Computed Torque control, the drive torque is calculated using the dynamic equations of the WMR in which the time varying

nature of the constraint forces and the frictional forces must be accounted. This is needed particularly when the WMR carries a dynamic load, such as a suspended weight, since the constraint loads on the wheels are then directly dependent on the dynamics of the load. The other case where constraint and friction forces are explicitly needed is that of traction limited motion [75] where the maximum wheel drive torque without wheel slip is limited by the Coulomb friction coefficient and the vertical wheel load.

3.4 Detailed Derivation of the Dynamic Equations

In the following sections, this five step procedure for the derivation of the dynamic equations of a WMR is applied. In the Kane's method, once the non-holonomic equations are obtained in Step 1, the WMR may be treated as separate bodies for which the generalised active and the generalised inertial forces are obtained using steps 2 to 4. The dynamic equations of the complete system are then obtained by the assembly in step 5.

As mentioned before, in the Kane's method, the non-holonomic nature of the system is retained in all the steps of the derivation through the partial velocities. It was also noted that this essential non-holonomic nature of the system is masked in both the Newton-Euler and the Lagrangian methods commonly used for the derivation of the dynamic equations of the WMR. In the Lagrangian approach, the non-holonomic nature of the system is introduced in the final step using the Lagrangian multipliers to represent the motion constraints between the generalised speeds. In the Newton-Euler approach, a force balance is applied to the components of the WMR to obtain the dynamic equations. Dependent speeds are eliminated using the constraint equations to obtain the dynamic equations for the independent speeds.

3.4.1 Steer Drive Wheel Unit

In a WMR, the types of wheels used and the particular wheel configuration adopted determines the nature of the motion constraints and hence, the permitted degrees of freedom. In the Kane's approach which focusses on the degrees of freedom, the derivation begins with an analysis of the motion constraints. The common wheel types and the dependency of the constraints are described first. In the derivation of the dynamic equations that follows, the different types of wheels are individually analyzed. Following the approach used by Chen [28], the steer-drive wheel unit is used as the standard model for all the steps of the derivation. The equations for other wheel types are then obtained by simplifications and substitutions in these equations. The effect of the payload on the dynamics of the WMR is then analyzed using the same five step approach.

3.4.1.1 Kinematics and motion constraints

For the kinematic analysis, the WMR is modelled as a rigid body mounted on three or more simple wheels. Each wheel has one rotational degree of freedom about the axis of symmetry. In addition, some or all the wheels may also have a second rotational degree of freedom about an axis, termed the steer axis, modelled in this derivation as being parallel to the vertical z-axis of the WMR. Due to the emphasis on the dynamics of the WMR, an inclined steering axis and non-conventional wheels are not specifically addressed. The results presented here may be extended to these cases using appropriate coordinate transformations. Using the number of rotational degrees of freedom, the simple wheels are classified for the present work as shown in Table 3.1 along with the degrees of freedom and symbols used.

Table 3.1 Classification of simple wheel types

Wheel Type	Rotational DOF	Steer DOF
Steer-Drive	$\dot{\theta}$	$\dot{\phi}$
Castor with swivel	$\dot{\gamma}$	$\dot{\delta}$
Steer only	Free wheel, ($\dot{\theta}$)	$\dot{\phi}$
Drive only	$\dot{\theta}$	Fixed
Castor without swivel	$\dot{\gamma}$	Fixed

The following derivation applies to a WMR, modelled as a system of interconnected rigid bodies, executing planar motion in an inertial (Cartesian) frame of reference. Planar motion implies that vertical motion of the body and roll and pitch motions are constrained, reducing the degrees of freedom to a maximum of 3. With the permitted maximum of 3 degrees of freedom in planar motion, the system can have independent linear velocities in the Cartesian x- and y-directions and a yaw rate or rotation about the Cartesian z-direction. Each wheel unit, depending on the type as defined in Table 3.1, may have one or two rotational degrees of freedom. However, the non-holonomic nature of the WMR system due to the no-slip condition at all the wheels, imposes motion constraints such that Cartesian speeds of the system and the steer and the rotational speeds of each wheel unit are related through non-holonomic equations.

3.4.1.2 Non-holonomic equations for a Steer-Drive Unit

The following derivation is for a steer-drive wheel unit since the non-holonomic equations for all the other wheel types in Table 3.1 may be obtained with suitable

substitutions. The geometric configuration of the steer-drive wheel unit is shown in Fig. 3.2. In the inertial coordinate system, n_i, the path of an (arbitrary) reference point, G, is assumed to be available from a path or a trajectory generator. The moving coordinate frame, ${}^1n_i$, is located with its origin at G ; for the following kinematic analysis, the orientation of the frame is arbitrary. When this analysis is applied to a WMR with a particular wheel configuration, the point G is identified with the chosen principal point of reference of the WMR. Thus the geometric parameters and the results derived in this section may be easily transferred to each particular wheel configuration. Also, the derivation does not assume a particular parametric scheme of the path and the Cartesian or the generalised coordinates may be substituted with their parametric forms at any stage if desired. The derivation may be extended to a prescribed trajectory as well.

In the inertial frame of reference, the prescribed linear velocity of G is given by

$$\begin{aligned} {}^{O}v_G &= \dot{x}n_1 + \dot{y}n_2 \\ &= (\dot{x}c\psi + \dot{y}s\psi)\,{}^1n_1 + (-\dot{x}s\psi + \dot{y}c\psi)\,{}^1n_2 \end{aligned} \tag{3.9}$$

where s( ) and c( ) are the sine and cosine functions; the prescribed angular velocity is

$${}^{O}\omega_G = \dot{\psi}n_3 = \dot{\psi}\,{}^1n_3 \tag{3.10}$$

The non-holonomic constraint equations are derived by applying the no slip condition to the point of contact of the wheel on the ground, i.e., by setting the instantaneous velocity of the point of contact in the inertial frame to zero.

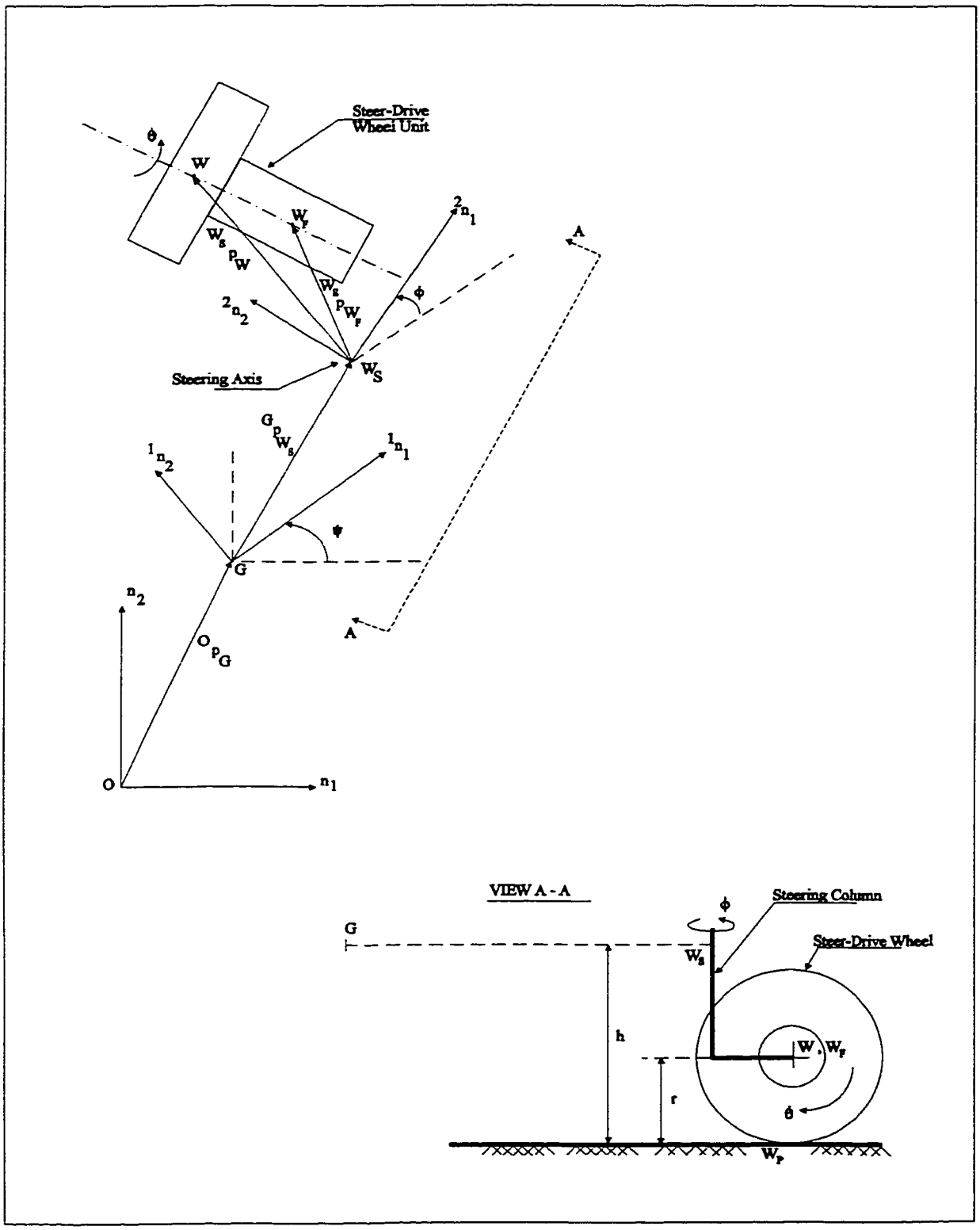

Figure 3.2 Position Vectors and Orientation Angles of Steer-Drive Wheel Unit in the Inertial Coordinate Frame.

The steer-drive wheel unit is modelled as three interconnected rigid bodies, viz., the hip, the steering column and the wheel, with one rotational degree of freedom at each joint. For the steer-drive wheel, the instantaneous velocity of the point of contact, W_p, of the wheel on the ground is derived by finding the velocities of the points of coupling namely, W_s and W. The coordinates of these points are shown in Fig. 3.2 and the position vectors are

$$\begin{aligned} {}^{G}p_{W_s} &= x_s\,{}^{1}n_1 + y_s\,{}^{1}n_2 \\ {}^{W_s}p_{W} &= x_w\,{}^{2}n_1 + y_w\,{}^{2}n_2 + z_w\,{}^{2}n_3 \\ {}^{W}p_{W_p} &= -r\,{}^{2}n_3 \end{aligned} \tag{3.11}$$

The coordinates of the velocity vectors are expressed in the ${}^{1}n_t$ frame. The velocity of the steer point, W_s, is given by

$$\begin{aligned} {}^{O}v_{W_s} &= {}^{O}v_{G} + {}^{O}\omega_{G} \times {}^{G}p_{W_s} \\ &= (\dot{x}c\psi + \dot{y}s\psi - \dot{\psi}y_s)\,{}^{1}n_1 + (-\dot{x}s\psi + \dot{y}c\psi + \dot{\psi}x_s)\,{}^{1}n_2 \end{aligned} \tag{3.12}$$

and the velocity of the centre of mass of the wheel, W, is given by

$$\begin{aligned} {}^{O}v_{W} &= {}^{O}v_{W_s} + {}^{O}\omega_{W_s} \times {}^{W_s}p_{W} \\ &= [\dot{x}c\psi + \dot{y}s\psi - \dot{\psi}y_s - (\dot{\psi} + \dot{\phi})(x_w s\phi + y_w c\phi)]\,{}^{1}n_1 \\ &\quad + [-\dot{x}s\psi + \dot{y}c\psi + \dot{\psi}x_s + (\dot{\psi} + \dot{\phi})(x_w c\phi - y_w s\phi)]\,{}^{1}n_2 \end{aligned} \tag{3.13}$$

Finally, the velocity of the point of contact of the wheel on the ground, W_p, is

$$\begin{aligned} {}^{O}v_{W_p} &= {}^{O}v_{W} + {}^{O}\omega_{W} \times {}^{W}p_{W_p} \\ &= [\dot{x}c\psi + \dot{y}s\psi - \dot{\psi}y_s - (\dot{\psi} + \dot{\phi})(x_w s\phi + y_w c\phi) - r\dot{\theta}c\phi]\,{}^{1}n_1 \\ &\quad + [-\dot{x}s\psi + \dot{y}c\psi + \dot{\psi}x_s + (\dot{\psi} + \dot{\phi})(x_w c\phi - y_w s\phi) - r\dot{\theta}s\phi]\,{}^{1}n_2 \end{aligned} \tag{3.14}$$

By the no slip condition, ${}^{O}v_{W_p} = 0$; equating each component of the velocity vector to 0, the

non-holonomic equations relating the five generalised speeds are

$$\begin{aligned} \dot{x}c\psi + \dot{y}s\psi - \psi y_g - (\psi + \dot{\phi})(x_w s\phi + y_w c\phi) - r\dot{\theta}c\phi &= 0 \\ -\dot{x}s\psi + \dot{y}c\psi + \psi x_g + (\psi + \dot{\phi})(x_w c\phi - y_w s\phi) - r\dot{\theta}s\phi &= 0 \end{aligned} \tag{3.15}$$

Five generalised coordinates, {x y ψ ϕ θ } are needed to describe the configuration of the steer-drive wheel unit in the inertial frame. However, the non-holonomic equations, Eqn.(3.15), indicate that the Cartesian speeds $\{ \dot{x}\ \dot{y}\ \dot{\psi} \}$ are dependent on the steer-drive speeds, $\{ \dot{\phi}\ \dot{\theta} \}$.

For the present derivation, the vehicle forward speed, u_1, the lateral speed, u_2, and the yaw rate, u_6, are chosen as the 3 independent generalised speeds for the system. The advantage of this choice of generalised speeds is the ease of prescribing and visualizing the path of the WMR. In terms of the Cartesian speeds, the generalised speeds are defined as

$$\begin{Bmatrix} u_1 \\ u_2 \\ u_6 \end{Bmatrix} = \begin{bmatrix} c\psi & s\psi & 0 \\ -s\psi & c\psi & 0 \\ 0 & 0 & 1 \end{bmatrix} \begin{Bmatrix} \dot{x} \\ \dot{y} \\ \dot{\psi} \end{Bmatrix} \tag{3.16}$$

As required by the definition of the generalised speeds, the transformation matrix is non-singular for all values of ψ. The above transformation may be inverted to yield the Cartesian speeds in terms of the generalised speeds as

$$\begin{Bmatrix} \dot{x} \\ \dot{y} \\ \dot{\psi} \end{Bmatrix} = \begin{bmatrix} c\psi & -s\psi & 0 \\ s\psi & c\psi & 0 \\ 0 & 0 & 1 \end{bmatrix} \begin{Bmatrix} u_1 \\ u_2 \\ u_6 \end{Bmatrix} \tag{3.17}$$

Using (3.17) and substituting for the cartesian speeds in the non-holonomic equations,

Eqn.(3.15), the elements of the coefficient matrix, A, in Eqn.(3.1) are obtained as

$$
\begin{aligned}
A_{11} &= \frac{1}{\Delta_A}(rs\phi) \\
A_{12} &= \frac{1}{\Delta_A}(-rc\phi) \\
A_{13} &= \frac{-r}{\Delta_A}(y_s s\phi + x_s c\phi + x_w) \\
A_{21} &= \frac{1}{\Delta_A}(x_w c\phi - y_w s\phi) \\
A_{22} &= \frac{1}{\Delta_A}(x_w s\phi + y_w c\phi) \\
A_{23} &= \frac{1}{\Delta_A}[-y_s(x_w c\phi - y_w s\phi) + x_s(x_w s\phi + y_w c\phi)]
\end{aligned}
\qquad \textbf{(3.18)}
$$

where

$$\Delta_A = rx_w$$

The criterion for the existence of a kinematic solution for the general case of inclined steering and steering offset distance has been investigated by Cheng and Rajagopalan [76]. In the present work, a non-zero offset value is assumed and $\Delta_A \neq 0$ in Eqn. (3.18).

3.4.1.3 Partial Velocities

The steer-drive wheel unit consists of stationary components with mass centre at W_f and the rotational components, viz., the wheel and drive train, with mass centre at W. Both masses are included in the analysis and the partial velocities of both these points are derived. In addition, the tire frictional force acts at the point of contact, W_p and the partial velocities of this point are also obtained. If one or both of these masses are assumed negligible in any particular application, some or all these partial velocities may be not be needed.

In order to compute constraint forces on the wheel, 3 'virtual' generalised speeds representing the upward translational speed (u_3) and the roll and the pitch rotational speeds

(u_4 and u_5) are included along with the 'real' generalised speeds, viz., the forward and the lateral translational speeds (u_1 and u_2) and the yaw rotational speed (u_6). In terms of the six generalised speeds, the prescribed linear and angular velocities of the reference point, G, are represented as

$$\begin{aligned} \{{}^{O}v_{G}\} &= (u_1\,{}^{1}n_1 + u_2\,{}^{1}n_2 + u_3\,{}^{1}n_3)^T \\ \{{}^{O}\omega_{G}\} &= (u_4\,{}^{1}n_1 + u_5\,{}^{1}n_2 + u_6\,{}^{1}n_3)^T \end{aligned} \qquad \textbf{(3.19)}$$

The derivation of the partial velocities is similar to the kinematic analysis carried out to develop the non-holonomic equations except for the introduction of the virtual generalised speeds. The velocity of the reference point, G, is propagated to obtain the velocity of the steer point, W_s as

$${}^{O}v_{W_s} = {}^{O}v_{G} + {}^{O}\omega_{G} \times {}^{G}p_{W_s} \qquad \textbf{(3.20)}$$

The velocity of the steer point is then used to obtain the velocities of the centres of mass, W_f and W, and of the point of contact, W_p, as

$$\begin{aligned} {}^{O}v_{W_f} &= {}^{O}v_{W_s} + {}^{O}\omega_{W_s} \times {}^{W_s}p_{W_f} \\ {}^{O}v_{W} &= {}^{O}v_{W_s} + {}^{O}\omega_{W_s} \times {}^{W_s}p_{W} \\ {}^{O}v_{W_p} &= {}^{O}v_{W} + {}^{O}\omega_{W} \times {}^{W}p_{W_p} \end{aligned} \qquad \textbf{(3.21)}$$

All the position vectors may be obtained from the geometric quantities shown in Fig. 3.2. The transformation matrix, $[{}^{1}T_2] = Rot({}^{1}n_3, -\phi)$, is used to convert the position vectors in the ${}^{2}n_i$ frame to the ${}^{1}n_i$ frame. The angular velocities of these two bodies represented by W_f and W are

$$
\begin{aligned}
{}^{O}\omega_{W_s} &= u_4\,{}^{1}n_1 + u_5\,{}^{1}n_2 + (u_6+\dot{\phi})\,{}^{1}n_3 \\
{}^{O}\omega_{W_f} &= {}^{O}\omega_{W_s} \\
{}^{O}\omega_{W} &= (u_4 - \dot{\theta}s\phi)\,{}^{1}n_1 + (u_5 + \dot{\theta}c\phi)\,{}^{1}n_2 + (u_6+\dot{\phi})\,{}^{1}n_3
\end{aligned}
\qquad \textbf{(3.22)}
$$

From the expressions for the linear velocities, Eqn. (3.21) and the angular velocities, Eqn.(3.22), the *holonomic* partial velocities of the six generalised speeds, u_i and the steer speed, $\dot{\phi}$ and the rotation speed, $\dot{\theta}$ have been collected and are given in Tables 3.2 and 3.3. The *non-holonomic* partial velocities are obtained using Eqn.(3.3) and the matrix elements in Eqn.(3.18). However, for the 'virtual' speeds u_3 , u_4 and u_5 , the expressions in Tables 3.2 and 3.3 are also the non-holonomic partial velocities.

3.4.1.4 Generalised Active Forces

The active forces and torques acting on the steer drive wheel unit are shown in Fig. 3.3. The drive torque, $\tau_d\,{}^{2}n_2$ acts on the rotational components of the wheel unit, W. The forces include the gravitational force, $-m_w g n_3$, acting at W; the (non-working) constraint forces, $Q_2\,{}^{2}n_2$ and $Q_3\,{}^{2}n_3$ acting at the point of contact, W_p ; and the longitudinal tire frictional force, $F_f\,{}^{2}n_1$, acting at W_p. The active forces acting on the stationary components, W_f, are the gravitational force, $-m_f g n_3$, acting at W_f; the steer torque, $\tau_s\,{}^{1}n_3$; and the reaction to the drive torque, $-\tau_d\,{}^{2}n_2$.

Using the partial velocities of the points W, W_f and W_p obtained in step 2, the generalised active forces for each generalised speed is obtained using Eqn.(3.4). It is to be noted that the partial velocity that must be used for the frictional force is that of the wheel, W, and not that of the point of contact, W_p since the frictional force is a force opposing the

Table.3.2 Holonomic Partial Velocities of the Steer-Drive Wheel Unit for the Generalised Speeds

	$v_t^{W_f}$	v_t^{W}	$v_t^{W_p}$
u_1	${}^1n_1$	${}^1n_1$	${}^1n_1$
u_2	${}^1n_2$	${}^1n_2$	${}^1n_2$
u_3	${}^1n_3$	${}^1n_3$	${}^1n_3$
u_4	$-z_f\,{}^1n_2-(x_f s\phi-y_f c\phi)\,{}^1n_3$	$-z_w\,{}^1n_2-(x_w s\phi-y_w c\phi)\,{}^1n_3$	$-(z_w-r)\,{}^1n_2-(y_s+x_w s\phi-y_w c\phi)\,{}^1n_3$
u_5	$z_f\,{}^1n_1-(x_s+x_f c\phi+y_f s\phi)\,{}^1n_3$	$z_w\,{}^1n_1-(x_s+x_w c\phi+y_w s\phi)\,{}^1n_3$	$(z_w-r)\,{}^1n_1-(x_s+x_w c\phi+y_w s\phi)\,{}^1n_3$
u_6	$-(y_s-x_f s\phi+y_f c\phi)\,{}^1n_1+(x_s+x_f c\phi+y_f s\phi)\,{}^1n_2$	$-(y_s-x_w s\phi+y_w c\phi)\,{}^1n_1+(x_s+x_w c\phi+y_w s\phi)\,{}^1n_2$	$-(y_s-x_w s\phi+y_w c\phi)\,{}^1n_1+(x_s+x_w c\phi+y_w s\phi)\,{}^1n_2$
$\dot{\phi}$	$(x_f s\phi-y_f c\phi)\,{}^1n_1+(x_f c\phi+y_f s\phi)\,{}^1n_2$	$(x_w s\phi-y_w c\phi)\,{}^1n_1+(x_w c\phi+y_w s\phi)\,{}^1n_2$	$(x_w s\phi-y_w c\phi)\,{}^1n_1+(x_w c\phi+y_w s\phi)\,{}^1n_2$
$\dot{\theta}$	0	0	$-rc\phi\,{}^1n_1-rs\phi\,{}^1n_2$

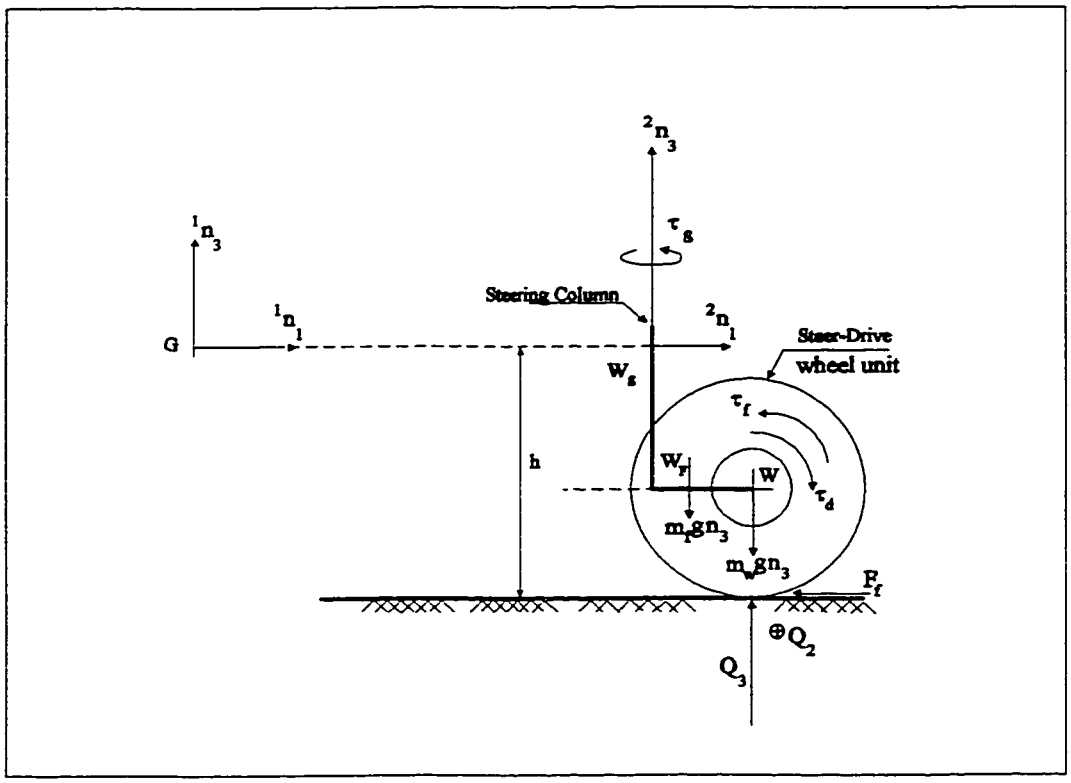

Figure 3.3 Active forces acting on the components of a steer-drive wheel unit.

Table 3.3 Holonomic Partial Angular Velocities for the Steer-Drive Wheel

	$\omega_t^{W_f}$	ω_t^{W}
u_1	0	0
u_2	0	0
u_3	0	0
u_4	$^1n_1$	$^1n_1$
u_5	$^1n_2$	$^1n_2$
u_6	$^1n_3$	$^1n_3$
$\dot{\phi}$	$^1n_3$	$^1n_3$
$\dot{\theta}$	0	$-s\phi\,^1n_1 + c\phi\,^1n_2$

linear motion of the vehicle. Another option that may be followed is to convert the frictional force into a frictional torque, $\tau_f{}^2\boldsymbol{n}_2$, using

$$\tau_f = {}^W\boldsymbol{p}_{W_p} \times \boldsymbol{F}_f = -rF_f{}^2\boldsymbol{n}_2 \tag{3.23}$$

The frictional force, F_f, obtained using the model, Eqn.(3.8) is a signed quantity depending on the direction of wheel rotation. Hence, the frictional torque in Eqn.(3.23) always opposes the drive torque. The generalised active force for each generalised speed corresponding to this frictional torque is obtained with the partial angular velocity of W, $\boldsymbol{\omega}_i^W$ and $\tau_f{}^2\boldsymbol{n}_2$.

3.4.1.5 Generalised Inertia Forces

The acceleration of the centre of mass of the rotational components of the wheel unit, ${}^O\boldsymbol{a}_W$, is obtained as the total derivative of the velocity, ${}^O\boldsymbol{v}_W$, given by Eqn.(3.21). When deriving the accelerations, it must be noted that only the 'real' generalised speeds, u_1, u_2 and u_6 are used and the 'virtual' speeds, u_3, u_4 and u_5, introduced to obtain the constraint forces, are set to zero. The acceleration of W is

$$\begin{aligned} {}^O\boldsymbol{a}_W = &\left({}^O\boldsymbol{a}_G + {}^O\boldsymbol{\omega}_G \times {}^O\boldsymbol{v}_G + {}^O\boldsymbol{\alpha}_G \times {}^G\boldsymbol{p}_{W_s} + {}^O\boldsymbol{\omega}_G \times {}^O\boldsymbol{\omega}_G \times {}^G\boldsymbol{p}_{W_s}\right) \\ &+\left({}^O\boldsymbol{\alpha}_{W_s} \times {}^{W_s}\boldsymbol{p}_W + {}^O\boldsymbol{\omega}_{W_s} \times {}^O\boldsymbol{\omega}_{W_s} \times {}^{W_s}\boldsymbol{p}_W\right) \end{aligned} \tag{3.24}$$

where the linear and angular accelerations are given by

$$\begin{aligned} {}^O\boldsymbol{a}_G &= \dot{u}_1{}^1\boldsymbol{n}_1 + \dot{u}_2{}^1\boldsymbol{n}_2 \\ {}^O\boldsymbol{\alpha}_G &= \dot{u}_6{}^1\boldsymbol{n}_3 \\ {}^O\boldsymbol{\alpha}_{W_s} &= (\dot{u}_6 + \ddot{\phi})\,{}^1\boldsymbol{n}_3 \end{aligned} \tag{3.25}$$

The angular acceleration, ${}^{O}\alpha_{W}$, of W is obtained as the total derivative of the sum of the angular velocities of W_s and W. It must be noted that the angular velocity of W ($= \dot{\theta}\,{}^{2}n_2$) is expressed in the moving frame attached to the axis of rotation and hence the angular acceleration would involve the time derivative of the transformation matrix, $[{}^{1}T_2]$. The angular acceleration of W is

$$\begin{aligned} {}^{O}\alpha_{W} &= \frac{d}{dt}\,{}^{O}\omega_{W} \\ &= \frac{d}{dt}\left({}^{O}\omega_{W_s} + {}^{W_s}\omega_{W}\right) \\ &= {}^{O}\alpha_{W_s} + \frac{d}{dt}\left(\dot{\theta}\,{}^{2}n_2\right) \\ &= {}^{O}\alpha_{W_s} + [{}^{1}T_2]\begin{Bmatrix} 0 \\ 0 \\ \ddot{\theta} \end{Bmatrix} + [{}^{O}\Omega_{W_s}][{}^{1}T_2]\begin{Bmatrix} 0 \\ 0 \\ \dot{\theta} \end{Bmatrix} \end{aligned} \qquad \textbf{(3.26)}$$

With the known inertial properties of the wheel and the accelerations computed above , the inertia force, R^{*W} and the inertia torque, T^{*W} for the rotational components are obtained using Eqn.(3.5).

Similarly, the acceleration of the centre of mass, W_f is given by

$$\begin{aligned} {}^{O}a_{W_f} = &\left({}^{O}a_{G} + {}^{O}\omega_{G} \times {}^{O}v_{G} + {}^{O}\alpha_{G} \times {}^{G}p_{W_s} + {}^{O}\omega_{G} \times {}^{O}\omega_{G} \times {}^{G}p_{W_s}\right) \\ &+ \left({}^{O}\alpha_{W_s} \times {}^{W_s}p_{W_f} + {}^{O}\omega_{W_s} \times {}^{O}\omega_{W_s} \times {}^{W_s}p_{W_f}\right) \end{aligned} \qquad \textbf{(3.27)}$$

and the angular acceleration is

$${}^{O}\alpha_{W_f} = {}^{O}\alpha_{W_s} \qquad \textbf{(3.28)}$$

With the known mass and the central inertia dyadic of the non-rotational components of the

wheel unit, the inertia force and the inertia torque are obtained using Eqn.(3.5).

Finally, using the inertia forces and the torques of the rotational and the non-rotational components of the wheel unit and the partial velocities of the respective centres of mass and the partial angular velocities of the bodies, the generalised inertia force, $\tilde{F}_t^*$, for each generalised speed, u_t is obtained by substitution in Eqn.(3.6).

3.4.2 Steer only Wheel

The kinematics of a steer only wheel unit, shown in Fig. 3.4, are identical to those of the steer-drive wheel unit. The non-holonomic equations for the steer-drive wheel unit, Eqn.(3.15), may be applied directly to a steer only wheel unit. Since wheel rotation is unactuated, the wheel is free wheeling and $\dot{\theta}$ gives the no-slip rotational speed. However, for control purposes, only the steer rate, $\dot{\phi}$ and the steer angle, ϕ are quantities of interest.

The partial velocities are identical to those of the steer-drive wheel. Even though the wheel is not driven, the partial velocity of W may be needed if the wheel has non-negligible inertial properties.

In the case of the steer only wheel, the drive torque on the wheel and the reaction on the wheel frame are absent. All the other active forces listed for the steer-drive wheel are present. The derivation of the generalised active forces for a steer only wheel are identical to the method used for the steer-drive wheel, setting the drive torque and it's reaction torque to zero. In case the masses of the stationary or the rotational components of the wheel are negligible, the gravitational forces may be set to zero as well.

For a steer only wheel with non-negligible inertial properties, the inertia force and

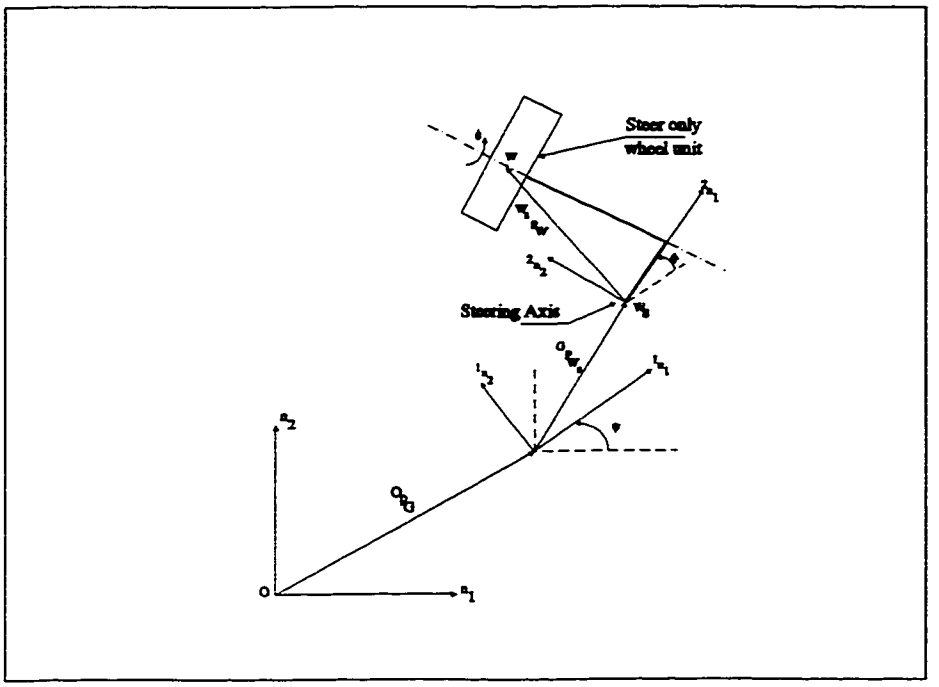

Figure 3.4 Position Vectors and Orientation Angles of a Steer only wheel unit.

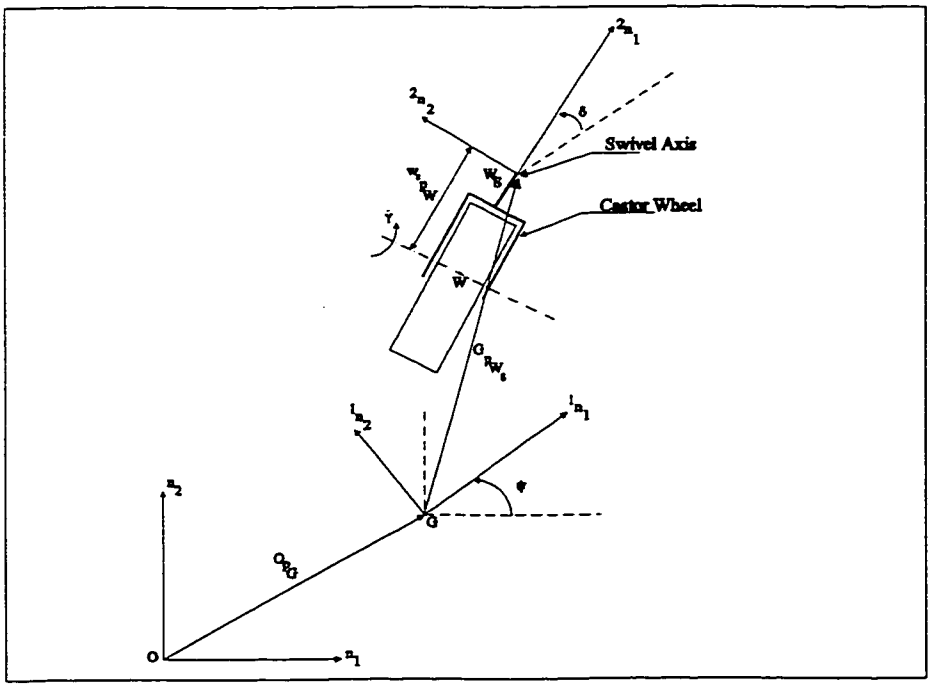

Figure 3.5 Position Vectors and Orientation Angles of a Castor with Swivel.

torque and the generalised inertia forces for the generalised speeds are identical to those of the steer-drive wheel unit. If the inertial properties of the rotational components or the stationary components are assumed negligible, the corresponding terms in Eqn.(3.5) and Eqn.(3.6) may be set to zero. A summary of these substitutions for the steer only wheel unit and the applicable equations is given in Table 3.4.

3.4.3 Castor with swivel

The kinematics of a castor with swivel, shown in Fig.3.5, are similar to those of the steer-drive wheel. The substitutions are one of nomenclature only. To obtain the non-holonomic equations, the rotational speed, $\dot{\gamma}$ and the swivel speed, $\dot{\delta}$ are substituted in Eqn.(3.15) along with the appropriate values for the geometric parameters. From the standpoint of control, both rotational degrees of freedom of the castor are unactuated and the non-holonomic equations give values of the instantaneous castor steer rate and the rotational speed in terms of the WMR path parameter values.

The partial velocities for a castor with swivel may be obtained from the expressions for the steer-drive wheel using the appropriate nomenclature. In most cases, the inertial properties of a castor are assumed negligible ; then, the only partial velocities needed are those of the point of contact of the castor on the ground to account for the rolling friction.

In this case, the only active forces considered are the constraint forces and the rolling friction forces acting at the point of contact of the castor on the ground. Since the castor is free to swivel, it cannot sustain any lateral force ; hence only the vertical constraint force need be considered. The steer and the drive torques are absent and the mass of the castor is usually

neglected. With these simplifications, the generalised active forces for the castor are obtained. The generalised inertia force for the castor is zero since the castor is assumed to have negligible inertial properties. In case this assumption is not made, the generalised inertia force is identical to those of the steer-drive wheel unit, the only substitutions being one of notation. A summary of these substitutions for the castor with swivel and the applicable equations is given in Table 3.5.

3.4.4 Drive only Wheel

For the case of a drive only wheel, Fig. 3.6, the wheel has one rotational degree of freedom only and the steer rate, $\dot{\phi} = 0$. The wheel unit loses one degree of freedom and becomes a 2 dof system. In this case, the forward speed, u_1, and the yaw rate, u_6 are used as the generalised speeds. For the drive only wheel, the following substitutions are made

$$\dot{\phi} = 0 \; ; \; \phi = 0 \; ; \; {}^{G}p_{W_s} = 0 \; ; \; {}^{G}p_{W} = {}^{W_s}p_{W} \qquad \textbf{(3.29)}$$

Using these substitutions, the non-holonomic equations for the constrained lateral speed, u_2 and the rotational speed, $\dot{\theta}$, are given by

$$u_2 = -x_w u_6 \; ; \; \dot{\theta} = \frac{1}{r}u_1 - \frac{y_w}{r}u_6 \qquad \textbf{(3.30)}$$

For this case only the partial velocities of W and W_p are required. The inertial properties of the non-rotating components of the wheel unit, e.g., the stator of the drive motor, may be included with those of the body of the WMR. The expressions in Table 3.2 and in Table 3.3 are first simplified using the parameter values indicated in Eqn.(3.29). The partial

Table 3. 4 Summary of Equations for Steer only Wheel Unit

	Applicable Parameters / Equations
Dependent Speeds	$\dot{\phi}, \dot{\theta}$
Geometric Substitutions	-
Step 1. Non-holonomic Equations	i. Eqn.(3.1), Eqn.(3.15) ii. Eqn.(3.18)
Step 2. Partial Velocities	i. Table 3.2 , Table 3.3 ii. Eqn.(3.3)
Step 3. Generalised Active Forces	i. τ_s, τ_f ; $-m_w g n_3$ ii. Eqn.(3.4)
Step 4. Generalised Inertia Forces	i. Eqn.(3.24), Eqn.(3.26) ii. Eqn.(3.5), Eqn.(3.6)

Table 3.5 Summary of Equations for Castor with swivel

	Applicable Parameters / Equations
Dependent Speeds	$\dot{\delta}, \dot{\gamma}$
Geometric Substitutions	$y_w = 0$
Step 1. Non-holonomic Equations	i. Eqn.(3.1), Eqn.(3.15) ii. Eqn.(3.18)
Step 2. Partial Velocities	i. Table 3.2 , Table 3.3 ii. Eqn.(3.3)
Step 3. Generalised Active Forces	i. τ_f ; $-m_w g n_3 \approx 0$ ii. Eqn.(3.4)
Step 4. Generalised Inertia Forces	$\vec{F}_i^{nw} \approx 0$

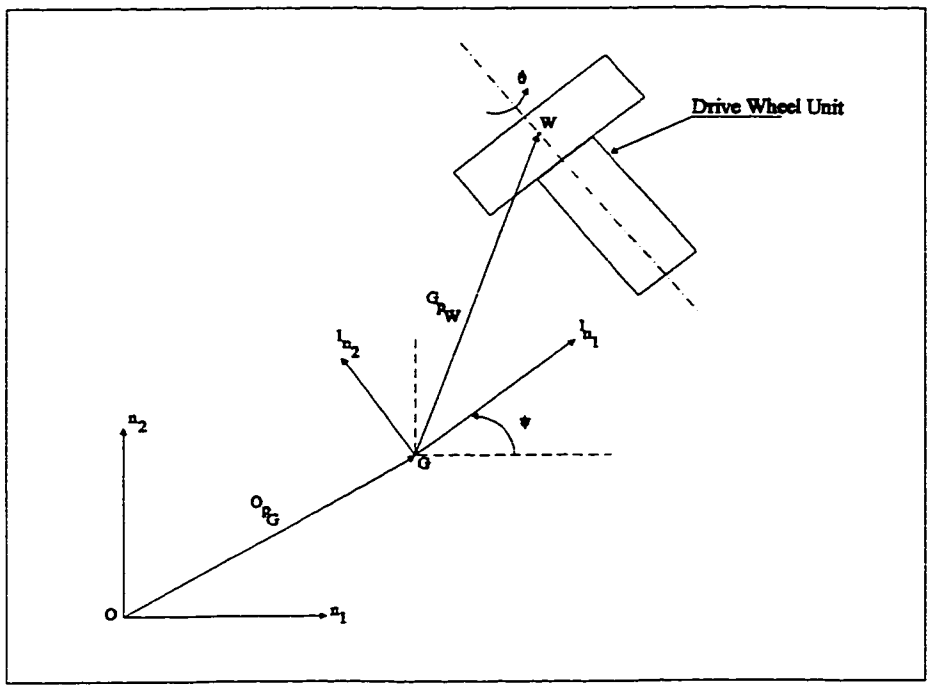

Figure 3.6 Position Vectors and Orientation Angles of Drive Only Wheel Unit

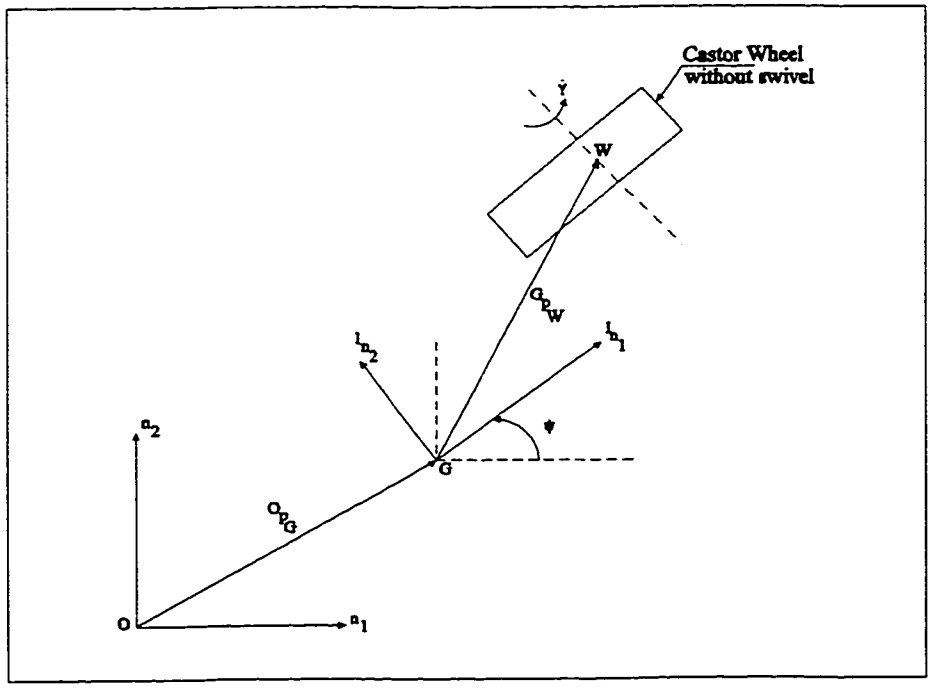

Figure 3.7 Position Vectors and Orientation Angles of a Castor without Swivel

velocities are then obtained using the non-holonomic equations, Eqn.(3.30) and the elements given in Tables 3.2 and 3.3.

For the drive only wheel, the steering acceleration is absent and the wheel coordinate frame, ${}^{2}n_{t}$ is identical to the frame, ${}^{1}n_{t}$ at the reference point, G. These simplifications may be expressed as

$$\begin{aligned} {}^{O}\alpha_{W_t} &= 0 \\ \left[{}^{1}T_{2}\right] &= [I]_{3\times 3} \end{aligned} \tag{3.31}$$

where I is the identity matrix. With these substitutions in Eqn.(3.24) for the acceleration of W, the inertia force and the inertia torque for the drive only wheel unit are obtained. The generalised inertia force, Eqn.(3.6), for each of the two generalised speeds is then obtained with the partial velocities of W.

In this case, the steer torque is absent and only the drive torque on the wheel is present. Also, the mass and the inertial properties of the non-rotational components of the wheel unit may be included with those of the payload; so, only the gravitational force acting at the mass centre, W, of the rotational components of the wheel unit need be considered. In addition, the constraint forces and the tire frictional forces acting at W_p are present. In the case of a drive only wheel, the reaction to the drive torque acts on the body of the WMR and must be accounted for in the dynamics of the payload as given in Section 3.5. Table 3.6 summarises the substitutions and the equations applicable to the drive only wheel unit.

3.4.5 Castor without swivel

The kinematics of a castor without swivel, shown in Fig. 3.7, are similar to those of the drive only wheel. The WMR has only 2-DOF. For the non-holonomic equations, the rotational speed $\dot{\gamma}$ is substituted in Eqn.(3.30) along with the appropriate positional values. The partial velocities, therefore, for this case are similar to those of the drive only wheel, differing only in nomenclature.

The simplifications regarding the torques and the masses of the components listed for the castor with swivel apply equally for this case as well. However, in this case, the castor is laterally constrained and hence will experience a lateral constraint force. The generalised active forces are derived for the frictional and the constraint forces.

As in the case of the castor with swivel, the inertial properties of the castor are normally neglected and the generalised inertia forces for the castor for both the generalised speeds are zero.

3.4.6 Effect of a Deadweight on WMR Dynamics

The presence of a payload on the WMR would affect the dynamic behaviour of the WMR as it directly influences both the active and the inertial forces of all the generalised speeds. The term payload in this context refers to all the dead weights carried by the WMR including the mass of the body of the WMR itself. Also, for each drive only wheel unit, the mass and the inertial quantities of the non-rotational components, such as the stator of the drive motor, can be added to those of the body of the WMR. Where an additional payload is placed on the WMR, the known mass and the inertial properties of the load are included with

Table 3.6 Summary of Equations for Drive only Wheel Unit

	Applicable Parameters and Equations
Dependent Speeds	$\dot{\theta}$; u_2
Geometric Substitutions	i. $x_s = 0$; $y_s = 0$ ii. $\phi = 0$; $\dot{\phi} = 0$
Step 1. Non-holonomic Equations	i. Eqn.(3.30)
Step 2. Partial Velocities	i. Table 3.2 , Table 3.3 ii. Eqn.(3.3) with $u_2 = -x_w u_6$
Step 3. Generalised Active Forces	i. τ_d, τ_f ; $-m_w g n_3$ ii. Eqn.(3.4)
Step 4. Generalised Inertia Forces	i. Eqn.(3.24,3.26) with ${}^O\alpha_{W_s} = 0$; ${}^1T_2 = I_{3\times3}$ ii. Eqn.(3.5), Eqn.(3.6)

Table 3.7 Summary of Equations for Castor without swivel

	Applicable Parameters and Equations
Dependent Speeds	$\dot{\gamma}$; u_2
Geometric Substitutions	i. $x_s = 0$; $y_s = 0$ ii. $\delta = 0$; $\dot{\delta} = 0$
Step 1. Non-holonomic Equations	i. Eqn.(3.30)
Step 2. Partial Velocities	i. Table 3.2 , Table 3.3 ii. Eqn.(3.3) with $u_2 = -x_w u_6$
Step 3. Generalised Active Forces	i. τ_f ; $-m_w g n_3 \approx 0$ ii. Eqn.(3.4)
Step 4. Generalised Inertia Forces	$\tilde{F}_i^{*w} \approx 0$

those of the body of the WMR using the parallel axis theorem.

The location of the centre of mass, D, of the payload in the vehicle reference frame, ${}^{1}n_{i}$ and the mass, m_d, and the central inertia dyadic, $\mathbf{I}_d$, are assumed known. Using the linear velocity, ${}^{O}v_{G}$, and the angular velocity, ${}^{O}\omega_{G}$, of the reference point, G, the linear and angular velocities of the centre of mass, D, are

$$\begin{aligned} {}^{O}v_{D} &= {}^{O}v_{G} + {}^{O}\omega_{G} \times {}^{G}p_{D} \\ {}^{O}\omega_{D} &= {}^{O}\omega_{G} \end{aligned} \qquad \textbf{(3.32)}$$

where the position vector of D from the reference point, G, is ${}^{G}p_{D} = (x_d {}^{1}n_1 + y_d {}^{1}n_2 + z_d {}^{1}n_3)$. The partial velocities, v_i^D, and the partial angular velocities, ω_i^D, are listed in Table 3.8.

If the wheel type and wheel configuration used in the WMR permit 3-DOF, the values listed in Table 3.8 are also the non-holonomic partial velocities and the partial angular velocities. For a WMR with only 2-DOF, the constrained lateral speed, u_2 is replaced using Eqn.(3.30) to obtain partial velocities of the independent generalised speeds, u_1 and u_6.

Table 3.8 Holonomic partial velocities of a deadweight

	v_i^D	ω_i^D
u_1	${}^{1}n_1$	0
u_2	${}^{1}n_2$	0
u_3	${}^{1}n_3$	0
u_4	$-z_d {}^{1}n_2 + y_d {}^{1}n_3$	${}^{1}n_1$
u_5	$z_d {}^{1}n_1 - x_d {}^{1}n_3$	${}^{1}n_2$
u_6	$-y_d {}^{1}n_1 + x_d {}^{1}n_2$	${}^{1}n_3$

For the deadweight payload, the only active force is the force due to gravity, $-m_D g\, {}^1\boldsymbol{n}_3$. However, additional active torques arising from the reactions to the steer torques and the drive torques must be introduced. In this derivation, the steer axes are assumed parallel to the vertical axis of the WMR. Therefore, the total reaction torque, $\boldsymbol{T}_s^D$, to steer torques from p steer-drive or steer only wheel units is expressed as

$$\boldsymbol{T}_s^D = \left(\sum_{k=1}^{p} -\tau_s^k \right) {}^1\boldsymbol{n}_3 \tag{3.33}$$

For each drive only unit, the reaction to the drive torque must be introduced. The total reaction torque, $\boldsymbol{T}_d^D$, to the drive torque from each of q drive only wheel units is given by

$$\boldsymbol{T}_d^D = \left(\sum_{k=1}^{q} -\tau_d^k \right) {}^1\boldsymbol{n}_2 \tag{3.34}$$

For drive only wheel units, the simplification that the wheel coordinate frame, ${}^2\boldsymbol{n}_i = {}^1\boldsymbol{n}_i$ has been used in Eqn.(3.34). In the case of steer-drive wheel units, the reaction to the drive torque has already been introduced as an active torque on W_f, in Section 4.3.2, Step 3 and should not be included in the summation above, Eqn.(3.34).

Hence, the generalised active force for the payload for each generalised speed u_i is given by

$$\tilde{F}_i^D = \bar{v}_i^D \cdot \left(-m_D g\, {}^1\boldsymbol{n}_3\right) + \bar{\omega}_i^D \cdot \left(\boldsymbol{T}_s^D + \boldsymbol{T}_d^D\right) \tag{3.35}$$

The linear acceleration of D is

$${}^O\boldsymbol{a}_D = {}^O\boldsymbol{a}_G + {}^O\omega_G \times {}^O\boldsymbol{v}_G + {}^O\alpha_G \times {}^G\boldsymbol{p}_D + {}^O\omega_G \times {}^O\omega_G \times {}^G\boldsymbol{p}_D \tag{3.36}$$

and the angular acceleration is

$$^{O}\alpha_{D} = {}^{O}\alpha_{G} \tag{3.37}$$

With the known inertial properties of the payload and the expressions for the linear and angular accelerations, the inertia force and torque are computed, Eqn.(3.5). Finally, the generalised inertia forces, Eqn.(3.6), for the payload are evaluated.

3.4.7 Effect of an active load on the WMR dynamics

Other than a payload which is a deadweight, the load carried by a WMR may be an active or live payload, such as a suspended load. In this case the load and the WMR behave as coupled rigid bodies and the dynamic model of the WMR must be augmented to reflect this coupling.

The Kane's method offers a clear advantage over the other classical methods when the dynamics of the load are to be added to the dynamic model of the WMR. The generalised active forces, $\tilde{F}_i^E$, and the generalised inertia forces, $\tilde{F}_i^{*E}$, for the load for the independent generalised speeds, including the degrees of freedom of the load, are obtained. The terms for the independent generalised speeds of the WMR are then simply added to the corresponding dynamic equations of the WMR. The generalised active and the generalised inertia force terms for the generalised speeds of the load provide the dynamic equations of the load itself. In the Lagrangian method, on the other hand, the Lagrangian of the coupled system must be obtained and the derivation of the dynamic equations for the generalised speeds must be repeated. Similarly, in the Newton-Euler method, the forces arising from the dynamic nature of the load must be introduced into the force balance of the WMR and the dynamic equations

must be derived. The Kane's method thus uses results previously obtained while retaining the essential coupled nature of the system.

In this section the effect of a suspended load on the dynamic behaviour of a WMR is studied. The active load is modelled as a mass of known inertial properties suspended by an inextensible, rigid sling. The sling is free to swing about the point of suspension. In this derivation, the arm is free to swing about the longitudinal axis of the WMR on the lateral plane. The load, therefore, has one degree of freedom; the methodology given here may be generalised to a case where the load has additional degrees of freedom by using corresponding generalised speeds in the derivation.

The load of mass, m_E, and centre of mass at E, is suspended from a point, H , as shown in Fig. 3.8. The position vector defining the point of suspension, H is

$$ {}^{G}p_{H} = x_h\,{}^{1}n_1 + y_h\,{}^{1}n_2 + z_h\,{}^{1}n_3 \qquad \textbf{(3.38)} $$

At the point of suspension, the load has a single rotational degree of freedom, ζ, about the vehicle ${}^{1}n_1$ axis. An intermediate coordinate frame, ${}^{3}n_i$, is located at H such that ${}^{3}n_1$ coincides with ${}^{1}n_1$ and ζ is the angle between ${}^{1}n_3$ and ${}^{3}n_3$. The centre of mass of the load is located at a distance z_E along ${}^{3}n_3$ so that the position vector is given by

$$ \begin{aligned} {}^{H}p_{E} &= -z_E\,{}^{3}n_3 = [{}^{1}T_3]\{0\ 0\ -z_E\}^T \\ &= z_E s\zeta\,{}^{1}n_2 - z_E c\zeta\,{}^{1}n_3 \end{aligned} \qquad \textbf{(3.39)} $$

The transformation matrix, $[{}^{1}T_3] = Rot({}^{1}n_1, -\zeta)$ is used to convert between the coordinate systems.

The generalised speed, u_7 , represents the rate of swing of the load and is defined as

$$u_7 \triangleq \dot{\zeta} \tag{3.40}$$

Step 1. Holonomic Equations

In the case of the suspended load, the load is free to swing with one rotational degree of freedom and so is a *holonomic* system. The swing rate, u_7 , Eqn.(3.40), is therefore an independent generalised speed of the system. The generalised speeds representing the WMR are still related through the non-holonomic equations appropriate for the particular wheel configuration.

Step 2. Partial Velocities

The velocity of the centre of mass, E,, in the inertial frame is obtained by propagating the velocity of the WMR through the point of suspension, H. In terms of the generalised speeds of the WMR, u_1 .. u_6, and the generalised speed, u_7 , of the load, the velocity of H is

$$^{O}v_{H} = {}^{O}v_{G} + {}^{O}\omega_{G} \times {}^{G}p_{H} \tag{3.41}$$

Propagating the velocity, the velocity of E in the inertial frame is

$$^{O}v_{E} = {}^{O}v_{H} + {}^{O}\omega_{H} \times {}^{H}p_{E} \tag{3.42}$$

and the angular velocity is

$$^{O}\omega_{E} = (u_4 + u_7)\,{}^{1}n_1 + u_5\,{}^{1}n_2 + u_6\,{}^{1}n_3 \tag{3.43}$$

The partial velocities, $\bar{v}_i^E$, and the partial angular velocities, $\bar{\omega}_i^E$, of the load for the

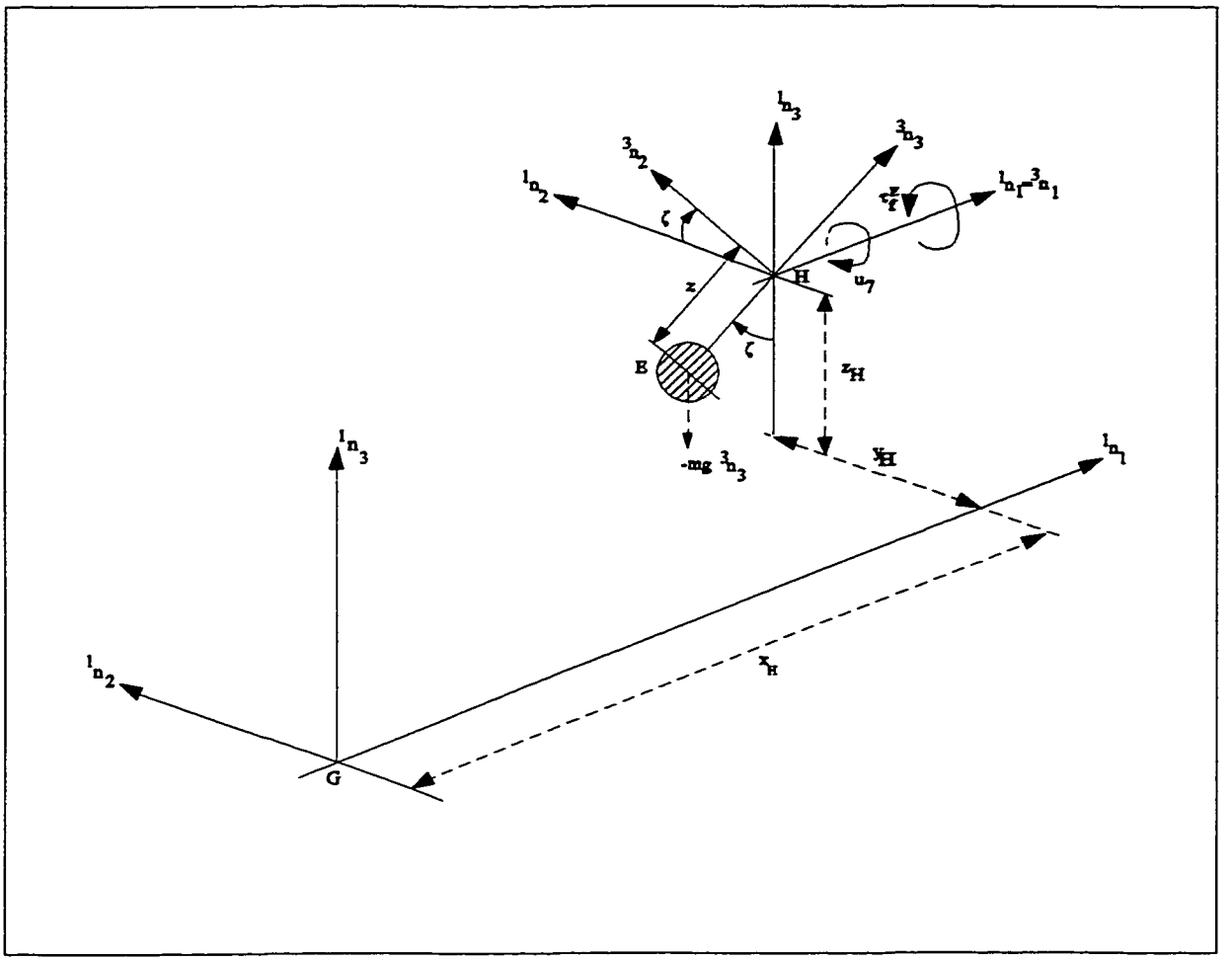

Figure 3.8 Geometric parameters and active forces on a suspended load.

Table 3.9 Partial velocities of the live load

	$\bar{v}_i^E$	$\bar{\omega}_i^E$
u_1	${}^1n_1$	0
u_2	${}^1n_2$	0
u_3	${}^1n_3$	0
u_4	$-(z_H - z_E c\zeta)\,{}^1n_2 + (y_H + z_E s\zeta)\,{}^1n_3$	${}^1n_1$
u_5	$(z_H - z_E c\zeta)\,{}^1n_1 - x_H\,{}^1n_3$	${}^1n_2$
u_6	$-(y_H + z_E s\zeta)\,{}^1n_1 + x_H\,{}^1n_2$	${}^1n_3$
u_7	$(z_E c\zeta)\,{}^1n_2 + (z_E s\zeta)\,{}^1n_3$	${}^1n_1$

generalised speeds, u_1 ..u_6 , of the WMR and u_7 , of the load are given in Table 3.9.

Step 3. Generalised Active Forces

Due to the mass of the load, the active force acting on the live load is the gravitational force, $-m_E g\, n_3$. In addition, a frictional torque, τ_f^E, acts on E due to friction at the point of suspension ; the frictional torque is modelled as

$$\tau_f^E = -(sgn\, u_7)\tau_f^E\, {}^3n_1 \qquad \textbf{(3.44)}$$

with the magnitude of the torque given by

$$\tau_f^E = k_1 + k_2 u_7 \qquad \textbf{(3.45)}$$

Using the partial velocities of the live load from Table 3.9, the generalised active forces, $\tilde{F}_i^E$ for the generalised speeds are obtained and are listed in Table 3.10a and Table 3.10b.

Table 3.10a. Generalised Active forces for the live load for u_1 .. u_4

u_1	u_2	u_3	u_4
0	0	$-m_E g$	$-m_E g(y_H + z_E s\zeta) + \tau_f^E$

Table 3.10b. Generalised Active forces for the live load for u_5 .. u_7

u_5	u_6	u_7
$x_H m_E g$	0	$-z_E m_E g s\zeta + \tau_f^E$

Step 4. Generalised Inertia Forces

The acceleration of the centre of mass, E, of the live load is obtained by taking the

total derivative of the velocity given in Eqn.(3.42).

$$
\begin{aligned}
{}^{O}a_{E} &= \frac{d}{dt}\,{}^{O}v_{E} \\
&= {}^{O}a_{G} + {}^{O}\alpha_{G}\times {}^{G}p_{H} + {}^{O}\omega_{G}\times {}^{O}\omega_{G}\times {}^{G}p_{H} \\
&\quad + {}^{O}\alpha_{H}\times {}^{H}p_{E} + {}^{O}\omega_{H}\times {}^{O}\omega_{H}\times {}^{H}p_{E}
\end{aligned}
\tag{3.46}
$$

where the angular acceleration of the suspended mass is given by

$$
{}^{O}\alpha_{H} = \dot{u}_{7}\,{}^{1}n_{1} + u_{7}u_{6}\,{}^{1}n_{2} + \dot{u}_{6}\,{}^{1}n_{3} \tag{3.47}
$$

With the known inertial properties of the suspended load, the inertia force and the inertia torque are obtained, Eqn.(3.5). Using the partial velocities of E given in Table 3.9, the generalised inertia force of the load for the independent generalised speeds are obtained.

Step 5. Assembly

For each independent generalised speed of the WMR, the generalised active force terms and the generalised inertia force terms for the suspended load are added to the corresponding terms representing the components of the WMR to obtain the dynamic equations for the coupled WMR-suspended load system. Similarly, the constraint equations are augmented with the generalised active force and generalised inertia force terms for the 'virtual' generalised speeds The dynamic equation of the load itself, corresponding to the generalised speed, u_7 , of the suspended load is given by

$$
\tilde{F}_{7}^{E} + \tilde{F}_{7}^{*E} = 0 \tag{3.48}
$$

3.5 Case studies for the proposed modelling methodology

The proposed dynamic modelling methodology is illustrated using case studies, viz., a tri-cycle configuration, a differentially driven WMR and an omnidirectional WMR. In these three cases the WMR is assumed to carry only a deadweight. The effect of the active payload is analyzed in the fourth case in which the differentially driven WMR carries a suspended payload. For each wheel configuration and load, the five step procedure is systematically applied and the resulting dynamic equations are provided. For each case, the set of equations representing the constraint forces is also derived.

3.5.1 WMR with tri-cycle wheel configuration

A WMR with wheels in a tricycle configuration, shown in Fig.3.9, is analyzed. The WMR has a steer-drive wheel unit in front and two castors without swivel in the rear. In this analysis, the mass and the inertial properties of the wheel frame, W_f, and the wheel, W, are assumed small enough to be neglected. The values of the various geometrical parameters for this configuration are listed in Table 3.11. The centre of mass, D, of the body of the WMR, is assumed coincident with the reference point, G, for simplicity.

Step 1: Non-holonomic equations

For the right and the left castors, when the geometrical parameters in Table 3.11 are substituted in Eqn.(3.30), the non-holonomic equations are

$$\begin{Bmatrix} \dot{\gamma}_R \\ \dot{\gamma}_L \end{Bmatrix} = \begin{bmatrix} \frac{1}{r} & \frac{b}{r} \\ \frac{1}{r} & -\frac{b}{r} \end{bmatrix} \begin{Bmatrix} u_1 \\ u_6 \end{Bmatrix} \qquad \textbf{(3.49)}$$

Since the castors have only 2-DOF, the lateral speed, u_2 is given by

$$u_2 = c u_6 \tag{3.50}$$

For the steer-drive wheel, substitution of the appropriate values of the physical parameters in Eqn.(3.1,3.15,3.18) yields

$$\begin{Bmatrix} \dot{\phi} \\ \dot{\theta} \end{Bmatrix} = \begin{bmatrix} -\frac{1}{d}s\phi & \frac{(l+c)}{d}c\phi - 1 \\ \frac{1}{r}c\phi & \frac{(l+c)}{r}s\phi \end{bmatrix} \begin{Bmatrix} u_1 \\ u_6 \end{Bmatrix} \tag{3.51}$$

Step 2: Non-Holonomic Partial Velocities

For the steer-drive wheel and the right and the left castors, the *holonomic* partial velocities are obtained from Table.3.2 and Table 3.3 using the values of the geometrical parameters in Table.3.11. The non-holonomic equations obtained in Step 1 above are then used to obtain the *non-holonomic* partial velocities using the procedure indicated in Eqn.(3.3). For the steer-drive wheel, the mass of W and that of W_f have been neglected. So, only the partial velocities of W_p , and the partial angular velocities of W and W_f are needed to obtain the dynamic equations. The non-holonomic partial velocities for the steer-drive wheel unit for each generalised speed are given in Table 3.13.

The castors are also assumed massless and only the partial velocities of the point of contact and the partial angular velocities are derived. For the body of the WMR, the partial velocities are derived using Eqn.(3.32) and the values given in Table.3.8. The non-holonomic partial velocities of the right castor and those of the body of the WMR are given in Table

3.14. The partial velocities of the left castor may be obtained by substituting the distance, b for -b in the expressions for the right castor.

Step 3: Generalised Active Forces

For the steer-drive wheel, the active forces are (i) drive torque, $\tau_d{}^2\boldsymbol{n}_2$ acting on W (ii) frictional torque, $\tau_f^{w\,2}\boldsymbol{n}_2$ acting on W (iii) reaction to drive torque, $-\tau_d{}^2\boldsymbol{n}_2$ acting on W_f (iv) steer torque, $\tau_s{}^1\boldsymbol{n}_3$ acting on W_f and (v) constraint forces $Q_2^{w\,2}\boldsymbol{n}_2+Q_3^{w\,2}\boldsymbol{n}_3$ acting at W_p.

For the castors, the active forces are (i) the constraint force on the right castor $Q_2^{r\,1}\boldsymbol{n}_2+Q_3^{r\,1}\boldsymbol{n}_3$ acting at the contact point, R_p (ii) the friction torque, $\tau_f^{r\,1}\boldsymbol{n}_2$ (iii) the constraint force on the left castor $Q_2^{l\,1}\boldsymbol{n}_2+Q_3^{l\,1}\boldsymbol{n}_3$ acting at L_p and (iv) the friction torque, $\tau_f^{l\,1}\boldsymbol{n}_2$. The only active force on the body of the WMR is the gravitational force $-m_d g\,{}^1\boldsymbol{n}_3$ acting at D. In addition, the body of the WMR is acted upon by the reaction to the steer torque, $-\tau_s{}^1\boldsymbol{n}_3$ and to that of the drive torque, $-\tau_d{}^2\boldsymbol{n}_2$. The generalised active forces for all these components are listed in Table 3.15.

Step 4: Generalised Inertia Forces

In this case, the only massive body is the body of the WMR itself. Hence, only the acceleration, ${}^o\boldsymbol{a}_D$, and the angular acceleration, ${}^o\boldsymbol{\alpha}_D$, of the centre of mass, D, are required. These are obtained using Eqn.(3.36,3.37) and are given by

$$\begin{aligned} {}^o\boldsymbol{a}_D &= \dot{u}_1\,{}^1\boldsymbol{n}_1+u_1u_6\,{}^1\boldsymbol{n}_2 \\ {}^o\boldsymbol{\alpha}_D &= \dot{u}_6\,{}^1\boldsymbol{n}_3 \end{aligned} \qquad \textbf{(3.52)}$$

The inertia force, $\boldsymbol{R}^{*D}$, and the inertia torque, $\boldsymbol{T}^{*D}$, are obtained using Eqn.(3.5) and are

$$
\begin{aligned}
R^{*D} &= -m_d \dot{u}_1 {}^1n_1 - m_d u_1 u_6 {}^1n_2 \\
T^{*D} &= -(I_3^d \dot{u}_6) {}^1n_3
\end{aligned}
\tag{3.53}
$$

where m_d and I_3^d are the mass and the moment of inertia of D with respect to the ${}^1n_3$ axis.

Using the partial velocities and the inertia force and the inertia torque, the generalised inertia forces corresponding to the generalised speeds are obtained. For the case of the tri-cycle configuration, the generalised inertia forces are listed in Table 3.15.

Step 5: Assembly

Collecting the generalised active forces and the generalised inertial forces corresponding to each of the independent generalised speed, the dynamic equations of the WMR are

$$
\begin{aligned}
m_d \dot{u}_1 &= \frac{(\tau_d + \tau_f^w)}{r} c\phi - \frac{\tau_s}{d} s\phi + \frac{(\tau_f^r + \tau_f^l)}{r} \\
I_3^w \dot{u}_6 &= \left(\frac{(l+c)}{d} c\phi - 1 \right) \tau_s + \frac{(l+c)}{r} s\phi (\tau_d + \tau_f^w) + \frac{b}{r} (\tau_f^r - \tau_f^l)
\end{aligned}
\tag{3.54}
$$

The generalised inertia and active force terms for the four 'virtual' generalised speeds in this case provide linear equations for the constraint forces at the wheels. These constraint forces are used to model the tire friction, Eqn.(3.8). Collecting terms and rearranging, the constraint equations are

$$
\begin{aligned}
Q_2^w c\phi + Q_2^r + Q_2^l &= m_d u_1 u_6 \\
Q_3^w + Q_3^r + Q_3^l &= m_d g \\
ds\phi Q_3^w + b(Q_3^r - Q_3^l) &= h m_d u_1 u_6 + \tau_d s\phi \\
-(l - dc\phi) Q_3^w + c(Q_3^r + Q_3^l) + h Q_2^w s\phi &= \tau_d c\phi
\end{aligned}
\tag{3.55}
$$

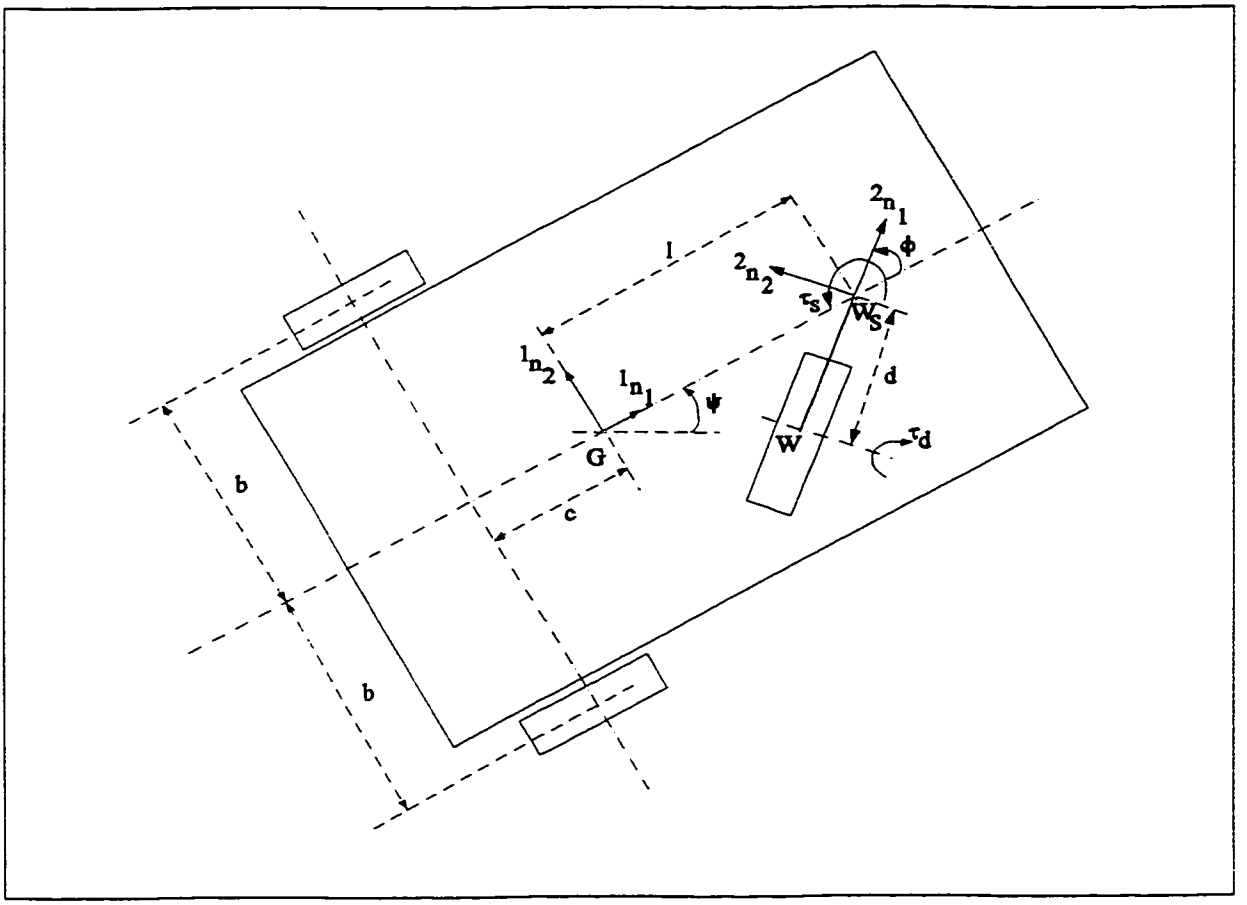

Figure 3.9 Geometrical Parameters and Drive Torques of Tricycle WMR

Table.3.11 Geometrical parameters used for the tri-cycle configuration

	x_s	y_s	x_w	y_w	z_w
Steer-Drive wheel	l	0	-d	0	-(h-r)
Right Castor	-	-	-c	-b	-(h-r)
Left Castor	-	-	-c	b	-(h-r)

Table 3.12 Partial velocities for the steer-drive wheel of the tri-cycle WMR

	$\vec{v}_t^{W_P}$	$\omega_t^{W_f}$	ω_t^{W}
u_1	0	$-\frac{1}{d}s\phi\ {}^1n_3$	$-\frac{1}{d}s\phi\ {}^1n_3+\frac{1}{r}c\phi\ {}^2n_2$
u_2	${}^1n_2$	0	0
u_3	${}^1n_3$	0	0
u_4	$h\ {}^1n_2-ds\phi\ {}^1n_3$	${}^1n_1$	${}^1n_1$
u_5	$-h\ {}^1n_1-(l-dc\phi)\ {}^1n_3$	${}^1n_2$	${}^1n_2$
u_6	0	$\frac{(l+c)}{d}c\phi\ {}^1n_3$	$\frac{(l+c)}{d}c\phi\ {}^1n_3+\frac{(l+c)}{r}s\phi\ {}^2n_2$

Table 3.13 Partial velocities of right castor and body of the tri-cycle WMR

	$\tilde{v}_i^{R_p}$	$\tilde{\omega}_i^R$	$\tilde{v}_i^D$	$\tilde{\omega}_i^D$
u_1	0	$\frac{1}{r}{}^1n_2$	${}^1n_1$	0
u_2	${}^1n_2$	0	${}^1n_2$	0
u_3	${}^1n_3$	0	${}^1n_3$	0
u_4	$h\,{}^1n_2 - b\,{}^1n_3$	${}^1n_1$	0	${}^1n_1$
u_5	$-h\,{}^1n_1 + c\,{}^1n_3$	${}^1n_2$	0	${}^1n_2$
u_6	0	$\frac{b}{r}{}^1n_2 + {}^1n_3$	0	${}^1n_3$

Table 3.14 Generalised active forces for the tri-cycle WMR

	$\tilde{F}_i^W$	$\tilde{F}_i^R$	$\tilde{F}_i^L$	$\tilde{F}_i^D$
u_1	$\frac{(\tau_d+\tau_f^w)}{r}c\phi - \frac{\tau_s}{d}s\phi$	$\frac{1}{r}\tau_f^r$	$\frac{1}{r}\tau_f^l$	0
u_2	$Q_2^w c\phi$	Q_2^r	Q_2^l	0
u_3	Q_3^w	Q_3^r	Q_3^l	$-m_d g$
u_4	$hQ_2^w c\phi - dQ_3^w s\phi$	$hQ_2^r - bQ_3^r$	$hQ_2^l + bQ_3^l$	$\tau_d s\phi$
u_5	$hQ_2^w s\phi - (l - dc\phi)Q_3^w$	cQ_3^r	cQ_3^l	$-\tau_d c\phi$
u_6	$\frac{(l+c)}{r}(\tau_d+\tau_f^w)s\phi + \frac{(l+c)}{d}\tau_s c\phi$	$\frac{b}{r}\tau_f^r$	$-\frac{b}{r}\tau_f^l$	$-\tau_s$

Table 3.15 Generalised Inertia Forces for the body of the tri-cycle WMR

	u_1	u_2	u_3	u_4	u_5	u_6
$\tilde{F}^{*D}$	$-m_d\dot{u}_1$	$-m_d u_1 u_6$	0	0	0	$-I_3^d\dot{u}_6$

3.5.2 A Differentially Driven WMR

The second wheel configuration analyzed is a differentially driven WMR with wheels in a diamond configuration as shown in Fig 3.10. The point of reference, G, is assumed coincident with the geometric centre of the WMR. The differentially driven wheels are set equidistant from G along the lateral mid plane of the WMR while two castors with swivel are set in the longitudinal axis equidistant from G. The radii of the wheels and the castors are assumed to be equal.

In this analysis, the mass and the inertial properties of the rotational components of the right and the left wheels, R and L, are assumed to be identical and are taken into consideration. Since the wheels are not steered, the inertial properties of the non-rotating components of the wheel units, with centres of mass at W_f, are assumed included with those of the body of the WMR. The centre of mass, D, of the body of the WMR, is assumed coincident with the reference point, G, for simplicity. The mass and the inertial properties of the castors are assumed negligible. The values of the geometrical parameters pertinent to this configuration are listed in Table 3.16.

Step 1: Non-holonomic equations

The drive wheel units used in this WMR are drive only wheel units and the simplifications given in Eqn.(3.29, 3.30) apply. In addition, since $x_w = 0$ in this differential drive configuration, the WMR has zero lateral speed, $u_2 = 0$. Using Eqn.(3.30) and the geometric parameters given in Table 3.16, the non-holonomic equations for the right and the left differential drive wheels, are

$$\begin{Bmatrix} \dot{\theta}_R \\ \dot{\theta}_L \end{Bmatrix} = \begin{bmatrix} \frac{1}{r} & \frac{b}{r} \\ \frac{1}{r} & -\frac{b}{r} \end{bmatrix} \begin{Bmatrix} u_1 \\ u_6 \end{Bmatrix} \tag{3.56}$$

The castors used in this configuration are free to swivel about the vertical axis at the point of attachment. The elements of the coefficient matrix, Eqn.(3.18), are evaluated with the geometric parameters given in Table 3.16. For the front castor, F, the non-holonomic equations obtained using Eqn.(3.1) are given by

$$\begin{Bmatrix} \dot{\delta}_F \\ \dot{\gamma}_F \end{Bmatrix} = \begin{bmatrix} -\frac{1}{d}s\delta & \frac{1}{d}(lc\delta - d) \\ \frac{1}{r}c\delta & \frac{l}{r}s\delta \end{bmatrix} \begin{Bmatrix} u_1 \\ u_6 \end{Bmatrix} \tag{3.57}$$

The equations for the rear castor, B, are obtained by substituting -l for l in Eqn.(3.57).

Step 2: Non-Holonomic Partial Velocities

For the differential drive wheels, the non-holonomic partial velocities needed are those of the respective centres of mass and the points of contact of the wheels on the ground. The non-holonomic partial angular velocities needed are those of the centres of mass only. The *holonomic* partial velocities of these points are obtained by substitution of the geometric parameter values in Table 3.2 and Table 3.3 with the steer angle set to zero. Then using the non-holonomic equations, Eqn.(3.56), the non-holonomic partial velocities are obtained. The non-holonomic partial velocities of the left drive wheel are listed in Table 3.17. The corresponding partial velocities for the right drive wheel are obtained by substituting -b for

b in the values listed in Table 3.17.

The castors are assumed massless and only the partial velocities of the points of contact of the castors on the ground are derived. For the body of the WMR, the partial velocities are derived using Table 3.4. The non-holonomic partial velocities of the front castor, F, and those of the body, D, of the WMR are given in Table 3.18. The partial velocities of the rear castor may be obtained by substituting the distance, -l for l in the expressions for the front castor.

Step 3: Generalised Active Forces

For the left-drive wheel, the active forces are (i) the gravitational force, $-m_l g\,{}^1\boldsymbol{n}_3$ at the centre of mass (ii) the drive torque, $\tau_d^l\,{}^1\boldsymbol{n}_2$ acting on L (iii) the frictional torque, $\tau_f^l\,{}^1\boldsymbol{n}_2$ acting on L and (iv) the constraint forces $Q_2^l\,{}^1\boldsymbol{n}_2 + Q_3^l\,{}^1\boldsymbol{n}_3$ acting at the point of contact, L_p.

For the front castor, the only active forces are (i) the constraint force $Q_3^f\,{}^1\boldsymbol{n}_3$ acting at the contact point, F_p and (ii) the friction torque, $\tau_f^f\,{}^2\boldsymbol{n}_2$. The active forces on the body, D, of the WMR are (i) the gravitational force $-m_d g\,{}^1\boldsymbol{n}_3$ acting at the centre of mass and (ii) the reaction to drive torques $-(\tau_d^l + \tau_d^r)\,{}^1\boldsymbol{n}_2$. The generalised active forces, $\tilde{F}_t$ are obtained by substituting the partial velocities and the active forces in Eqn.(3.4). The generalised active forces for the body, D of the WMR are listed in Table 3.19a. The generalised active forces for the left drive wheel, L, the right drive wheel, R, the front castor, F and for the rear castor, B are listed in Table 3.19b.

Step 4: Inertia Forces

For the sake of illustration, the inertial properties of the rotational components of the wheels are also taken into account in this case. Hence, along with the acceleration, ${}^O\boldsymbol{a}_D$, and

the angular acceleration, ${}^{O}\alpha_{D}$, of the centre of mass, D, of the WMR, the accelerations of the centres of mass of the drive wheels are also required.

For the centre of mass, D, the accelerations are obtained using Eqn.(3.36,3.37) and are given by

$$\begin{aligned} {}^{O}a_{D} &= \dot{u}_1\,{}^{1}n_1 + u_1u_6\,{}^{1}n_2 \\ {}^{O}\alpha_{D} &= \dot{u}_6\,{}^{1}n_3 \end{aligned} \tag{3.58}$$

The inertia force, R^{*D}, and the inertia torque, T^{*D}, from Eqn.(3.5) are

$$\begin{aligned} R^{*D} &= -m_d\dot{u}_1\,{}^{1}n_1 - m_d u_1u_6\,{}^{1}n_2 \\ T^{*D} &= -(I_3^{d}\dot{u}_6)\,{}^{1}n_3 \end{aligned} \tag{3.59}$$

where m_d and I_3^{d} are the mass and the moment of inertia of D with respect to the ${}^{1}n_3$ axis. For the left wheel, L, the acceleration is computed using Eqn.(3.24) and is

$${}^{O}a_{L} = (\dot{u}_1 - b\dot{u}_6)\,{}^{1}n_1 + (u_1u_6 - bu_6^2)\,{}^{1}n_2 \tag{3.60}$$

Using Eqn.(3.26), the angular acceleration is

$${}^{O}\alpha_{L} = -\dot{\theta}_L u_6\,{}^{1}n_1 + \dot{\theta}_L\,{}^{1}n_2 + \dot{u}_6\,{}^{1}n_3 \tag{3.61}$$

From the known inertial properties of the wheel, the inertia force and the inertia torque are

$$\begin{aligned} R^{*L} &= -m_l(\dot{u}_1 - b\dot{u}_6)\,{}^{1}n_1 - m_l(u_1u_6 - bu_6^2)\,{}^{1}n_2 \\ T^{*L} &= \dot{\theta}u_6(I_2^{l} - 2I_1^{l})\,{}^{1}n_1 - \dot{\theta}_L I_2^{l}\,{}^{1}n_2 - \dot{u}_6 I_1^{l}\,{}^{1}n_3 \end{aligned} \tag{3.62}$$

where, due to the symmetry of the wheel about its axis of rotation, $I_1^l = I_3^l$.

Using the partial velocities and the inertia forces and the inertia torques, Eqn.(3.4,3.7), the generalised inertia forces corresponding to the generalised speeds are obtained. For the case of the differential drive WMR, the generalised inertia forces for the body of the WMR are listed in Table 3.20a and those for the drive wheels in Table 3.20b. The castors have been assumed to have negligible inertial properties and hence do not contribute to the generalised inertia force.

Step 5: Assembly

Collecting the generalised active forces, Tables 3.19a, 3.19b and the generalised inertia forces, Tables 3.20a, 3.20b corresponding to the independent generalised speeds, u_1 and u_6, the dynamic equations of the differential drive WMR are

$$\begin{aligned}(m_d+2m_w+\frac{2}{r^2}I_2^w)\dot{u}_1 &= \frac{(\tau_d^l+\tau_d^r)}{r}+\frac{(\tau_f^l+\tau_f^r)}{r}+\frac{(\tau_f^f+\tau_f^b)}{r}c\delta \\ (I_3^d+2b^2m_w+2I_1^w+\frac{2b^2}{r^2}I_2^w)\dot{u}_6 &= \frac{b}{r}(\tau_d^r-\tau_d^l)+\frac{b}{r}(\tau_f^r-\tau_f^l)+\frac{l}{r}s\delta\,(\tau_f^f+\tau_f^b)\end{aligned} \qquad \textbf{(3.63)}$$

It has been assumed that the two drive wheels have identical inertial properties, m_w and I_t^w.

The generalised inertia and active force terms for the four 'virtual' generalised speeds provide the equations to obtain the constraint forces at the wheels as

$$\begin{aligned}Q_2^r+Q_2^l &= (m_d+2m_w)u_1u_6 \\ Q_3^r+Q_3^l+Q_3^f+Q_3^b &= m_dg+2m_wg \\ b(Q_3^l-Q_3^r)+ds\delta\,(Q_3^b-Q_3^f)+h(Q_2^l+Q_2^r) &= u_1u_6(2m_w(h-r)-\frac{2}{r}(I_2^w-2I_1^w)) \\ l(Q_3^b-Q_3^f)+dc\delta\,(Q_3^f+Q_3^b) &= \dot{u}_1(\frac{2}{r}I_2^w-2m_w(h-r))\end{aligned} \qquad \textbf{(3.64)}$$

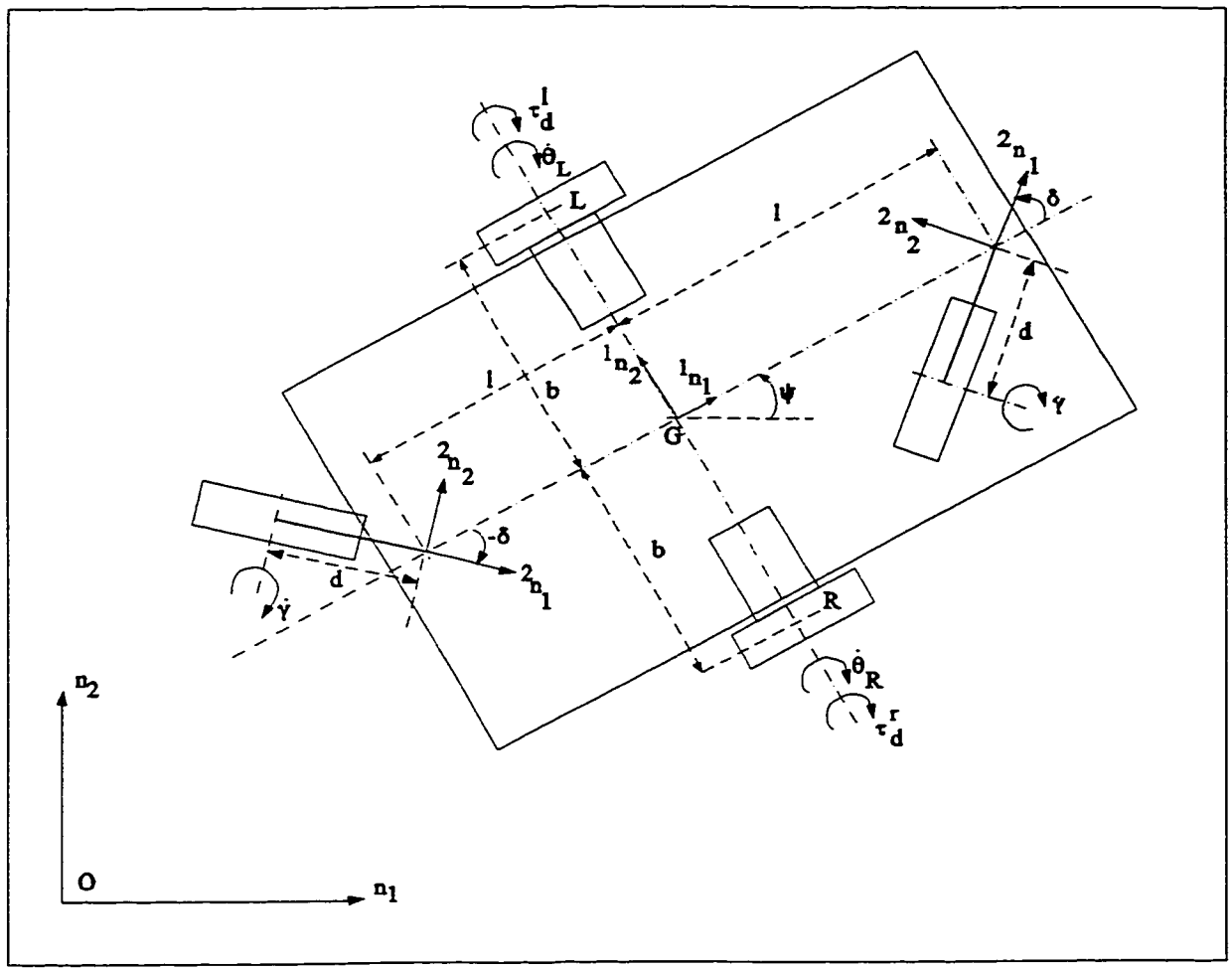

Figure 3.10 Geometric Parameters and Active Torques of a Differentially Driven WMR

Table 3.16 Geometrical parameters used for the Differential-Drive configuration

	x_s	y_s	x_w	y_w	z_w
Right drive wheel, R	-	-	-	-b	-(h-r)
Left drive wheel, L	-	-	-	b	-(h-r)
Front Castor, F	l	0	-d	0	-(h-r)
Rear Castor, B	-l	0	-d	0	-(h-r)

Table 3.17 Non-holonomic Partial Velocities for the Left Drive Wheel

	$\bar{v}_i^L$	$\bar{v}_i^{L_P}$	$\bar{\omega}_i^L$
u_1	${}^1n_1$	0	$\frac{1}{r}\,{}^1n_2$
u_2	${}^1n_2$	${}^1n_2$	0
u_3	${}^1n_3$	${}^1n_3$	0
u_4	$(h-r)\,{}^1n_2+b\,{}^1n_3$	$h\,{}^1n_2+b\,{}^1n_3$	${}^1n_1$
u_5	$-(h-r)\,{}^1n_1$	$-h\,{}^1n_1$	${}^1n_2$
u_6	$-b\,{}^1n_1$	0	$-\frac{b}{r}\,{}^1n_2+{}^1n_3$

Table 3.18 Partial velocities of Front Castor and Body of WMR

	$\bar{\omega}_i^F$	$\bar{v}_i^{F_P}$	$\bar{v}_i^D$	$\bar{\omega}_i^D$
u_1	$-\frac{1}{d}s\delta\,{}^1n_3+\frac{1}{r}c\delta\,{}^2n_2$	0	${}^1n_1$	0
u_2	0	${}^1n_2$	${}^1n_2$	0
u_3	0	${}^1n_3$	${}^1n_3$	0
u_4	${}^1n_1$	$h\,{}^1n_2-ds\delta\,{}^1n_3$	0	${}^1n_1$
u_5	${}^1n_2$	$-h\,{}^1n_1-(l-dc\delta)\,{}^1n_3$	0	${}^1n_2$
u_6	$\frac{l}{d}c\delta\,{}^1n_3+\frac{l}{r}s\delta\,{}^2n_2$	0	0	${}^1n_3$

Table 3.19a Generalised Active Forces for the Body of the WMR

	u_1	u_2	u_3	u_4	u_5	u_6
$\tilde{F}_i^D$	0	0	$-m_d g$	0	$-(\tau_d^r+\tau_d^l)$	0

Table 3.19b Generalised Active Forces for Drive wheels and Castors

	$\tilde{F}_i^L$	$\tilde{F}_i^R$	$\tilde{F}_i^F$	$\tilde{F}_i^B$
u_1	$\frac{(\tau_d^l+\tau_f^l)}{r}$	$\frac{(\tau_d^r+\tau_f^r)}{r}$	$\frac{\tau_f^f}{r}c\delta$	$\frac{\tau_f^b}{r}c\delta$
u_2	Q_2^l	Q_2^r	0	0
u_3	$Q_3^l - m_l g$	$Q_3^r - m_r g$	Q_3^f	Q_3^b
u_4	$hQ_2^l + b(Q_3^l - m_l g)$	$hQ_2^r - b(Q_3^r - m_r g)$	$-dQ_3^f s\delta$	$dQ_3^b s\delta$
u_5	τ_d^l	τ_d^r	$-(l-dc\delta)Q_3^f$	$(l+dc\delta)Q_3^b$
u_6	$-\frac{b}{r}(\tau_d^l+\tau_f^l)$	$\frac{b}{r}(\tau_d^r+\tau_f^r)$	$\frac{l}{r}s\delta\,\tau_f^f$	$\frac{l}{r}s\delta\,\tau_f^b$

Table 3.20a Generalised Inertia Forces for the centre of mass, D

	u_1	u_2	u_3	u_4	u_5	u_6
$\tilde{F}_i^{*D}$	$-m_d\dot{u}_1$	$-m_d u_1 u_6$	0	0	0	$-\dot{u}_6 I_3^d$

Table 3.20b Generalised Inertia Forces for the wheels' centres of mass, L and R

	$\tilde{F}_i^{*L}$	$\tilde{F}_i^{*R}$
u_1	$-m_l(\dot{u}_1 - b\dot{u}_6) - \frac{1}{r}\dot{\theta}_L I_2^l$	$-m_r(\dot{u}_1 + b\dot{u}_6) - \frac{1}{r}\dot{\theta}_R I_2^r$
u_2	$-m_l(u_1u_6 - bu_6^2)$	$-m_r(u_1u_6 + bu_6^2)$
u_3	0	0
u_4	$-m_l(h-r)(u_1u_6 - bu_6^2) + \dot{\theta}_L u_6(I_2^l - 2I_1^l)$	$-m_r(h-r)(u_1u_6 + bu_6^2) + \dot{\theta}_R u_6(I_2^r - 2I_1^r)$
u_5	$m_l(h-r)(\dot{u}_1 - b\dot{u}_6) - \dot{\theta}_L I_2^l$	$m_r(h-r)(\dot{u}_1 + b\dot{u}_6) - \dot{\theta}_R I_2^r$
u_6	$bm_l(\dot{u}_1 - b\dot{u}_6) + \frac{b}{r}\dot{\theta}_L I_2^l - \dot{u}_6 I_1^l$	$-bm_r(\dot{u}_1 + b\dot{u}_6) - \frac{b}{r}\dot{\theta}_R I_2^r - \dot{u}_6 I_1^r$

3.5.3 An Omnidirectional WMR

For the third case, an omnidirectional WMR with four steer-drive wheels in a rectangular configuration, shown in Fig.3.11, is analyzed. With the four steer-drive units, the WMR can have independent forward and lateral speeds and a yaw rate in the floor frame. In this analysis, only the mass and the inertial properties of the body, D, of the WMR are considered. The reference point, G, is chosen such that the four steer-drive units are symmetric about it. The centre of mass, D, of the body of the WMR, is assumed coincident with G. The mass and the inertial properties of the wheel frame, W_f, and the wheel, W, are assumed small enough to be neglected. The values of the various geometrical parameters for this configuration are listed in Table 3.21.

In the following derivation, only dynamic quantities for the Left-Front wheel unit, indicated in Fig.3.11 by 1, are obtained. The quantities for the other units may be obtained by substitution of the appropriate geometric values from the Table 3.21. When the dynamic equations are assembled, the steer rate, the steer angle and the rotational rate terms are superscripted and a summation over the four wheel units is implied.

Step 1: Non-holonomic equations

For the Left-Front steer-drive wheel unit, the non-holonomic equations are obtained using Eqn.(3.1) with the elements of the coefficient matrix, Eqn.(3.18) evaluated using the values of the geometrical parameters in Table 3.21. For clarity of presentation, the subscripts on the rotational speeds $\dot{\phi}$ and $\dot{\theta}$ are not indicated in the following equations.

$$\begin{Bmatrix} \dot{\phi} \\ \dot{\theta} \end{Bmatrix} = \begin{bmatrix} -\frac{1}{d}s\phi & \frac{1}{d}c\phi & \frac{(bs\phi + lc\phi - d)}{d} \\ \frac{1}{r}c\phi & \frac{1}{r}s\phi & \frac{(ls\phi - bc\phi)}{r} \end{bmatrix} \begin{Bmatrix} u_1 \\ u_2 \\ u_6 \end{Bmatrix} \tag{3.65}$$

It must be mentioned that the omnidirectional WMR imposes kinematic constraints on the steer rate and the rotational speed of each of the four steer-drive wheel units. The speeds must be chosen such that the Ackerman's steering requirement is met by the path parameters. This issue falls under the area of trajectory generation and is not addressed here.

Step 2: Non-Holonomic Partial Velocities

For the steer-drive wheel the *holonomic* partial velocities are obtained from Table 3.2 and Table 3.3. The non-holonomic equations are then used to obtain the *non-holonomic* partial velocities using Eqn.(3.3) to eliminate the dependent speeds. For the steer-drive wheel unit, the mass of W and that of W_f have been neglected. So, only the partial velocities of W_p and the partial angular velocities of W and W_f are needed to obtain the dynamic equations. These non-holonomic partial velocities are listed in Table 3.22a. Since the mass centre, D, of the body of the WMR, is coincident with the reference point, G, the partial velocities are easily written down and are given in Table 3.22b.

Step 3: Generalised Active Forces

For the Left-Front steer-drive wheel, the active forces (superscripted with 1) are (i) drive torque, $\tau_d^{1\,2}\boldsymbol{n}_2$ acting on W (ii) frictional torque, $\tau_f^{1\,2}\boldsymbol{n}_2$ acting on W (iii) reaction to drive torque, $-\tau_d^{1\,2}\boldsymbol{n}_2$ acting on W_f (iv) steer torque, $\tau_s^{1\,1}\boldsymbol{n}_3$ acting on W_f and (v) constraint forces $Q_2^{1\,2}\boldsymbol{n}_2 + Q_3^{1\,2}\boldsymbol{n}_3$ acting at W_p.

For the mass centre, D, of the WMR, the active forces are (i) gravitational force $-m_d g\,{}^1n_3$ acting at D (ii) the reaction to the steer torque, $-\tau_s^k\,{}^1n_3$, for each of k wheel units and (iii) the reaction to the drive torque, $-\tau_d^k\,{}^2n_2$, for each of k wheel units. In this case, k = 4 for the omnidirectional WMR.

The generalised active forces for the Left-Front steer-drive wheel unit for the independent generalised speeds are listed in Table 3.23a and those for the 'virtual' speeds in Table 3.23b. Active forces and torques are explicitly superscripted here. Similarly, the generalised active forces for the centre of mass, D, of the body of the WMR are obtained and are listed in Table 3.24.

Step 4: Generalised Inertia Forces

In this case, the only massive body is the body of the WMR itself. Hence, only the acceleration, ${}^O a_D$, and the angular acceleration, ${}^O\alpha_D$, of the centre of mass, D, are required. These are obtained using Eqn.(3.36,3.37) and are given by

$$\begin{aligned} {}^O a_D &= (\dot{u}_1 - u_2 u_6)\,{}^1n_1 + (\dot{u}_2 + u_1 u_6)\,{}^1n_2 \\ {}^O\alpha_D &= \dot{u}_6\,{}^1n_3 \end{aligned} \qquad \textbf{(3.66)}$$

The inertia force, R^{*D}, and the inertia torque, T^{*D}, are obtained using Eqn.(3.5) and are

$$\begin{aligned} R^{*D} &= -m_d(\dot{u}_1 - u_2 u_6)\,{}^1n_1 - m_d(\dot{u}_2 + u_1 u_6)\,{}^1n_2 \\ T^{*D} &= -(I_3^d \dot{u}_6)\,{}^1n_3 \end{aligned} \qquad \textbf{(3.67)}$$

where m_d and I_3^d are the mass and the moment of inertia of D with respect to the ${}^1n_3$ axis.

Using the partial velocities and the inertia force and the inertia torque, the generalised inertia forces corresponding to the generalised speeds are obtained, Eqn.(3.6). For the case of the omnidirectional WMR, the generalised inertial forces are listed in Table 3.25.

Step 5: Assembly

Collecting the generalised active forces and the generalised inertia forces corresponding to each of the independent generalised speed, the dynamic equations of the omnidirectional WMR are

$$
\begin{aligned}
m_d \dot{u}_1 &= m_d u_2 u_6 - \sum_{k=1}^{4} \left(\frac{\tau_s^k}{d} s\phi^k + \frac{(\tau_d^k + \tau_f^k)}{r} c\phi^k \right) \\
m_d \dot{u}_2 &= -m_d u_1 u_6 + \sum_{k=1}^{4} \left(\frac{\tau_s^k}{d} c\phi^k + \frac{(\tau_d^k + \tau_f^k)}{r} s\phi^k \right) \\
I_3^d \dot{u}_6 &= \sum_{k=1}^{4} \left(\frac{\tau_s^k}{d} (b\, s\phi + l c\phi - d)^k + \frac{(\tau_d^k + \tau_f^k)}{r} (l s\phi - b\, c\phi)^k \right)
\end{aligned}
\tag{3.68}
$$

The superscripts indicate each of the four steer-drive wheel units.

The equations expressing the constraint forces at the wheels are given by collecting the generalised active and the inertial forces corresponding to the 'virtual' generalised speeds. These equations are

$$
\begin{aligned}
Q_3^k - m_d g &= 0 \\
h Q_2^k c\phi^k + (b - d s\phi)^k Q_3^k + \tau_d^k s\phi^k &= 0 \\
h Q_2^k s\phi^k - (l - d c\phi)^k Q_3^k - \tau_d^k c\phi^k &= 0
\end{aligned}
\tag{3.69}
$$

The subscript indicates that the appropriate values of the geometric quantities are to be substituted and the summation carried out over the four steer-drive wheel units.

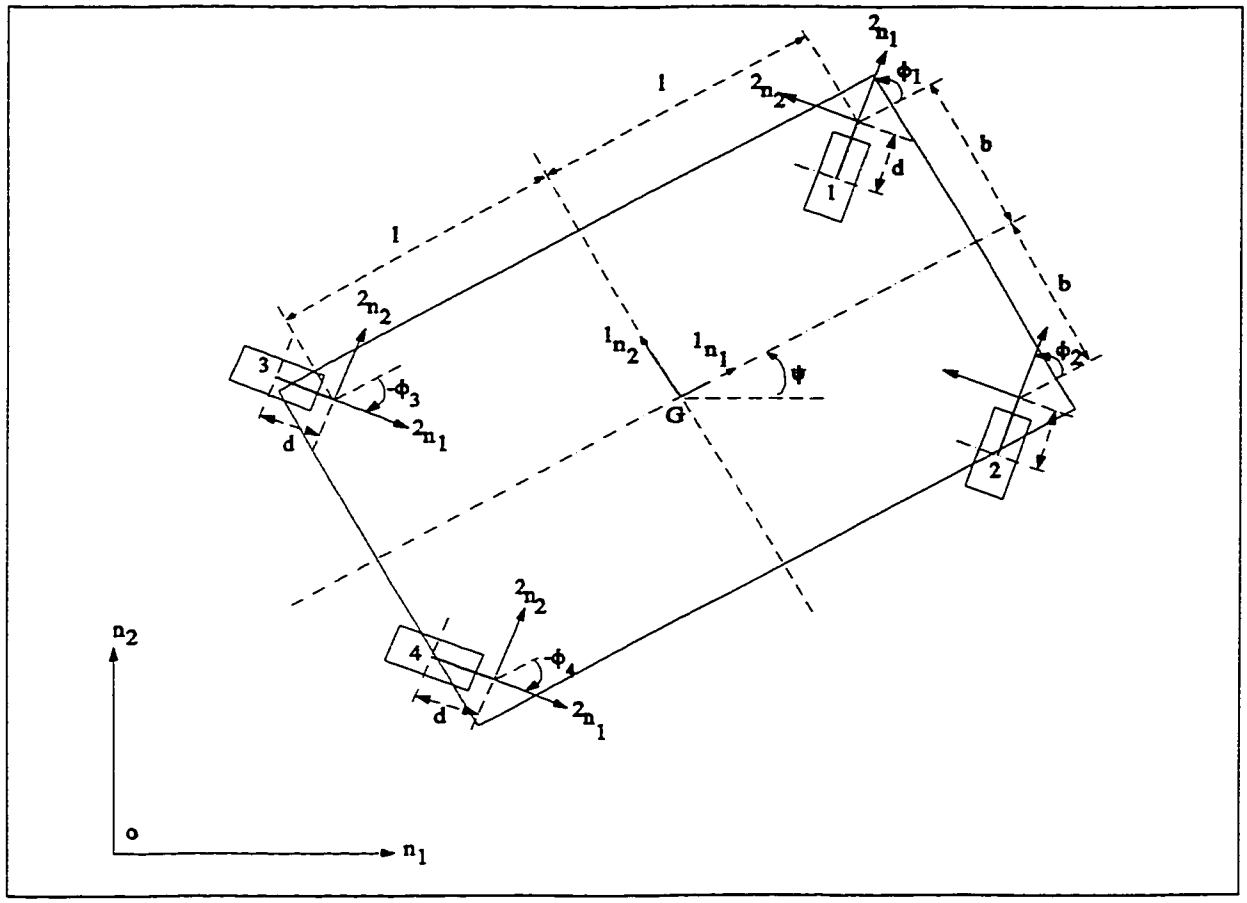

Figure 3.11 Geometrical Parameters of Omnidirectional WMR

Table 3.21 Geometrical parameters used for the Omnidirectional configuration

	x_s	y_s	x_w	y_w	z_w
Steer-Drive wheel #1 (Left - Front)	l	b	-d	0	-(h-r)
Steer-Drive wheel #2 (Right - Front)	l	-b	-d	0	-(h-r)
Steer-Drive wheel #3 (Left - Rear)	-l	b	-d	0	-(h-r)
Steer-Drive wheel #4 (Right - Rear)	-l	-b	-d	0	-(h-r)

Table 3.22a. Non-holonomic Partial Velocities for the Steer-Drive Wheel (Left-Front)

	$\bar{v}_i^{W_p}$	$\bar{\omega}_i^{W_f}$	$\bar{\omega}_i^{W}$
u_1	0	$-\frac{1}{d}s\phi\ {}^1n_3$	$-\frac{1}{d}s\phi\ {}^1n_3+\frac{1}{r}c\phi\ {}^2n_2$
u_2	0	$\frac{1}{d}c\phi\ {}^1n_3$	$\frac{1}{d}c\phi\ {}^1n_3+\frac{1}{r}s\phi\ {}^2n_2$
u_3	${}^1n_3$	0	0
u_4	$h\ {}^1n_2+(b-ds\phi)\ {}^1n_3$	${}^1n_1$	${}^1n_1$
u_5	$-h\ {}^1n_1-(l-dc\phi)\ {}^1n_3$	${}^1n_2$	${}^1n_2$
u_6	0	$\frac{(bs\phi+lc\phi)}{d}\ {}^1n_3$	$\frac{(bs\phi+lc\phi)}{d}\ {}^1n_3$ $+\frac{(ls\phi-bc\phi)}{r}\ {}^2n_2$

Table 3.22b Partial velocities of the mass centre, D, of WMR

	u_1	u_2	u_3	u_4	u_5	u_6
$\bar{v}_i^D$	${}^1\boldsymbol{n}_1$	${}^1\boldsymbol{n}_2$	${}^1\boldsymbol{n}_3$	0	0	0
$\bar{\omega}_i^D$	0	0	0	${}^1\boldsymbol{n}_1$	${}^1\boldsymbol{n}_2$	${}^1\boldsymbol{n}_3$

Table 3.23a Generalised Active Forces for the Left-Front unit for 'actual' speeds.

	u_1	u_2	u_6
F_i^1	$-\frac{\tau_s^1}{d}s\phi+\frac{(\tau_d^1+\tau_f^1)}{r}c\phi$	$\frac{\tau_s^1}{d}c\phi+\frac{(\tau_d^1+\tau_f^1)}{r}s\phi$	$\frac{(b\,s\phi+l\,c\phi)}{d}\tau_s^1$ $+\frac{(l\,s\phi-b\,c\phi)}{r}(\tau_d^1+\tau_f^1)$

Table 3.23b Generalised Active Forces for the Left-Front unit for 'virtual' speeds

	u_3	u_4	u_5
F_i^1	Q_3^1	$(h\,c\phi)Q_2^1+(b-d\,s\phi)Q_3^1$	$(h\,s\phi)Q_2^1-(l-d\,c\phi)Q_3^1$

Table 3.24 Generalised Active Forces for the centre of mass D

	u_1	u_2	u_3	u_4	u_5	u_6
F_i^D	0	0	$-m_d g$	$\tau_d^k s\phi^k$	$-\tau_d^k c\phi^k$	$-\tau_s^k$

Table 3.25 Generalised Inertial Forces for the centre of mass, D.

	u_1	u_2	u_3	u_4	u_5	u_6
$\bar{F}^{*D}$	$-m_d(\dot{u}_1-u_2u_6)$	$-m_d(\dot{u}_2+u_1u_6)$	0	0	0	$-I_3^d\dot{u}_6$

3.5.4 A Differentially Driven WMR carrying a suspended load

In order to illustrate the application of the proposed modelling scheme to WMRs carrying active payloads, a differentially driven WMR carrying a suspended load is analyzed. Since the addition of the suspended load does not affect the non-holonomic nature of the WMR, the dynamic equations for the particular wheel configuration may simply be augmented with the generalised active and inertia terms for the load. As mentioned in Section 3.2, this special feature offered by the proposed modelling scheme is an advantage over the Newton-Euler and the Lagrangian methods.

In order to illustrate the methodology , the differentially driven WMR used in the case study in Section 3.5.2 is assumed to carry a suspended load, as shown in Fig.3.12. The load is suspended from a point, H, along the longitudinal axis of the WMR. The load is suspended by a sling of length, z, and is free to swing along the lateral plane of the WMR. The angle of swing, ζ, and the generalised speed, $u_7 = \dot{\zeta}$ are used to describe the motion of the load.

In the following derivation, only the generalised active and the generalised inertia terms for the suspended load for the generalised speeds are obtained. In the assembly of the dynamic equations in Step 5, all the results obtained in Section 3.5.2 for the WMR alone are used along with the results obtained here to obtain the equations of motion for the WMR - suspended load coupled system.

Step 1. Non-holonomic equations

Since the non-holonomic equations of the WMR are already available, Eqn.(3.56, 3.57) and the suspended load is a holonomic system, this step is redundant in this derivation.

Step 2. Partial Velocities

The velocity of the centre of mass, E, of the suspended load is obtained from Eqn.(3.42) using the geometrical values shown in Fig.3.12. Substituting the values of the geometric parameters for the load in the terms given in Table 3.9, the partial velocities of the centre of mass, E, of the load are obtained and are listed in Table 3.26.

Step 3. Generalised Active Forces

The active forces are the gravitational force, $-m_E g\,{}^1\boldsymbol{n}_3$, acting at the centre of mass, E and the frictional torque, $\tau_f^E\,{}^3\boldsymbol{n}_1$, due to sliding friction at the point of suspension. Using the partial velocities in Table 3.26, the generalised active forces for the seven generalised speeds are obtained and are listed in Table 3.27.

Step 4: Generalised Inertia Forces

The acceleration of the centre of mass, E, given by Eqn.(3.46) is

$$\begin{aligned} {}^O\boldsymbol{a}_E &= \frac{\mathrm{d}}{\mathrm{dt}}\,{}^O\boldsymbol{v}_E \\ &= (\dot{u}_1 - z\dot{u}_6 s\zeta - i u_6^2 - 2z u_7 u_6 c\zeta)\,{}^1\boldsymbol{n}_1 \\ &\quad + (i\dot{u}_6 + z\dot{u}_7 c\zeta + u_1 u_6 - z u_6^2 s\zeta - z u_7^2 s\zeta)\,{}^1\boldsymbol{n}_2 \\ &\quad + (z\dot{u}_7 s\zeta + z u_7^2 c\zeta)\,{}^1\boldsymbol{n}_3 \end{aligned} \tag{3.70}$$

and the angular acceleration, Eqn.(3.47) is

$$\begin{aligned} {}^O\boldsymbol{\alpha}_E &= \frac{\mathrm{d}}{\mathrm{dt}}\,{}^O\boldsymbol{\omega}_E \\ &= \dot{u}_7\,{}^1\boldsymbol{n}_1 + u_7 u_6\,{}^1\boldsymbol{n}_2 + \dot{u}_6\,{}^1\boldsymbol{n}_3 \end{aligned} \tag{3.71}$$

Using the acceleration, Eqn.(3.71), the inertia force acting on the mass centre, E, is

$$F^{*E} = -m_E\, {}^{O}a_E \tag{3.72}$$

and the inertia torque, Eqn.(3.5), is

$$\begin{aligned} T^{*E} = & -\left[I_1^E \dot{u}_7 - u_6^2 s\zeta\, c\zeta\, (I_2^E - I_3^E)\right] {}^3\boldsymbol{n}_1 \\ & -\left[(u_7 u_6 c\zeta + \dot{u}_6 s\zeta) I_2^E - u_7 u_6 c\zeta\, (I_2^E - I_3^E)\right] {}^3\boldsymbol{n}_2 \\ & -\left[(-u_7 u_6 s\zeta + \dot{u}_6 c\zeta) I_3^E - u_7 u_6 s\zeta\, (I_1^E - I_2^E)\right] {}^3\boldsymbol{n}_3 \end{aligned} \tag{3.73}$$

where, with no loss of generality, I_i^E are the principal moments of inertia of the load for the centre of mass, E, and the ${}^3\boldsymbol{n}_i$ axes are the principal axes. The generalised inertia forces corresponding to the generalised speeds for the load are listed in Table 3.28.

Step 5: Assembly

The terms representing the generalised active forces, Table 3.27 , and the generalised inertia forces, Table 3.28, for the generalised speeds, u_1 and u_6 , are added to the dynamic equations of the differential drive WMR, Eqn.(3.63), to obtain the dynamic equations of the WMR with a suspended load. The generalised force terms for u_7 provide the dynamic equation for the suspended load. The dynamic equations for the WMR and the suspended load may be expressed as

$$[M(q)]\{\dot{u}\} = [D(u,q)] + \{\tau\} \tag{3.74}$$

where the generalised coordinate, $q = \{\zeta\}$, the vector of generalised speeds, $u = \{u_1\ u_6\ u_7\}^T$ and the vector of generalised accelerations, $\{\dot{u}\} = \{\dot{u}_1\ \dot{u}_6\ \dot{u}_7\}^T$.

In Eqn.(3.74), the symmetric mass matrix, $[M(q)]$ is

$$\begin{bmatrix} m_D+2m_W+m_E+\frac{2}{r^2}I_2^W & -zm_E s\zeta & 0 \\ -zm_E s\zeta & 2b^2(m_W+\frac{I_2^W}{r^2})+I_3^E+2I_1^W+m_E(z^2s^2\zeta+i^2)+I_2^E s^2\zeta+I_3^E c^2\zeta & zim_E c\zeta \\ 0 & zim_E c\zeta & z^2m_E+I_1^E \end{bmatrix}$$

The cross coupling matrix expressing the Coriolis and centrifugal terms, $[D(u,q)]$ is

$$\begin{bmatrix} im_E u_6^2+2zm_E u_7 u_6 c\zeta \\ u_7 u_6 s2\zeta(I_3^E-I_2^E-z^2m_E)-im_E u_1 u_6+zim_E u_7^2 s\zeta \\ -\frac{1}{2}u_6^2 s2\zeta(I_3^E-I_2^E-z^2m_E)-zm_E u_1 u_6 c\zeta \end{bmatrix}$$

and the drive and frictional torques, $\{\tau\}$, are

$$\begin{Bmatrix} \frac{(\tau_d^l+\tau_d^r)}{r}+\frac{(\tau_f^l+\tau_f^r)}{r}+\frac{(\tau_f^f+\tau_f^b)}{r}c\delta \\ \frac{b}{r}(\tau_d^r-\tau_d^l)+\frac{b}{r}(\tau_f^r-\tau_f^l)+\frac{l}{r}s\delta(\tau_f^f+\tau_f^b) \\ -zm_E g s\zeta+\tau_f^E \end{Bmatrix}$$

Finally, the constraint forces acting at the wheels of the WMR and the corresponding rolling frictional torque are obtained by augmenting the constraint equations, Eqn.(3.64), with the generalised active forces, Table 3.27 and generalised inertia forces, Table 3.28 for the generalised speeds, u_2 .. u_5 . In addition to the four equations obtained, two further equations based on the wheel configuration are used to solve for the six constraint forces. Since the drive wheels are symmetric about the longitudinal axis of the WMR, the lateral constraint force at the right drive wheel is assumed equal to the lateral force on the left wheel. The

vertical load on the wheels and the castors depends on the dead weight due to the body of the WMR, m_D, and the live load of the suspended mass, m_E; in addition, each wheel carries the weight of the wheel unit, m_W. The sum of the vertical load on the two drive wheels is assumed to be the weight of the two drive units in addition to half of the dead weight plus the live load. The two castors carry half of the dead weight and the live load. The load on each wheel or on each castor depends on the coupled dynamics of the WMR and the load and is calculated using the constraint equations.

Using the generalised active and inertia forces for u_2, the lateral constraint forces are

$$Q_2^r + Q_2^l = (m_d + 2m_w + m_E)u_1u_6 + im_E\dot{u}_6 + zm_E\dot{u}_7c\zeta - zs\zeta(u_6^2 + u_7^2) \qquad \textbf{(3.78)}$$

where, due to symmetry, $Q_2^r = Q_2^l$

The sum of the vertical loads on the wheels are obtained from the generalised force terms for u_3 as

$$Q_3^r + Q_3^l = \frac{1}{2}[g(m_d + m_E) + m_E(z\dot{u}_7s\zeta + zu_7^2c\zeta)] + 2m_w \qquad \textbf{(3.79)}$$

and the total vertical load on the castors are

$$Q_3^f + Q_3^b = \frac{1}{2}[g(m_d + m_E) + m_E(z\dot{u}_7s\zeta + zu_7^2c\zeta)] \qquad \textbf{(3.80)}$$

Using the generalised force terms for u_5, the difference of the vertical loads on the castors induced by the motion of the WMR-suspended load system is

$$
\begin{aligned}
I(Q_3^b - Q_3^f) = & -im_E g + \dot{u}_1\left[\frac{2}{r}I_2^w - 2m_w(h-r) + m_E(k - zc\zeta)\right] \\
& - m_E(k - zc\zeta)(z\dot{u}_6 s\zeta + iu_6^2 + 2zu_7 u_6 c\zeta) \\
& + I_1^E u_7 u_6 + (I_3^E - I_2^E)(u_7 u_6 c2\zeta + \dot{u}_6 c\zeta s\zeta) \\
& - im_E(z\dot{u}_7 s\zeta + zu_7^2 c\zeta) + dc\delta(Q_3^f + Q_3^b)
\end{aligned}
\tag{3.81}
$$

The difference between the vertical loads on the right and the left wheels is obtained using the generalised forces for u_4 as

$$
\begin{aligned}
b(Q_3^l - Q_3^r) = & zm_E g s\zeta - \tau_f^E - m_E k(i\dot{u}_6 + z\dot{u}_7 c\zeta - zu_6^2 s\zeta - zu_7^2 s\zeta) \\
& + u_1 u_6\left[2m_w(h-r) - m_E(k - zc\zeta) - \frac{2}{r}(I_2^w - 2I_1^w)\right] \\
& + zm_E(i\dot{u}_6 c\zeta + z\dot{u}_7 - zu_6^2 c\zeta s\zeta) + ds\delta(Q_3^b - Q_3^f) \\
& + [I_1^E \dot{u}_7 - u_6^2 s\zeta c\zeta(I_2^E - I_3^E)] + h(Q_2^l + Q_2^r)
\end{aligned}
\tag{3.82}
$$

The dynamic vertical loads on each wheel and castor are then obtained as

$$
\begin{aligned}
Q_3^r &= \frac{(Q_3^r + Q_3^l)}{2} + \frac{(Q_3^r - Q_3^l)}{2} \\
Q_3^l &= \frac{(Q_3^r + Q_3^l)}{2} - \frac{(Q_3^r - Q_3^l)}{2} \\
Q_3^f &= \frac{(Q_3^f + Q_3^b)}{2} + \frac{(Q_3^f - Q_3^b)}{2} \\
Q_3^b &= \frac{(Q_3^f + Q_3^b)}{2} - \frac{(Q_3^f - Q_3^b)}{2}
\end{aligned}
\tag{3.83}
$$

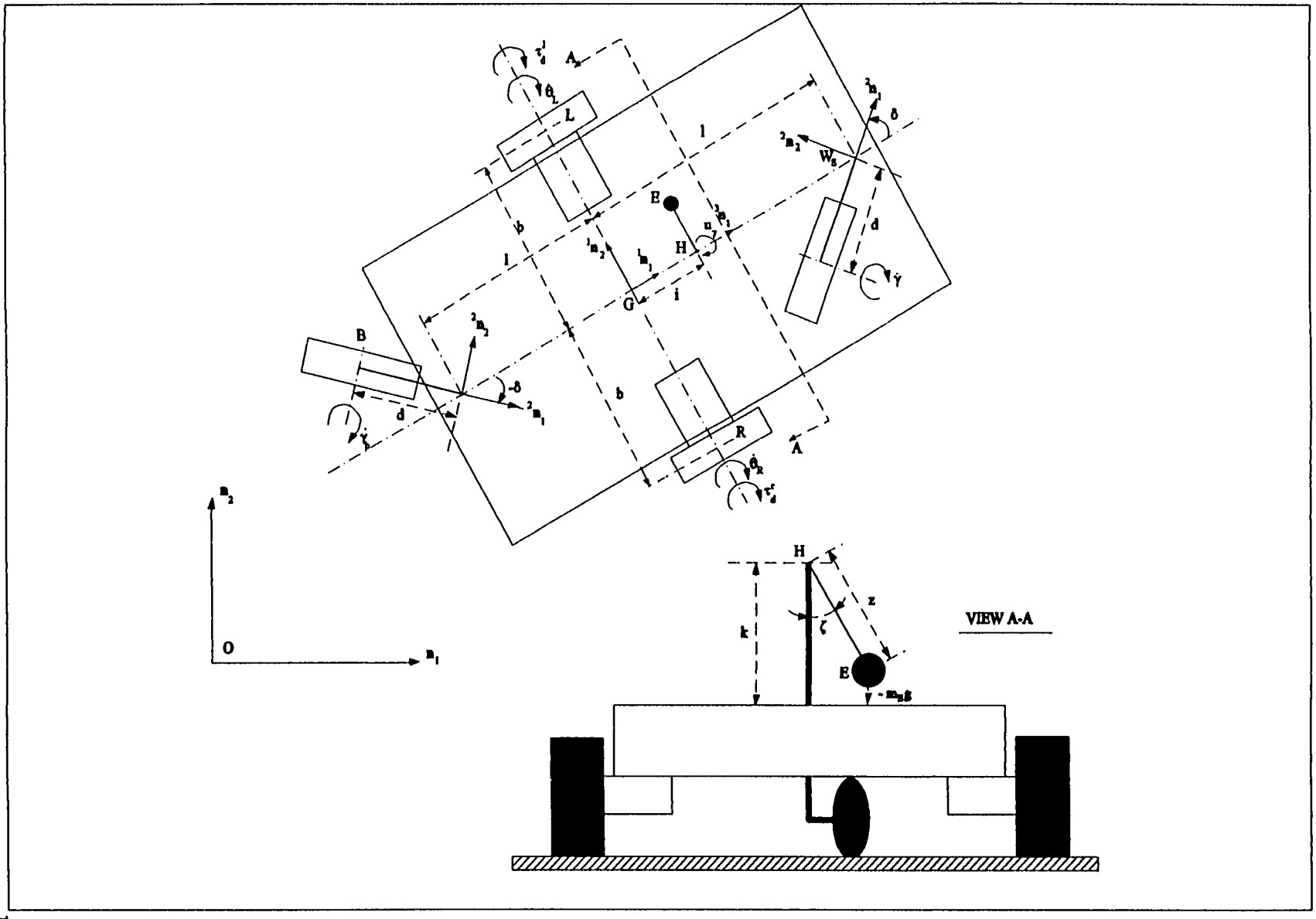

Figure 3.12 Geometric Parameters of a Differential Drive WMR with a Suspended Load.

Table 3.26 Partial Velocities of the centre of mass, E, of the suspended load.

	$\bar{v}_i^E$	$\bar{\omega}_i^E$
u_1	${}^1n_1$	0
u_2	${}^1n_2$	0
u_3	${}^1n_3$	0
u_4	$-(k-zc\zeta){}^1n_2+zs\zeta{}^1n_3$	${}^1n_1$
u_5	$(k-zc\zeta){}^1n_1-i{}^1n_3$	${}^1n_2$
u_6	$-zs\zeta{}^1n_1+i{}^1n_2$	${}^1n_3$
u_7	$zc\zeta{}^1n_2+zs\zeta{}^1n_3$	${}^1n_1$

Table 3.27 Generalised Active Forces for the Live Load

	$\tilde{F}_i^E$
u_1	0
u_2	0
u_3	$-m_E g$
u_4	$-zm_E gs\zeta+\tau_f^E$
u_5	$im_E g$
u_6	0
u_7	$-zm_E gs\zeta+\tau_f^E$

Table 3.28 Generalised Inertia Forces for the Generalised Speeds for the Live Load.

	$\tilde{F}_i^{*E}$
u_1	$-m_E(\dot{u}_1 - z\dot{u}_6 s\zeta - iu_6^2 - 2zu_7u_6c\zeta)$
u_2	$-m_E(i\dot{u}_6 + z\dot{u}_7c\zeta + u_1u_6 - zu_6^2s\zeta - zu_7^2s\zeta)$
u_3	$-m_E(z\dot{u}_7s\zeta + zu_7^2c\zeta)$
u_4	$km_E(i\dot{u}_6 + z\dot{u}_7c\zeta + u_1u_6 - zu_6^2s\zeta - zu_7^2s\zeta) - zm_E(i\dot{u}_6c\zeta + u_1u_6c\zeta - zu_6^2c\zeta s\zeta)$ $-\left[I_1^E\dot{u}_7 - u_6^2s\zeta c\zeta(I_2^E - I_3^E)\right]$
u_5	$-m_E(k - zc\zeta)(\dot{u}_1 - z\dot{u}_6s\zeta - iu_6^2 - 2zu_7u_6c\zeta) + im_E(z\dot{u}_7s\zeta + zu_7^2c\zeta)$ $-(I_3^E - I_2^E)(u_7u_6c2\zeta + \dot{u}_6c\zeta s\zeta) - I_1^Eu_7u_6$
u_6	$zm_Es\zeta(\dot{u}_1 - z\dot{u}_6s\zeta - 2zu_7u_6c\zeta) - im_E(i\dot{u}_6 + z\dot{u}_7c\zeta + u_1u_6 - zu_7^2s\zeta)$ $+(I_3^E - I_2^E)u_7u_6s2\zeta - I_2^E\dot{u}_6s^2\zeta - I_3^E\dot{u}_6c^2\zeta$
u_7	$-m_E(iz\dot{u}_6c\zeta + zu_1u_6c\zeta - z^2u_6^2c\zeta s\zeta + z^2\dot{u}_7)$ $I_1^E\dot{u}_7 + (I_2^E - I_3^E)u_6^2s\zeta c\zeta$

3.6 Summary

Using the Kane's approach, a generalised 5-step procedure has been developed to deduce the dynamics of a WMR with common wheel types and wheel configurations and subject to both deadweight and active payload conditions. In the derivation of the dynamic equations, this approach permits the use of any natural set of generalised speeds representing the degrees of freedom of the non-holonomic system. Consequently, in this approach there are only as many dynamic equations as there are degrees of freedom unlike the redundant set of equations obtained in both the Newton-Euler and the Lagrangian approaches. The proposed modelling scheme incorporates closed-chains and higher pair joints and incorporates friction as well as unsensed and unactuated joints. Using 'virtual' generalised speeds, the method also provides a set of linear equations to obtain the dynamic loads experienced by the wheels during motion.

The first step in this proposed scheme is to obtain the non-holonomic equations for the specific wheel configuration and for the types of wheels used in the WMR being analyzed. Partial velocities and partial angular velocities of specific points of interest, such as the mass centres of the various rigid bodies, are then obtained in step 2. These partial velocities embody the motion constraints present in the system due to which the action of a force is propagated to all the components in the closed chain. In step 3, the generalised active forces arising from the applied forces and torques on each rigid body for each independent generalised speed are obtained. Correspondingly, the generalised inertia force terms due to the mass and the inertia of the various rigid bodies in the WMR are obtained in step 4. The final step is an assembly of the generalised active and generalised inertia force terms to obtain

the dynamic equations of the system.

The steer-drive wheel has been utilised as the generic wheel type in the derivation of the dynamic equations. The simplifications and substitutions to be made when the generic model is applied to other wheel types have been discussed and results have been tabulated for ease of reference. In order to account for the different loading conditions, the five step procedure has been applied to a deadweight payload which includes the body of the WMR itself. A suspended load with a single rotational degree of freedom has been analyzed in order to illustrate the case of active loads. A general geometric configuration for the suspended load has been employed and the results have been tabulated. Thus the procedure, the assembly methodology and the results presented for the generic model may be applied to a WMR with any specific wheel configuration.

In addition, the proposed methodology addresses the issue of modelling the dynamic loads on the wheels of a WMR by introducing 'virtual' generalised speeds. In the literature, these wheel loads, which depend on the applied and inertial forces, are simplified to be constants and equal to the static loads on the wheels. In order to obtain the wheel loads, the same 5-step procedure is applied for each 'virtual' generalised speed. The dynamic equations obtained for these generalised speeds provide a set of linear equations which are solved to obtain the constraint forces acting on the wheels. These constraint forces are required to model the rolling and steering friction forces acting at the points of contact of the wheels and castors on the ground. For model based control of systems where joint friction is dominant such as in a WMR, knowledge of the constraint and friction forces at the wheels is essential. The effect of the trajectory parameters and the nature of the load carried by the WMR on tire

friction forces must also be computed in traction limited motion to avoid wheel slippage and consequent loss of trajectory following accuracy.

The application of the proposed modelling scheme to a specific WMR has been illustrated using four case studies. The wheel configuration used in each case has been chosen from literature. A WMR with a steer-drive wheel in front and two castors at the rear in a tri-cycle configuration has been chosen as Case 1. The geometric values for this configuration have been substituted in the tabulated results for the wheel types in order to obtain the generalised active and inertia forces. 'Virtual' generalised speeds have been used to obtain both the lateral and the vertical wheel loads. A differentially driven WMR with two independently driven wheel units in the lateral plane and two free wheeling castors in the longitudinal plane has been used for the second case. The experimental platform, CONCIC III, employs this wheel configuration. An omnidirectional WMR with four independent steer-drive wheel units has been used as the third case. This configuration provides three degrees of freedom to the WMR. In these three cases the WMR is assumed to carry a deadweight. In order to illustrate application to active payloads, the differentially driven WMR in Case 2 is analyzed while carrying a suspended load. The set of dynamic equations and the system of equations for the constraint forces acting on the wheels for each case have been provided.

Chapter 4

Model Based Control

4.1 Introduction

The literature review on the control of mobile and stationary robots presented in Chapter 2 indicates that the inclusion of the dynamics of the robot in the control structure improves the trajectory tracking performance [e.g., 15, 39, 44, 45]. In the case of mobile robots, the only reported experimental work on model-based control was carried out at the Centre for Industrial Control (CIC), Dept. of Mechanical Engineering, Concordia University, Montreal [13, 15, 48]. This work, though the pioneering work in model based control of mobile robots, was limited in two respects:

(i) the control structure focusses on modifying only the vehicle speed based on the error information ;

(ii) studies only the effects of changes in the dead weight carried by the vehicle on the the trajectory tracking performance.

This thesis addresses two control issues not dealt with in the literature for WMRs. The first issue deals with the structure of the controller for dynamic compensation. The second issue focusses on studying the effect of and the compensation scheme for live loads (dynamic loads such as a suspended mass). These two issues have been addressed as these are mainly industrial applications requiring control schemes that could assure good trajectory following performance with changes in the dynamics of the vehicle and in the operating environment.

The literature provides a large number of schemes for model based control of dynamic systems, the Feed Forward and the Resolved Acceleration Control being two such schemes

implemented for process control applications and for robot manipulators. The investigations reported in this chapter include the suitability and the performance of a feedforward compensation scheme making use of the inverse dynamics of the WMR along with a conventional PD feedback scheme. A similar approach was adopted to control the MIT DDArm by An, Atkeson and Hollerbach [39].

Control of robot arms using the model based scheme, the Resolved Acceleration Control, was proposed by Luh, Walker and Paul [40] and an implementation has been reported earlier in the literature [39]. This thesis adopts a similar structure for the Resolved Acceleration control scheme. The inverse dynamic model of the WMR is used to compute the actuator torques as in the case of robot manipulators [39, 40] and of WMRs by Barakat and Rajagopalan [13, 15, 48]. In a serial manipulator, the forces propagate from the end effector to the base while the velocities propagate from the base to the end effector. The same is not true for WMRs. In the case of WMRs, there is strong coupling between the joints and hence a control scheme that worked well for robot arms may not produce the same performance for WMRs.

The control problem examined here is the execution of a pre-planned trajectory by the WMR under active and deadweight payload conditions. Trajectory in this context implies a parametric two dimensional path in the Cartesian x-y plane with time as the parameter. The actual trajectory followed by the WMR is evaluated by dead reckoning using measured values of wheel speeds. In this work, cartesian position feedback, using camera vision [3] for example, is not used since the focus is on the dynamic model of the WMR and on model based control schemes. With dead reckoning, the trajectory is planned off-line and the desired

cartesian position, velocity and acceleration for every sampling instant of the digital controller are stored in a look up table in the computer memory. Using measured values of wheel speeds and the non-holonomic equations, the actual cartesian trajectory parameters are evaluated. It must be pointed out that the model based control schemes in *this thesis do not require actual acceleration* values and hence these are neither measured nor evaluated.

The control algorithms applied to the modified CONCIC II [15], labelled as CONCIC III, the differentially driven WMR described in Section 1.3 and used for the experimental work in this thesis are detailed in this chapter. The Independent Joint PD Controller using the joint position and velocity feedback of each actuator/wheel is discussed in Section 4.2.1. In Section 4.2.2, the Cartesian PD Controller, a variation of the Independent Joint PD controller using the independent cartesian speeds of the WMR is proposed. The Feed Forward (FF) controller, a model based controller using the dynamic model only for off-line calculations of the drive torque, is discussed in Section 4.3. Finally, the Computed Torque (CT) controller which utilises the dynamic model to compute the actuator drive torques on-line during WMR motion is discussed in Section 4.4. The cartesian version of the CT control scheme, also termed the Resolved Acceleration control scheme, is discussed in Section 4.4.1. A variation of the CT control scheme which computes and uses resolved joint accelerations for torque calculations is presented in Section 4.4.2. The performances of these controllers are studied by simulation in Chapter 6 and are validated through experimentation, the results of which are given in Chapter 7.

4.2 Proportional-Derivative (PD) Controller

The literature review indicates that PD controllers have been widely used for stationary robots and for WMRs as well. Due to this popularity of PD controllers and the availability of published results, the performances of the dynamic model based controllers are compared in this thesis with that of the conventional PD controller. The PD controllers are driven entirely by errors in the (kinematic) motion parameters and utilize neither the dynamic model nor any known inertial properties of the system under control.

The PD controller may be classified as joint level or cartesian level depending on the nature of the feedback signals used by the controller. In a joint level PD controller, the desired trajectory is specified in terms of the position and velocity of each joint as functions of time. In the case of a WMR, the angular position and the rotational speed of each wheel (driving and steering) are specified. Measured values of wheel speed and position are then used during trajectory execution to compute the controller output. In the case of the serial link stationary robots, the joint speeds form a set of linearly independent generalised speeds and an independent PD controller may be applied to each joint. Due to this nature, in robotic literature, PD controllers are called Independent Joint PD controllers [39, 74]. However, in the case of a WMR, all the generalised speeds are not linearly independent and the Jacobian matrix is sometimes rank deficient. Due to the motion constraints in a WMR, the joints may not be decoupled and independent PD controllers used for each joint as in stationary robots. Thus, for a WMR, the PD controller may be designed to use any convenient set of independent generalised speeds for feedback.

The Cartesian PD controller formulated in this thesis uses position and velocity errors

in the inertial floor frame which is the task space of the WMR. For example, for the discussions on the dynamics in Chapter 3, it was shown that the cartesian speeds of the differentially driven WMR are represented by the generalised speeds u_1 and u_6 which are the forward speed and the yaw rate of the WMR. The generalised speeds are available either by direct measurement or by estimation using measured joint speeds and the non-holonomic equations. Generalised position of the WMR in the inertial floor frame is represented by the path length and by the orientation of the WMR. These values are obtained by integrating the non-holonomic equations using measured joint speeds. The joint speeds are obtained using either tachometers or optical encoders. Direct measurement of the cartesian position and velocity values is less popular and has been applied to stationary robots using gyros or optical triangulation schemes, to name two methods. Cost and the lack of instruments to accurately measure and provide the information in real-time are the main reasons for this approach to be less popular.

4.2.1 Independent Joint PD Controller

As mentioned earlier, in a joint level PD controller, errors in each joint's position and speed are used to compute the controller output. For each independent joint, the control output is calculated using the PD control algorithm as

$$\begin{aligned} \tau_d &= [K_v]\{e_{\dot{\theta}}\} + [K_p]\{e_{\theta}\} \\ e_{\dot{\theta}} &= \dot{\theta}_d - \dot{\theta}_a \\ e_{\theta} &= \theta_d - \theta_a \end{aligned} \tag{4.1}$$

where e_{θ} , $e_{\dot{\theta}}$ are the joint position and velocity errors. The desired joint position is θ_d , and

the joint velocity is $\dot{\theta}_d$. The desired trajectory for stationary and for mobile robots is normally specified in terms of cartesian values only. In the case of stationary robots which are holonomic systems, the cartesian values may be converted into joint values using the inverse kinematic formulation. For the non-holonomic WMR systems, the desired cartesian values are converted to desired joint values, namely the desired joint positions (θ_d) and the desired joint velocities $(\dot{\theta}_d)$, by numerically integrating the non-holonomic relations from some known initial condition. The actual joint positions, (θ_a) and velocities, $(\dot{\theta}_a)$ are directly measured using a feedback device such as an encoder. In the case of non-redundant stationary robots which are holonomic systems , each joint provides a degree of freedom for the robotic system when the end effector is moving freely without making contact with the environment. Hence, for robotic systems where the number of actuated joints equals the number of degrees of freedom (without redundancy), a joint PD controller may be applied to each of the actuated joints. Position and velocity of each joint are measured and used by the controller. However, for a non-holonomic system such as a WMR, the number of actuated joints sometimes exceeds the number of degrees of freedom. In this case, if Independent Joint PD controllers are applied to all the actuated joints, wheel slip and consequent loss of control will result. A number of independent joints representing the degrees of freedom of the mobile robot are chosen by the designer and the joint level PD controller is applied only to those joints. The control output for the other joints are calculated as functions of the independent control values using kinematic model of the WMR. The structure of the Independent Joint PD controller for a general WMR system is shown in Fig.4.1. The WMR in Fig.4.1 has M number of actuated joints but is assumed to have only N degrees of freedom, with ($N \leq M$). In this

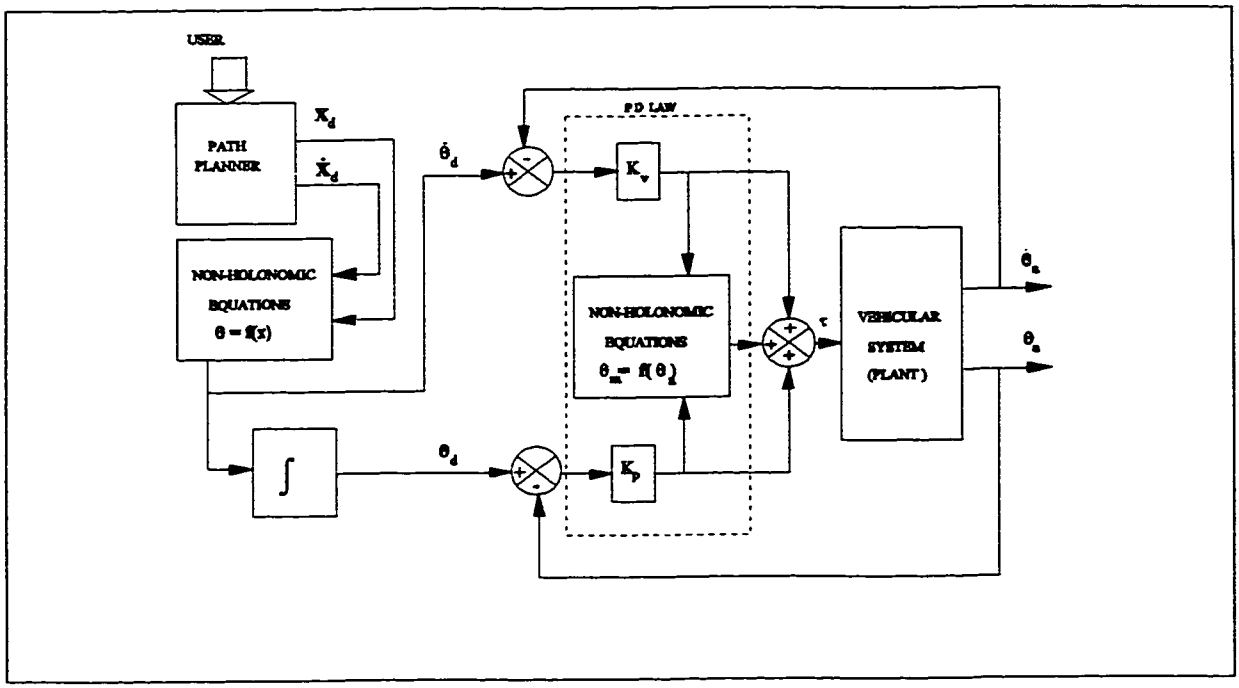

Figure 4.1 Independent Joint Proportional Derivative (PD) Control Scheme for a WMR with N-degrees of freedom and M actuated joints (M ≥ N).

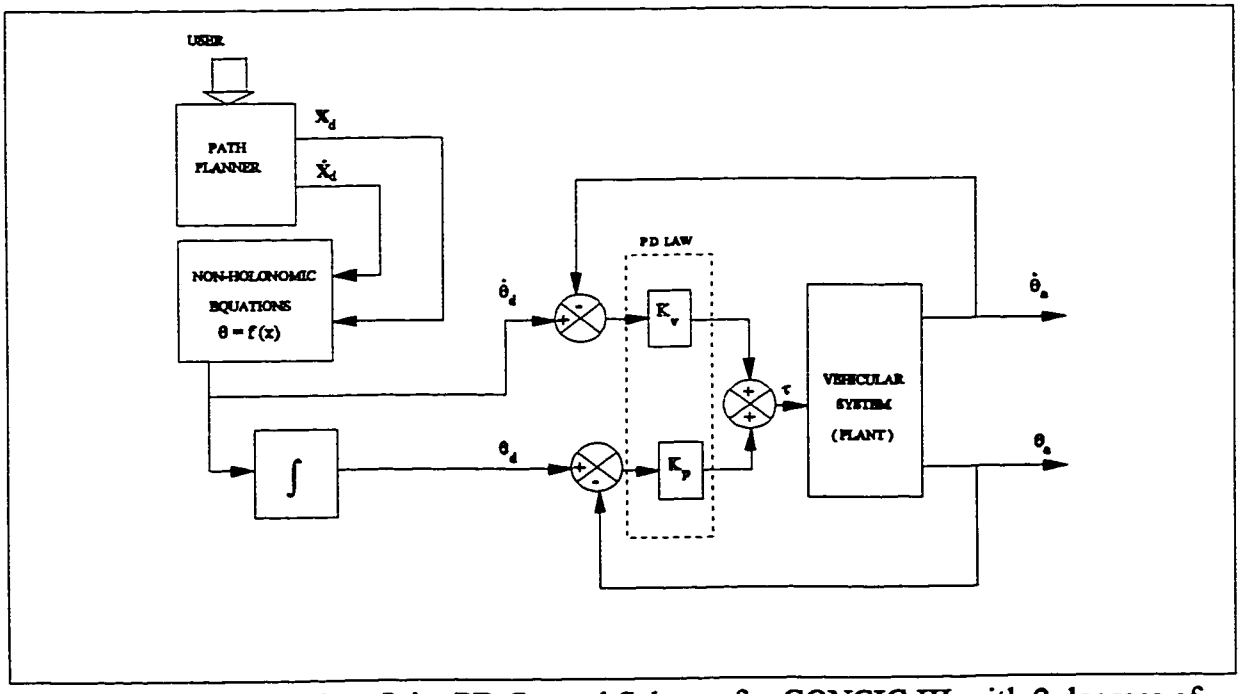

Figure 4.2 Independent Joint PD Control Scheme for CONCIC III with 2 degrees of freedom and 2 actuated joints.

case only N of the joints may be independently actuated while the other (M - N) joints are kinematically constrained. In this case only the N independent joint positions and velocities are measured and used by the N number of Independent Joint PD controllers. The controller output for the other (M-N) joints is computed using the non-holonomic equations as

$$\{\tau\}_{m-n} = [J]_{(m-n)m}\{\tau\}_n \qquad (4.2)$$

where the matrix and the vector dimensions are denoted by the subscripts. **J** is the Jacobian matrix that provides the non-holonomic relations between the independent and the dependent joint speeds.

For the differentially driven CONCIC III with one pair of differentially driven wheel units, the number of degrees of freedom of the system equals the number of actuated joints, namely 2. In this case the Independent Joint PD controller may be applied to each actuated joint. For the CONCIC III, the feedback PD control loop for one joint is shown in Fig.4.2. For this WMR, N equals M in Eqn.(4.2) and an Independent Joint PD controller provides the drive output for each actuated joint. Hence, the non-holonomic relations do not appear in the control loop.

4.2.2 Cartesian PD Controller

The WMR operates in the inertial floor frame and any cartesian frame attached to the floor frame may be regarded as the task space of the mobile robot. The cartesian coordinates then form the natural choice to specify the trajectory of the WMR. The number of degrees of freedom dictates the number of independent cartesian speeds that may be specified for the

trajectory of the WMR. The Cartesian PD controller, Fig.4.3, uses errors in the cartesian kinematic values to compute the control output. The control output is then converted to actuator drive torques using the non-holonomic equations. Using the cartesian kinematic errors, the control output vector, **c** , from the Cartesian PD controller is obtained as

$$\begin{aligned} \{c\} &= [K_v]\{e_u\} + [K_p]\{e_s\} \\ e_u &= u_d - u_a \\ e_s &= s_d - s_a \end{aligned} \tag{4.3}$$

where **u** is the vector of cartesian speeds and **s** is the cartesian position. The control output vector is the set of corrective forces applied in the cartesian coordinate system. The corrective drive torques for the drive wheels are obtained by equating the power input to the WMR in the cartesian and joint systems as

$$u^T \cdot c = \theta^T \cdot \tau \tag{4.4}$$

Using the non-holonomic equations to eliminate the speeds, the drive torques are given by

$$\tau = [J]^T c \tag{4.5}$$

The control scheme for the Cartesian PD controller applied to the CONCIC III is shown in Fig.4.4. Corresponding to the 2 degrees of freedom, the cartesian speeds chosen are the two independent generalised speeds, namely, the forward speed, u_1 and the yaw rate, u_6 . Integrating the speeds, the desired cartesian position values specified in the trajectory are the path length, s_1 , and the orientation angle, ψ . The path length and the orientation are computed with respect to some user specified origin in the inertial floor frame. In this thesis,

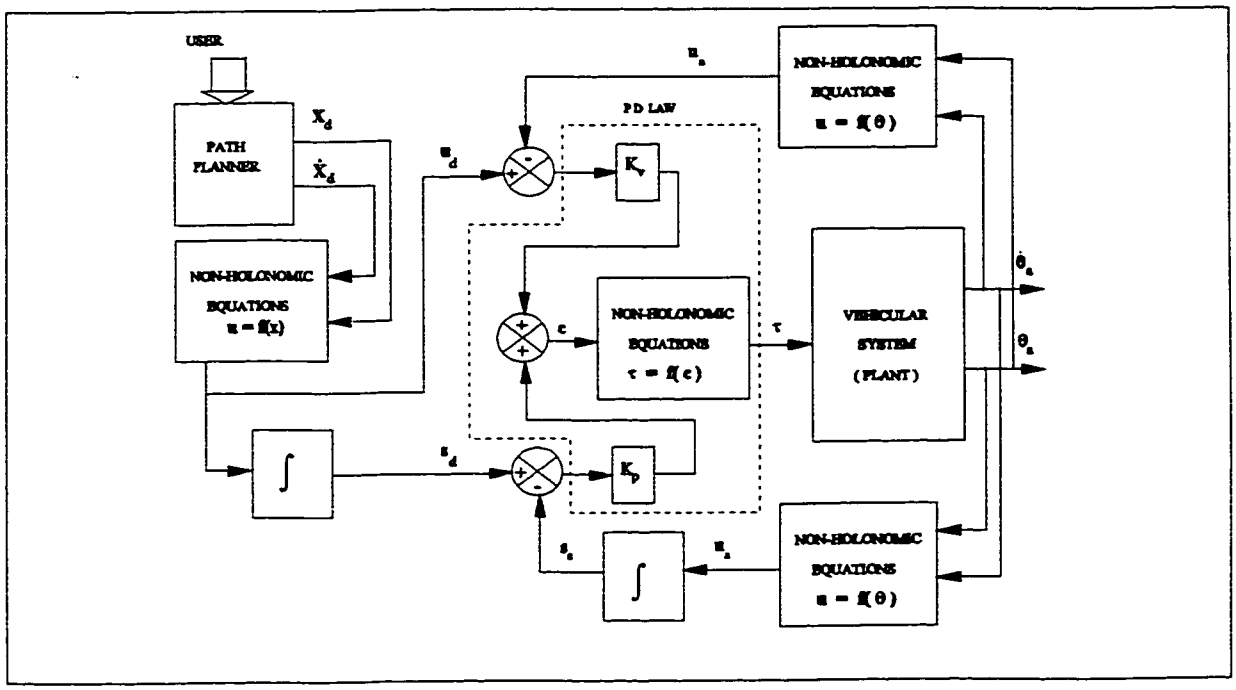

Figure 4.3 Cartesian PD Control Scheme for a WMR with feed back of joint parameters.

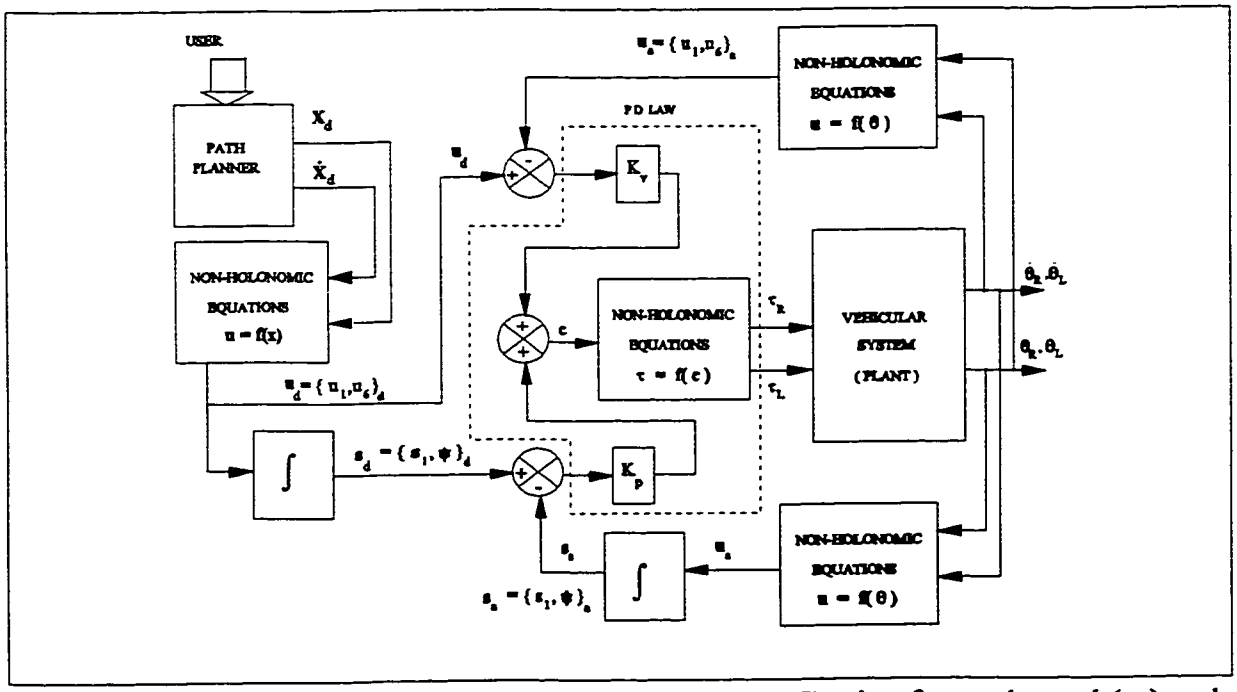

Figure 4.4 Cartesian PD Control Scheme for CONCIC III using forward speed (u_1) and yaw rate (u_6) and feed back of right and left wheel speeds.

at the commencement of the trajectory, the floor frame and the coordinate frame fixed to the WMR are assumed to be coincident and aligned with each other. The forward speed, u_1, of the WMR is integrated to provide the path length from the origin of the floor frame. In Fig.4.4, the generalised speeds are shown by the vector, **u**, and the cartesian positions by **s**. Using the kinematic errors, the control output vector, c_1, from the Cartesian PD controller applied to the forward speed is obtained as

$$\begin{aligned} c_1 &= K_v * \dot{e}_{u_1} + K_p * e_{s_1} \\ \dot{e}_{u_1} &= u_{1d} - u_{1a} \\ e_{s_1} &= s_{1d} - s_{1a} \end{aligned} \tag{4.6}$$

where the cartesian path length, $s_1 = \int_0^T u_1 dt$.

Similarly, the output from the controller applied to the yaw rate, u_6, is given by

$$\begin{aligned} c_6 &= K_v * \dot{e}_{u_6} + K_p * e_{\psi} \\ \dot{e}_{u_6} &= u_{6d} - u_{6a} \\ e_{\psi} &= \psi_d - \psi_a \end{aligned} \tag{4.7}$$

in which the angle of yaw, $\psi = \int_0^T u_6 dt$.

The control output vector, $c = \{c_1 \; c_6\}^T$, is the set of corrective forces applied in the cartesian coordinate system. Substituting the non-holonomic equations for CONCIC III in Eqn.(4.5), the drive torques are computed using the following relations

$$\begin{Bmatrix} \tau_R \\ \tau_L \end{Bmatrix} = \frac{r}{2} \begin{bmatrix} 1 & \frac{1}{b} \\ 1 & -\frac{1}{b} \end{bmatrix} \begin{Bmatrix} c_1 \\ c_6 \end{Bmatrix} \tag{4.8}$$

4.3 Feed Forward Controller

The structure of the Feed Forward (FF) controller proposed in this thesis is similar to the conventional FF controller in classical control theory and the feedforward component is similar to the one adopted by An, Atkeson and Hollerbach [39] for the model based control of the MIT DDArm . In this control scheme, the inverse dynamic model of the WMR with estimated values of the model parameters is used to compute the actuator drive torques for the desired trajectory. These feedforward torques are computed and are stored in a look-up table corresponding to the instances of time used to specify the trajectory. When the WMR tracks the trajectory, the drive torques are computed as the sum of the feedforward torques and feedback torques computed using a PD feedback controller for errors arising from unmodelled dynamics and uncertain model parameter values.

For stationary and mobile robots, the primary advantage of the feedforward controller is that the dynamic model of the system can be included without imposing additional computational burden as the computations are carried out off-line unlike other non-linear control schemes, such as Computed Torque Controller. In addition, actuator saturation may be checked and corrected since the nominal drive torques are computed and are available for every instance of the desired trajectory. If actuator saturation is seen to occur at any segment of the trajectory, the trajectory parameters may be suitably modified. In the case of WMRs, an additional advantage offered by the FF controller is that of indicating possible wheel slippage when the drive torque exceeds the Coulomb frictional force at the wheel [75]. The dynamic model developed and used for the Feed Forward Controller also computes the

dynamic wheel loads and the frictional forces at the tires. For a preplanned trajectory over a known terrain, if the coefficient of Coulomb friction is known for the tire material and the surface, occurrence of wheel slippage due to the applied drive torque may be checked during the computation of the feedforward torques. The non-holonomic equations form the basis of the dynamic model derived in this thesis under the assumption of no-slip at the wheels; hence the model-based controllers may not compensate for wheel slip when drive torques exceed the wheel slippage limit. In such torque limited trajectories, the wheel frictional forces and the feedforward torques may be used to check for wheel slippage and to modify the desired trajectory accordingly. These checks and corrections, which are naturally iterative, are done off-line only and hence pose neither convergence problems nor computational over heads on the digital controller during trajectory tracking operation. In this thesis, wheel slippage has been assumed to be negligible and the dynamic equations have been derived based on the non-holonomic nature of the WMR system. In the experimental work, wheel slippage and actuator saturation have both been specifically avoided by using the feedforward torques to modify the trajectory parameter values.

The Feed Forward Controller shown in Fig.4.5, consists of two parts, viz., the dynamic model based Feed Forward Torques and the error driven Independent Joint PD controller. Using the dynamic model and estimated inertial parameters of the WMR, the feedforward drive torques are computed off-line for the desired trajectory parameter values. In the ideal case, with a perfect dynamic model and with the estimated model parameter values identical to the actual values, the actual trajectory will be identical to the desired one. In practice, an Independent Joint PD (IJPD) controller is needed to correct trajectory errors

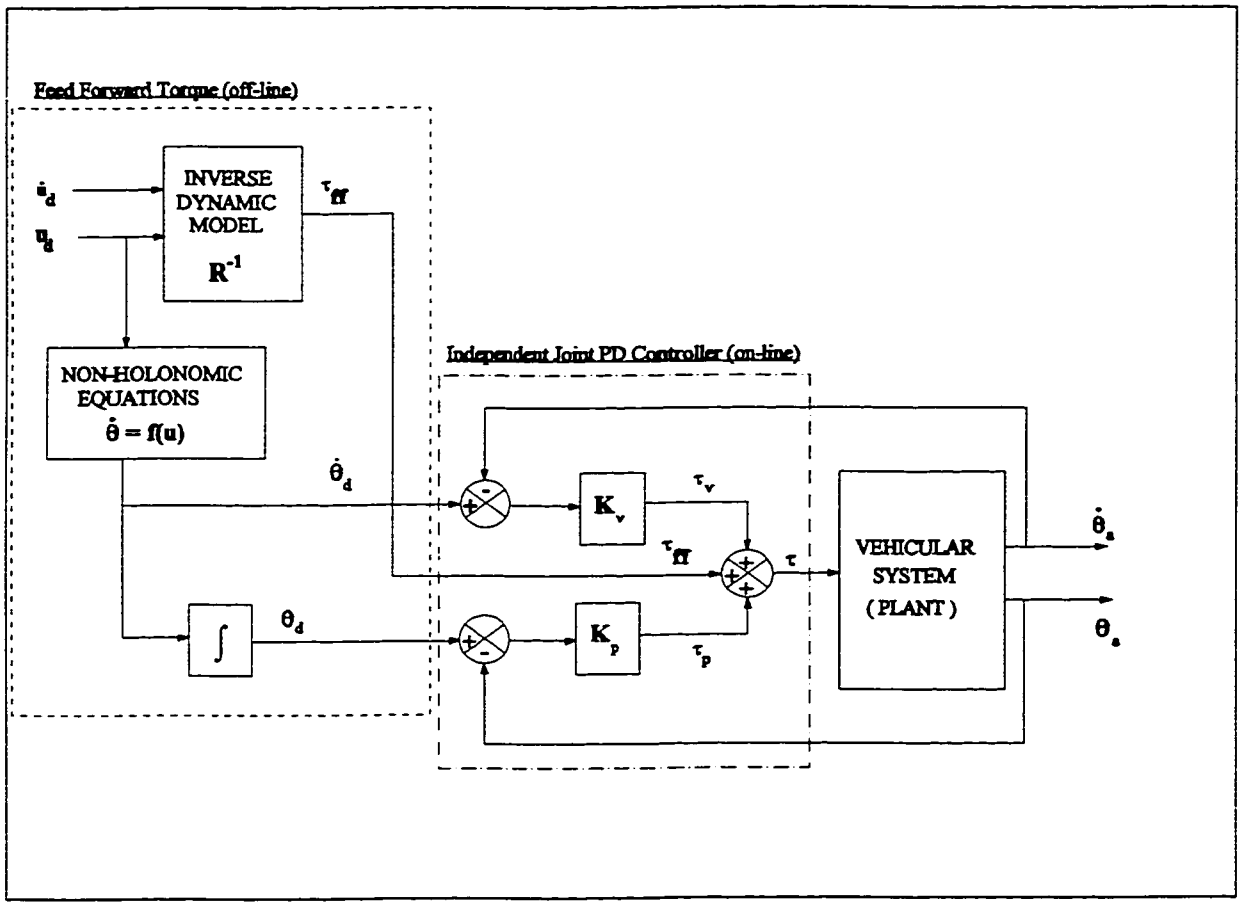

Figure 4.5 Structure of the general form of a Feed Forward Controller for a WMR.

arising from unmodelled dynamics and errors in the estimated values of the inertial and geometrical parameter values of the vehicle (WMR). The feedforward torque is computed off-line using the relation

$$\begin{aligned} \tau_{ff} &= \hat{R}^{-1}(\dot{u}_d, u_d) \\ &= [\hat{M}]\{\dot{u}_d\} + [\hat{H}(u_d, q_d)] + \hat{t}_f \end{aligned} \tag{4.9}$$

The feedback torque is computed on-line using the expression

$$\begin{aligned} \tau_{fb} &= [K_v]\{e_{\dot{\theta}}\} + [K_p]\{e_\theta\} \\ e_{\dot{\theta}} &= \dot{\theta}_d - \dot{\theta}_a \\ e_\theta &= \theta_d - \theta_a \end{aligned} \tag{4.10}$$

The resultant drive torque is

$$\tau_d = \tau_{ff} + \tau_{fb} \tag{4.11}$$

where, τ_{ff} represents the feedforward torques estimated off-line using the inverse dynamic model, $\hat{R}^{-1}$ and τ_{fb} are the correctional torques from the PD controller. In the inverse dynamic model, $\hat{M}$ is the mass matrix, $\hat{H}$ is the matrix containing the Coriolis and centrifugal terms and $\hat{t}_f$ denotes frictional terms. The notation, ^ indicates that the corresponding terms are computed using estimated values of the inertial and other model parameters.

For the case of a unladen WMR or a WMR carrying a deadweight, the mass matrix is a constant; however, for the case with an active load, the mass matrix is a function of the angle of swing (ζ) of the suspended load. In practice, the suspended load acts as a unactuated and unsensed joint and the angle of swing, (ζ) must be predicted by a dynamic model

describing the motion imparted by the load and the vehicle movement. In addition, for the case of a WMR executing planar motion in the cartesian XY plane carrying a deadweight payload, gravitational forces affect only the constraint forces on the wheels and hence the tire frictional forces; they do not appear explicitly in the dynamic equations. When the WMR carries an active payload, the gravitational forces acting on the suspended load do affect the independent generalised speeds and appear explicitly in the dynamic equations. Incorporating these modifications in the dynamic model derived in Section 3.4.7, the feedforward torques for a WMR carrying a suspended load are given by

$$\tau_{ff} = [\hat{M}(\zeta)]\{\dot{u}_d \;\; \ddot{\zeta}\}^T + [\hat{H}(u_d, q_d, \dot{\zeta}, \zeta)] + \hat{G}(\zeta) + t_f \qquad \textbf{(4.12)}$$

where the mass matrix is an explicit function of the angle of swing and the acceleration vector has been augmented with the acceleration of the suspended load. The swing rate and the swing angle appear in the matrix of Coriolis and centrifugal terms and the gravitational terms are given by the G matrix. The dynamic equation of the suspended load provides the acceleration, the swing rate and angle.

Since the feedforward torques are computed off-line using estimated values of the model parameters, uncertainty in these values may degrade the performance of the controller. This is explored in the simulation studies where a 20% difference in the estimated values of the model parameters from their nominal values is introduced to study the effect on the performance of the Feed Forward Controller. The results of this study are presented in Chapter 6.

4.4 Computed Torque Controller

The structure of the Computed Torque (CT) Controller used in this thesis is based on the Resolved Acceleration control algorithm proposed and tested on a six joint serial link manipulator, the Stanford Arm, by Luh, Walker and Paul [40]. The method is an extension of the Resolved Motion Rate Controller proposed by Whitney [41] for prostheses and for stationary manipulators. This technique uses the idea of 'inverse problem' [40] or 'non-linearity cancellation' [39] for the control of the non-linear manipulator system.

In the 'inverse problem' algorithm as proposed for a serial link manipulator the controller uses the desired acceleration, velocity and position generated by the path planner and errors in the position and velocity of the end effector to compute the 'resolved' acceleration. For position control of the end effector of the manipulator, the Resolved Acceleration Controller proposed by Luh, Walker and Paul [40] uses the desired and the actual trajectories in the cartesian work space of the robot. With estimated values of the model parameters and the actual trajectory parameter values, the inverse dynamic model is used to compute the drive torques of the actuators for the resolved acceleration. These estimated model parameters are measured and/or calculated by physical experiments. If the estimated inverse dynamic model is exactly equal to the actual model of the robot, then the controller cancels the non-linearities and the robot tracks the desired trajectory accurately. Even where the estimated values and the actual values are different, it has been reported in the literature that asymptotic convergence of the actual trajectory to the desired trajectory in every sample interval has been achieved [40]. The inverse dynamic model and the drive torques are thus computed on-line using the values of the actual position and velocity of the

manipulator. In the context of this thesis, the Resolved Acceleration Controller using cartesian trajectory values is referred to as the Cartesian Computed Torque Controller.

An et al. [39] developed and implemented the dynamic model based Computed Torque Controller for the MIT DDArm. This control scheme uses the Resolved Acceleration algorithm in the joint space of the robot to directly compute the resolved joint accelerations in terms of the desired joint accelerations provided by the path planner. The trajectory is specified in terms of desired joint acceleration, velocity and position and the measured joint parameters are directly used to compute the resolved joint accelerations. The inverse dynamic model of the manipulator is used to compute the joint torques. This controller structure is referred to here as the Independent Joint Level Computed Torque Controller.

In this thesis, the Computed Torque control algorithm is applied in both the joint space and in the cartesian space of the mobile robot to study their performance. For the differentially driven CONCIC III, the number of independent joints equals the degrees of freedom of the robot and this permits the application of the CT controller to compute either the resolved joint accelerations or the resolved rate of the generalised speeds, here after referred to as the resolved generalised accelerations. Unlike the serial link manipulator, the cartesian speeds of the WMR are related to the joint speeds through non-integrable differential equations. The cartesian accelerations are thus related through non-linear second order differential equations to the joint accelerations. This provides the motivation for the comparison between a cartesian resolved acceleration controller and a controller using resolved joint accelerations. For planar motion of the WMR in the floor frame, the trajectory of the WMR is prescribed using higher order polynomial segments in the cartesian XY plane,

hence the cartesian accelerations are available as continuous functions of time.

4.4.1 Cartesian Computed Torque Controller

The Cartesian Computed Torque Controller aims at reducing the position and the orientation errors of the WMR in the cartesian work space to a prescribed minimum value in the vicinity of zero. The path of the mobile robot is pre-planned and the cartesian position, velocity and the accelerations are available from the path planner. In the Cartesian Computed Torque controller shown in Fig. 4.6, the desired generalised accelerations, $(\dot{u}_d)$, from the trajectory generator and the errors in the generalised speeds and the cartesian path lengths of the WMR from a PD filter are used to compute the resolved generalised accelerations, $(\dot{u})$, as

$$\begin{aligned} \dot{u} &= \dot{u}_d + K_v e_v + K_p e_p \\ e_v &= u_d - u_a \\ e_p &= \int u_d dt - \int u_a dt \end{aligned} \qquad (4.13)$$

The cartesian path lengths are obtained by integrating the generalised speeds. The actual generalised speed, ($\mathbf{u}_a$), and the actual path length are obtained, as for the Cartesian PD Controller in Section 4.4.2, from the non-holonomic equations using measured values of the joint speeds. Since the non-holonomic equations apply only for no-slip conditions at the wheels of the WMR, the model implicitly assumes this condition. The drive torques for the actuators are then computed using the resolved generalised accelerations, the actual generalised speeds and the cartesian positions in the inverse dynamic model, $(\hat{R}^{-1})$, of the WMR. The drive torques for the actuators for the case of a WMR executing planar motion

carrying a deadweight (payload) are thus obtained as

$$\begin{aligned} \tau_d &= \hat{R}^{-1}(\ddot{u}, u_a, s_a) \\ &= [\hat{M}]\{\ddot{u}\} + [\hat{H}(u_a, s_a)] + t_f \end{aligned} \tag{4.14}$$

where, the actual generalised speeds ($\mathbf{u_a}$) are computed from the non-holonomic equations using the measured values of the joint speeds. The cartesian position or path length and orientation ($\mathbf{s_a}$) are obtained by integrating the generalised speeds. In the case of the deadweight payload, the mass matrix, $\hat{M}$ is a constant and may be computed off-line. However, unlike the case of the Feed Forward Controller, the cross coupling matrix, $\hat{H}$ is now a function of the actual generalised speeds and positions and has to be computed during trajectory execution at every sampling instant. As in the case of the Feed Forward Controller in Section 4.3, the notation (^) on these matrices indicates that the inertial parameters of the model are estimated values only. The frictional torques, t_{ff} are also obtained on-line with the tire friction model, Eqn.(3.8). The wheel loads are computed by the dynamic model using the equations for the constraint forces and the actual trajectory parameters.

The modifications to the dynamic equations for the case of a suspended load as given in Section 4.3 apply to the Computed Torque Controller as well. The mass matrix, $\hat{M}(\zeta)$, the cross coupling matrix, $\hat{H}(u_a, q_a, \dot{\zeta}, \zeta)$ and the additional gravitational terms must be computed using the swing angle and the swing rate of the suspended load. However, the suspended load is a unactuated and unsensed joint and these values are not measured. Hence, the controller estimates these values using the dynamic equation of the suspended load using the resolved generalised accelerations and measured speeds and positions. In the computation of

the drive torques using the inverse dynamic model, the vector of resolved generalised accelerations, $\ddot{u}$ must be augmented with the estimated swing acceleration, $\ddot{\zeta}$ obtained from the forward dynamic model of the suspended load.

Even if the inverse dynamic model contains errors due to unmodelled dynamics or uncertain parameter values, it has been shown by Luh, Walker and Paul [40] that the actual trajectory converges asymptotically to the desired trajectory if the controller gains used to compute the resolved acceleration are chosen appropriately and the sampling frequency of the digital controller is sufficiently high. Quoting as an illustration of the value of the sampling frequency, the Resolved Acceleration Controller implemented on the Stanford Arm by Luh, Walker and Paul [40] used a sampling frequency of 87 Hz.

For the CONCIC III, the forward speed, u_1, of the mobile robot and the yaw rate, u_6, are chosen as the two independent generalised speeds corresponding to the two degrees of freedom. During motion, these two speeds are obtained using the measured values of the joint speeds and the non-holonomic relations. Integrating the generalised speeds, the cartesian path length, s_1, and the angle of yaw, ψ, of the WMR are used to denote the position and the orientation angle in the work space. Kinematic errors in the cartesian positions and speeds are used by the Cartesian Computed Torque Controller to compute the resolved generalised acceleration. The structure of the controller is shown in Fig.4.6. The drive torques for the two actuators are then computed using the resolved generalised speed and the actual values of the generalised speeds and positions. The dynamic wheel loads and the frictional forces are computed by the inverse dynamic model using the actual values of the generalised speeds and positions.

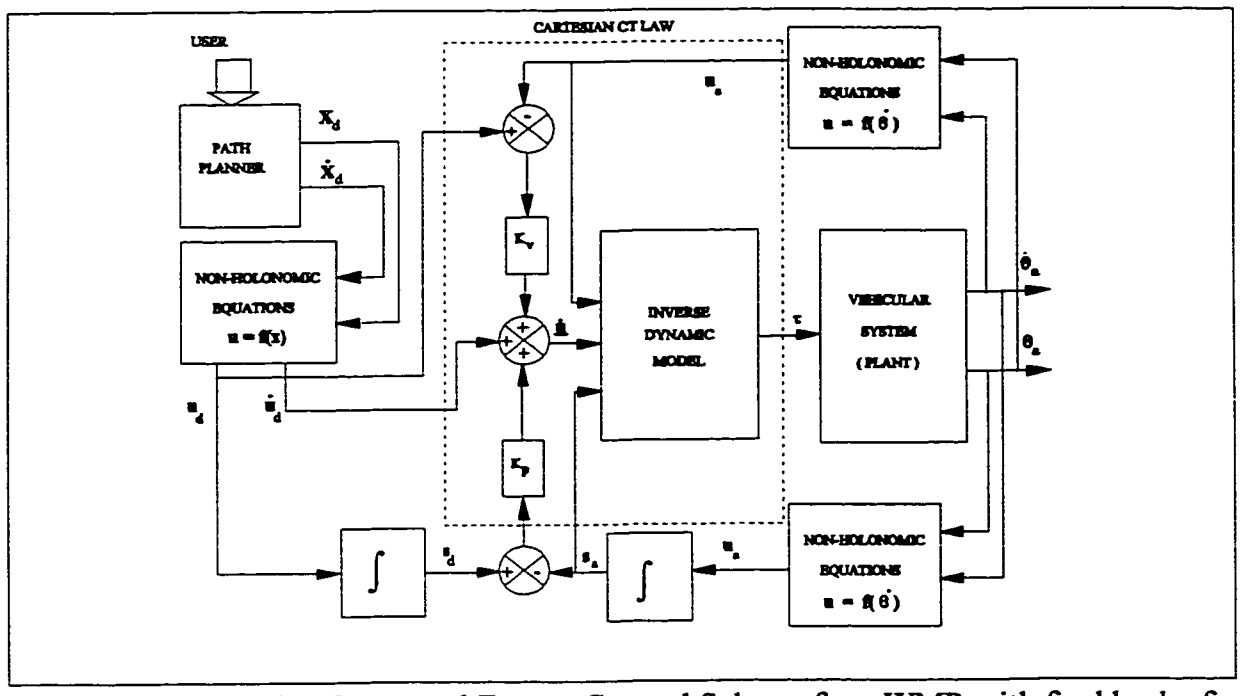

Figure 4.6 Cartesian Computed Torque Control Scheme for a WMR with feed back of joint parameters.

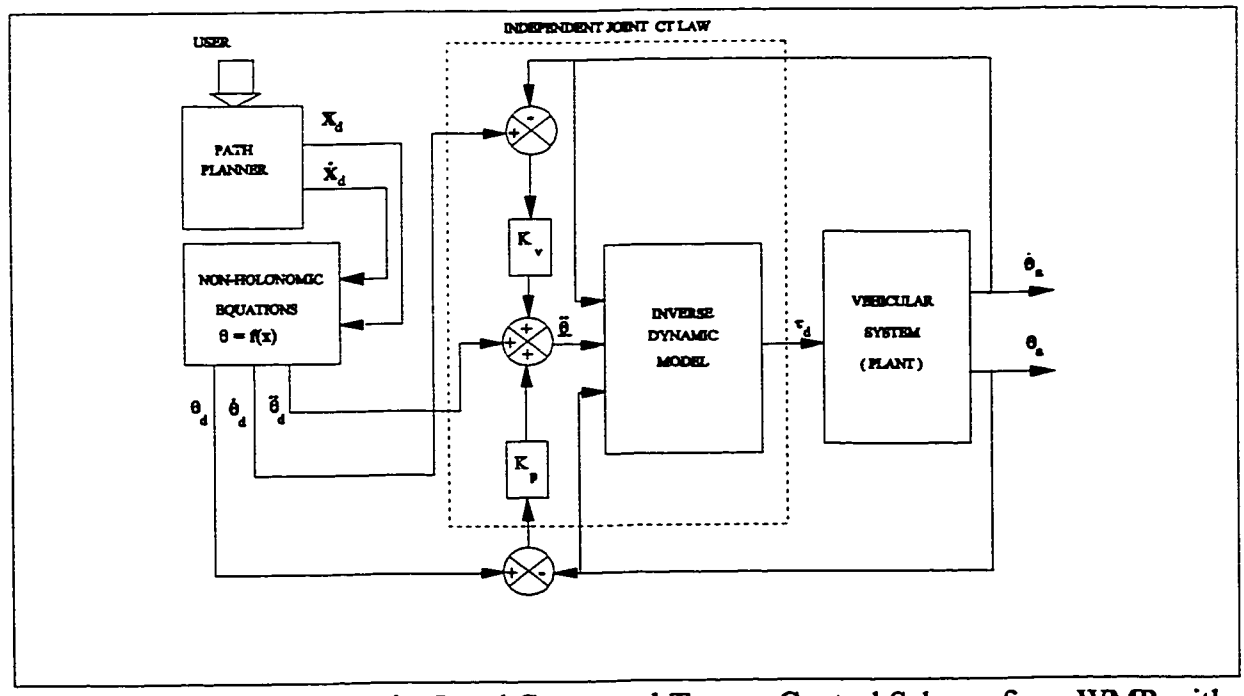

Figure 4.7 Independent Joint Level Computed Torque Control Scheme for a WMR with feed back of joints' speed and position.

4.4.2 Independent Joint Level Computed Torque Controller

The Independent Joint Level Computed Torque Controller applies the Resolved Acceleration algorithm to the joint space of the WMR. The Independent Joint Level Computed Torque Controller is shown in Fig.4.7. The desired trajectory specified by the user in task space coordinates is converted by the path planner to joint parameter values using the non-holonomic relations. During trajectory execution, the joint speeds and positions are measured by feedback devices. The set of resolved joint accelerations, $\underline{\ddot{\theta}}$,for the independent joints of the WMR is thus given by

$$\begin{aligned} \underline{\ddot{\theta}} &= \underline{\ddot{\theta}}_d + K_v e_{\dot{\theta}} + K_p e_{\theta} \\ e_{\dot{\theta}} &= \dot{\theta}_d - \dot{\theta}_a \\ e_{\theta} &= \theta_d - \theta_a \end{aligned} \tag{4.15}$$

where the desired joint accelerations ($\ddot{\theta}_d$), joint speeds ($\dot{\theta}_d$) and positions (θ_d) are available from the trajectory planner. The measured joint values are denoted by the actual speeds ($\dot{\theta}_a$) and positions (θ_a). The drive torques are then computed using the inverse dynamic model for the resolved joint accelerations and the actual joint speeds and positions as

$$\begin{aligned} \tau_d &= \hat{R}^{-1}(\underline{\ddot{\theta}}, \dot{\theta}_a, \theta_a) \\ &= [\hat{M}]\{\underline{\ddot{\theta}}\} + [\hat{H}(\dot{\theta}_a, \theta_a)] + t_f \end{aligned} \tag{4.16}$$

in which $\hat{R}^{-1}$ is used to denote the inverse dynamic model of the mobile robot. The dynamics of the WMR are described in terms of the joint variables for the Independent Joint CT Controller. The computation of the mass and the cross coupling matrices for the case of payload are carried out similar to the Cartesian CT Controller presented in Section 4.4.1.

4.5 Summary

In this chapter, the two dynamic model based controllers, namely, the Feed Forward Controller and the Computed Torque Controller, being applied for trajectory control of a WMR have been described in detail. The general form of the controller structure is explained first and then the specific structure as applied to CONCIC III, the WMR being used for the experimental validation, is given. For a non-holonomic system, such as a WMR, any set of speeds representing the degrees of freedom of the system may be used as the independent generalised speeds for describing the dynamic behaviour of the system. Hence, for control purposes, the effect of applying either cartesian speeds or joint speeds as the independent generalised speeds is studied by constructing the Computed Torque Controller in cartesian space and also in joint space. The Proportional Derivative Controller used to provide a baseline for the comparison of controller performance is also described both in the Cartesian and in the Independent Joint structure.

Chapter 5

Path Planning and Trajectory Generation

5.1 Introduction

One of the common applications of a WMR in industry is the robot moving a payload between two stations in a specified time interval. The natural straight line path between the two stations may have to be modified due to path constraints imposed by the presence of intervening obstacles. As in the case of stationary serial link manipulator arms, the path is specified in the cartesian task space of the robot and not in the joint space because it is easier to visualize the position and orientation of the robot in cartesian coordinates [77]. However, unlike serial link manipulators, the non-holonomic nature of the WMR does not permit a one-to-one inverse kinematic solution of the joint coordinates when the cartesian coordinates of the path are specified. These joint values are needed by any trajectory error driven controller since the actual trajectory is usually measured in terms of joint speeds and positions. For such non-holonomic systems, the motion constraint equations, which are non-integrable first order differential equations in the case of a WMR, have to be integrated numerically to obtain the joint coordinate values with respect to some specified initial condition. This also permits verifying and correcting for kinematic constraints such as maximum permissible steer angle.

In this chapter, the topic of path planning and trajectory generation for the WMR is discussed in Section 5.2. The path planning schemes proposed by Nelson [78, 79] for a WMR for a straight line path and for a lane change have been adopted in this thesis. With the cartesian path so specified, the trajectory is generated using a fifth order polynomial with time

as the independent parameter. Detailed derivations of the path planning scheme and trajectory generation for a lane change or a straight line path are presented in Section 5.3. These two trajectories have been chosen since the effects of linear acceleration on controller performance are seen during a straight line trajectory while a lane change introduces the effects of angular acceleration. Pertinent details are summarised in Section 5.4.

5.2 Path Planning for a WMR

The path of a reference vector (end effector for robot arms and a vector at the mass centre for WMRs) may be specified using a series of points, called knot points or interpolation points [77], at which the cartesian position and orientation are prescribed. The prescribed path is subject to kinematic and dynamic constraints imposed by the construction of the robot and by the operating environment. In a mobile robot, the user may also impose additional constraints on the forward and angular speeds and accelerations primarily for safety reasons. In industrial applications the WMR is restricted to planar motion only and the knot points may be connected by any two dimensional curve in the cartesian XY plane. Any such curve may be defined in terms of a parameter, s, as

$$\{x\ ,\ y\} = \{x(s)\ ,\ y(s)\} \tag{5.1}$$

where s is the length along the curve from any initial point on it. Such a parametrization is termed regular or arc length parametrization [80]. In addition to the cartesian position at each knot point, the orientation, $\psi(s)$, of the WMR is also specified. In the case of a differential drive WMR, the orientation of the WMR also coincides with the instantaneous heading of the

mobile robot and is given by

$$\psi(s) = \tan^{-1}\left\{\frac{y'(s)}{x'(s)}\right\} \tag{5.2}$$

where the prime denotes differentiation with respect to the path length parameter (s).

The properties of a parametric curve used to specify non-stop motion of the robot between two successive knot points have been enumerated by Kanayama [58]. The first requirement on the curve describing the path of the WMR is that of continuity. In addition, the orientation of the robot and the heading must also be continuous. Any discontinuity in the heading of the robot translates to a discontinuity in the forward speed of the WMR which makes motion not feasible since it requires infinite acceleration. The derivative of the orientation, $\psi(s)$, with respect to the arc length parameter, s, is the curvature denoted as, $\kappa(s) = \psi'(s)$. The inverse of the curvature at any point on the curve equals the radius of curvature of the curve at that point. In path planning for WMRs, continuity of curvature is required to assure feasible values of angular accelerations and to provide a smooth change in the centrifugal force.

In their work on path planning for WMRs, Kanayama [58] defines a posture $P = (x, y, \theta, \kappa)$, as the quadruple of cartesian coordinates, orientation and curvature. The path is thus given by a set of postures, $\{P_i\}$ where $i = 1..n$. If a curve, C, starts at P_1 and ends at P_n and satisfies the position, orientation and curvature at every intermediate posture, then C is said to satisfy P or is said to be a solution of P. The path planning problem for a WMR may be stated as finding a solution when a pair of postures is given.

For a general path, the curvature at each posture, P_i, is specified by the user and is

normally not equal to zero. For the interpolation of the quadruple of position, orientation and curvature values between the two postures, any set of basis functions may be used. Following the method presented by Nelson [78, 79], for straight line and lane change paths the monomial basis up to fifth order is chosen. The complete path is expressed as a composite of fifth order polynomial segments and in each segment, the cartesian Y-coordinates are expressed as a polynomial function of the X-coordinate values.

The path parameter values are then converted to trajectories by expressing the independent X-coordinate in the case of straight line or lane change paths as a function of time. In this work, as in the case of stationary manipulators [39], fifth order polynomials of time are used so that continuity of velocity and acceleration are assured. The equations used for path planning and trajectory generation are derived in the following sections.

5.3 Lane Change Trajectory Generation

In an industrial application, the WMR may have to make a smooth transition between two parallel lanes while travelling in the same direction. An example of such a manoeuvre is when the WMR has to be parked at a work station as shown in Fig.5.1. The WMR leaves the main path in a smooth double turn without much reduction in its forward speed. Having entered the parallel path in the parking bay, it decelerates down to a dead stop. A similar manoeuvre but with acceleration to the normal forward speed is used when the WMR leaves the parking bay and enters the main path. Since such a lane change path must have continuous curvature to avoid abrupt changes in acceleration, a 'Lazy-S' type curve [78] composed of a single quintic polynomial is used. The complete manoeuvre consists of steady straight line

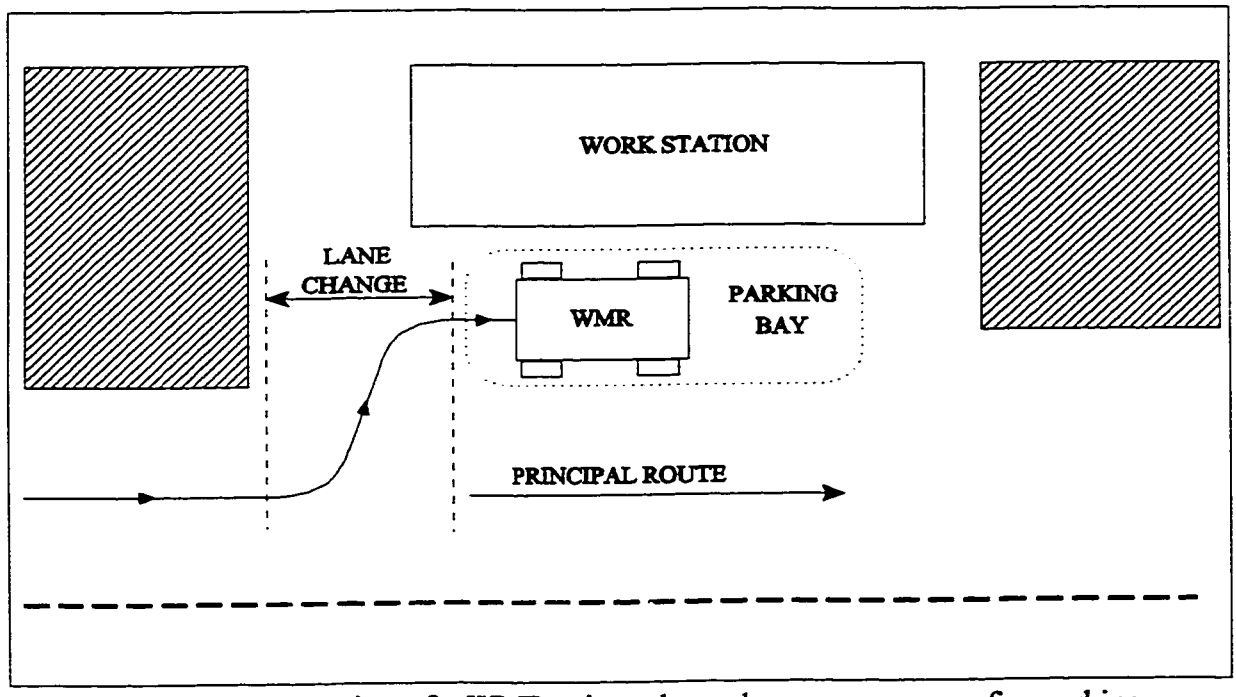

Figure 5.1 Illustration of a WMR using a lane change manoeuvre for parking.

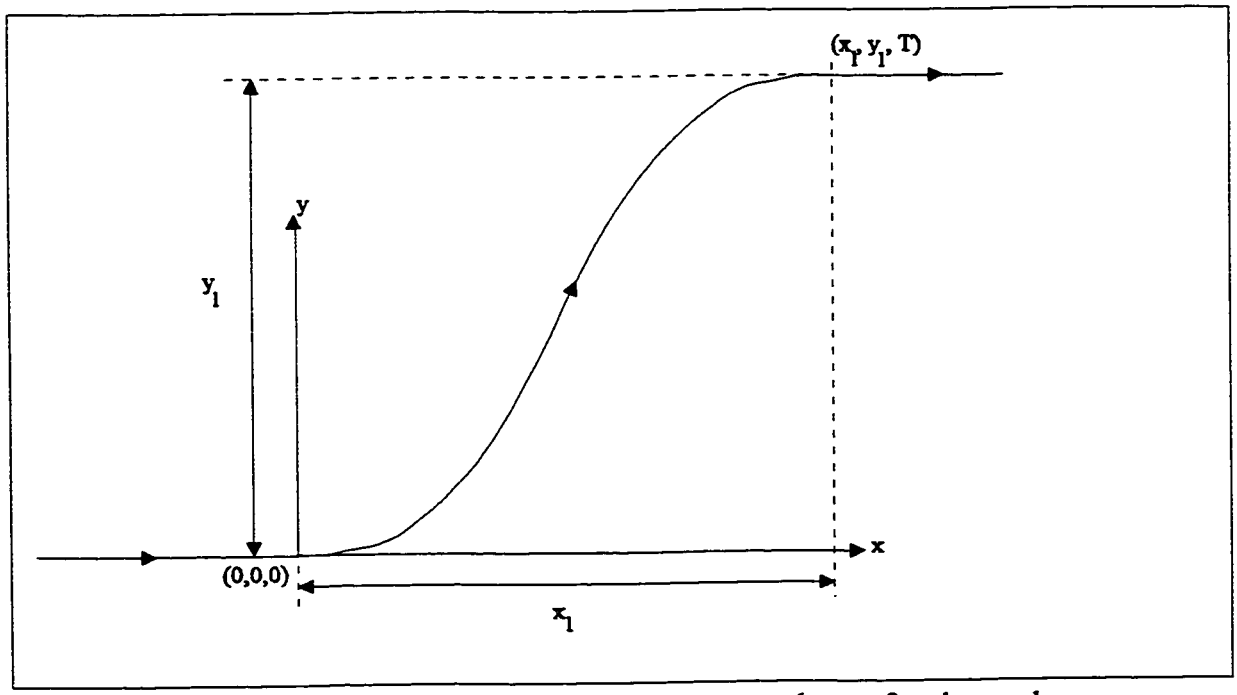

Figure 5.2 Coordinate definition and parameter values of a lane change manoeuvre using a quintic polynomial segment [70].

motion of the WMR as it enters the lane change path. Following the lane change, the WMR exits in a steady straight line motion along the new parallel direction.

In path planning, the Cartesian x-coordinate is chosen to be the independent parameter for the curve and the Cartesian y-coordinate is expressed as

$$y(x) = a_0 + a_1 x + a_2 x^2 + a_3 x^3 + a_4 x^4 + a_5 x^5 \tag{5.3}$$

For the piecewise path segments used, the simple monomial form in Eqn. (5.3) assures continuity of derivatives of up to the fourth order for all values of x. The definition of the coordinate system used in this derivation is shown in Fig. 5.2. For simplicity and with no loss of generality, the x-direction for the lane change is assumed to be aligned with the x-coordinate direction of the floor frame. If the lane change coordinate directions do not coincide with the axes of the floor frame, a local coordinate frame oriented in the requisite direction may be established and related to the floor frame through a rotational transformation. In Fig.5.2, the origin of the coordinate frame is located at the point of entry of the lane change. The total distance travelled in the x-direction during the lane change is measured by the distance, x_l . The distance between the two parallel paths of the WMR is measured by the change in the y-coordinate, y_l . Using these distances to characterize the lane change manoeuvre, the local coordinates may be normalised as

$$\chi = \frac{x}{x_l} \qquad y'(x) = \left(\frac{y_l}{x_l}\right)\eta'(\xi)$$

$$\eta(\chi) = \frac{y(x)}{y_l} \qquad y''(x) = \left(\frac{y_l}{x_l^2}\right)\eta''(\xi) \tag{5.4}$$

where differentiation with respect to the independent variable is denoted by a prime.

The WMR enters the lane change segment from a straight line path and exits along a straight line path. The conditions imposed on the lane change path are continuity of position, slope and curvature at both the entry and the exit points. For any planar curve in the cartesian xy plane, the curvature is given by

$$\kappa(x) = \frac{(d^2y/dx^2)}{[1+(dy/dx)^2]^{3/2}} \tag{5.5}$$

For the lane change curve, continuity of curvature at both the ends reduces to the second derivative being zero. The six constraints imposed on the lane change path may be expressed as

$$\begin{aligned} &\eta(0) = 0 \; ; \; \eta'(0) = 0 \; ; \; \eta''(0) = 0 \\ &\eta(1) = 1 \; ; \; \eta'(1) = 0 \; ; \; \eta''(1) = 0 \end{aligned} \tag{5.6}$$

Normalising Eqn.(5.3), differentiating it twice and using the six constraint equations gives the following set of linear equations for the six coefficients

$$\begin{aligned} &a_0 = a_1 = a_2 = 0 \\ &a_3 x_l^3 + a_4 x_l^4 + a_5 x_l^5 = y_l \\ &3a_3 + 4a_4 x_l + 5a_5 x_l^2 = 0 \\ &3a_3 + 6a_4 x_l + 10a_5 x_l^2 = 0 \end{aligned} \tag{5.7}$$

Solving for the non-zero coefficients, the lane change curve may be expressed in parametric form as

$$\eta(\chi) = 10\chi^3 - 15\chi^4 + 6\chi^5 \tag{5.8}$$

This simple three term function provides the required continuous curvature path for the lane change. The maximum curvature and the rate of change of the curvature are both dependent on the characteristic distances, x_l and y_l.

The lane change path is converted into a trajectory by expressing the x-coordinate as a function of time. In this thesis, a quintic polynomial is chosen so that continuity of acceleration and rate of change of acceleration are both assured. In addition, the results obtained for the lane change path may be directly applied for trajectory generation as well. The quintic polynomial relating the x-coordinate to time is given by

$$x(t) = c_0 + c_1 t + c_2 t^2 + c_3 t^3 + c_4 t^4 + c_5 t^5 \qquad \textbf{(5.9)}$$

Using the x-distance, x_l, travelled during the manoeuvre and the total time taken, T, for the lane change, the variables in the function are normalised as

$$\tau = \frac{t}{T} \; ; \; \chi(\tau) = \frac{x(t)}{x_l} \qquad \textbf{(5.10)}$$

The constraints imposed on the trajectory are continuity of position, speed and acceleration in the x-direction. The WMR enters and exits the lane change manoeuvre with non-zero velocity ; this velocity equals the forward speed of the WMR in the straight line entry and exit sections. The mobile robot is assumed to be following steady straight line motion in these sections so that the forward acceleration at entry and at exit are both zero. These constraints, expressed in terms of the normalised variables, are expressed as

$$\begin{aligned} \chi(0) &= 0 \; ; \; \chi'(0) = \chi_0' \; ; \; \chi''(0) = 0 \\ \chi(1) &= 1 \; ; \; \chi'(1) = \chi_1' \; ; \; \chi''(1) = 0 \end{aligned} \qquad \textbf{(5.11)}$$

The velocity end conditions are obtained from the forward speed, u_1 , of the WMR in the straight entry and exit sections as

$$\chi_0' = \left(\frac{T}{x_l}\right) u_1(0) \; ; \; \chi_1' = \left(\frac{T}{x_l}\right) u_1(1) \tag{5.12}$$

in which u_1 is the generalised speed representing the forward speed of the WMR.

Taking the first and the second derivative of the quintic polynomial and substituting the constraint equations yields the following set of linear equations for the coefficients

$$c_0 = c_2 = 0 \; ; \; c_1 = \chi_0'$$

$$\begin{bmatrix} 3 & 4 & 5 \\ 3 & 6 & 10 \\ 1 & 1 & 1 \end{bmatrix} \begin{Bmatrix} c_3 \\ c_4 \\ c_5 \end{Bmatrix} = \begin{Bmatrix} \chi_1' - \chi_0' \\ 0 \\ 1 - \chi_0' \end{Bmatrix} \tag{5.13}$$

Having related the x-coordinate of the path to time, the y-components of the velocity and the acceleration are obtained using the chain rule of differentiation as

$$\begin{aligned} \dot{y}(t) &= y'(x)\dot{x} \\ \ddot{y}(t) &= y''(x)\dot{x}^2 + y'(x)\ddot{x} \end{aligned} \tag{5.14}$$

where the dot is used to denote derivative with respect to time and the prime, differentiation with respect to x.

For the Cartesian PD controller and for the model based FF and CT controllers, the trajectory needs to be specified in terms of the path lengths and the generalised speeds and accelerations. For the Independent Joint PD controller, the joint positions, speeds and accelerations need be specified. The non-holonomic equations are used to obtain these

trajectory parameters from the Cartesian values. The following derivation refers to the differentially driven CONCIC III. This methodology may be generalised for other wheel configurations using the appropriate non-holonomic equations.

The non-holonomic equations relating the generalised speeds and the cartesian speeds, Eqn.(3.16), simplified for a differential drive using Eqn.(3.30) are

$$\begin{aligned} u_1 &= \dot{x}c\psi + \dot{y}s\psi \\ u_6 &= \dot{\psi} \end{aligned} \tag{5.15}$$

where ψ denotes vehicle orientation and $\dot{\psi}$ is the yaw rate. The yaw rate is obtained in terms of the Cartesian speeds by differentiating the constraint of zero lateral speed

$$u_2 = -\dot{x}s\psi + \dot{y}c\psi = 0 \tag{5.16}$$

Taking the time derivative and rearranging,

$$u_6 = \dot{\psi} = \frac{1}{u_1}(-\ddot{x}s\psi + \ddot{y}c\psi) \tag{5.17}$$

For the lane change manoeuvre, by definition the forward speed, $u_1 \neq 0$; hence Eqn.(5.17) may be used to compute the yaw rate. Taking the time derivatives of Eqn.(5.15) and rearranging, the generalised accelerations are given by

$$\begin{aligned} \dot{u}_1 &= \ddot{x}c\psi + \ddot{y}s\psi \\ \dot{u}_6 &= \frac{1}{u_1}(-\ddot{x}s\psi + \ddot{y}c\psi) - \frac{2\dot{u}_1 u_6}{u_1} \end{aligned} \tag{5.18}$$

Since the x-coordinate is given by a quintic polynomial, the third derivative is a continuous function of time. The third derivative of y is given by

$$\ddot{y}(t) = y'''(x)\dot{x}^3 + 3y''(x)\dot{x}\ddot{x} + y'(x)\dddot{x} \tag{5.19}$$

The cartesian path length, s, is obtained by numerically integrating the non-holonomic equations Eqn.(5.15) using known initial conditions.

For the differential drive, the Jacobian matrix, **J**, is a constant. From the generalised speeds and accelerations, the joint trajectory parameters are obtained as

$$\begin{aligned} \dot{\theta} &= [J]^{-1}\dot{u} \\ \ddot{\theta} &= [J]^{-1}\ddot{u} \end{aligned} \tag{5.20}$$

The joint positions are obtained by integrating the joint speeds from known initial conditions. With no loss of generality, the initial values of the joints are assumed to be zero for the trajectory. For straight line trajectories, the same quintic polynomial scheme is adopted with the y-coordinate and all its derivatives held at zero.

5.4 Summary

This chapter describes the path planning and the trajectory generation methods used in this thesis work. Issues related to path planning and trajectory generation for WMRs for industrial applications are discussed. For planar motion, the path of the WMR is specified by a set of knot points at which the position and the orientation of the mobile robot in the floor frame are specified. The knot points are connected by any two dimensional curve in the cartesian XY plane. The prescribed path is subject to kinematic and dynamic constraints imposed by the construction of the robot and by the operating environment. For WMRs, constraints on the forward and angular speeds and accelerations require that the orientation

and the heading be continuous for any set of interpolation curves used.

In this thesis, straight line and lane change trajectories have been chosen for the evaluation of the performances of model based controllers. A straight line trajectory shows the effects of linear acceleration on the performance of the controllers while the lane change trajectory introduces the effects of angular acceleration. The path planning scheme for a lane change using quintic polynomial segments proposed by Nelson [78, 79] has been adopted. The straight line path is generated by setting the distance between the parallel paths in a lane change to zero. The cartesian xy path generated by this scheme is then converted into a trajectory by expressing the independent x-coordinate as a fifth order polynomial of time. This method has been adopted so that the results obtained in the path planning section may be directly applied to trajectory generation as well. The complete set of equations required for path planning and trajectory generation have been derived and discussed.

Chapter 6

Simulation Studies

6.1 Introduction

In the study of the dynamics and the control of a mechanical system such as a WMR, simulations performed on a digital computer using mathematical models offer valuable insights into the dynamic behaviour and the response of the system to a control action. The reliability of the results obtained from these simulations rests on the rigour employed in the construction of the mathematical models of the systems and the values of the various parameters used.

To study the dynamic behaviour of a WMR, the forward dynamic model of the system is used to compute the generalised accelerations for a given set of drive torques and operating conditions, such as the trajectory, the payload and the tire friction values. For a WMR executing planar motion, the generalised coordinates used to describe the configuration of the robot are cyclic coordinates and do not appear in the dynamic equations. Hence the forward dynamic equations, which are coupled non-linear first order differential equations in terms of the generalised speeds, are numerically integrated to simulate the actual motion of the system. In model based controllers, the inverse dynamic model is used to compute the drive torques for a given set of accelerations and operating conditions. Once the simulation program has been constructed, the effects of a variety of operating parameters, for example, different trajectories and payloads, may be easily studied by modifying these values in the simulation. Dynamic simulations also permit verifying and correcting for dynamic constraints imposed by

the construction of the WMR, such as actuator saturation due to large control signals and wheel slippage due to excessive drive torques.

Furthermore, in the case of a non-holonomic system such as a WMR, computer simulations are necessary to verify that kinematic constraints such as the maximum permissible steering angle of a steering wheel are not exceeded at any point in the desired trajectory. For a WMR, the cartesian task space and the joint space variables are related by non-integrable first order differential equations and not by simple transformation matrices as in the case of a stationary manipulator. Thus, during the computer simulation, the first order differential equations expressing the non-holonomic relations can be numerically integrated using the desired path parameters, normally specified in cartesian values, to obtain the joint parameter values.

In this chapter, the results of computer simulations carried out to compare the performances of the model based Feed Forward and Computed Torque controllers and the conventional PD controller in the dynamic control of a WMR are presented and discussed. Section 6.2 describes the structure of the program used for the simulations. The programming environment chosen was MATLAB®, a numeric computation and visualization software. The two trajectories chosen for the simulations were a straight line path and a lane change manoeuvre. The same trajectories were also used for the experimental work, described in Chapter 8, on controller performances. Section 6.3 is devoted to the presentation and the discussion of the results from the straight line trajectory. Simulation results from the lane change trajectory used in the experimental work are presented in Section 6.4. The simulations are then extended to a comparison of the performances of the PD and the CT controllers for

a lane change trajectory involving higher speeds and accelerations. These results are used to highlight the advantage of including the dynamic model of the WMR in the control loop. In Section 6.6, the importance of including the dynamic nature of wheel loads in the model are shown by simulations for three lane change trajectories of increasing values of linear and angular accelerations. The simulations presented in Section 6.7 explore issues related to the influence of errors in the estimated inertial and frictional parameter values used in the dynamic model on the performance of the controllers. The chapter concludes with a summary of the pertinent results in Section 6.8.

6.2 Structure of the Simulation Programmes

The programs used for the simulations were all written in the programming environment provided by MATLAB®. This general purpose numeric computation and visualization software was chosen because of the large number of function libraries available specifically for control studies. Further details of the programming environment and the library functions may be found in the Reference Guide [81]

For these simulations, the desired trajectories are generated using the lane change algorithm described in Section 5.3. The desired time of execution of each trajectory segment, the cartesian position and speed values are chosen such that the trajectories may be used for the experimental work as well. Since dead reckoning method of guidance has been adopted, the desired trajectory parameters at each sampling instant of the control loop are stored in a data file. With the user defined input values, the coefficients of the piecewise polynomial segments of the trajectory are computed. The values of the desired trajectory parameters at

each sampling instant of the controller are then generated. The desired joint speeds are obtained from the cartesian values using the non-holonomic relations. The joint speeds are numerically integrated to obtain the desired joint positions. These desired joint trajectory files are generated for the PD controller in order to avoid the numerical integration and other computations on-line.

The structure of the simulation programme is shown in Fig.6.1. The values of the kinematic and inertial parameters of the experimental WMR, CONCIC III, being used in this study are built-in constants in the programme. The desired trajectory values, and the feed forward torque values in the case of the FF controller, are a priori information for the vehicle. Each execution of the main control loop corresponds to one sampling interval of the digital controller. In the simulations, the initial values of all the motion parameters are set to zero and the wheel vertical loads are set equal to their static values.

For the forward dynamics, the Runge-Kutta fourth and fifth order numerical quadrature scheme has been used. At the end of the desired trajectory, the simulations are continued in order to permit controller actions to decay to their steady state values. In the case of the WMR, motion ceases when the drive torques fall below the static friction values in the actuators. In these simulations, the dry friction values of 0.05 N.m obtained during the calibration of the motor sets has been used as the stopping criterion.

In order to obtain the feedforward torques required by the FF controller, the simulation programme is modified to run in an open loop without the control section. The desired acceleration and cartesian speeds are substituted into the inverse dynamic model to obtain the feedforward drive torques. The dynamic vertical loads on the wheels are obtained

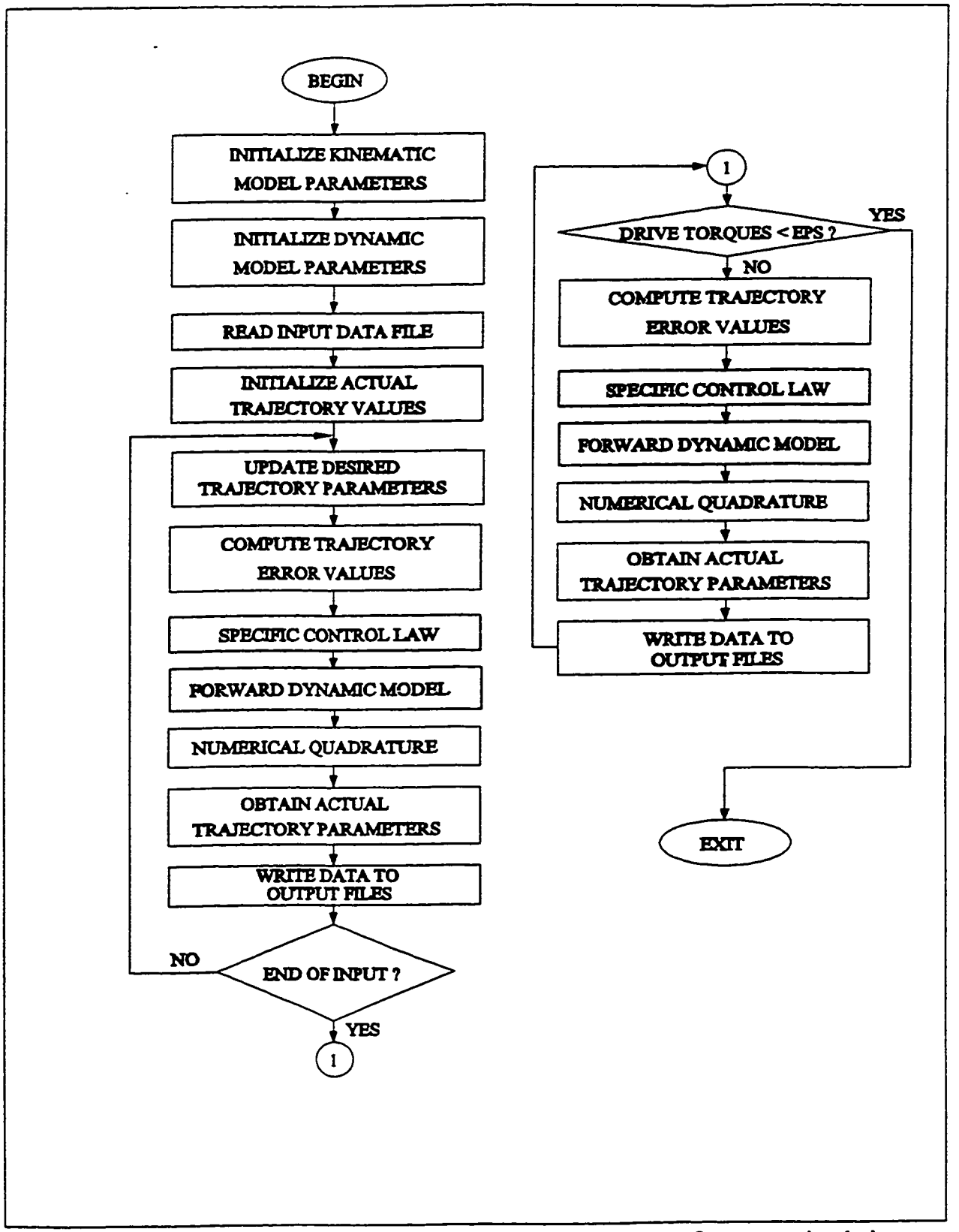

Figure 6.1 Structure of programme for dynamic controller performance simulation.

using the desired cartesian trajectory parameter values. Using the vertical loads, the frictional forces at the contact patches of the tires and in the actuators and in the drive gear trains are obtained with the desired joint parameter values. The feedforward torques are used to check for actuator saturation and, if necessary, modify the desired trajectory parameter values iteratively.

6.3 Straight Line Trajectory

In order to study the performances of the controllers only for forward acceleration of the WMR, a straight line trajectory was chosen. The same trajectory parameters are used in the experimental trajectory, termed SL_2, described in Section 8.2. The WMR in the simulations is the CONCIC III and the values of the geometrical and inertial parameters used are the estimated values given in Appendix C.

The profiles of the trajectory parameters used are shown in Fig.6.2. The WMR starts from rest and accelerates to a maximum speed of 1 $m.s^{-1}$ in a time of 9.5s. The forward speed used in the trajectory is the maximum forward speed for the drive wheel units on CONCIC III. The maximum acceleration during this phase is 0.16 $m.s^{-2}$. This is also the maximum permissible value of acceleration without saturating the power amplifiers at the settings of the peak and the continuous current limits used in the experimental work. The trajectory is symmetric about the mid-point and the WMR decelerates to a stop in a time period of 9.5s.

The value of the acceleration specified in this trajectory was chosen such that the maximum feedforward actuator current is 11.6 amps which is just over 90% of the continuous current limit of 12.5 amps set in the power amplifiers. This maximum value of the acceleration

was arrived at in an iterative fashion as described below. When the trajectory parameters for this straight line trajectory were generated, the maximum forward speed was first fixed at 1 $m.s^{-1}$. An initial estimate of the total time for the trajectory was done assuming constant acceleration and a ramping velocity profile. For this duration of trajectory and for the maximum forward speed, the trajectory parameters were generated using the algorithm described in Section 5.3. Then, using the inverse dynamic model of the WMR, the feedforward torques and the corresponding actuator feedforward currents were generated for these trajectory parameter values. The maximum feedforward current required during the trajectory was then compared with the continuous current limit set in the power amplifiers. The total time for the trajectory was then iteratively adjusted till the acceptable acceleration and current values were obtained.

The results of the simulations are shown in Fig.6.3, a plot of instantaneous errors in the path length, and in Fig.6.4 which shows instantaneous values of errors in the forward speed of the WMR during the trajectory. In the simulations, the heading of the WMR stayed true on the straight line due to the absence of random disturbances, such as uneven floor conditions, experienced during the experimental work. Hence, the heading and the yaw rate plots are not shown. A summary of the performance indices for the three controllers is given in Table 6.1.

A comparison of the performance indices for the path length and the forward speed of the WMR shows that the performances of both the model based controllers are better than those of the PD controller. The differences in value between the FF and the CT controller performance indices are not significant.

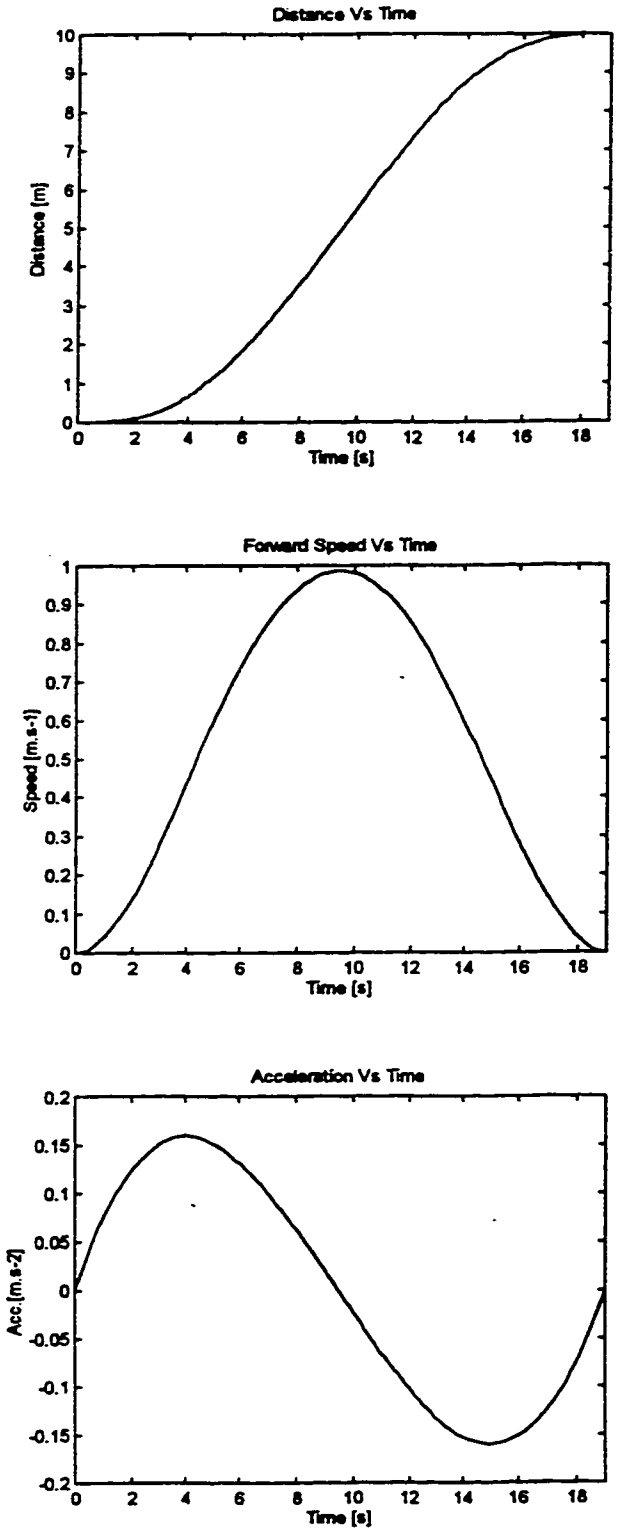

Figure 6.2 Desired parameters of the simulated straight line trajectory, SL_2.

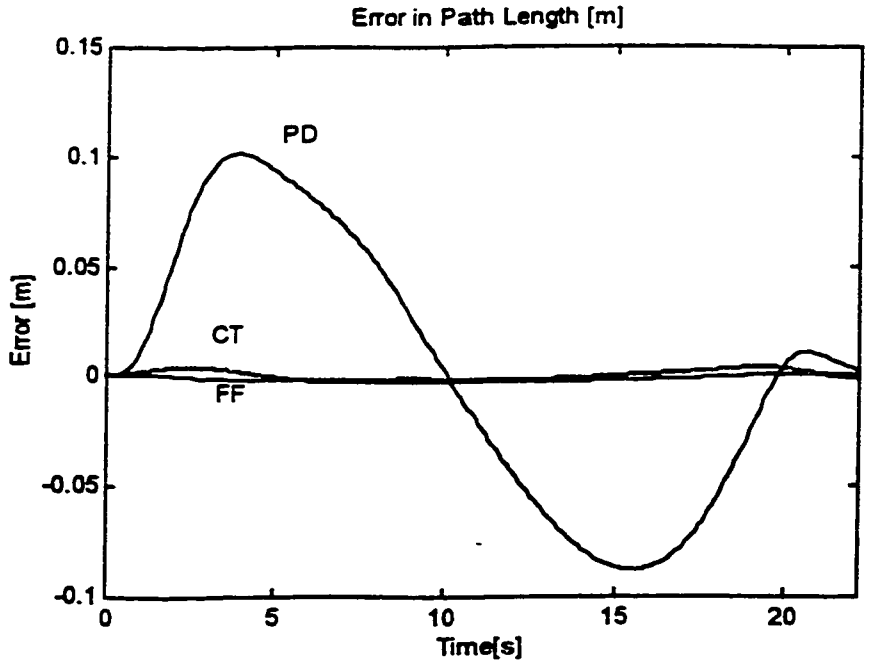

Figure 6.3 Errors in path length for the simulated straight line trajectory, SL_2, for the PD, the FF and the CT controllers.

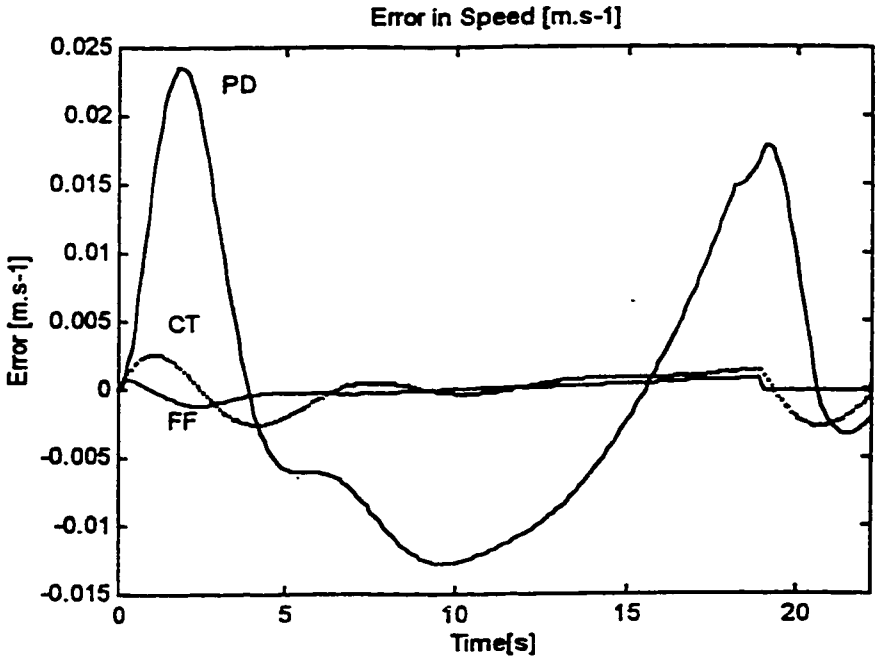

Figure 6.4 Errors in the forward speed for the simulated straight line trajectory, SL_2, for the PD, the FF and the CT controllers..

Controller	Path Length Error RMS [m]	Path Length Error Max.[m]	Path Length Error SS.[m]	Forward Speed Error RMS [$m.s^{-1}$]
PD	0.061	0.102	< 0.01	0.012
FF	0.002	-0.003	< 0.01	0.005
CT	0.002	0.004	< 0.01	0.001

Table 6.1 Values of the performance indices for the simulated straight line trajectory

The CT controller tracks the desired forward speed with errors in the range of ± 0.002 $m.s^{-1}$ and the oscillatory response resembles that of an underdamped system. The gains used to compute the resolved acceleration are equal in numerical value to the gains used for the PD controller. The gain values chosen for the simulations introduce oscillations in the resolved acceleration about the desired acceleration values. This forces the controller to under-compensate for the inertial load initially and then to over-compensate as the accumulated errors in speed and position increase. The steady state error of the CT controller is less than 0.001m in the simulations.

The FF controller, which uses the feed forward torques in an open loop, shows an over compensation during the initial part of the trajectory. The feed forward drive torques have been compensated using the inverse of the dynamic model used in the simulations. Theoretically, the FF controller should then show zero errors during trajectory tracking. However, the feed forward drive torques are piecewise constant values and are changed only

at the sampling instants of the digital controller. The WMR system, however, responds to these inputs during the sample interval thereby inducing errors in forward speed and consequently in path length. The steady state offset for the FF is less than 0.001m as well.

In the performance of the PD controller, the speed of the WMR during the acceleration phase lags behind the desired speed and the position error of the WMR consequently shows a rising trend. The maximum errors of 0.1m in path length and $0.023 m.s^{-1}$ in forward speed coincide with the instant of peak forward acceleration. The error values decrease as the acceleration falls to zero and the WMR reaches top speed at the mid point of the trajectory. The error pattern is mirrored about the horizontal axis, symmetrically in the case of the path length, during the deceleration in the second half of the trajectory. The WMR comes to rest with a steady state error of less than 0.001m.

6.4 Lane Change Trajectory

In order to study the performances of the controllers under the combined action of forward and angular accelerations, a lane change trajectory was used. In addition, the WMR was simulated carrying a suspended load of identical geometrical and inertial values as the load used in the experiments. The active payload consists of a mass of 20 Kg suspended from a point 0.65m vertically above the centre of mass by an rigid arm of length 0.4m. The arm is fixed to a rod mounted on bearings so that the mass is free to oscillate about the transverse plane of the WMR. A similar arrangement is used for the suspended load in the experimental work as well. The trajectory parameters were generated using the lane change trajectory generation scheme given in Section 5.3 and the profiles of the desired trajectory parameters

are shown in Fig.6.5. The WMR starts from rest and accelerates to a top speed of 1 $m.s^{-1}$ in 10s during the lane change. The maximum forward acceleration during this phase is 0.144 $m.s^{-2}$ .The distance between the two lanes is 1 m and the total time for the trajectory is 20s. The maximum yaw rate for the turn is 0.0442 $rad.s^{-1}$ and the angular acceleration is 0.0137 $rad.s^{-2}$. Since the WMR regains its original heading at the end of the lane change, the yaw rates are positive in the first part of the lane change and are negative in the second half. The trajectory generator also provides smooth angular acceleration values with no discontinuous jumps in the junction between the two symmetric parts of the trajectory.

The results of the simulated performances of the controllers are shown in Fig.6.6 and Fig.6.7 for the instantaneous errors in the path length and the forward speed of the WMR. Fig.6.8 compares errors in the heading of the WMR and Fig.6.9 shows the errors in the yaw rate. The values of the indices used to compare the performances of the controllers are summarised in Table 6.2.

The performances of the model based controllers, as indicated by the values of the errors, are better than that of the PD controller. The trends in the errors for the forward speed and the path length are similar to those for the straight line trajectory. However, the difference between the CT and the FF performance indices for both the path length and the forward speed are seen to be higher than for the straight line trajectory. In the lane change trajectory, both the forward and the angular accelerations are functions of time while the feed forward torques in the case of the FF controller and the drive torques computed using the inverse dynamic model in the case of the CT controller are piecewise constant values. The errors in orientation and position have to be compensated by a feedback

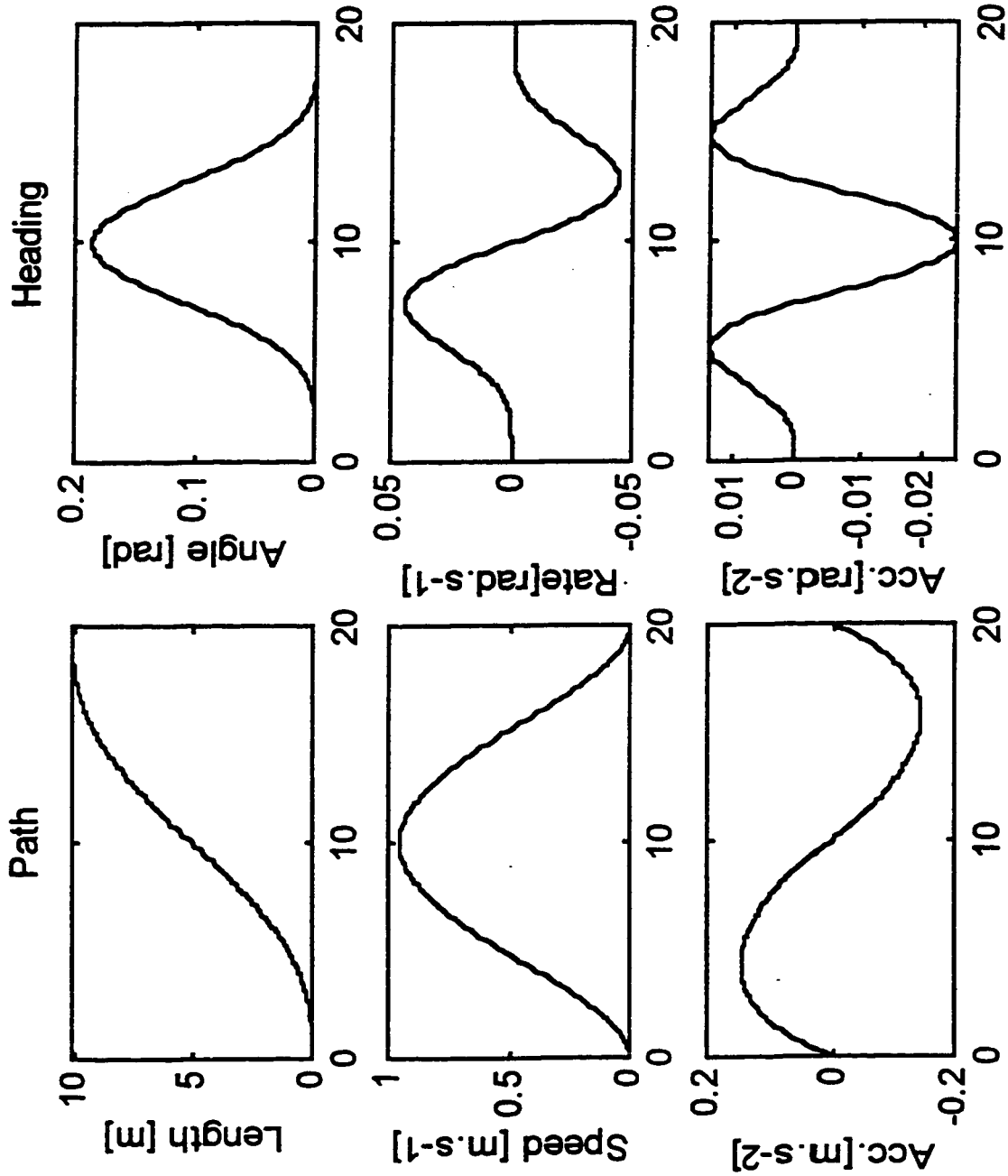

Figure 6.5 Desired path and heading parameters for the simulated lane change trajectory, LC_2

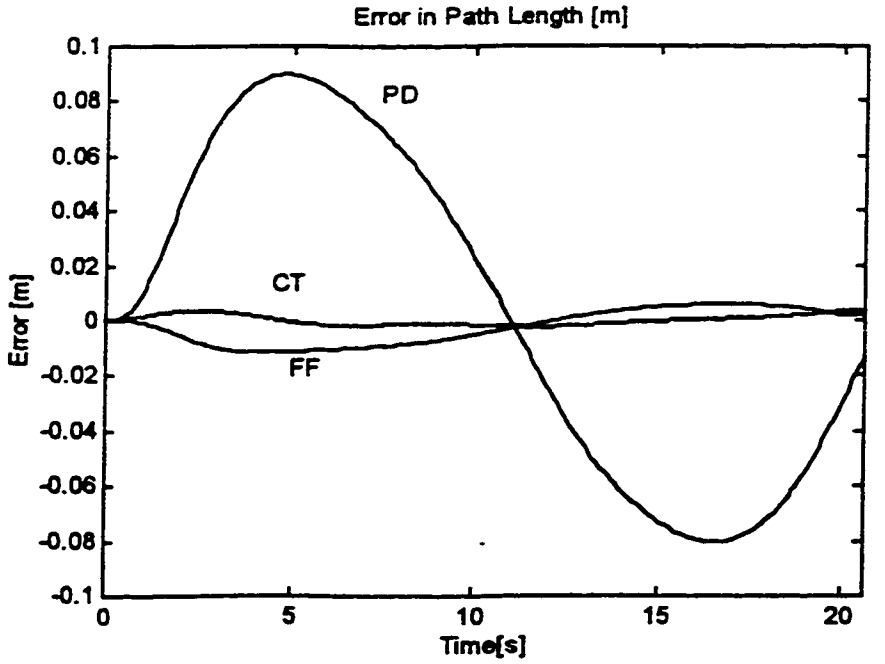

Figure 6.6 Instantaneous errors in path length for the simulated lane change trajectory, LC_2, for the PD, the FF and the CT controllers.

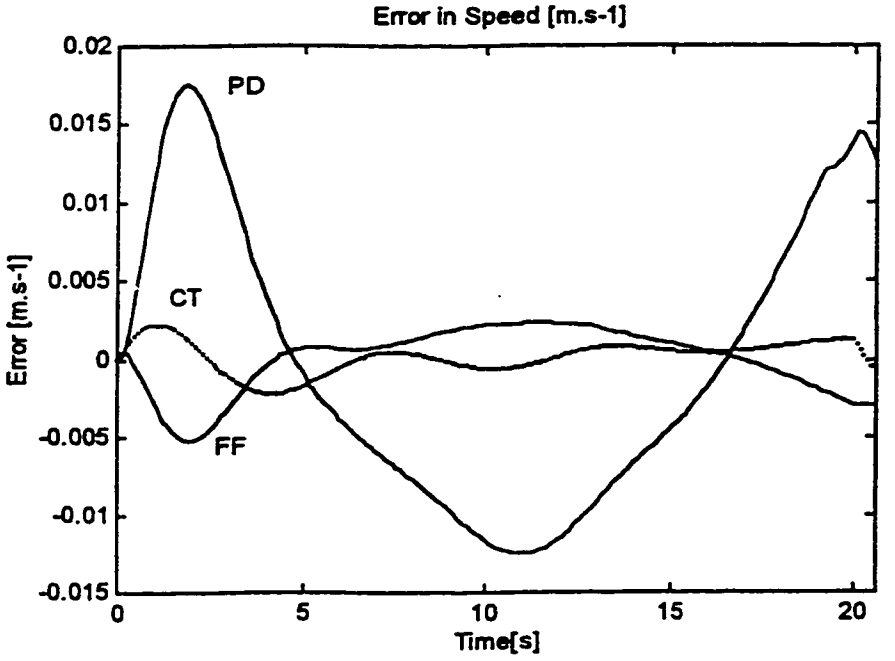

Figure 6.7 Instantaneous errors in forward speed for the simulated lane change trajectory, LC_2, for the PD, the FF and the CT controllers.

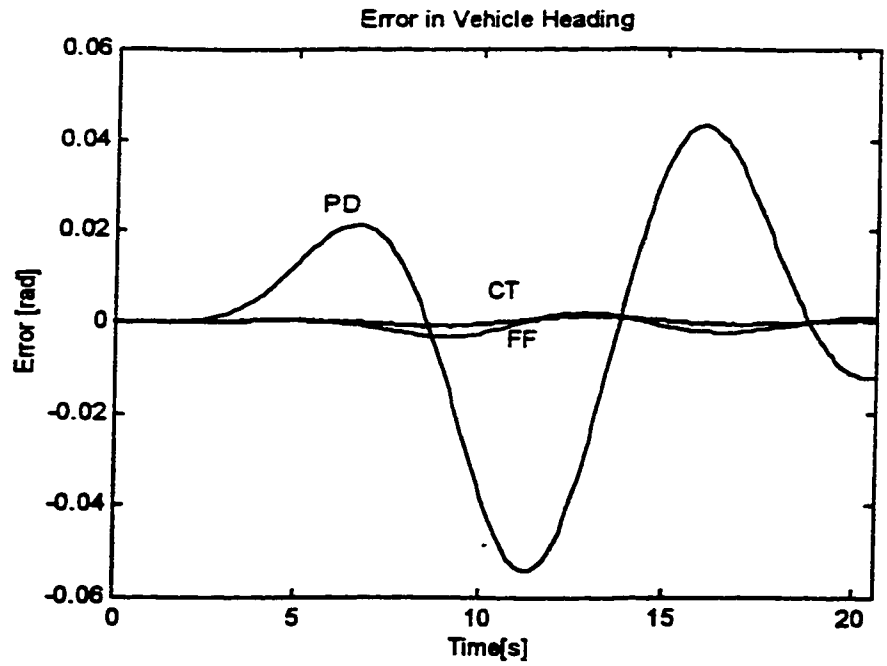

Figure 6.8 Instantaneous errors in vehicle heading for the simulated lane change trajectory, LC_2, for the PD, the FF and the CT controllers.

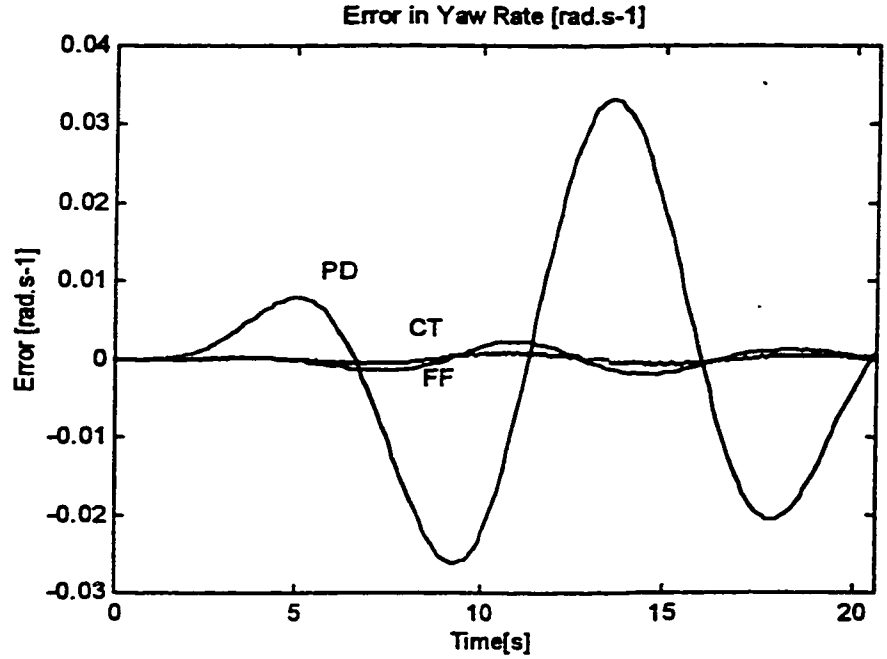

Figure 6.9 Instantaneous errors in yaw rate for the simulated lane change trajectory, LC_2, for the PD, the FF and the CT controllers.

Controller	Path Length RMS [m]	Path Length Max.[m]	Path Length SS.[m]	Forward Speed RMS [$m.s^{-1}$]	Heading RMS [rad.]	Heading Max.[rad.]	Heading SS.[rad.]	Yaw Rate RMS [$rad.s^{-1}$]
PD	0.06	0.09	<0.01	0.009	0.025	-0.054	-0.01	0.016
FF	0.007	-0.012	<0.01	0.002	0.002	-0.003	< 0.001	0.001
CT	0.002	0.003	<0.01	0.001	0.001	0.001	< 0.001	< 0.001

Table 6.2 Values of the performance indices for the path length, the forward speed, the heading and the yaw rate of CONCIC III obtained during the simulated execution of the lane change trajectory , Section 6.3.

(N.B: RMS = Root Mean Square value ; Max. = Maximum value ; SS. = Steady State value)

Desired Trajectory Parameters: Single segment lane change carrying a suspended load of 20 Kg. on a 0.4m long load arm.

Maximum forward speed : 1.0 $m.s^{-1}$; Maximum yaw rate: 0.0442 $rad.s^{-1}$

Total duration of the trajectory: 20 s.

Maximum Acceleration: 0.1444 $m.s^{-2}$; Maximum angular acceleration: 0.0137 $rad.s^{-2}$

controller for the FF controller whereas the CT controller uses the inverse dynamic model for error compensation. This results in the quicker convergence of the actual and the desired trajectories for the CT controller with smaller values of instantaneous errors.

6.5 Lane Change Trajectory at High Speeds

In order to compare the performance of the dynamic model based CT controller with that of the PD controller at speeds above those used in the experimental work, a second lane change trajectory was chosen. The inertial properties of the active payload were also increased above those used in the experimental work. The simulated payload is 40 Kg at the end of an arm of length 0.5m fixed to a point 0.75m vertically above the mass centre of the WMR. In this lane change trajectory, the WMR accelerates to a maximum forward speed of 1.9 $m.s^{-1}$ in a time of 5s. The maximum value of the forward acceleration during this phase is 0.578 $m.s^{-2}$. The distance between the two lanes is maintained at 1 m so that the WMR experiences a maximum angular acceleration of 0.102 $rad.s^{-2}$ at the mid point of the trajectory and reaches a maximum yaw rate of 0.089 $rad.s^{-1}$. The profiles of desired trajectory parameters during this lane change trajectory are shown in Fig.6.10.

The inverse dynamic model was evaluated for the desired trajectory in order to ensure that the drive torques at the wheels did not exceed the Coulomb friction present. As mentioned in Section 3.1, the inverse dynamic model used in the CT controller has been derived on the assumption of no-slip at the wheels. Hence the desired trajectory must be generated such that the non-holonomic nature of the system is preserved. The effect of the motion of the suspended mass on the vertical load acting on the drive wheels and thereby on

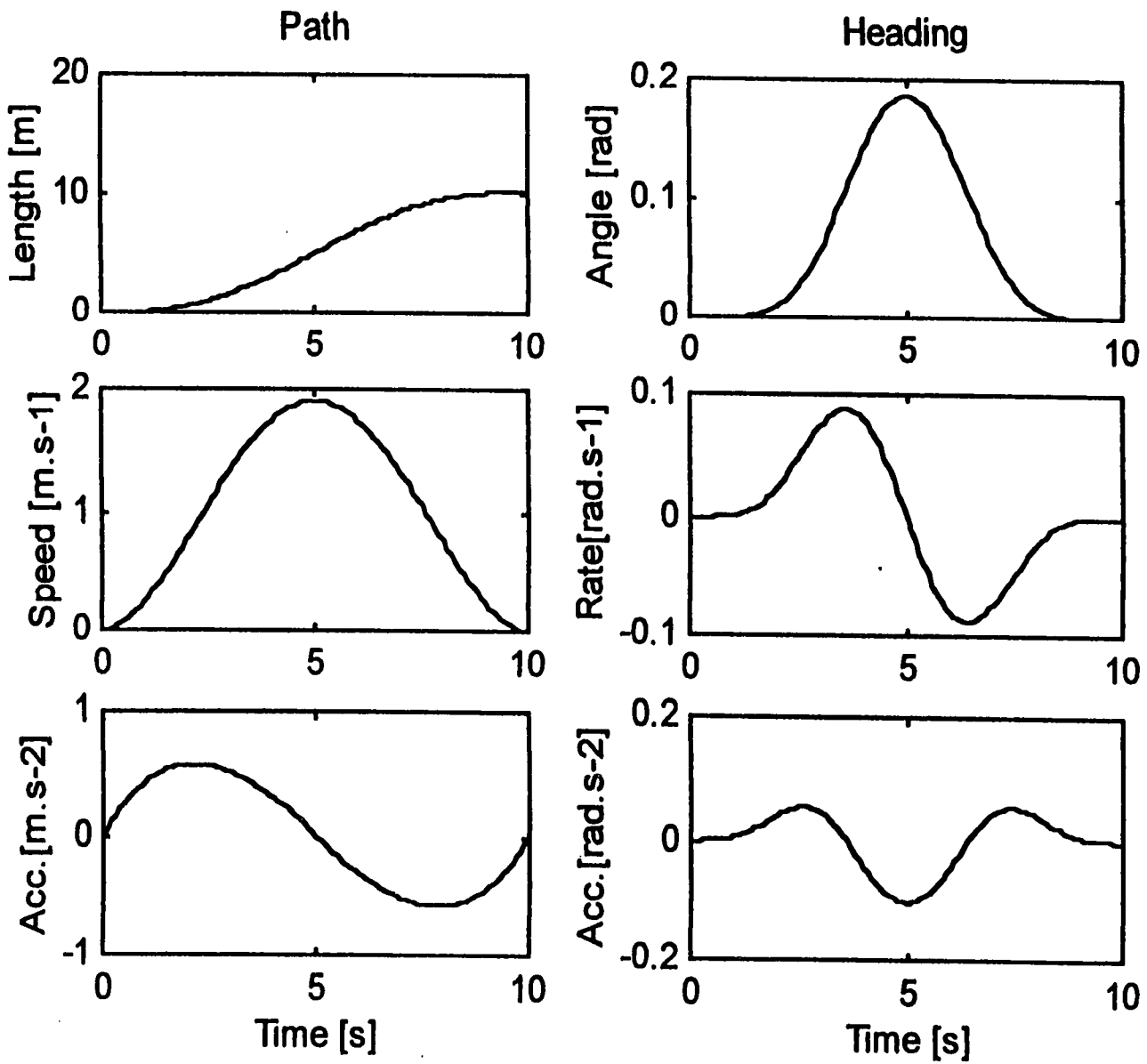

Figure 6.10 Desired trajectory parameters for the simulated lane change trajectory at high speed, LC_2.

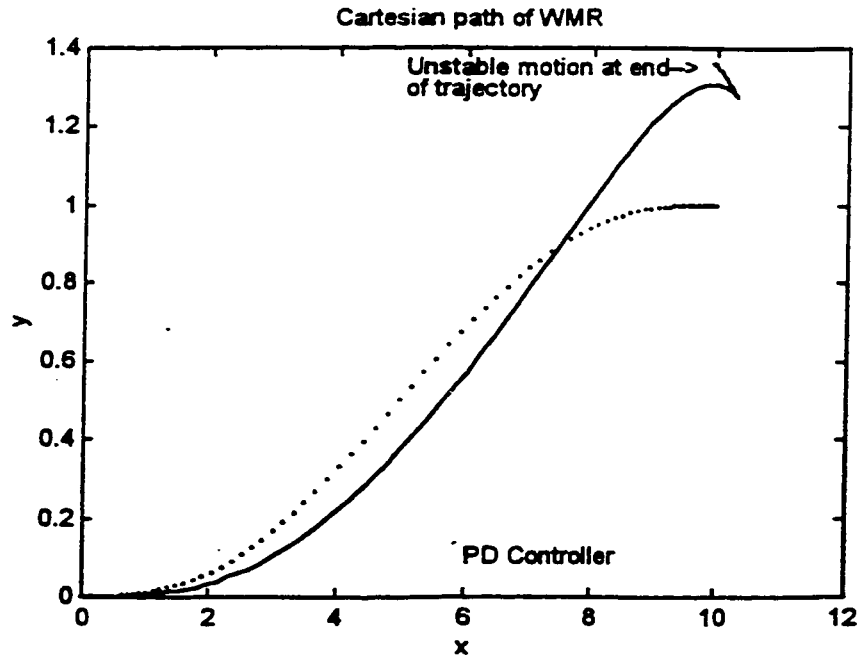

Figure 6.11 Cartesian path of the WMR for high speed lane change under the PD controller.

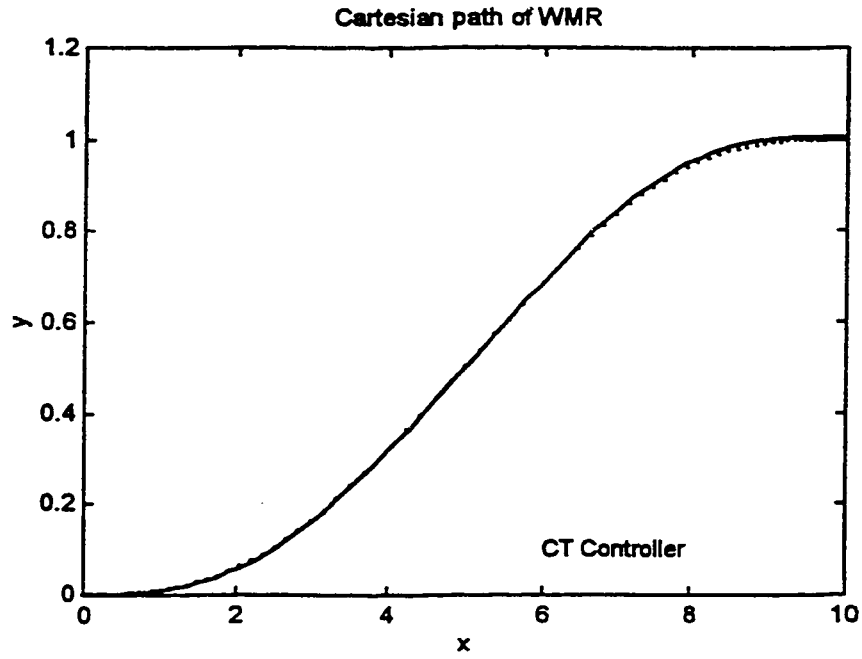

Figure 6.12 Cartesian path of the WMR for high speed lane change under the CT controller.

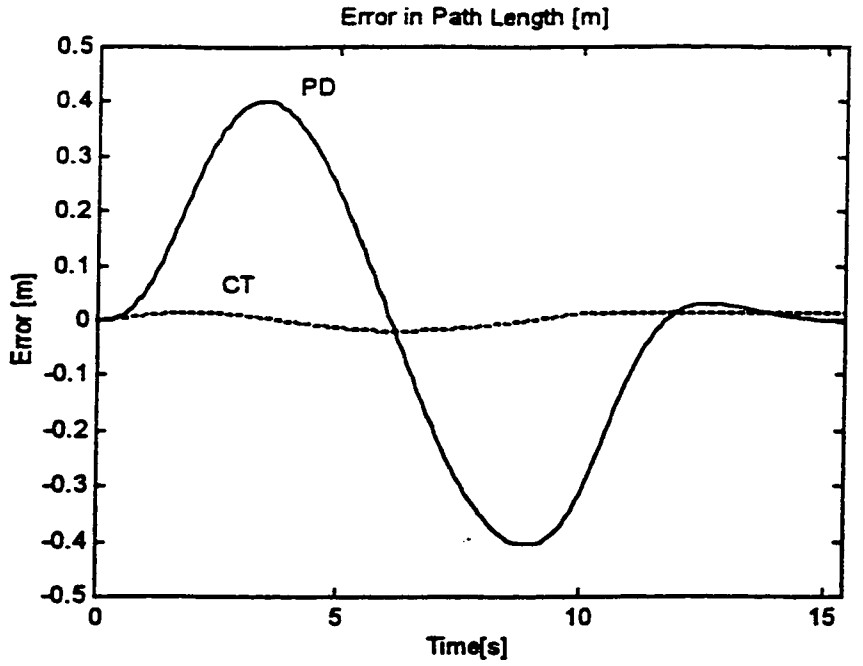

Figure 6.13 Plots of the instantaneous errors in path length for the PD and the CT controllers for the high speed lane change trajectory, LC_2.

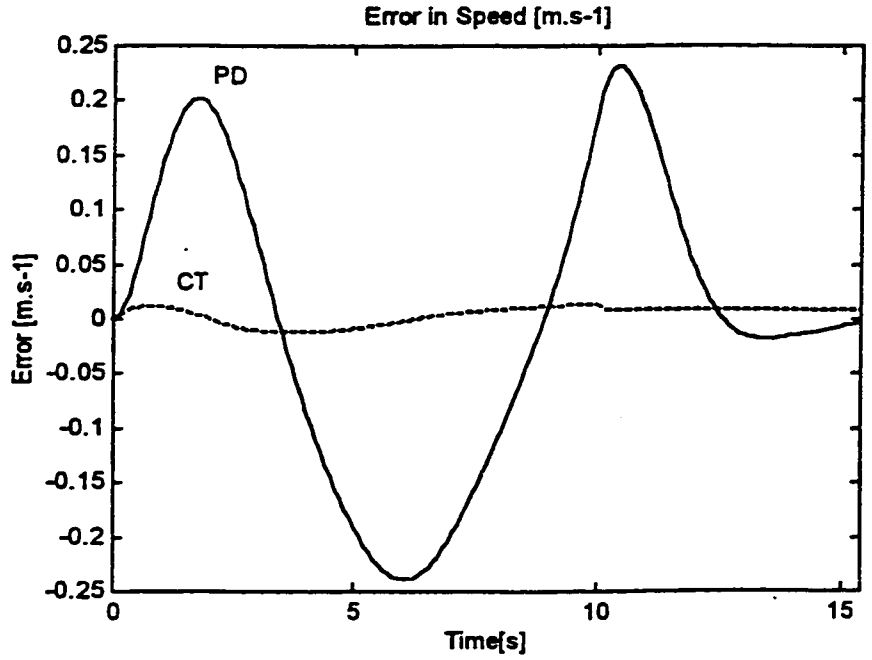

Figure 6.14 Plots of the instantaneous errors in forward speed for the PD and the CT controllers for the high speed lane change trajectory, LC_2.

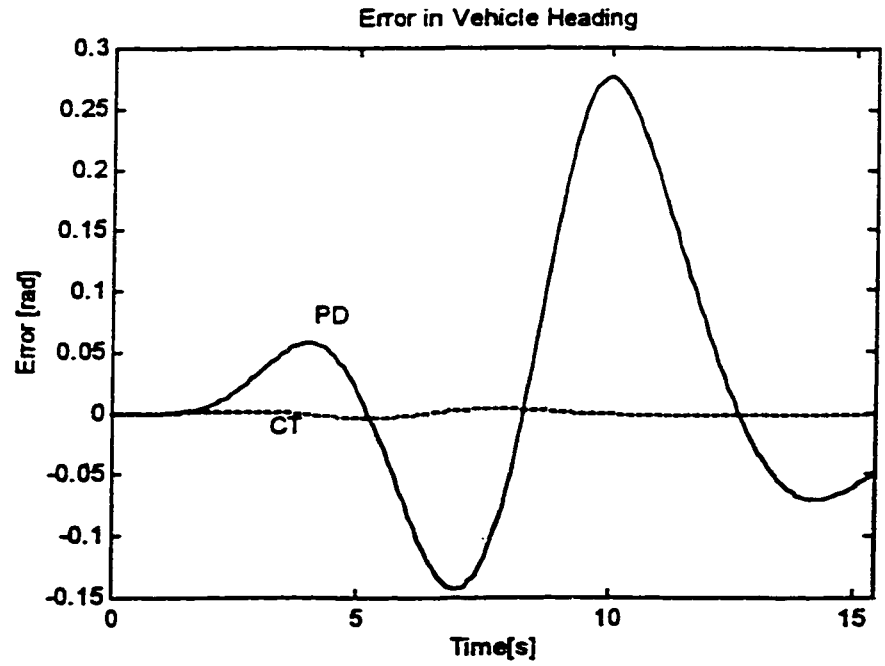

Figure 6.15 Plots of the instantaneous errors in vehicle heading for the PD and the CT controllers for the high speed lane change trajectory, LC_2.

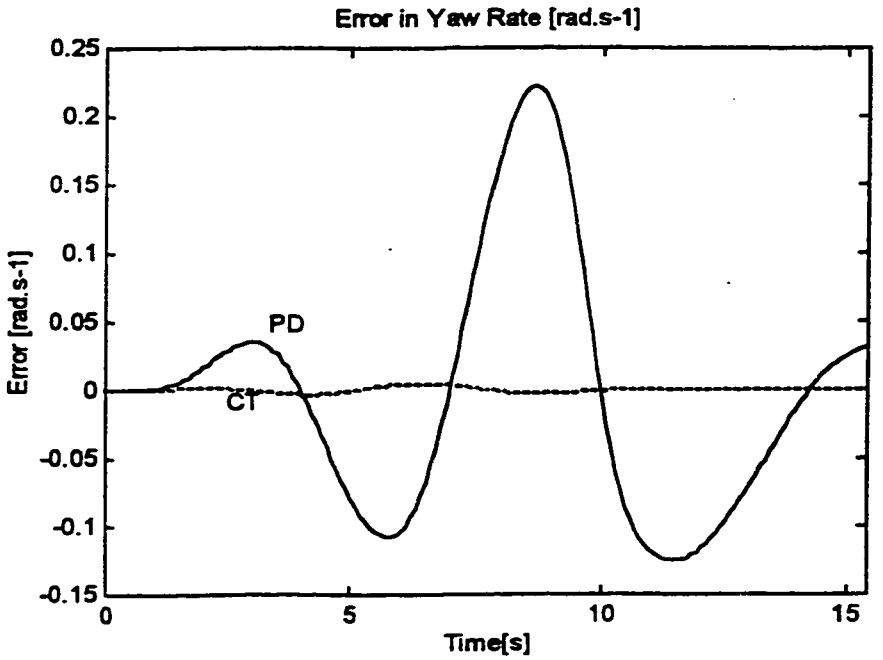

Figure 6.16 Plots of the instantaneous errors in yaw rate for the PD and the CT controllers for the high speed lane change trajectory, LC_2.

the Coulomb friction at the contact patch of the wheels during the trajectory was evaluated using the dynamic model of the load.

CT Controller	Path Length [m]	Forward Speed [$m.s^{-1}$]	Heading [rad.]	Yaw Rate [$rad.s^{-1}$]
RMS	0.012	0.009	0.002	0.002
Max.	-0.019	0.014	0.004	0.0045

Table 6.3 Values of the performance indices for the CT controller for the simulated lane change trajectory at high speed

The trajectory tracking performance of the CT controller is shown in Fig.6.11 and that of the PD controller in Fig.6.12, both as the path followed by the WMR in the floor frame. The model based controller is able to follow the desired path even with the disturbances from the suspended load. The performance indices for the CT controller are listed in Table 6.3. The RMS error in forward speed is less than 0.5% of the maximum speed reached by the WMR during the trajectory and the maximum instantaneous forward speed error is 1%. For yaw rates, the RMS value is 2.5% and the maximum instantaneous error value is 5% of the maximum desired yaw rate.

Comparisons of the instantaneous errors in the four trajectory parameters for the CT controller with those for the PD controller are shown in Fig.6.13 for the path length, Fig.6.14 for the forward speed, Fig.6.15 for the heading and Fig.6.16 for the yaw rate. The FF

controller, using the inverse of the dynamic model representing the WMR, performs equally with the CT controller in the simulations and is not shown in the figures for clarity. These figures show that the higher values of the accelerations and speeds used in this trajectory along with the higher value of the suspended payload affect the performance of the CT controller marginally. However, the figures highlight the increasingly poor trajectory tracking performance of the PD controller. This poor performance is due to the action of the higher inertial loads arising from the accelerations of the WMR compounded by the dynamics of the suspended load. The increased angular acceleration induces large orientation errors and overshoots at the points of maximum angular acceleration. The path of the WMR diverges from the desired path even with the feed back compensation provided by the PD controller. At the end of the desired trajectory, the WMR drifts away from the goal position of the WMR.

This drift at the end of the trajectory obeys the observations by Samson and Ait-Abderrahim [54], on feedback stabilization around a given terminal configuration for a WMR. They have proven that the actual trajectory of the WMR can be made to converge towards the desired trajectory generated for an ideal 'virtual' cart by stable feed back control as long as the virtual cart is moving. However, when the reference cart comes to rest, no stabilizing feed back exists. The values of the performance indices for the PD controller are not given since the WMR diverges from the goal position.

6.6 Side Forces and Wheel Vertical Loads

One of the issues specifically addressed in the dynamic modelling methodology developed in this thesis is the inclusion of the dynamic nature of the vertical loads and the side forces acting on the wheels of the WMR. The magnitude of the dominant frictional forces present at the contact patches of the tires are directly dependent on these forces. The survey of the literature given in Section 2.3 on the dynamic modelling schemes employed for WMRs shows that these forces are usually assumed to remain at their static values throughout the trajectory.

In order to validate the observation that the dynamic nature of these forces is not negligible and must be taken into account, a set of lane change simulations were performed for CONCIC III. The first trajectory used was the lane change trajectory described in Section 6.4. In order to study only the effect of the dynamic behaviour of the WMR, the suspended load was removed in these simulations. The linear and angular accelerations were then increased to the values of lane change trajectory used in Section 6.5. In the third trajectory, the accelerations were further increased to obtain wheel loads under these conditions. The values of the trajectory parameters for each trajectory are given in Table 6.4. The forward speeds and yaw rates used in these simulations are found in industrial and transit applications of WMRs [11].

The side forces acting on the right drive wheel of the CONCIC III during each trajectory are shown in Fig.6.17 for Trajectory I (labelled Slow Lane Change, SLC_1), in Fig.6.19 for the medium speed lane change, MLC_1 and for the high speed lane change, HLC_1 in Fig.6.21. The instantaneous vertical loads on the right drive wheel, expressed as

a ratio of the static wheel load under stationary conditions, are shown in Figs.6.18, 6.20 and 6.22 for the three trajectories respectively. A summary of the maximum side force and the maximum wheel load ratio for each trajectory are given in Table 6.4.

A comparison of the side forces indicates that the magnitude of the force increases as the square of the maximum yaw rate. The side forces on the wheels for a WMR carrying a deadweight are due to the centrifugal forces, which in turn are dependent on the square of the angular speed. The dynamic fluctuations in the vertical wheel load depend on both the forward and the angular accelerations of the WMR. For the lane change trajectory with the highest acceleration values, HLC_1, the ratio rises to 125% of the static wheel load. The side force acting on the left drive wheel is equal to that on the right wheel. However, the vertical loads on the two wheels are mirror images of each other. The motion of the WMR transfers the loads between the wheels, so that an increase in the load on one wheel results in a decrease in the vertical load on the other. In the case of the drive wheel, a 25% reduction in the vertical load will reduce the available Coulomb frictional force at the tire by the same percentage. Hence, if the controller does not compensate for this reduction, the applied drive torque may exceed the friction limit and wheel slippage will result. In the case of a model based controller, the changes in the frictional forces due to the dynamic vertical loads must be taken into account to compute the drive torques.

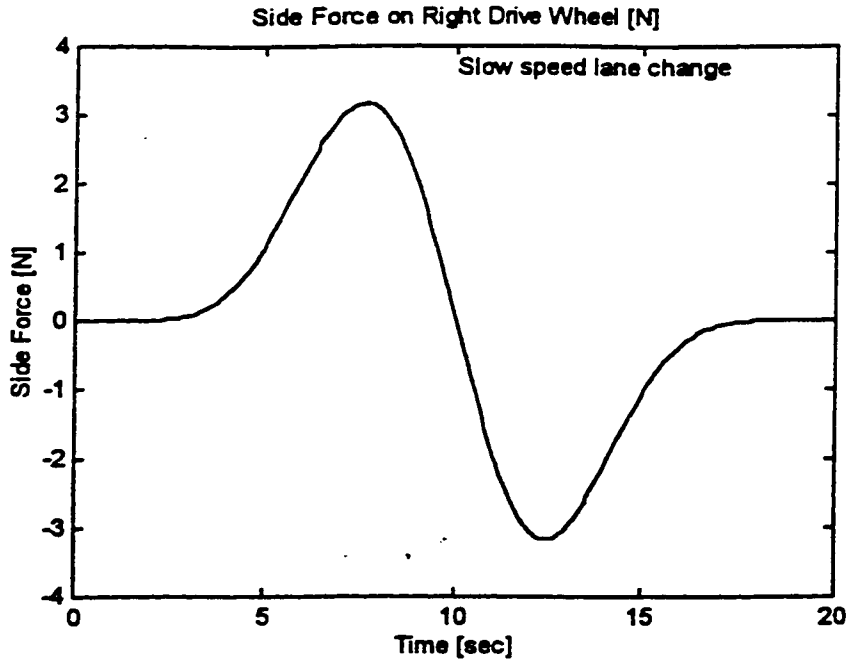

Figure 6.17 Side force on drive wheel (right) during the slow speed lane change,SLC-1.

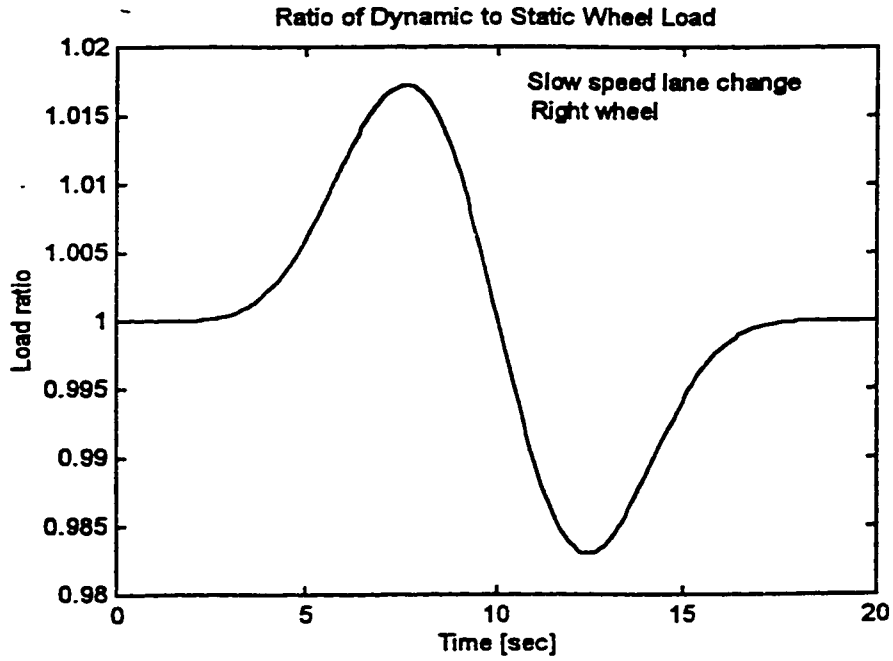

Figure 6.18 Ratio of the instantaneous dynamic vertical load to the stationary load on a drive wheel (right) during the slow speed lane change, SLC_1.

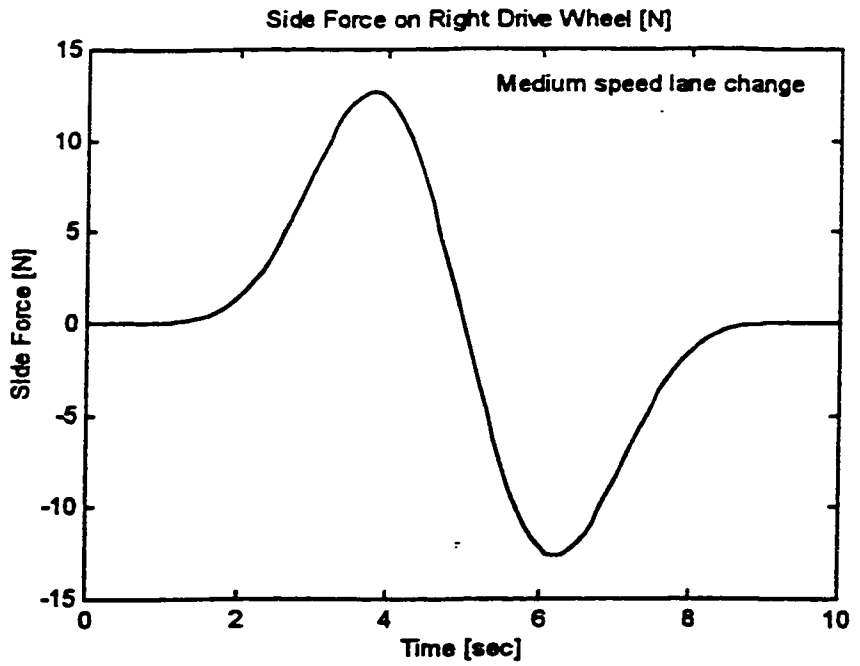

Figure 6.19 Side force on drive wheel (right) during the medium speed lane change,MLC-1.

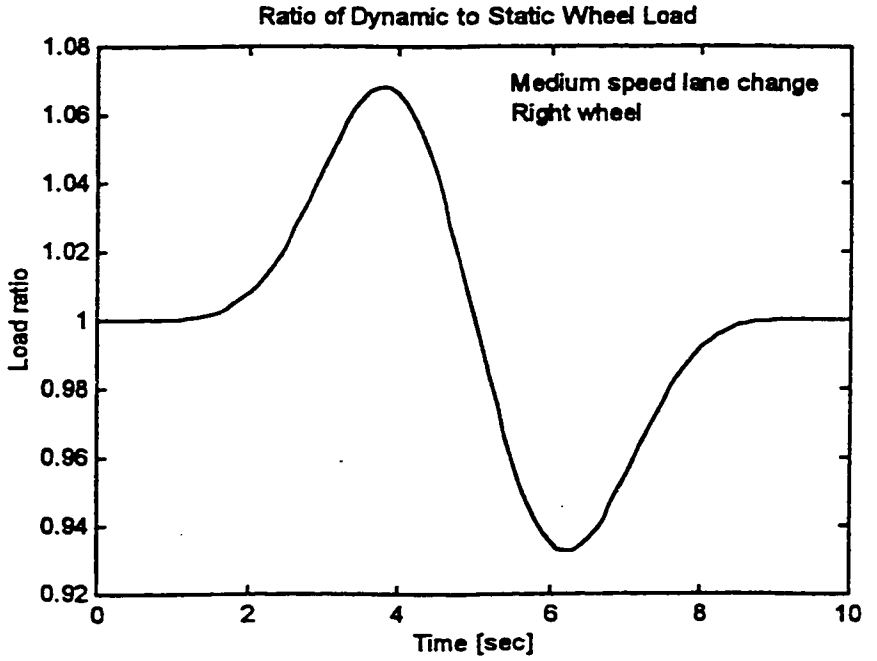

Figure 6.20 Ratio of the instantaneous dynamic vertical load to the staionary load on a drive wheel (right) during the medium speed lane change, MLC_1.

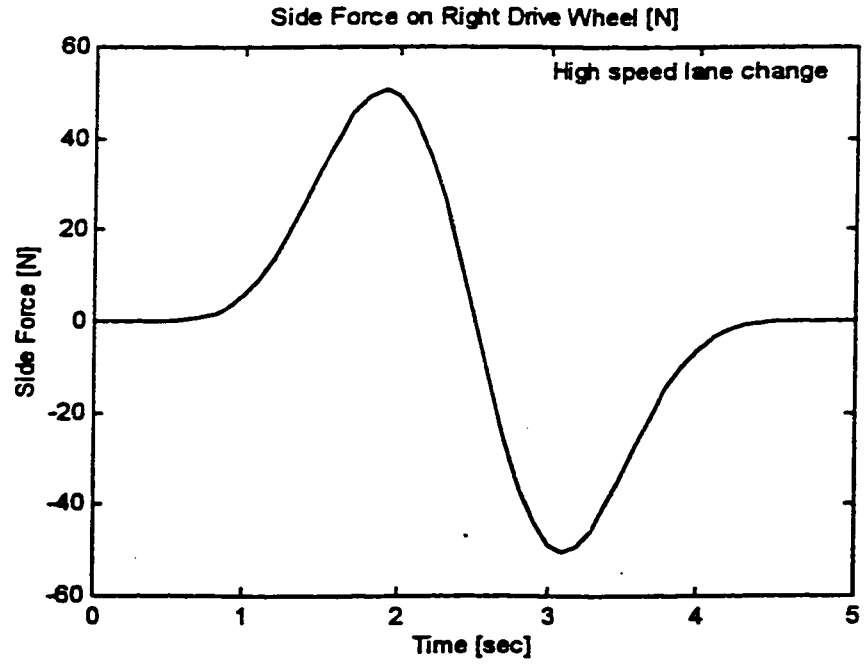

Figure 6.21 Side force on drive wheel (right) during the high speed lane change,HLC-1.

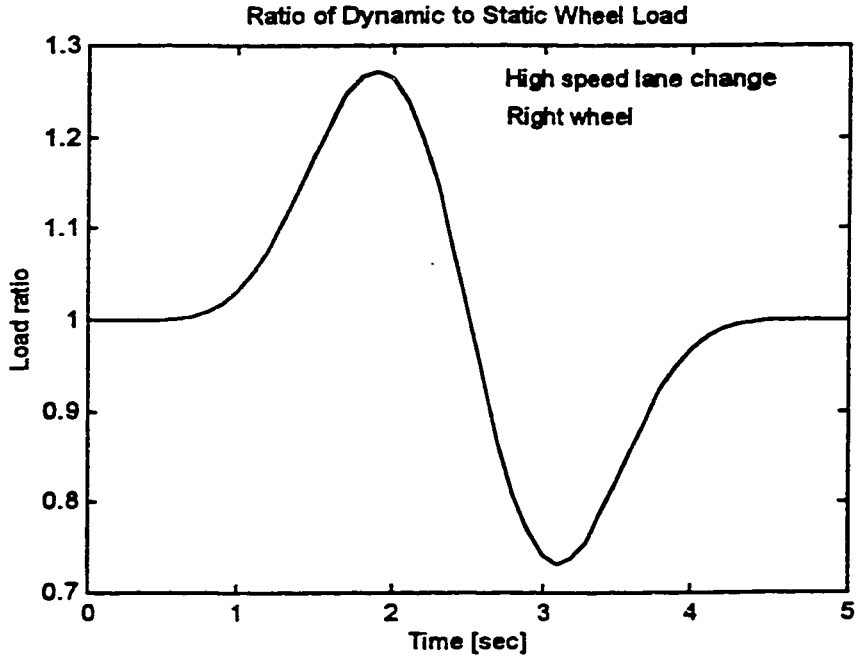

Figure 6.22 Ratio of the instantaneous dynamic vertical load to the staionary load on a drive wheel (right) during the high speed lane change, HLC_1.

Trajectory	Duration [s]	Forward Speed [$m.s^{-1}$]	Linear Acceleration [$m.s^{-2}$]	Yaw Rate [$rad.s^{-1}$]	Angular Acceleration [$rad.s^{-2}$]	Max. Side Force [N]	Max. Vertical Load Ratio [-]
SLC_1	20	1	0.14	0.044	-0.026	3.18	1.017
MLC_1	10	2	0.578	0.089	-0.102	12.71	1.068
HLC_1	5	4	2.308	0.177	-0.408	50.8	1.27

Table 6.4 Trajectory parameters and comparison of maximum side forces and vertical loads on drive wheels during lane change trajectories at three different linear and angular accelerations.

6.7 Effects of Errors in the Estimates of Inertial and Frictional Parameters

The behaviour of CONCIC III under the model based Feed Forward controller during the experimental trials did not bear out the predictions of the simulations presented in this chapter. For the CT controller, the simulations indicate the correct trend though the numerical values of the performance indices differ substantially. An analysis of the experimental results indicated that the source of the differences may lie in differences between the estimated values of the inertial and frictional parameters used in the dynamic model and the actual values for the WMR. In particular, it was surmised that the inertial parameters in the model had been overestimated while the frictional model gave an underestimate of the actual frictional forces in the actuator and the tire. In order to investigate this hypothesis, simulations for the three controllers were performed in which the inertial parameters were overestimated by a value of 20% while the frictional values were assumed to be double the modelled value. The trajectory used in the simulation was the lane change trajectory presented in Section 6.4. The results obtained for each controller for the simulated case in which the modelled values exactly match the actual values are termed 'Nominal' in the set of error plots, Fig.6.23 to Fig.6.26 for the PD controller, Fig.6.27 to Fig.6.30 for the FF controller and Fig.6.31 to Fig.6.34 for the CT controller. The 20% overestimate in inertial values are termed 'Inertial'. To study the effect of an underestimated frictional value, the frictional forces computed by the friction model were increased by 100% and the performance curves obtained for this case are termed 'Frictional'. The inertial values were maintained at their nominal values for these simulations. Finally, simulations were performed with the inertial parameters overestimated by 20% and the frictional parameters underestimated by 100% and the resulting performance

curves for each controller are labelled 'Both'. The figures show the influence of the parameters on the instantaneous errors in the trajectory parameters for each controller. In these figures, it is the effect of the inertial and the frictional parameters, either individually or in conjunction, on the errors that is important and not the numerical values of these changes.

The PD controller shows no change in the pattern of instantaneous errors during the trajectory, either for the overestimated inertial parameter values or for the underestimated frictional parameters. The inertial terms increase the magnitude of the errors in path length and the forward speed. In these simulations, the gains of the controller were left unchanged and the decrease in the inertia leads to higher values of overshoots. Friction on the other hand, adds damping to the closed loop response and the effect is seen as an improvement in the position errors. With regards to orientation, the decrease in the inertia, decreases the value of the errors while friction increases it. These relative changes in magnitudes of the errors are brought about by the particular values of the controller gains and the trends in the errors remain unaltered.

For both the model based controllers on the other hand, the effects of changes in the inertial parameters are similar in nature and are very pronounced. For the FF controller, the 20% overestimation in the inertial values, produces a fourfold increase in the instantaneous errors in the path length and the forward speed. The overestimated feed forward drive torques during the acceleration phase of the trajectory produce large errors in the forward speed and consequently in the path length as well. Similarly, during the deceleration phase, the braking torques used to slow the WMR are larger than the required values and the trajectory lags behind the desired trajectory. Friction on the other hand is seen to produce only a marginal

decrease in the values of the position errors due to its damping effect. The effect of the inertial and frictional parameters on the orientation errors are similar to the effect on position. The 20% overestimation in the inertial parameters produces a four fold increase in the magnitude of the error in the heading and a three fold increase in the errors in yaw rate.

For the CT controller, the effect of overestimation in inertial parameters on the error in the path length and the forward speed, shown in Fig.6.31 and Fig.6.32, is to make the WMR lead the reference trajectory in the acceleration phase where the nominal errors are lagging. Increased friction, on the other hand, increases the lagging errors in this phase of the trajectory. During the deceleration phase, the CT controller overcompensates for the inertia of the WMR and the actual trajectory lags behind the desired values. The effects on orientation errors, shown in Figs. 6.33 and 6.34, show a similar trend for changes in the inertial and the frictional terms, with the inertial effects being more dominant.

The results of these simulations bear a close resemblance to the behaviour of the model based controllers during the experimental work. For lane change trajectories, large leading errors in the forward speed and the position were observed during the acceleration phase for the FF and the CT controller. The magnitudes of the errors for the CT controller were however much smaller than those for the FF controller, as indicated by the performance indices given in Chapter 8. During the deceleration phase, the large lagging errors indicated by the simulations were also observed. The trends in the errors in orientation and yaw rate in these simulations were seen in the experimental results as well.

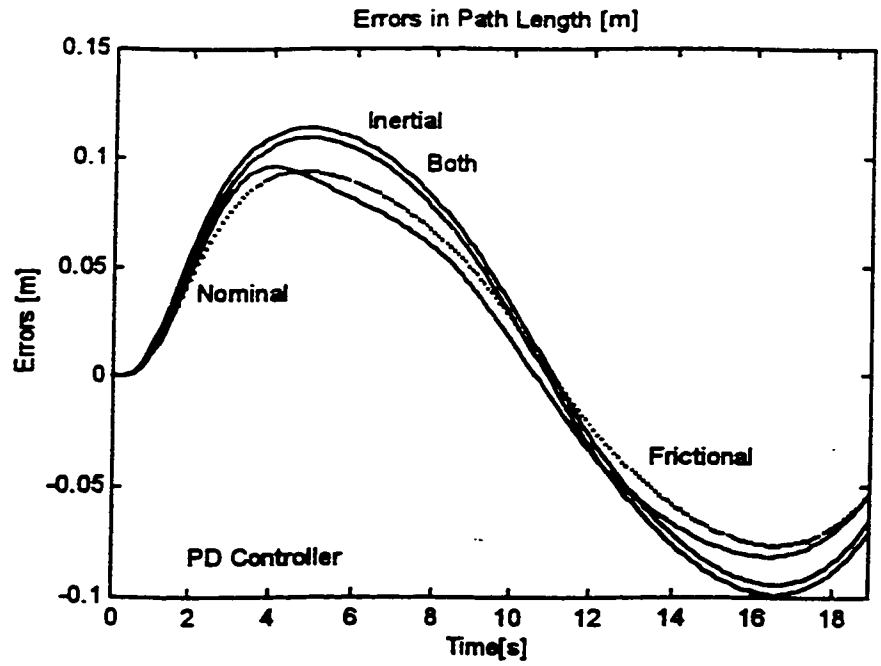

Figure 6.23 Influence on errors in path length due to differences between modelled and actual inertial and/or frictional parameters for a PD controller.

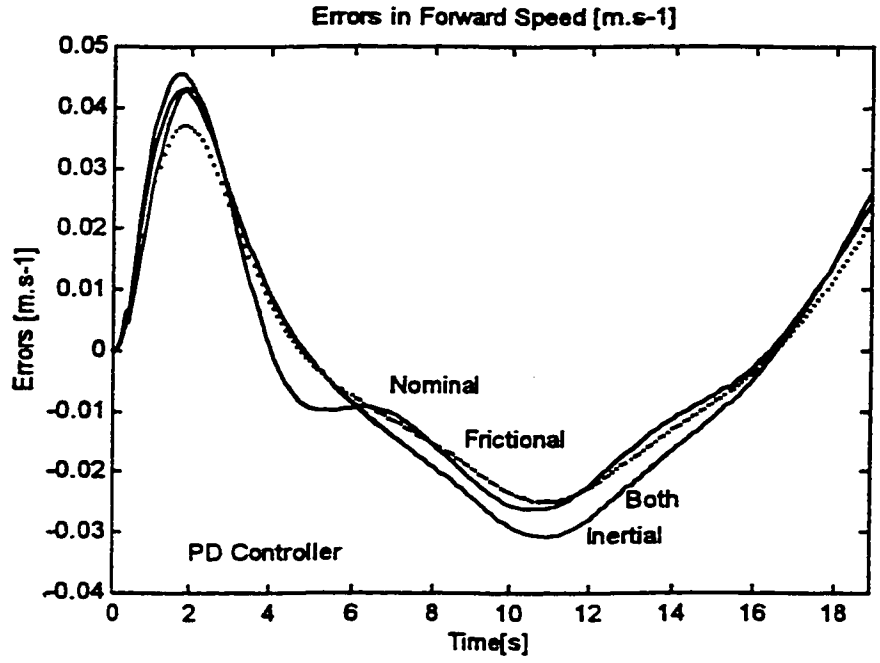

Figure 6.24 Influence on errors in forward speed due to differences between modelled and actual inertial and/or frictional parameters for a PD controller.

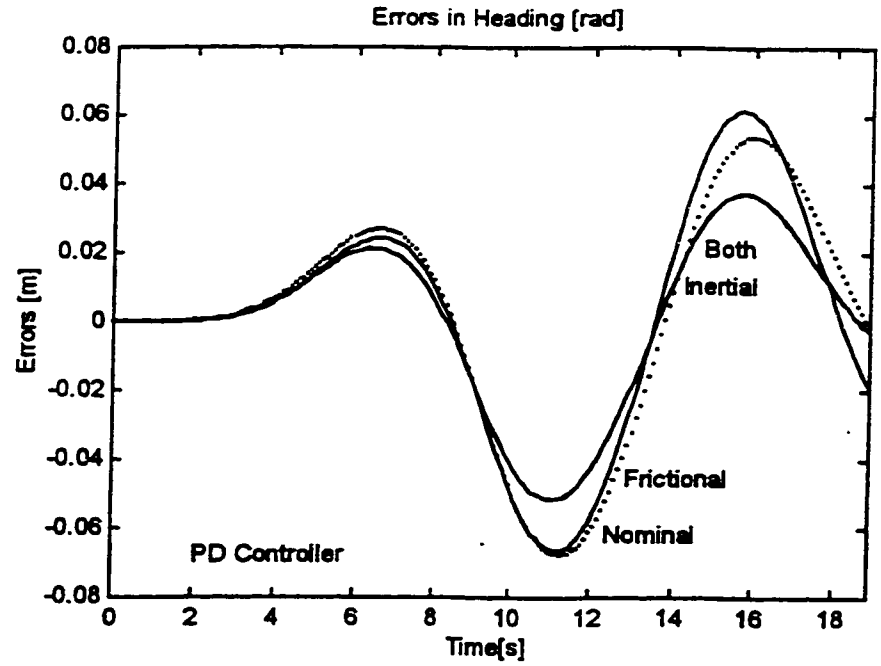

Figure 6.25 Influence on errors in vehicle heading due to differences between modelled and actual inertial and/or frictional parameters for a PD controller.

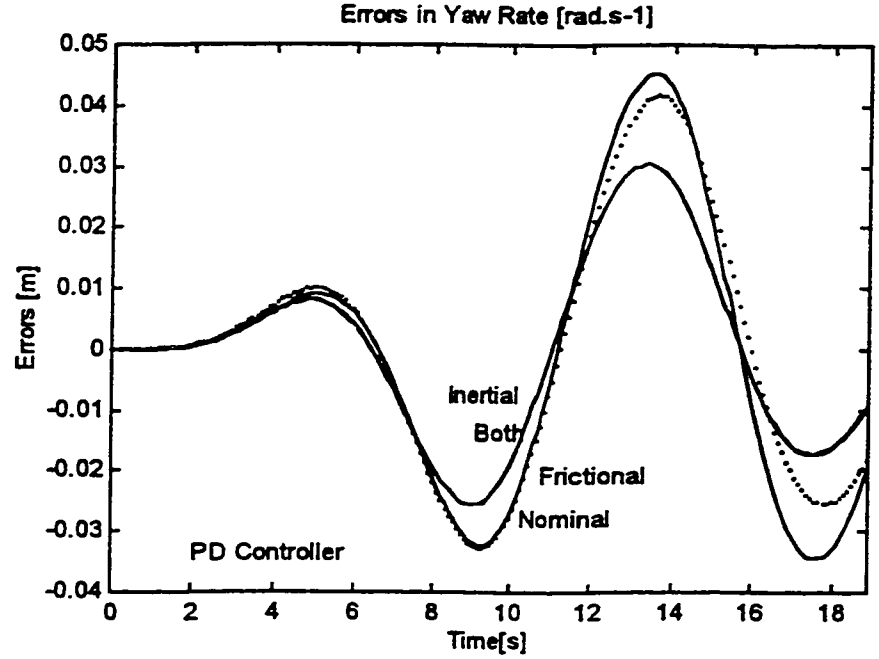

Figure 6.26 Influence on errors in yaw rate due to differences between modelled and actual inertial and/or frictional parameters for a PD controller.

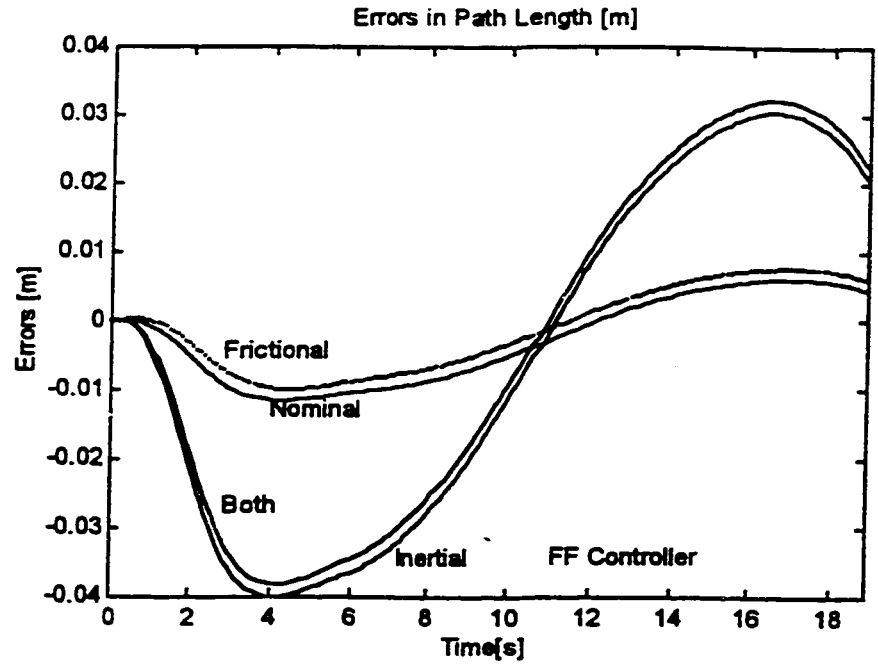

Figure 6.27 Influence on errors in path length due to differences between modelled and actual inertial and/or frictional parameters for a FF controller.

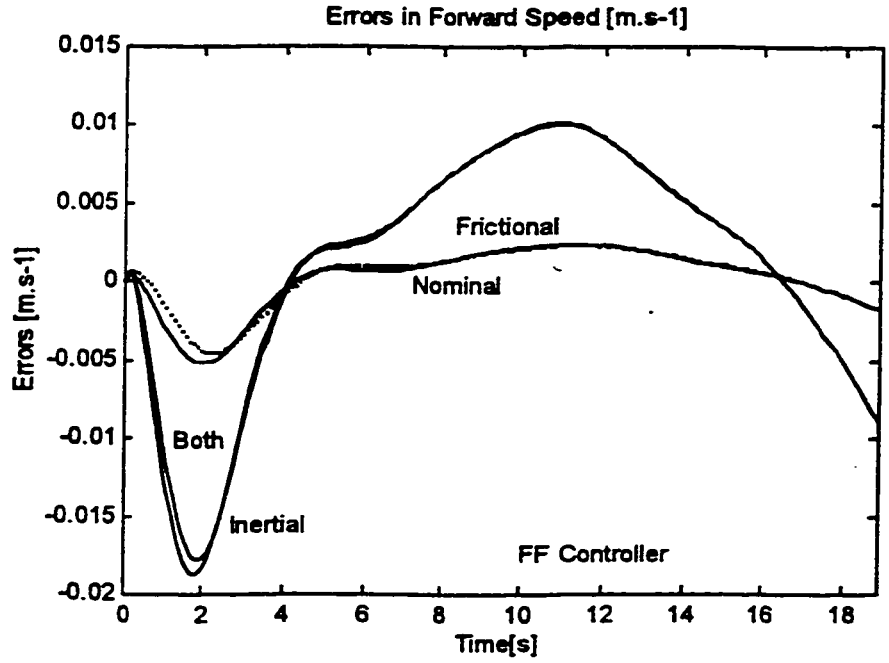

Figure 6.28 Influence on errors in forward speed due to differences between modelled and actual inertial and/or frictional parameters for a FF controller.

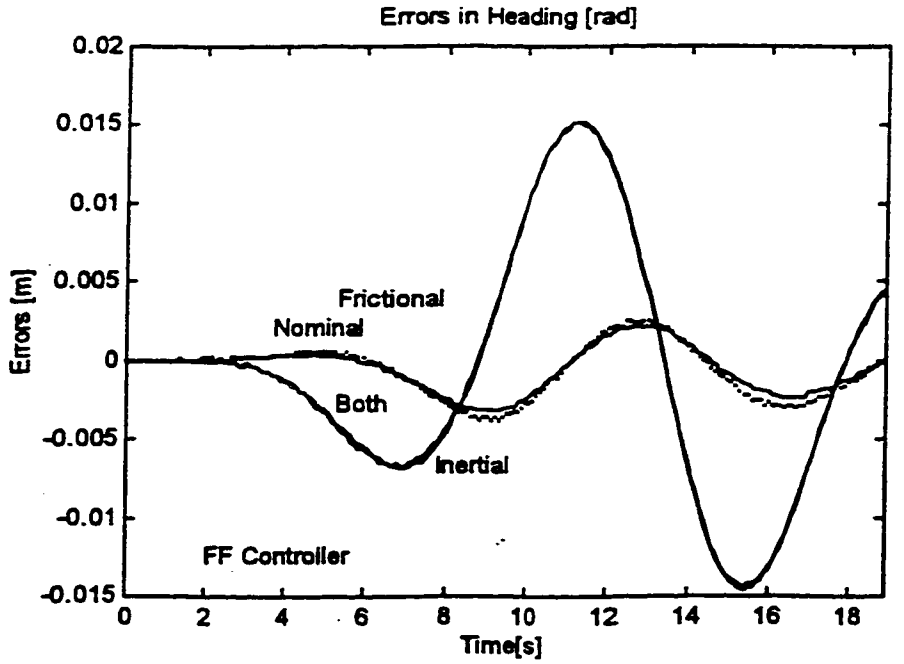

Figure 6.29 Influence on errors in vehicle heading due to differences between modelled and actual inertial and/or frictional parameters for a FF controller.

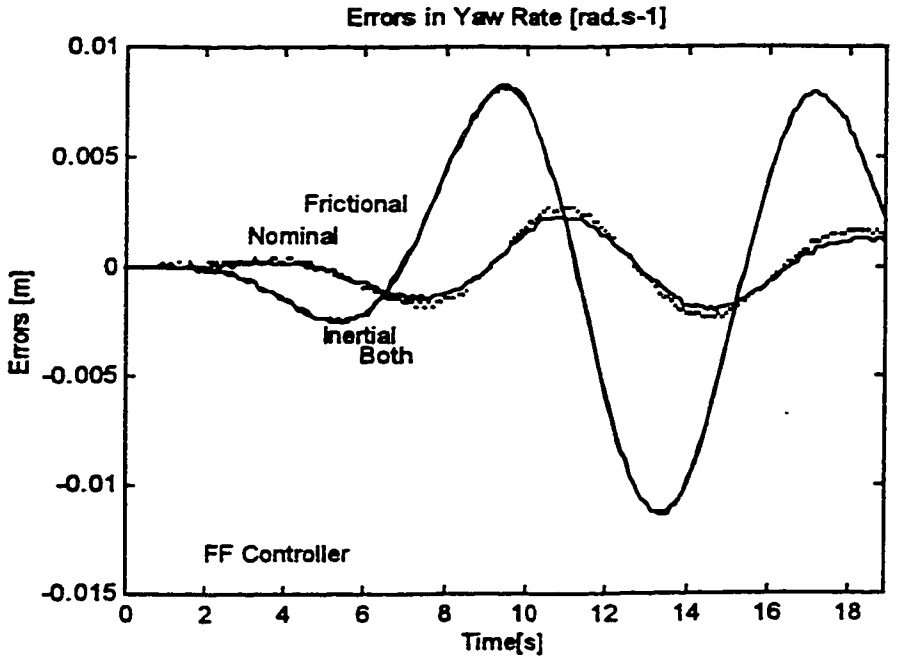

Figure 6.30 Influence on errors in yaw rate due to differences between modelled and actual inertial and/or frictional parameters for a FF controller.

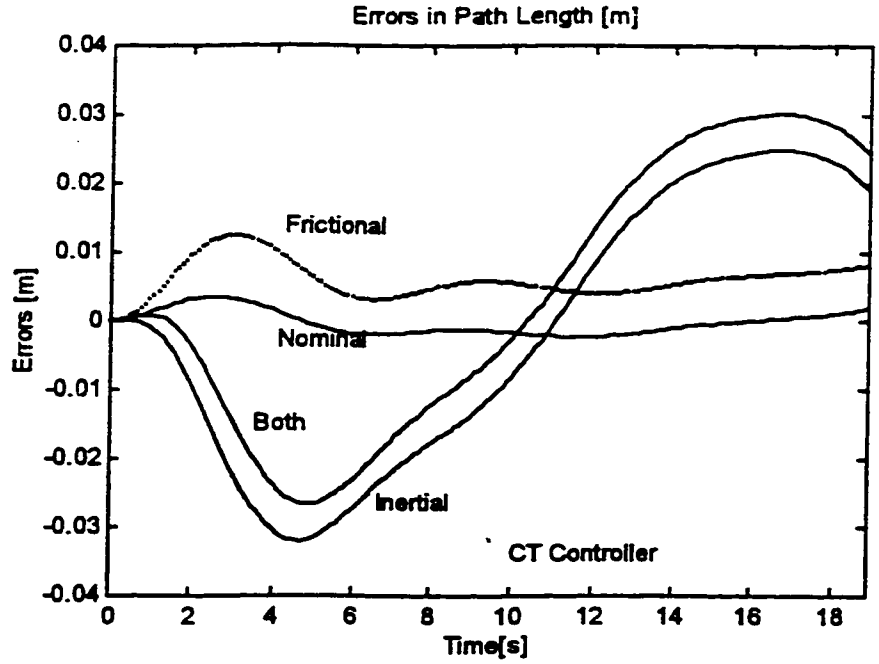

Figure 6.31 Influence on errors in path length due to differences between modelled and actual inertial and/or frictional parameters for a CT controller.

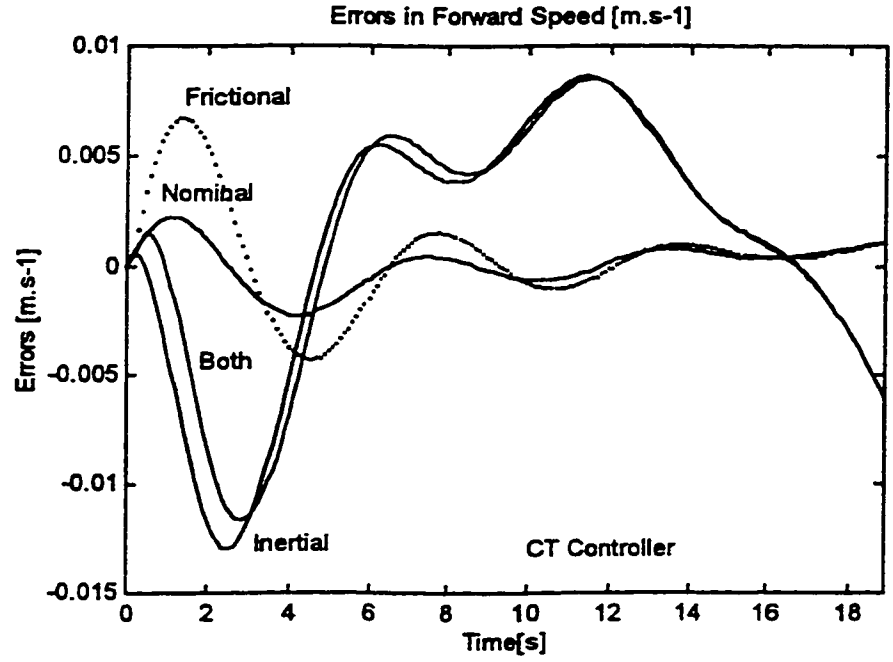

Figure 6.32 Influence on errors in forward speed due to differences between modelled and actual inertial and/or frictional parameters for a CT controller.

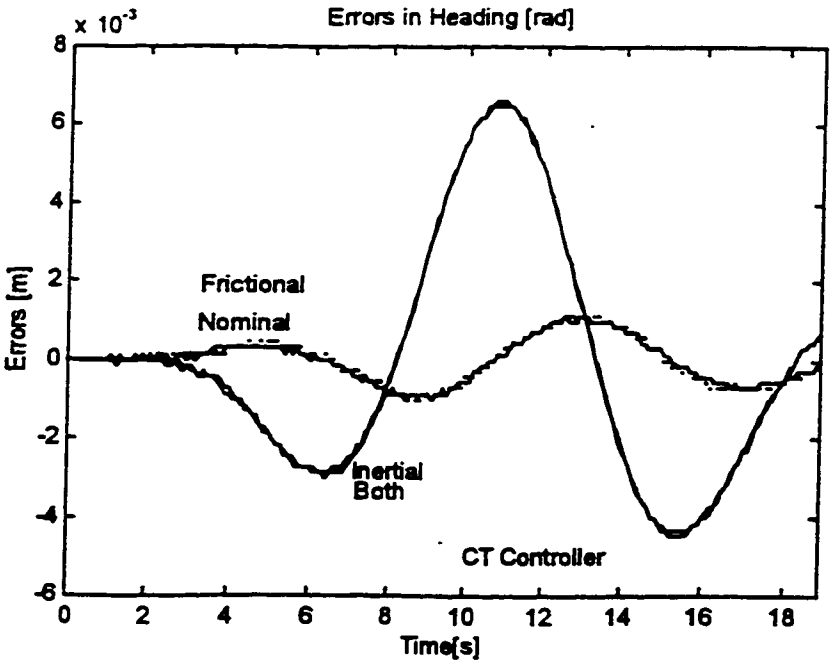

Figure 6.33 Influence on errors in vehicle heading due to differences between modelled and actual inertial and/or frictional parameters for a CT controller.

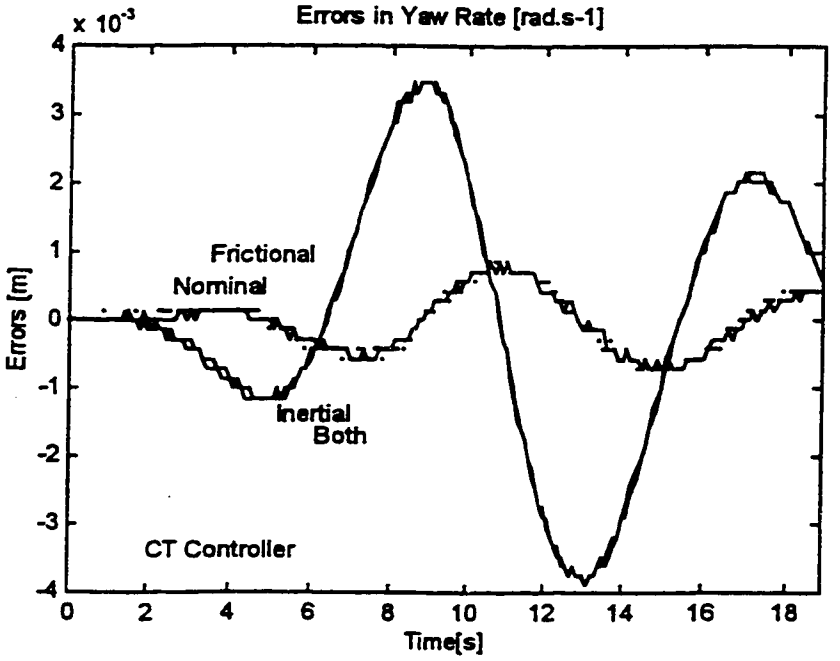

Figure 6.34 Influence on errors in yaw rate due to differences between modelled and actual inertial and/or frictional parameters for a CT controller.

6.8 Summary

In this chapter, results obtained from simulations of the dynamic behaviour of the WMR for the PD, the FF and the CT controllers under various operating conditions are presented. These results are used to compare and to evaluate the performances of the controllers. A straight line trajectory, with values of parameters later used in the experimental investigations, indicates that both the model based controllers perform equally well and the performance indices used for comparison show that they outperform the PD controller. These results are further borne out by the simulations of the lane change trajectory in which the model based controllers are observed to perform well in tracking the desired orientation of the WMR as well. The simulations are then extended to a lane change trajectory with values of speeds and accelerations higher than those possible on the experimental WMR. These trajectory values, however, exist in industrial applications of WMRs. A comparison of the performances of the controllers indicates that the CT controller is able to track the trajectory with marginal increases in the values of the errors. However, the PD controller is unable to compensate for the accelerations and the WMR diverges from the goal position.

The second set of simulations are performed to underline the necessity to account for the dynamic nature of the side forces and the vertical loads acting on the wheels of the WMR. The magnitude of the frictional forces in the actuators and in the contact patches of the tires depend on these forces. Simulations done for three lane change trajectories for the CONCIC III show that a four fold increase in the angular speed results in a sixteen fold increase in the side force. Similarly, for the acceleration values used in this simulation, the vertical load is seen to increase to 125% of the static value. These large changes in the magnitudes of the

forces must be taken into account by a model based control scheme.

Finally, the effects of differences between estimated and actual values of inertial and frictional parameter values on the performance of the controllers have been investigated. These simulations were done specifically to verify the reasons proposed in Chapter 8 to explain the behaviour of the FF controller. The large leading errors during periods of acceleration and the large lagging errors during deceleration for the FF controller observed during the experimental investigations were analyzed to be due to errors in the over estimates of the inertial values of the WMR. In addition, it was reasoned that the frictional forces obtained from the tire friction and the actuator friction models under estimated the actual values, leading to the performances observed. The simulations, performed for a 20% overestimation in the inertial values and estimates of frictional values half those actually present, indicate trends similar to those seen during the experimental work.

Chapter 7

System Description of the Experimental Setup

7.1 Introduction

This chapter describes the interface and the support hardware systems and the control software used for the experimental investigations. The tests have been carried out on the experimental platform, CONCIC III, described in Section 1.3, under generalised loading conditions and realistic trajectories and manoeuvres. The vehicle frame was modified to carry the suspended mass used as the active load in the experimental work. The digital to analog interface circuitry has been updated to provide better resolution and speed and more versatile data acquisition facilities. The control software for each controller was developed in a modular form using a template developed as part of this work. The template provides all the modules necessary to initialize and setup the interface hardware and the data acquisition segments, so that the user may use the software with minor modifications to implement various digital controllers on this experimental platform.

The modifications done to the wheel configuration, to the vehicle frame to carry the suspended load and to the control hardware of the CONCIC III for the present experimental investigations are described in Section 7.2. Using flow charts, the software template and the control software used for each control strategy are explained in Section 7.3. This section also discusses the data acquisition capabilities provided by this hardware configuration. Section 7.4 describes the interrupt handling segment and some special methods developed in this work to provide stable handling of asynchronous interrupts on two PC-AT interrupt levels. These

features were implemented to prevent conflict between the interrupt from the sample interval timer for the digital controller and the interrupt signalling an error from the data acquisition card. The chapter concludes with a summary of the important features of the hardware setup, the software template and the digital control segments presented in this chapter.

7.2 The Experimental Platform, CONCIC III

The experimental investigations have been carried out using the mobile robot, CONCIC III, described in Section 1.3 with some modifications. This experimental platform was developed by Mehrabi, Cheng and Hemami [10] and Mehrabi [6] for investigations on the dynamic modelling and the synthesis of an optimal controller for a WMR. A diamond wheel configuration with front and rear steer drive units and two fixed castors on the transverse mid-plane on either side of the geometric centre was used.

For the present investigations, for reasons cited below, a diamond wheel configuration is used with differentially driven wheels in the transverse mid-plane on either side of the geometric centre. The same differential drive configuration was used by Rajagopalan [3], Rajagopalan and Cheng [4] and by Rajagopalan and Barakat [14] for CONCIC II. In the configuration used by Mehrabi [6], the fixed castors in the mid plane impose a restriction on the turning radius of the vehicle. Moreover, the drive input to the front and the rear drive wheels must be perfectly matched to avoid longitudinal slip and the steering angles matched to prevent side slip of the wheels. The reduction gearing used in the steering mechanism is prone to backlash errors and hence, to mismatched steering angles. In the differential drive only two individual drive inputs to the two wheels are required making the kinematic and the

dynamic models simpler and easier to compute in real-time for model based control.

7.2.1 Drive Wheel Units and Power Amplifiers

The drive units used are D.C. motor-in-wheel drive units manufactured by Schabmuller Corporation, West Germany. These units were first used by Rajagopalan and Cheng [4] on the CONCIC II and have been adopted as the standard drive sets on the experimental mobile robots built at the CIC since then. The drive units are rated at 4.05 N.m stall torque and 1.2 $m.s^{-1}$ maximum forward speed. Hardened rubber 0.15 m diameter wheels capable of supporting a maximum load of 200 N are used. Appendix B gives full details of these drive units and the no-load friction calibration carried out as part of this investigation. The power amplifier used for each motor is a PWM servo amplifier manufactured by Advanced Motion Controls, Camarillo, California. These pulse width modulated amplifiers are used in the current mode of operation in which the current supplied to the motors is proportional to the voltage of the input signal. Pertinent details obtained from the manufacturer's specifications are presented in Appendix B along with the results obtained from the calibration of each amplifier. Using the data given by Rajagopalan and Barakat [14] and by Barakat [15] for the peak and the steady state current values required to drive CONCIC III, the gains of the amplifiers were adjusted to provide a peak current of 25 amps and a maximum continuous current of 12.5 amps. The calibration curves of the amplifiers indicate that response is linear in this chosen range of amperage.

7.2.2 Control Loop Hardware

The control loop hardware configuration used for the experimental work is shown in Fig. 7.1. The hardware configuration is built around two interface cards. The AT-MIO-16 general purpose data acquisition card manufactured by National Instruments, Austin,Texas is used for all the Digital to Analog and the Analog to Digital signal conversions and for sample interval timing. The LM Interface card designed and built at the CIC, provides decoding for the shaft encoders using LM629 motion control chips. The Parallel Peripheral Interface 8255 chip available on the card is used as a toggle switch for the PC-AT IRQ5 used in the configuration.

The DAC interface between the digital controller and the power amplifiers is provided by the two 12-bit DAC analog output channels available on the AT-MIO-16 data acquisition board. This interface board was chosen because of the DAC and the high speed data acquisition (up to 1 MHz) facilities provided by a single card. In addition, three 16-bit timers are also available for accurate sample interval timing for the digital control loop. The NIDAQ software running in a DOS environment comprises of a wide set of pre-compiled C-functions for common control and data acquisition applications. This facilitates the development of the interface software. The reference manuals [82] provide full details of the hardware on the AT-MIO-16 card and on the NIDAQ software functions.

In the present experimental work, a dead reckoning method is adopted for guidance of the WMR in the floor frame. The dead reckoning method requires accurate measurement of the speed and the position of each wheel using some form of feedback device, such as a tachometer or incremental shaft encoder. In this hardware configuration, the method used by

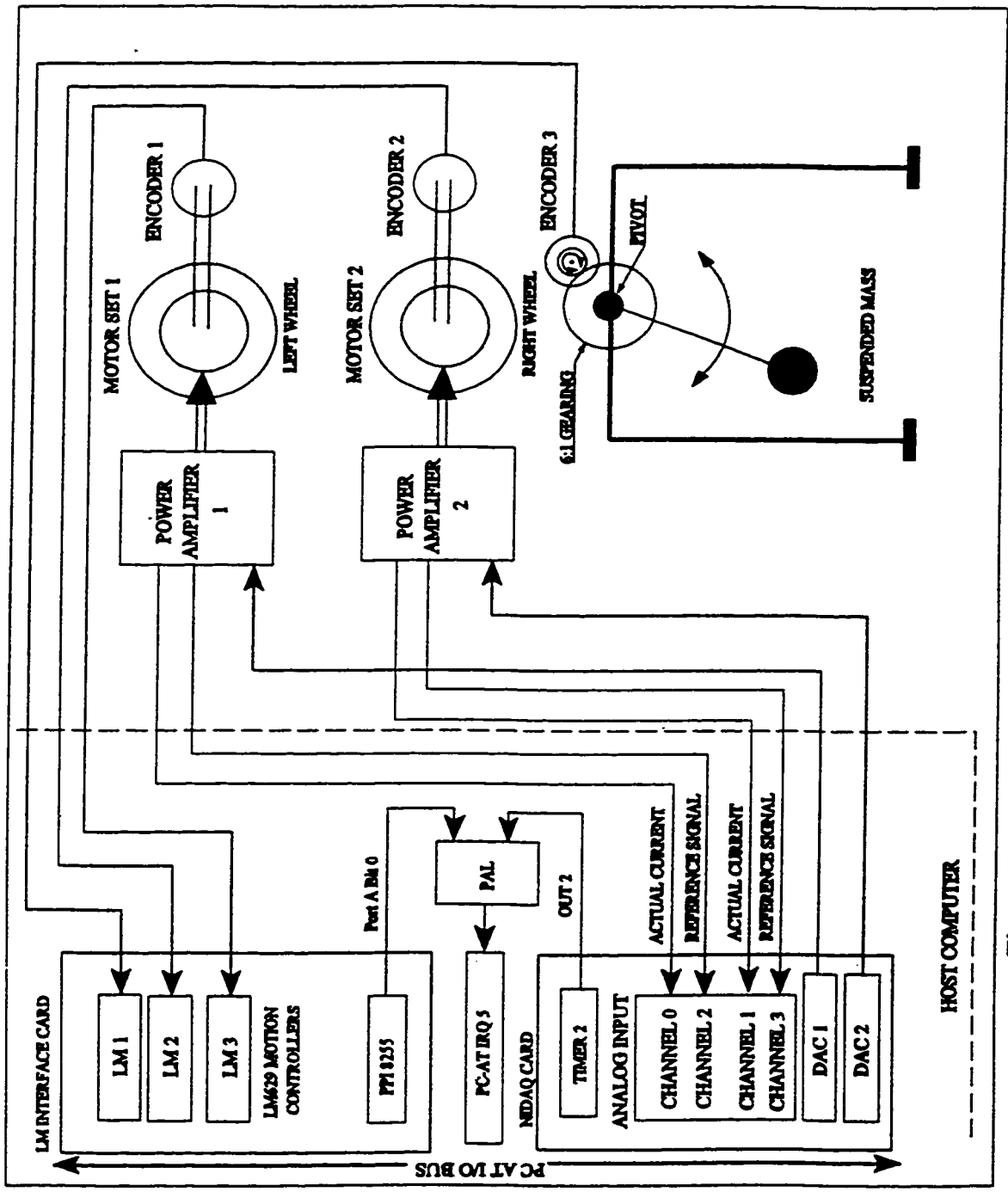

Figure 7.1 Schematic of the computer interface for CONCIC III.

Rajagopalan [3] and later by Mehrabi [6] has been adopted. The speed and position of each drive wheel are measured using 1024-line quadrature incremental shaft encoders mounted integral with the motor shaft in the drive units. The two digital signals on the A and the B channels from each encoder are decoded using LM629 motion control chips interfaced to the PC-AT bus by the LM Interface card. The LM629 motion control chips, manufactured by National Semiconductor Laboratories, are designed to use encoder feedback signals and hence provide high speed decoding and read back of both position and velocity of the motor. Full details on the programming and the use of the LM629 chips may be found in the reference manuals [83]. However, for the present investigations, only position read back is done and motor speed is computed using first differences.

In order to study the effect of a dynamic load on the behaviour of the mobile robot and the performance of the controller, a suspended load free to swing along the transverse plane of the WMR is used, as shown in Fig.7.2. The load is attached to the end of a rigid arm fitted securely to a horizontal shaft. The shaft is mounted on plummer blocks on each end and is free to rotate about its longitudinal axis which coincides with the longitudinal axis of CONCIC III. The plummer blocks are used to reduce friction to a minimum and to permit the load to swing like a simple pendulum due to any angular acceleration of the WMR. A 256-line quadrature incremental optical shaft encoder is used to measure the amplified angular position of the load. The schematic of the hardware configuration is shown in Fig.7.1. A 1:6 step up gear arrangement is used for the encoder to amplify the expected small oscillations of the load and the load shaft. The signal is decoded using a LM629 chip as adopted for the wheel encoders. This LM629 chip is also interfaced to the PC-AT bus on the LM Interface card.

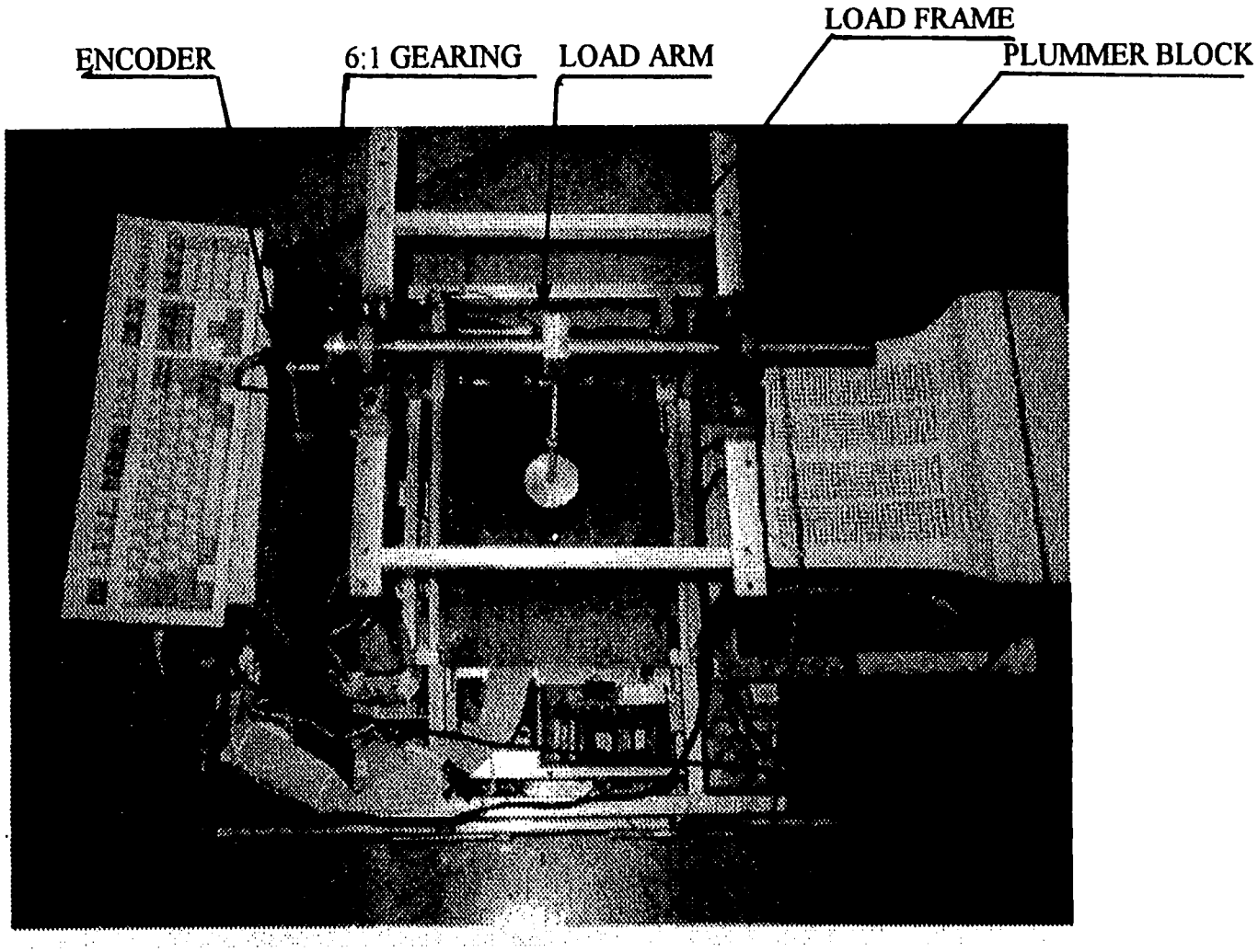

Figure 7.2 Cradle assembly for suspended load on the CONCIC III

7.3 Control Software

The control software comprises of a series of modules written in C. In the following sections the overall flow of the control programs for the three control schemes, viz., the PD controller, the FF controller and the CT controller are described. The numerous initialisation, data acquisition and termination features common to the three control programs permit the use of a template to construct the control software. The template is described in Section 7.3.1 using a flow chart. The program segments containing the control law for each type of controller are explained in the Sections 7.3.2 for the PD controller, Section 7.3.3 for the FF controller and 7.3.4 for the CT controller.

7.3.1 Template for the Control Software

The control program used for each controller is structured such that a common template program may be used for the main body and only modifications in the segment containing the control law are required. The template, shown in Fig. 7.3, comprises of all the essential initialisation and data acquisition features designed for the experimental work. The template comprises of three distinct sections for initialisation, for trajectory execution using the feedback control law and finally for data transfer to disk.

The initialisation section comprises of four primary modules used for,

(i) the memory allocation and the establishment of the linked lists used to hold both the input desired trajectory information as well as the data acquired during actual trajectory execution;

(ii) the initialisation of the NI DAQ card, allocating memory for the data acquisition

buffer ; the primary function used on this card are the analog output, the multi-channel analog input scan functions and the timer used as the sample interval timer for the control loop;

(iii) the reset and the initialisation of the LM629 chips used to decode the optical encoders used as the wheel position and speed feedback devices and

(iv) the initialisation of the PC-AT interrupt IRQ5 used to flag the sample intervals of the control loop.

At each step in the initialisation, the status of the device or the function is checked and the error status is echoed back on the screen. In case of hardware errors or if the user deems necessary, the program may be aborted at any step. Dynamic memory and linked lists are used for both the input data and the acquired data to reduce the time required for data transfers to a minimum, so that high sample rates for the digital control loop may be possible. In addition, by using the Random Access Memory (RAM) to store the data during program execution, the hard drive is not accessed and may be powered down. This follows the approach adopted by Rajagopalan [3] and Rajagopalan and Cheng [4] for CONCIC II. This protects the platters and the read head mechanism in the hard drive from physical damage. Once the initialisation is done and the desired trajectory file has been successfully read and stored in the linked list, the execution of the main control loop begins.

The control loop, shown in detail in Fig.7.4, contains modules to read the motors' positions and speeds, to use the control law to compute the control signals and to output the control signals to the amplifiers / motor sets through the DAC devices. The desired trajectory parameters are updated from the input data linked list. After the completion of the desired

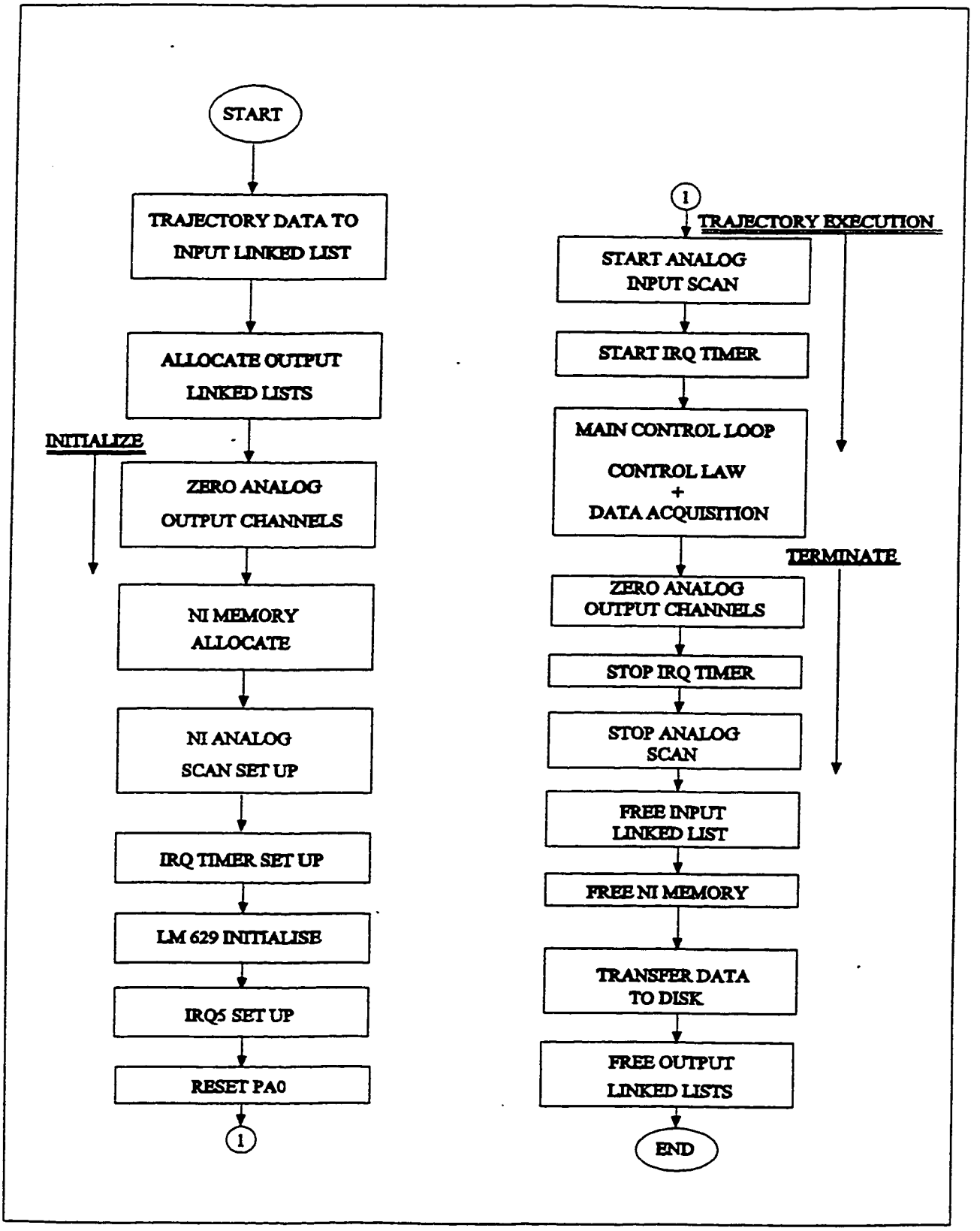

Figure 7.3 Template of control software.

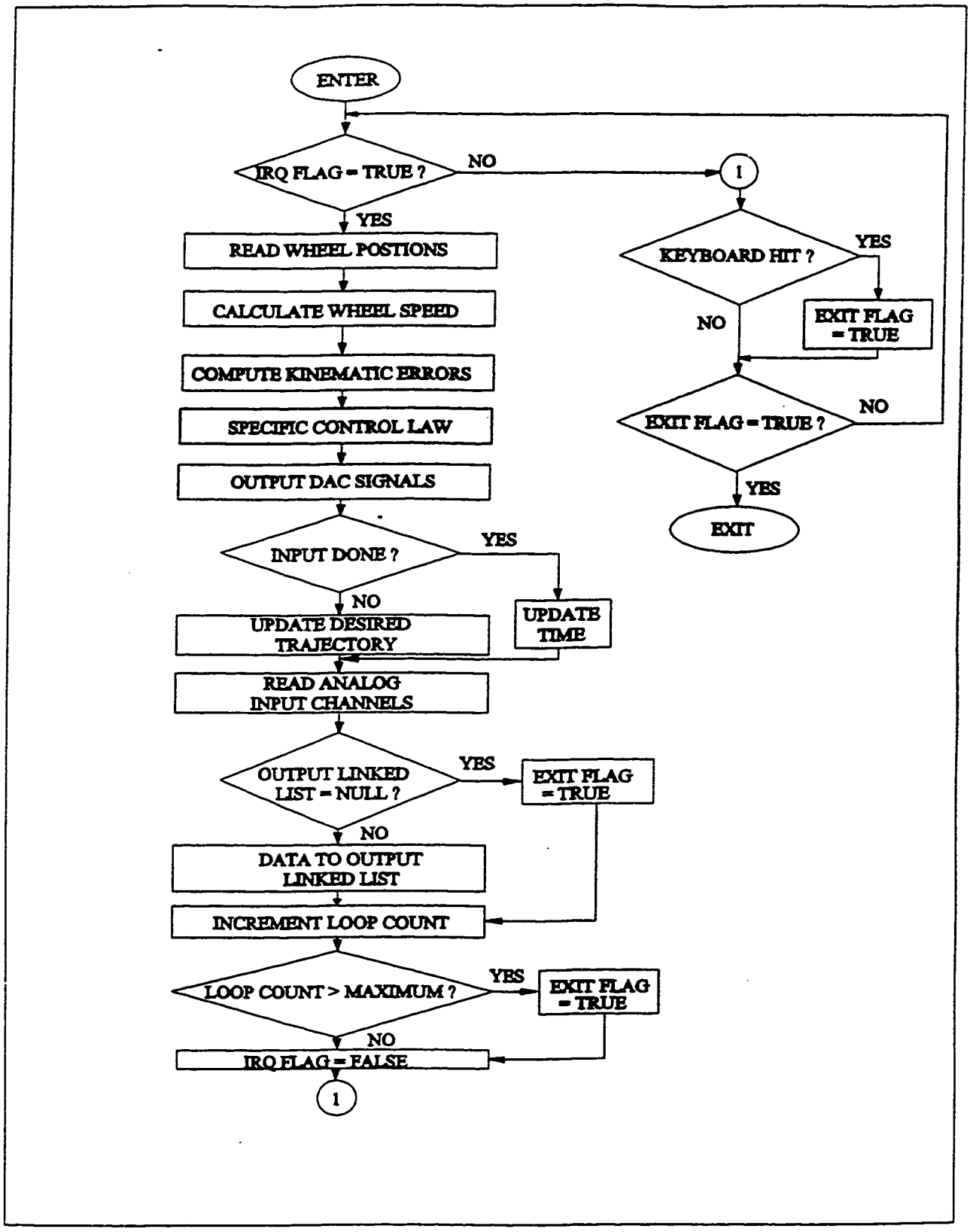

Figure 7.4 Details of Control Law and Data Acquisition Segment

trajectory, the control loop is designed to continue executing for a further period so that the system has adequate time to settle down to the steady state values. In the experimental work, a time period of 10 s is used. In Fig.7.4, the variable loop_count which contains the current time value during execution is tested against the maximum value which is equal to the period for the desired trajectory plus the extra time provided. The execution of the control loop depends on the condition of the exit flag. As shown in Fig.7.4, any software or hardware errors trapped during execution of the loop or if the control loop terminates successfully, sets the condition to TRUE, thereby terminating execution of the control loop. This ensures that all the physical devices are reset and the dynamic memory freed before control is returned to the operating system.

The data acquisition from the NI DAQ analog input devices is done in the control loop and the data is transferred to the output linked lists. Two output lists are maintained - one for the actual trajectory parameter values, viz., the left and the right wheel positions and speeds and the other for the two control signals computed by the control law and the actual value of the amperage drawn by each motor as read back from the power amplifiers. Using the NIDAQ channels, a moving average window is maintained for the actual current values read back from the amplifiers. Sixteen values are read in a block and the average is computed to reduce the effect of the high frequency noise present on these signals due to the PWM switching frequency of 33 Khz used by the power amplifiers. Blocks of sixteen values are used since the time required to compute the average value may be minimised by replacing the division by a faster bit shift operation.

At the end of the trajectory execution section, all the physical devices used by the

controller are reset. In Fig. 7.3, this section is labelled the Terminate section. Chief among these are the DAC analog output channels which are set to zero ; the sample interval timer and the data acquisition scan interval timer are both stopped. The original PC-AT IRQ5 interrupt vector is restored in the vector list and the interrupt mask register in the PC Programmable Interrupt Controller, PIC 8259, is restored to its value before program execution. The dynamic memory used by the input linked list and the data acquisition memory buffer are freed. Since the hard disk is powered down and is not used, the data in the output linked lists are written to floppy drives. The dynamic memory used by the output linked lists is freed to the heap space and the program terminates.

7.3.2 PD Control Law Software Segment

The Independent Joint PD control law utilises errors in the positions and the speeds of the drive wheels to compute the control output. At each execution of the control loop segment, shown in Fig.7.5, the positions, θ_a , of the two wheels are read using the position read back command for the LM629 chips. The speeds, $\dot{\theta}_a$, are obtained by using first differences. The errors between the desired and the actual trajectory parameters, ϵ_θ and $\epsilon_{\dot{\theta}}$, are used to compute the control signals with user defined PD gains, K_p and K_v . The numerical values of the control signals, C, correspond to the DAC output voltage; hence, the signals are checked against the maximum possible DAC output voltage of $\pm$ 10 V to prevent saturation. Since the amplifiers are in current mode of operation, they supply the amperage corresponding to the DAC output to the motors.

In the Cartesian PD controller, shown in Fig.7.6, the Jacobian matrix, **J** , representing

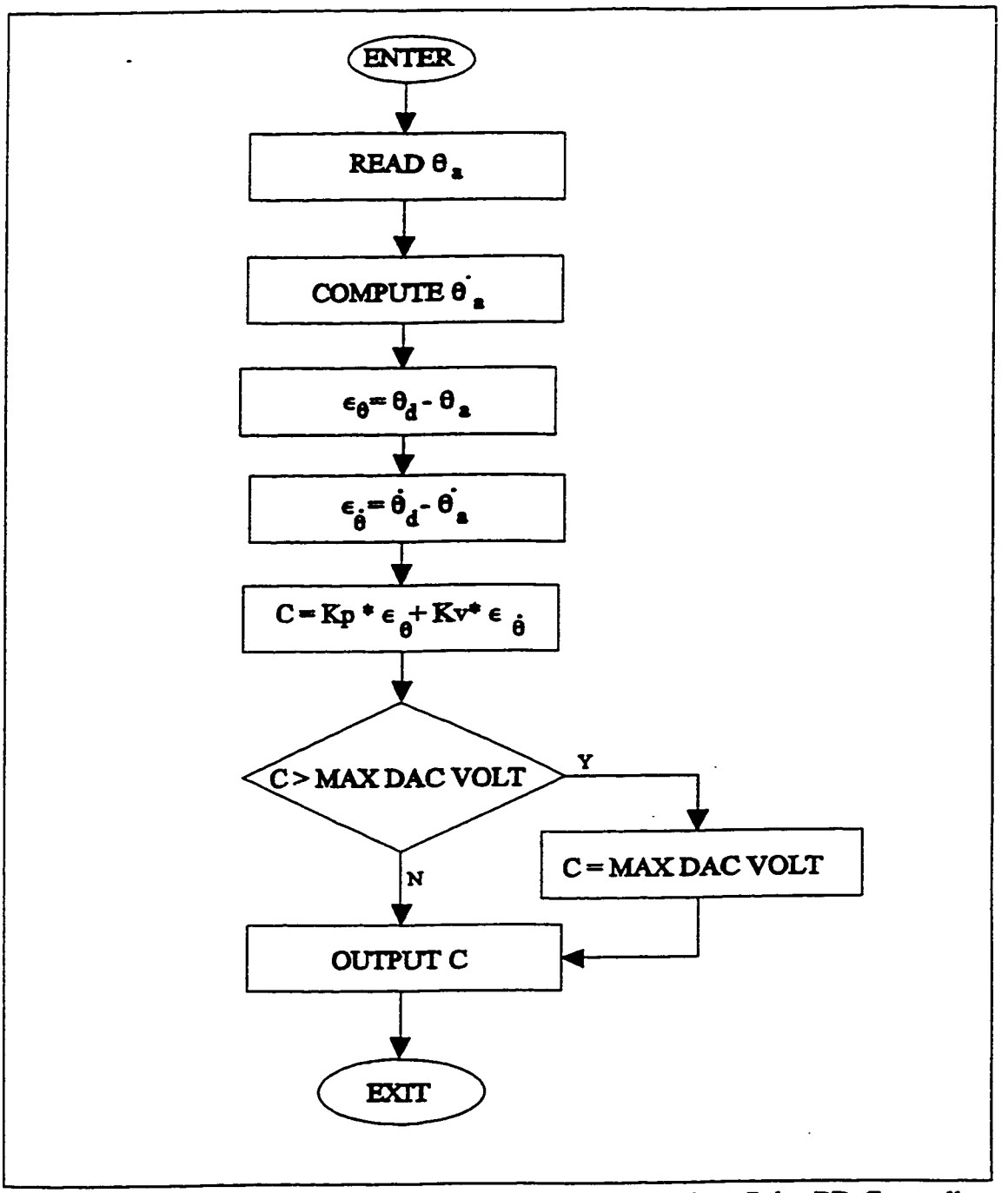

Figure 7.5 Flowchart of control segment for the Independent Joint PD Controller.

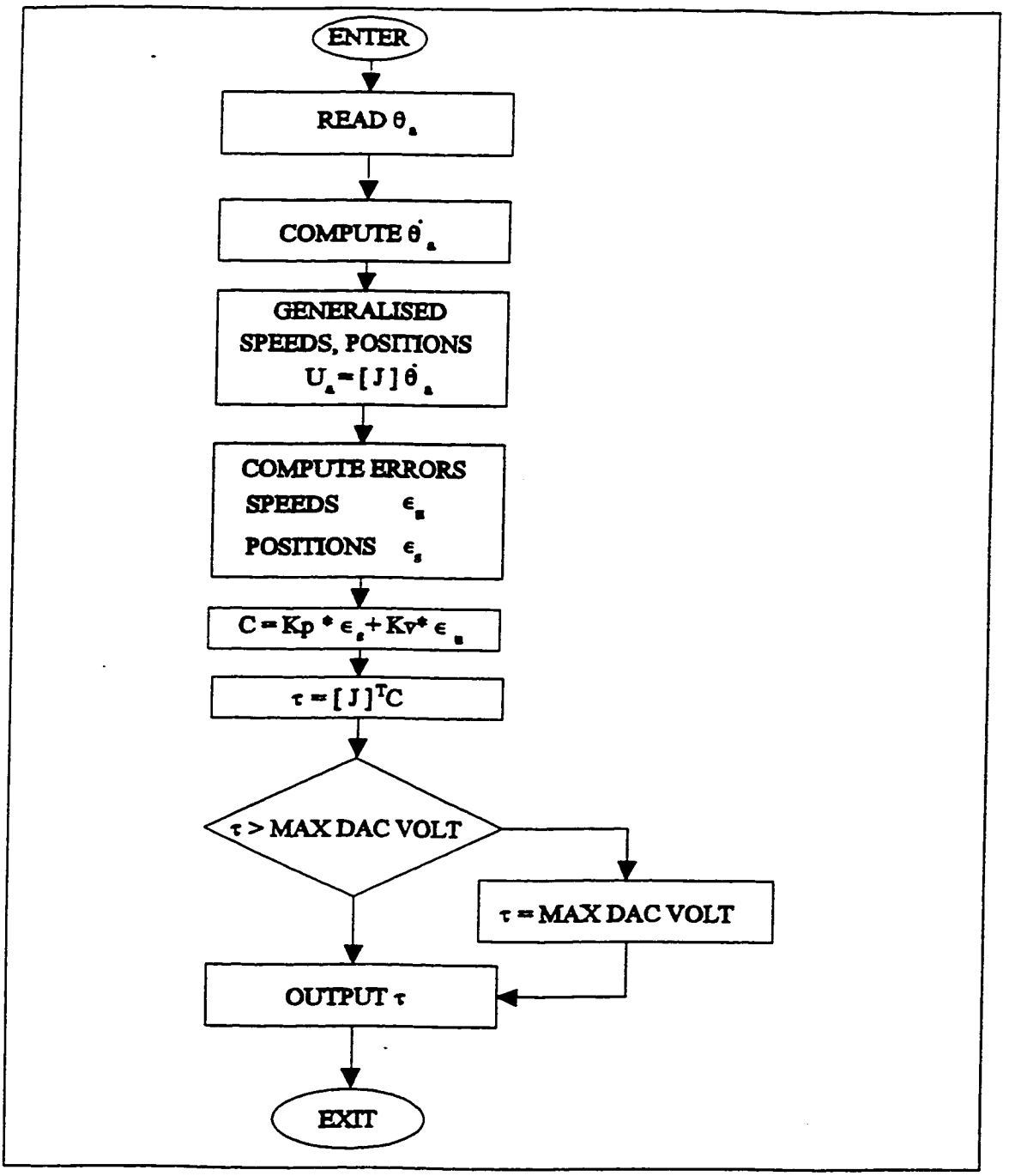

Figure 7.6 Flow chart of control segment for Cartesian PD controller.

the non-holonomic relations is used to convert the joint speeds, $\dot{\theta}_a$ into generalised speeds, u_a. In the case of the differential drive configuration, the Jacobian is only dependent on constant geometrical values, viz., the radius of the drive wheel and the wheel span. Hence, the same Jacobian matrix is used to convert joint positions, θ_a , to cartesian generalised coordinates, s_a , chosen in this work to comprise the path length and heading angle. For the CONCIC III, the Jacobian matrix is computed and stored before execution of the control segment. For the general case where the Jacobian is a function of the generalised coordinates, it must be computed in real-time. Also, to obtain the generalised coordinate values from the generalised speeds, a numerical integration scheme must be implemented in the control loop. For the case of the Cartesian PD controller, the desired trajectory is specified in terms of the cartesian path length and heading angle. The computation of the control outputs proceeds with errors in the generalised coordinates and speeds using the user specified PD gains, K_p and K_v. The control signals, C, are then converted back to DAC outputs, τ , which translate to motor currents and to actuator drive torques, using the transpose of the Jacobian, J^T.

7.3.3 Feed Forward Control Law Segment

The Feed Forward control law comprises of two parallel paths - the feedforward control signals computed offline and the feedback control signals from a Independent Joint PD controller. The feedforward control signals, corresponding to DAC voltages, are read from a data file and are transferred to a linked list in the same initialisation segment as the desired trajectory parameters. During control loop execution, the corresponding feedforward control signal values are read off this look up table and are added to the feedback control

signal from the Independent Joint PD controller described in Section 7.3.2. For the Feed Forward Controller, only the Independent Joint PD controller has been implemented. Since the control loop segment is similar to that of the PD controller, shown in Fig.7.5, with only the addition of the feedforward signals, a separate flow chart for the Feed Forward controller is not provided.

7.3.4 Cartesian Computed Torque Control Law Segment

The Cartesian Computed Torque controller, shown in Fig.7.7, refers to the case of the WMR carrying the suspended load. For the case of a deadweight payload, the segments related to the load parameters and the load dynamic model are not used. The mass matrix **M**, being a constant in the deadweight case, is computed before the execution of the control loop. The control scheme uses errors, ϵ_u and ϵ_s, in the generalised trajectory parameters to modify the desired acceleration, $\ddot{u}_d$ to the resolved generalised acceleration, $\ddot{u}$. As in the case of the Cartesian PD controller, shown in Fig. 7.6, the actual generalised trajectory parameters, u_a and s_a, are obtained from the wheel speeds, $\dot{\theta}_a$ and positions, θ_a using the Jacobian matrix, **J**, for the transformation. The angle of swing, ζ, is read from the LM629 chip used for the load. The rate of swing, $\dot{\zeta}$, is computed as the first difference of the position. The dynamic model of the suspended load is used to compute the acceleration of the load using the resolved accelerations, $\ddot{u}$. For the suspended load case, the mass matrix, **M** and the matrix containing the centrifugal and the coriolis terms, referred to as the cross coupling matrix, **D**, in Fig.7.7, are computed in real-time in the control segment. The inertial redistribution of the vertical loads on the wheels, **Q**, is then computed and used to provide the frictional torque,

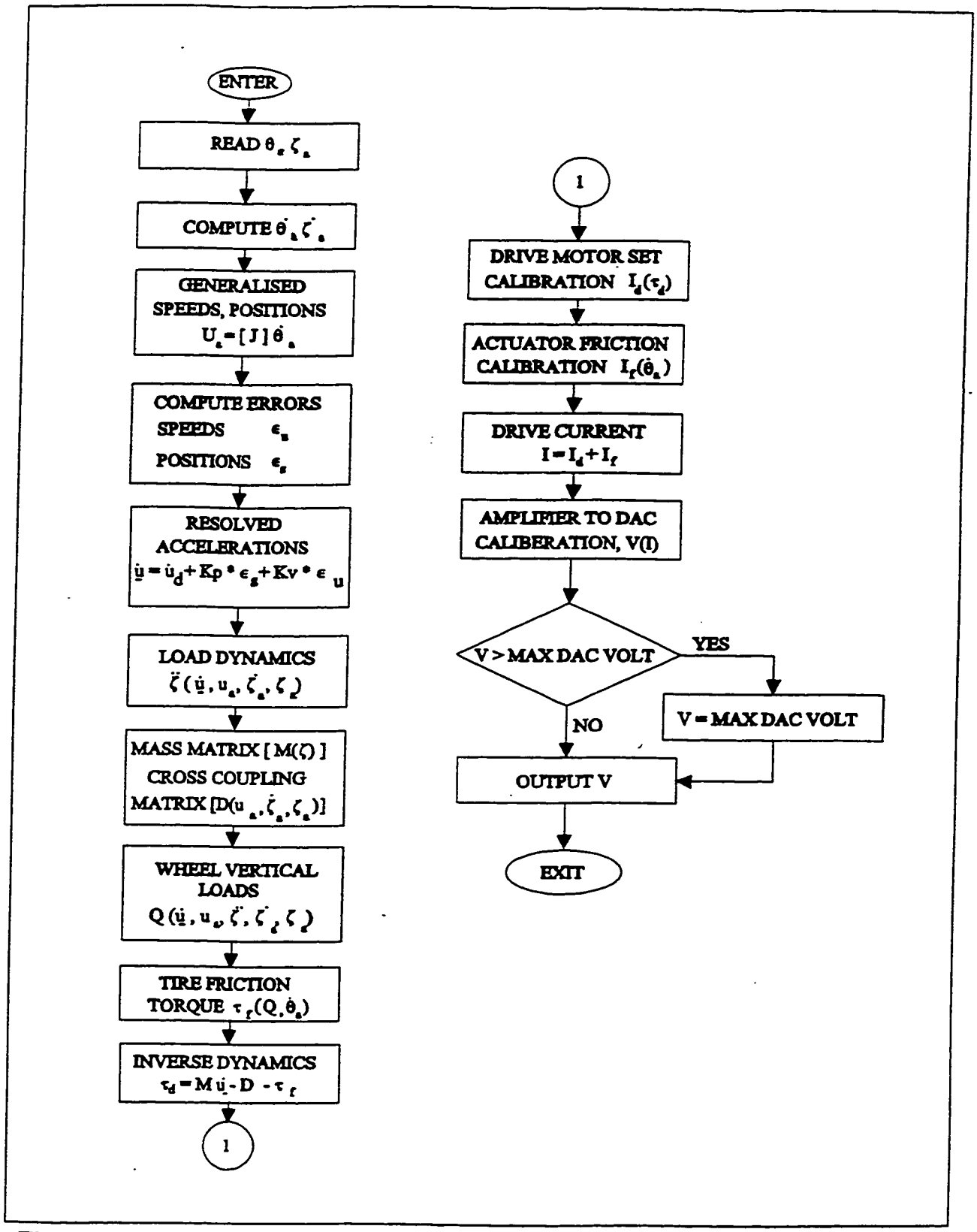

Figure 7.7 Flowchart of control segment of the Cartesian Computed Torque Controller.

τ_f due to tire friction. The resolved acceleration and the actual trajectory parameter values are then substituted in the inverse dynamic model of the WMR-suspended load system to compute the drive torques, τ_d for the actuators. The drive torque values are then converted to amplifier current values, I_d using the calibration data of the drive motors. The no-load friction in the actuators have been calibrated for different wheel speeds and is given in Appendix B. The calibration is used to compute the current, I_f, for actuator friction. The total amperage, I, computed by the CT controller is converted to DAC voltage value, V, for each wheel using the calibration curves of the amplifiers provided in Appendix B. The voltage is checked against the maximum permissible DAC voltage to prevent errors due to saturation.

7.3.5 Independent Joint Computed Torque Control Law Segment

For the Independent Joint Computed Torque Controller the inverse dynamic equations of the WMR are directly expressed in terms of the joint parameters. The actual values read back from the encoders are used to compute the resolved joint accelerations and then the drive torques using the inverse dynamic model. Except for the conversion between the joint parameters and the generalised parameters in the case of the Cartesian Computed Torque controller described in Section 7.3.4, the control law segment for the Independent Joint Computed Torque controller for CONCIC III is identical to that shown in Fig. 7.7. The dead weight and the suspended load cases are dealt in a manner similar to the Cartesian Computed Torque Controller.

7.4 Interrupt Handling Segment

Caution must be exercised when using one PC-AT interrupt level for the sample interval timer for the digital controller and another interrupt level for error signals from the interface card providing digital to analog interface and data acquisition. A conflict occurs between these interrupt levels when the actuator output is at its maximum corresponding to large control output from the DAC. Even though the NIDAQ software automatically truncates the value if the maximum DAC voltage is exceeded, it also issues an interrupt indicating analog output error. Under these conditions, the simultaneous interrupts from the NIDAQ card and from the sample interval timer for the digital controller conflict with each other leading to a unpredictable termination of the control programme being executed.

The flow chart of the interrupt handler for IRQ5, used in this setup for the sample interval timer of the digital controller, is shown in Fig.7.8. To keep the Interrupt Service Routine (ISR) execution time short, a flag is used to indicate every occurrence of the interrupt signal. When using multiple interrupt levels for asynchronous timers, as in this setup, the following precautions help prevent conflicts between interrupts and the consequent unpredictable behaviour of the processor

- on entry to the ISR, ***do not mask all*** the interrupt levels in the PC-AT Programmable Interrupt Controller, PIC 8259;
- on exit from the ISR, issue a ***Specific End Of Interrupt*** (EOI) command with the appropriate OCW2 [84]

If, as in the present hardware set up, the timer signal used to generate the interrupt signal is an inverted square wave with a small duty cycle value, it holds the interrupt line at

the TTL high level (=5 V) between successive interrupt signals. This prolonged logic high level on the PC-AT IRQ line is prone to problems, even though by design [84], this should not be the case. These problems are addressed and rectified using the Parallel Peripheral Interface (PPI 8255) and Generic Array Logic (PAL) chips shown in Fig. 7.1.

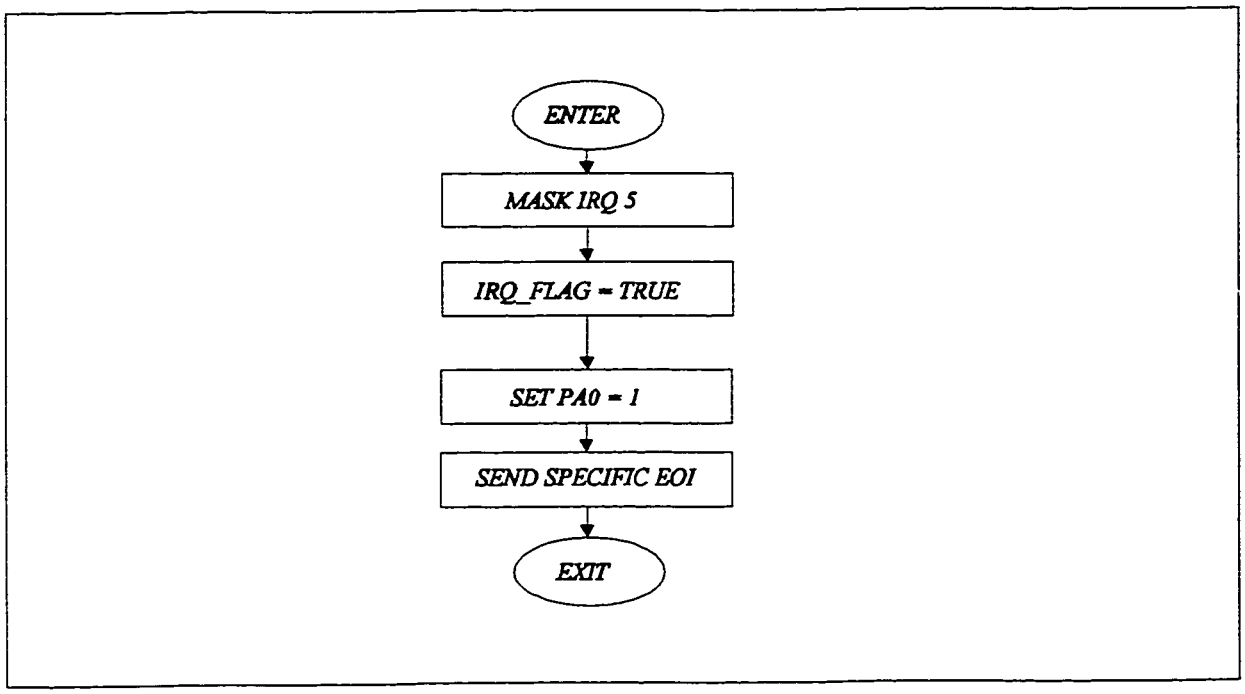

Figure 7.8 Flowchart of Interrupt Handler for PC-AT Interrupt Request (IRQ5) used for the sample interval timer for the digital controller.

The software solutions adopted for the interrupt handler are

- masking ***only*** IRQ5 on entry to the ISR. An Exclusive OR (XOR) command is used to set only bit 5 in the original interrupt mask word, as set by the BIOS, to one. The interrupt level is unmasked in the control loop segment of the main program. This

segment should be executed only at each sample period and hence the unmasking of IRQ5 is done in this segment

- a specific EOI command, (OCW2 = 0x65), for interrupt level 5 is issued in the ISR.

In addition, one bit of the Port A (PA0) available on the PPI 8255 chip, interfaced for the present purpose on the LM Interface card, is used to reset the interrupt line to the logic low state at the end of the execution of the ISR. The GAL chip is used as a state machine with the timer signal and the PA0 as input signals and the interrupt signal as the output. The logic states are shown in Fig. 7.9.

7.5 Summary

In this chapter, a description of the modifications done to carry the suspended mass used as the active load on CONCIC III, the experimental platform designed and developed at the CIC is provided. The improvements made to the digital to analog interface and data acquisition hardware used on CONCIC III are also given. These changes provide higher speed and better resolution in the interface and versatility and speed for data acquisition. A programme with a modular structure has been developed so that a variety of digital controllers may be implemented and tested on this hardware setup. A detailed description of this programme and its constituent software modules are given for reference. Using flowcharts, the programme segments for the conventional PD controller as well as the model based FF and CT controllers are described. Finally, some cautionary notes are provided on the use of multiple PC-AT interrupt levels for asynchronous timers for the sample interval timing of the digital controller and for the interface and data acquisition card. These notes are

intended to help prevent conflicts arising between these interrupt levels. The hardware using a PPI 8255 chip and a GAL chip developed as part of this work to guard against such conflicts between the two interrupt levels used in this setup is described. In addition, the construction of the interrupt handler used for the sample interval timer is described to provide a specific example of the interrupt handling methodology discussed.

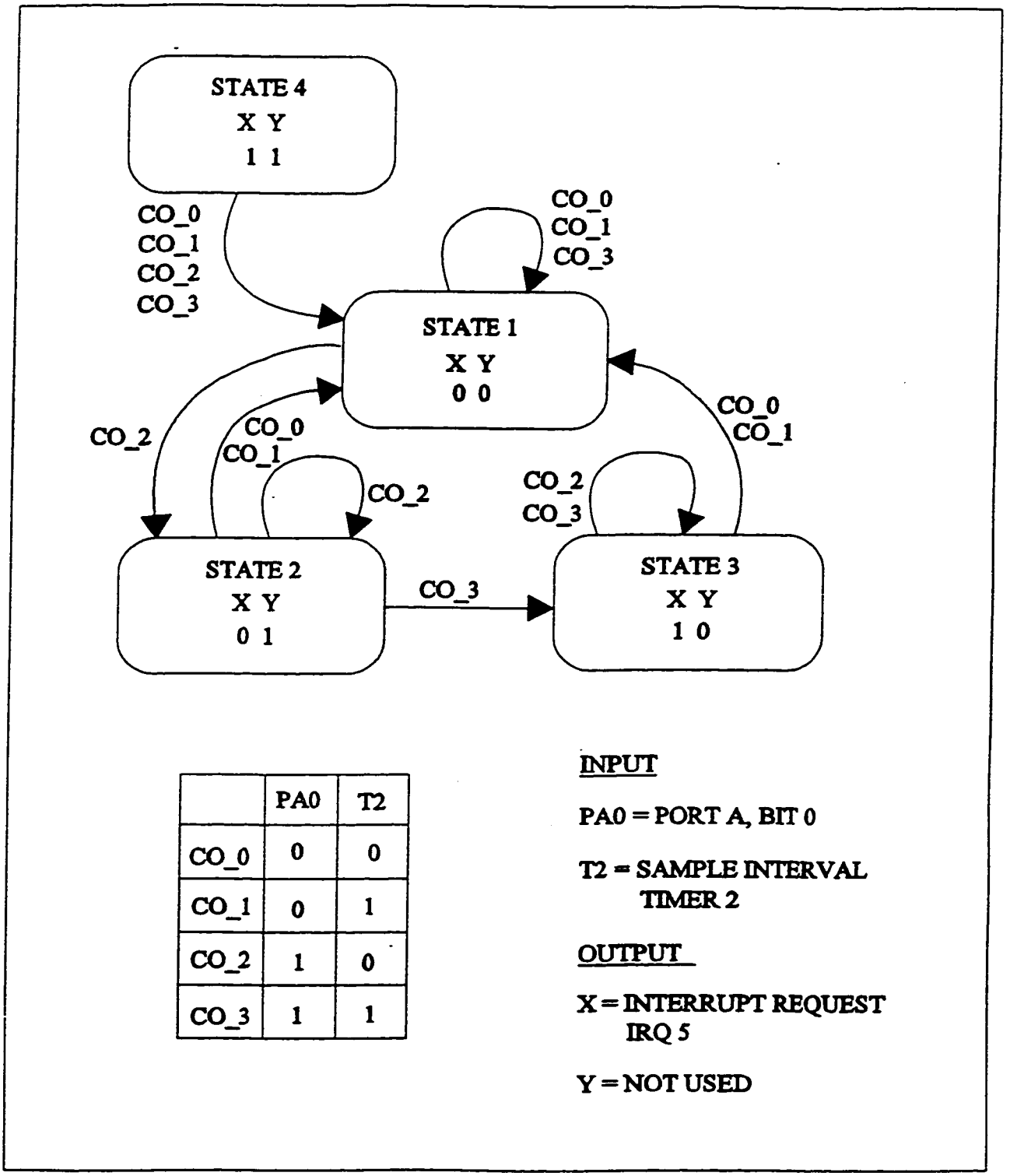

	PA0	T2
CO_0	0	0
CO_1	0	1
CO_2	1	0
CO_3	1	1

Figure 7.9 State Diagram for IRQ 5 Interrupt Request Signal Generation.

Chapter 8

Discussion of Experimental Investigations

8.1 Introduction

This chapter discusses the experimental investigations performed to study the performances of model based Feed Forward Controller described in Section 4.3 and the Computed Torque Controller proposed in Section 4.4 in the dynamic control of a WMR. The objective of this thesis research of evaluating model based control schemes has been supported by experimental work since only simulations, as correctly pointed out by Leahy, Valavanis and Saridis [42], may give misleading results. The present experimental work draws upon the vast experience on WMR guidance and control available at the CIC through the continued experimental work carried out since 1985.

Previous experimental work on Computed Torque Control of a WMR carried out by Rajagopalan and Barakat [13, 14] and by Barakat [15] at the CIC has indicated that the inclusion of the inverse dynamic model in the control loop leads to better trajectory tracking. The work was carried out for straight line trajectories with dead weight payloads. In the present work, the investigations are being extended to include angular accelerations induced by a lane change manoeuvre when the WMR is carrying a suspended load. The inverse dynamic model used in this thesis for the model based controllers is derived using the generalised methodology proposed in Chapter 3. As mentioned earlier, this model accounts fully for the inertial and the frictional terms compared to the models discussed in the literature and those used for Computed Torque control [14]. In addition, including the effects of the

Coriolis and the centrifugal forces and accounting for the dynamic redistribution of the vertical loads on the wheels during periods of acceleration are additional features in the model developed in Chapter 3 of this thesis. In the simulation studies on the side forces and the vertical loads on the wheels presented in Section 6.6, the magnitudes and the effects of these forces are shown to be significant during a common manoeuvre such as a lane change. The presence of a dynamic load such as the suspended load amplifies these effects.

In Section 8.2 three relevant topics, viz., the generation of the desired trajectory, the tuning of the gains used in the controllers and the frequency used for the digital control loop are presented. These topics and the accompanying discussions apply to all the experimental work presented later. Two straight line trajectories, of differing forward speeds and accelerations, are used in the first part of the experimental work so that the dynamic model may be adequately verified. The load carried by the WMR is a deadweight only. The criterion used for the comparison of performances is the Root Mean Square (RMS) values of the errors in path length, vehicle heading angle, forward speed and yaw rate. By using these cartesian error values, the trajectory tracking behaviour of the WMR in the floor frame is evident. The results obtained from these straight line trajectory trials are presented in Sections 8.3.1 and 8.3.2. Error plots for each controller and a tabulation of typical error indices obtained from the experimental work are provided.

As mentioned in Section 4.2, for the differential drive configuration used in CONCIC III, the Cartesian PD controller and the Independent Joint PD controller are similar in performance because the coefficients of the Jacobian matrix depend only on the constant geometric parameters and are independent of the generalised coordinates. Due to the same

reason, the difference in the performances of the Cartesian CT controller presented in Section 4.4.1 and the Independent Joint CT controller proposed in Section 4.42 showed insignificant differences during the experimental investiagations. Hence the results presented in this chapter refer only to the Independent Joint PD controller, the FF controller using a Independent Joint PD controller for feedback compensation and the Cartesian CT controller only.

In the second part, two lane change trajectories of differing values of linear and angular speeds and accelerations are used when the WMR is carrying a suspended load. In these tests, the forward speed by the WMR is the maximum speed possible with the motor-in-wheel drive units used on the CONCIC III. Sections 8.4.3 and 8.4.4 present and discuss the results of these tests. The summary of the results obtained from the experimental investigations and the conclusions drawn from them are given in Section 8.5.

8.2 Trajectory Generation, Controller gains and Sampling Frequency

Straight line trajectories are used in the first part of the experimental work in order to study the performances of the controllers under relatively simple operating conditions involving only forward acceleration and a dead weight as the payload. The lane change trajectory when the WMR carries a suspended load is then used for more rigorous testing. Some specific features of the trajectory generation scheme presented in Chapter 5 are discussed here. The use of controllers requires the user to choose values for the controller gains. The choice of the gains used for the experiments is justified in this section. The choice of the sampling frequency of the digital control system used for the controllers is also discussed. These three issues are discussed for all the controllers evaluated in this thesis.

8.2.1 Desired Trajectory Parameters

The straight line trajectory used in the first part of the experimental work is composed of 3 segments, the acceleration, the steady speed and the deceleration stages. A typical 3-segment straight line trajectory is shown in Fig.8.1. The desired trajectory parameters for each segment have been generated using the fifth order polynomial scheme for a lane change trajectory, described in Section 5.2, with the lane change distance set to zero. The trajectory generation scheme provides for a smooth matching of forward velocities at the junctions of the segments since the accelerations are continuous. However, the forward accelerations are only piecewise continuous and the sharp breaks at the junctions are seen in the acceleration curve given in Fig.8.1. However, if the 3-segment trajectory generation scheme was applied to a lane change, it was observed that the discontinuous jumps in the linear and the angular accelerations led to jerky response of the WMR at points of transition from one segment to the other, especially when using the CT controller. Hence, a single segment lane change trajectory is used in order to eliminate the drawbacks in the trajectory generation scheme from affecting the performance of the controllers, which is the objective of this work.

8.2.2 Controller Gains

The performance of a controller depends on the values of the gains used in the control scheme for a chosen operating condition. In practice, one needs to modify the gains based on the operating conditions in order to enhance the performance of a controller. However, in this work, constant gains are used for the controllers since the objective is to evaluate their perfomances under different operting conditions. In addition, the same numerical values of

the gains are used for all the controllers in all the experimental trials carried out in order to obviate unfair performance enhancement by the trial and error tuning schemes usually adopted. Further, it is the objective of this research to illustrate the effectiveness of the model based controllers in self-adapting to the changes in the operating conditions. This implies that the performance of these controllers under various operating conditions does not require gain tuning while only nominal gains are used for the entire operating range of the vehicle. Though the order of magnitude tuning methods such as the Zeigler-Nichols methods [84] for PID controllers may be used, the final choice is still based on trial and error only. Moreover, no such tuning scheme has been proposed in the literature for the model based controllers.

The PD controller was tuned by trial and error for the straight line trajectory shown in Fig. 8.1. The PD gain values of $K_p = 1.0$ and $K_d = 0.5$ which have been chosen gave the minimum RMS error index of 0.05m in these trials . It is possible that we may find a wide range of values for K_p and K_d that would provide similar performance. The same values of gains were used subsequently for the FF and the CT controllers as well for all the experimental trials.

8.2.3 Sampling Frequency for the Digital Control Loop

The performance of digital controllers is dependent on the sampling frequency chosen. In this experimental work, the sampling frequency is chosen to be 10 Hz, and is based on the system time constant. The mechanical time constant of the CONCIC III estimated from results presented by Barakat [15] for straight line motion is of the order of 1 sec. From the results given by Mehrabi [6] for CONCIC III with front and rear drive-steer wheels, the time

constant around the yaw axis is an order of magnitude larger. Hence the slow sampling rate used in this experimental work is still well below the aliasing limit of 500 ms set by sampling theory for this mechanical system. The reasons for this choice of sampling frequency are

- to provide enough time for the Cartesian Computed Torque controller to compute the complete inverse dynamic model for the suspended load case and
- to restrict the size of the input data file containing the desired trajectory values to less than the 64 Kilobyte page size restrictions present in the PC architecture.

The time required to compute only the inverse dynamic model for the WMR carrying the suspended load has been measured to be in the range of 30 ms to 40 ms. This includes the time required to read the wheel positions, compute the wheel speeds and proceed with the evaluation of the drive torques using the inverse dynamic model. The inverse dynamic model requires the computation of the mass and the cross coupling matrices and also the dynamic redistribution of the wheel loads and the consequent tire frictional forces. The load swing acceleration is estimated using the dynamic model of the suspended load with actual angle of swing read back from the encoder. Of all the control schemes evaluated in this work, this is the computation that was measured to take the longest duration. No special programming methodology was attempted to optimize the code, to use assembly language programming or to reduce the number of arithmetic functions or calls to transcendental functions, such as sine and cosine evaluations. The time for data acquisition, manipulation and transfer to the buffer adds marginally to this computation time during the actual experimental work.

The second reason pertains to guidance using dead reckoning in which the desired trajectory is generated off-line and is stored in a look up table in the computer memory. Each

row in the look up table contains the desired trajectory parameters at the chosen sample intervals, which is 100 ms in this case. The values on each row for the Cartesian level controllers are time, path distance, heading angle, forward speed, yaw rate, forward acceleration and angular acceleration. For the Independent Joint PD, the Feed Forward and the Joint Level CT Controllers, the motors' positions, speeds and accelerations are provided since the feedback control schemes use measured joint level values during trajectory execution. Using the PC-AT interrupt and the sample interval timer the trajectory parameters are updated at 100 ms intervals. For the desired trajectory parameters required by control schemes being used in this thesis, each row in the table contains 7 floating point double precision values. Double precision was used to be consistent with the NIDAQ function library. Each data structure thus requires 56 bytes of memory ; with the additional 4 bytes needed for the far pointer in the linked list, the memory required per row is 60 bytes. In the construction of the programme, only Far pointers provided by the C-language are used. These Far pointers used for the linked list of input data cannot cross page boundaries [86, 87] and hence the total amount of dynamic memory available for the linked list holding the desired trajectory parameter values is 64 Kbytes. This permits a maximum of 1000 rows of data only. At 10 Hz, this provides a maximum trajectory duration of about 2 minutes. Increasing the frequency of the digital control loop would then incur a proportional restriction on the total time period of the trajectory. So, as a trade off , the 10 Hz sampling was chosen since it was seen that the results obtained were relevant and provided enough information to evaluate the performances of the controllers. With more advanced programming skill, these limitations placed by the program structure on the sampling frequency may be overcome.

8.3 Experimental Investigations

The performances of the model based controllers were evaluated in tracking straight line trajectories and lane change manoeuvres. As mentioned earlier in Section 5.2, both these trajectories are used in industrial applications of WMRs. Of these, the straigth line trajectory involves only linear acceleration and thus helps quantify controller performance under this condition. In the experimental work, two straight line trajectories have been used. In the first trajectory the WMR is programmed to attain only 50% of the maximum speed of 1 $m.s^{-1}$ permitted by the wheel drive units. In the second straight line trajectory, the magnitude of the acceleration and the maximum speed reached by the vehicle are increased to twice the value used in the first straight line trajectory. This is done in order to study the effectiveness of the controllers for different forward accelerations. The lane change manoeuvre introduces the effect of angular acceleration and yaw motion on the performance of the controllers. In the lane change trajectories, the forward speed and acceleration have been maintained close to the values used for the second straight line trajectory. The angular acceleration in the second lane change trajectory is twice the value used in the first lane change manoeuver. This introduction of one dynamic effect at a time permits the evaluation of the controllers to this one factor in as close to isolation as practically feasible.

8.3.1 Straight Line Trajectory

In this straight line trajectory (SL_1), the WMR accelerates from rest to reach a maximum forward speed of 0.5 $m.s^{-1}$ in a time of 15 s. The desired trajectory parameters are shown in Fig 8.1. The maximum acceleration attained by the WMR during this stage is 0.8

$m.s^{-2}$. Having attained the desired forward speed, the WMR coasts for 10 s at 0.5 m/s. This steady forward speed section is included to provide time for any overshoots to die down before the commencement of the deceleration stage. Simulations of this straight line trajectory indicated that the PD controller is prone to such overshoots. After the period of coasting, the WMR decelerates smoothly to a stop in a time of 15 s.

This trajectory was used for all the preliminary testing of the hardware systems of CONCIC III as well as the controller software. The tuning of the PD controller was also carried out during these trials. The controller gains were set at 1.0 and 0.5 for the PD and the FF controller ; the same numerical values were used for the computation of the resolved accelerations from the position and velocity errors in the Computed Torque controller. The tests were carried out on a rough concrete floor resembling an industrial environment. The trajectory was repeatedly executed in the same location with the WMR running in the same direction to assure repeatability and to validate the results of the performance comparisons. All other factors, such as the state of the batteries were held constant within the practical limits.

The left and the right wheel positions and speeds were recorded during trajectory execution in the data acquisition buffer at 100 ms intervals. The actual cartesian path of the WMR has been reconstructed from these values using the kinematic model. The difference between the desired and the actual trajectory parameters for the path length for the Independent Joint PD controller, the Feed Forward Controller and the Cartesian Computed Torque controller are shown in Fig. 8.2. Fig 8.3 presents errors in the forward speed, Fig. 8.4 errors in the vehicle heading angle and Fig. 8.5 shows errors in the yaw rate. Typical values

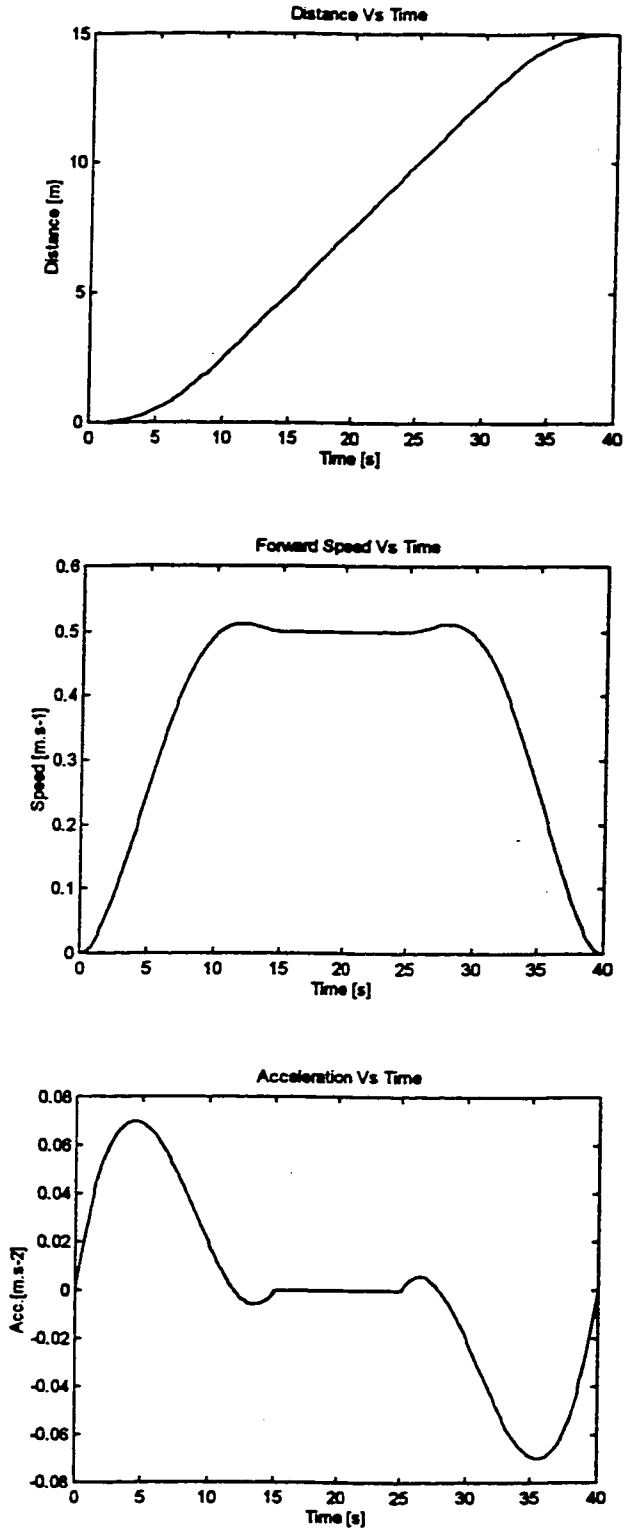

Figure 8.1 Desired parameters for the straight line trajectory, SL_1.

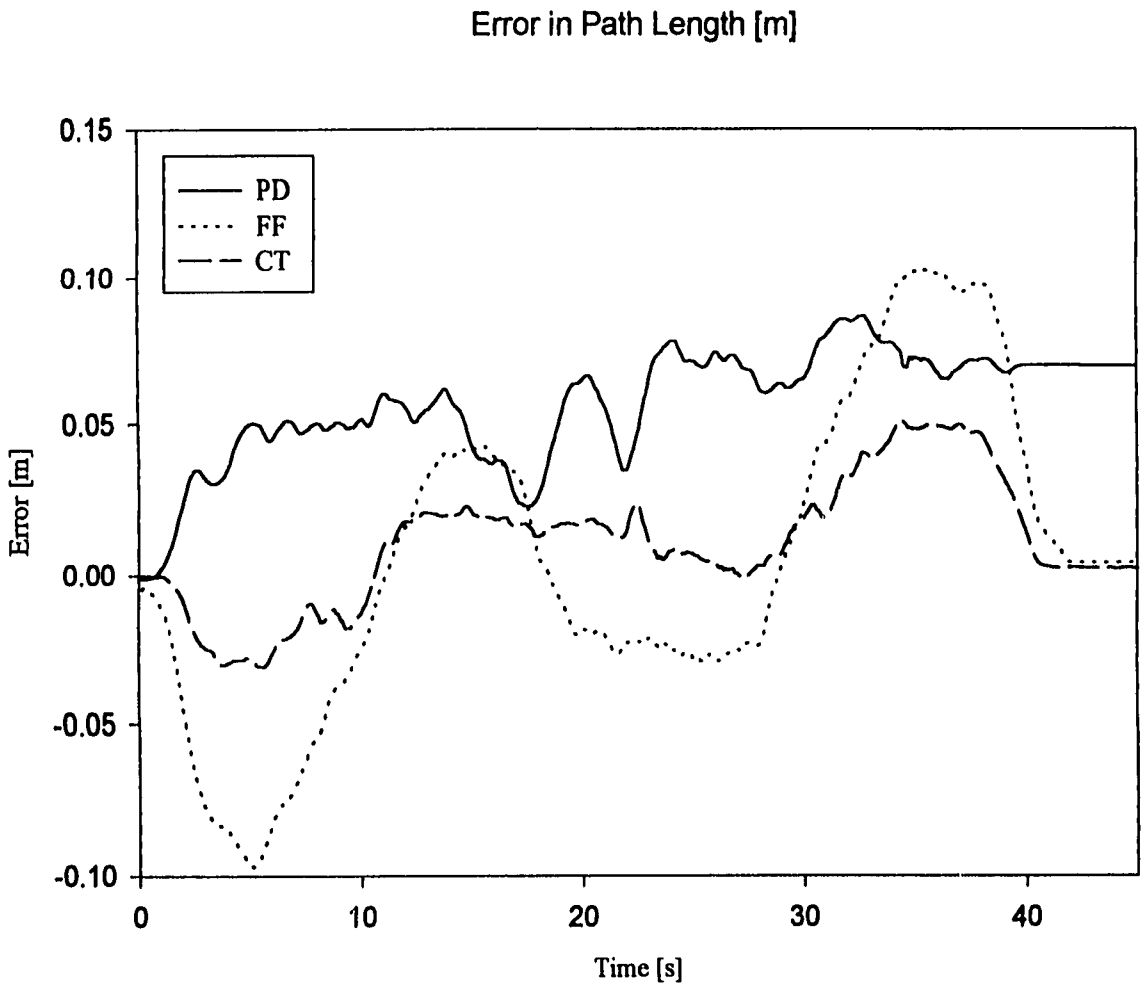

Figure 8.2 Errors in the path length during the straight line trajectory, SL_1.

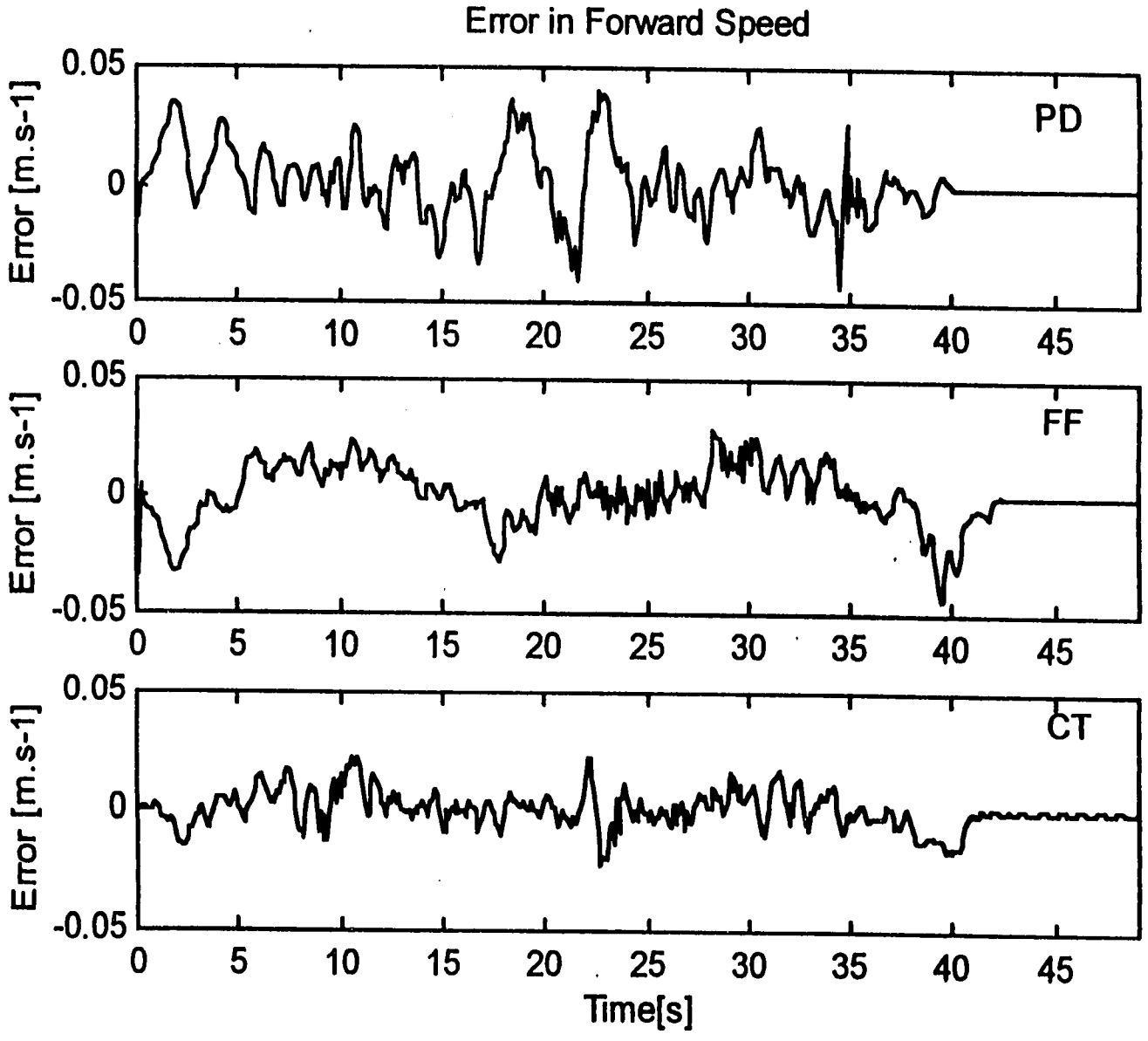

Figure 8.3 Errors in the forward speed during the straight line trajectory (SL_1).

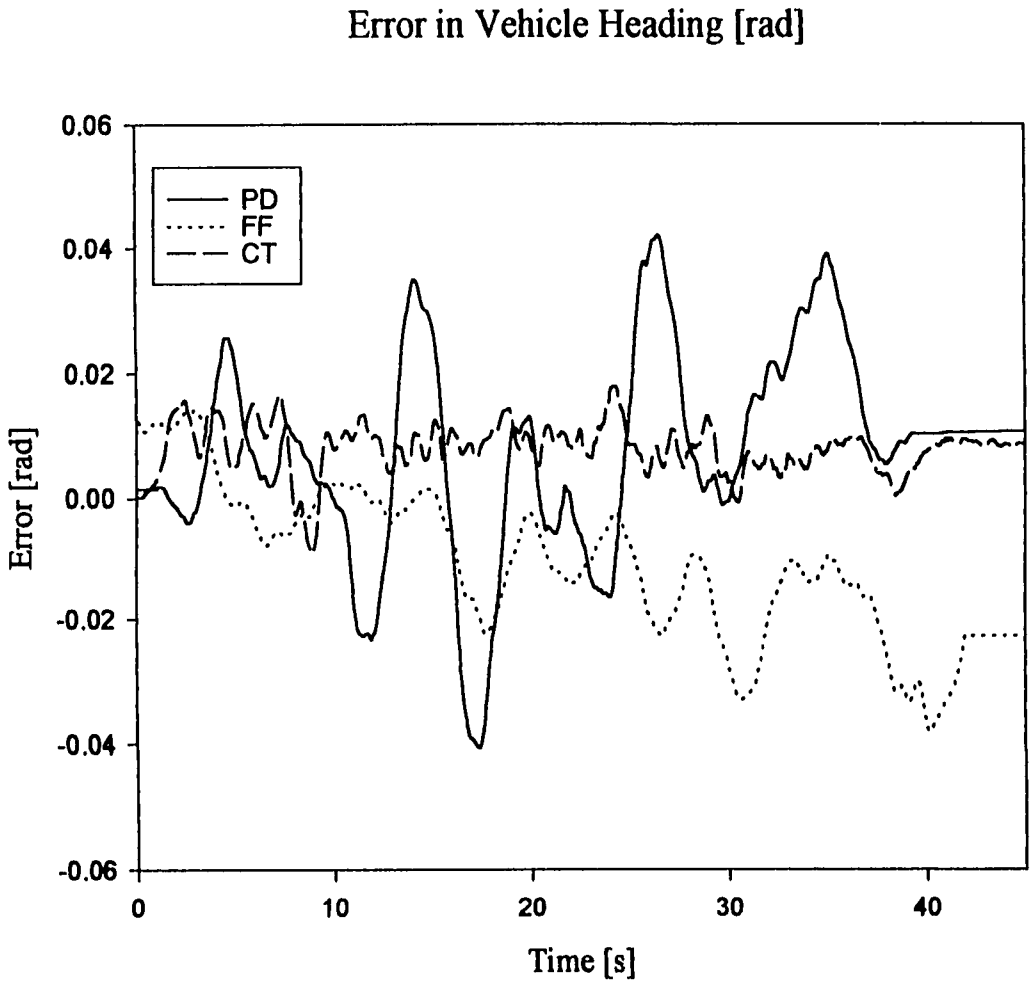

Figure 8.4 Errors in the heading angle during the straight line trajectory SL_1.

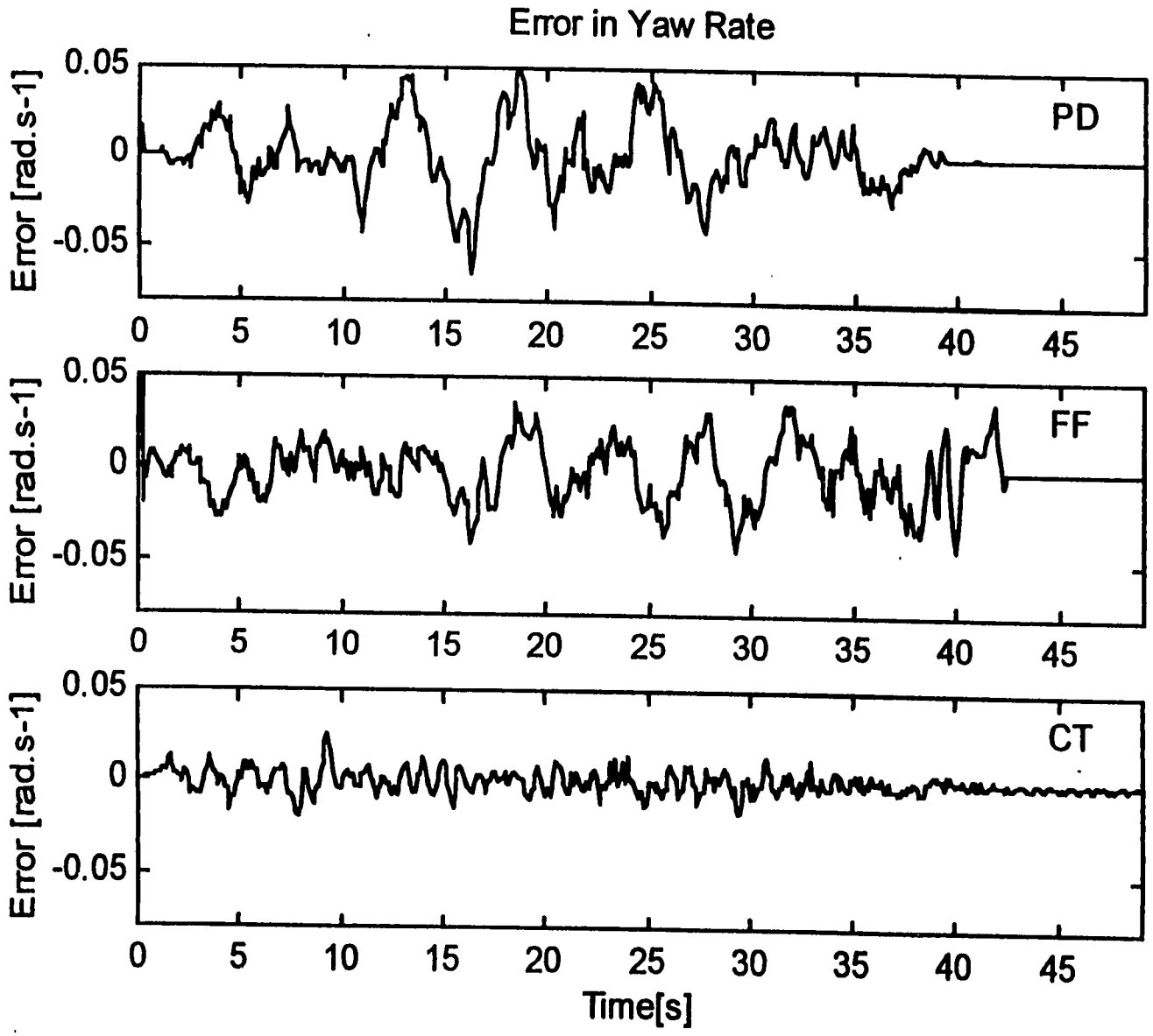

Figure 8.5 Errors in yaw rate during the straight line trajectory (SL_1).

Table 8.1

Typical values of the performance indices for the 3-segment straight line trajectory, SL_1.

Duration of trajectory 40 s

Maximum forward speed : 0.512 $m.s^{-1}$

Maximum Acceleration: 0.07 $m.s^{-2}$

Controller	Path Length Error RMS [m]	Path Length Error Max.[m]	Path Length Error SS.[m]	Forward Speed Error RMS [$m.s^{-1}$]	Heading Error RMS [rad.]	Heading Error Max.[rad.]	Heading Error SS.[rad.]	Yaw Rate Error RMS [$rad.s^{-1}$]
PD	0.0673	0.0867	0.07	0.0147	0.0194	0.0421	0.011	0.0182
FF	0.0552	-0.1031	0.0042	0.0131	0.019	-0.038	-0.0227	0.0205
CT	0.0248	0.051	0.002	0.0076	0.005	0.009	0.004	0.0116

(N.B: RMS = Root Mean Square value ; Max. = Maximum value ; SS. = Steady State value)

of the RMS performance index for cartesian position and forward speed and for the heading angle and yaw rate for the PD, the FF and the CT controllers are given in Table.8.1. The maximum and the steady state error values for position and heading are also given for reference.

In Fig.8.2, the error in the position for the PD controller is always positive indicating that the actual position of the WMR lags behind the desired value throughout the trajectory. The steady state error is due to the lack of the integral action in the PD scheme. The CT controller, however, overcorrects during the acceleration phase of the trajectory and the actual forward speed of the WMR is faster than the desired value. The magnitude of the error decreases as the acceleration diminishes and the WMR reaches steady forward speed at 15s. There is an error of 0.02m during the steady speed phase. During the deceleration stage, the trend is similar to that during the acceleration phase but with positive values of errors. The behaviour of the FF controller resembles that of the CT controller but the magnitudes of the RMS error values are more than twice the corresponding values for the CT controller. The feedforward torque during the acceleration phase is overcompensating and the vehicle accelerates faster than the desired trajectory value. The feedforward torques act as open loop excitation and the error increases until maximum acceleration is attained. The correction due to the feedback PD part of the FF controller marginally reduces the errors as the gains are not large enough to provide faster corrections. The rate of decrease in the error in the phase where the acceleration decreases and the vehicle reaches steady forward speed is seen to be much steeper than that of the CT controller. During the deceleration phase, the feedforward part undercompensates and large lagging errors result.

A comparison of the performance indices for the position and the orientation errors shows that the RMS values for the CT controller are less than 50% those for the PD and the FF controller. The RMS values of the errors in the forward speed and the yaw rate for the CT controller show the same trend when compared with those of the PD and the FF controllers.

The values of the errors in position for the model based controllers are seen to resemble a mirror image of the desired acceleration curve for the trajectory given in Fig.8.1. In the case of the straight line trajectory, the terms in the cross coupling matrix are all zero since the angular velocity is zero. Hence, for any given drive torque, the dynamic behaviour of the WMR, while executing a straight line trajectory, is governed by the inertial forces and the frictional forces only. Frictional forces, as used in this context, refer only to rolling frictional forces and include both tire friction and friction in the actuators. Of these two force terms, the inertial forces are dependent on the forward acceleration and the frictional forces, on the wheel speed. If the inertial parameters of the WMR are overestimated in the inverse dynamic model used by both the model based controllers , the controller output will be higher than the required value during periods of acceleration ; during deceleration, on the other hand, the negative current used by the controller to brake the WMR will be higher than the required value and the WMR decelerates faster than desired. In addition, at low forward speeds, the rolling frictional forces are small and the system behaves as a underdamped system giving rise to large rates of change of errors. As the forward speed increases, the frictional terms become dominant making the system overdamped and slowing the system response. This leads to large lagging errors. In the inverse dynamic model, an under estimate of the magnitude of friction by the friction model will complement errors from overestimated inertial parameters

resulting in large errors, especially at higher speeds. In the case of the CT controller, the errors in position and speed make the value of the resolved acceleration non-zero even when the desired acceleration is zero, as in the mid-portion of the trajectory. Hence the CT controller is able to compensate for the poor estimates of the inertial and frictional parameters during trajectory execution. In the FF controller, the corrective action is provided only by the feedback PD part which provides slower response as mentioned earlier.

The performance indices for the orientation indicates that the CT controller provides a balanced control of the two drive wheels throughout the trajectory. Uneven control outputs to the two drive wheels in this differentially driven WMR make the heading oscillate about the straight path desired. This tendency is seen in the case of the FF and the PD controller, both of which do not use the dynamic model for feedback compensation.

8.3.2 Straight Line Trajectory

In order to explore further the effects of the forward speed and the acceleration on the performances of the dynamic controllers, the second straight line trajectory (SL_2) is used. The profiles of the desired trajectory parameters, shown in Fig.8.6, resemble those of the trajectory SL_1 except that the steady forward speed section has been removed. The WMR starts from rest and accelerates to a maximum speed of 1 m/s in a time of 9.5s. The maximum acceleration during this phase is 0.16 $m.s^{-2}$. This is also the maximum permissible value of acceleration without saturating the power amplifiers. The trajectory is symmetric about the mid-point and the WMR decelerates to a stop in a time period of 9.5s. The value of the acceleration specified in this trajectory was chosen such that the maximum feedforward

actuator current is 11.6 amps which is just over 90% of the continuous current limit of 12.5 amps set in the power amplifiers.

The performances of the controllers while executing this straight line trajectory are shown in Fig.8.7 to Fig.8.10. The RMS, maximum and steady state performance indices for the path length, the forward speed, the heading angle and the yaw rate are recorded in Table 8.2. Comparison of the error plots obtained for SL_1 and SL_2 shows that the model based controllers exhibit the same tendency to overcompensate during periods of acceleration when the forward speed is low, as in the early phase of the trajectory. The magnitude of the acceleration for SL_2 is twice that used for SL_1 ; comparison of the RMS and maximum values of errors for the FF controller for the two trajectories indicate that these error indices show a similar two-fold increase. The increase in error indices in the case of the CT controller is 50%. The higher forward speed used for this trajectory increases the rolling friction at the tires and the viscous friction in the actuators. This increased friction complements the overestimated braking torque during deceleration, leading to greater magnitudes of errors. The CT controller exhibits the overcompensation during the high acceleration and low speed phases at either end of the trajectory and the under compensation during the high speed and low acceleration mid-phase as shown in Fig.8.8.

The plots of heading and yaw rate errors, Fig.8.9 and Fig.8.10, show that the CT controller is able to maintain the desired straight heading by providing balanced wheel speeds. This Cartesian based controller computes the heading and the yaw rate from the two wheel positions and speeds. Hence feedback compensation using errors in the cartesian trajectory parameters accounts for the non-holonomic behaviour of the WMR and tends to balance the

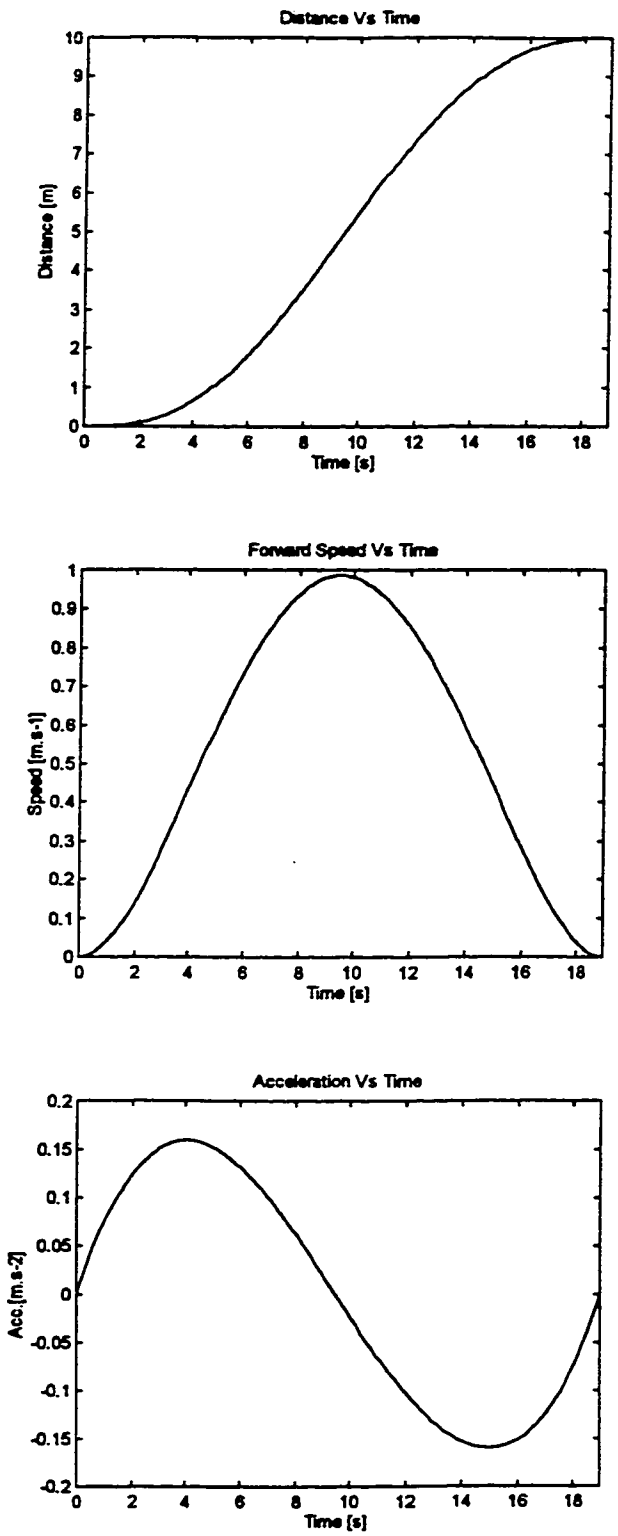

Figure 8.6 Desired parameters of the straight line trajectory, SL_2.

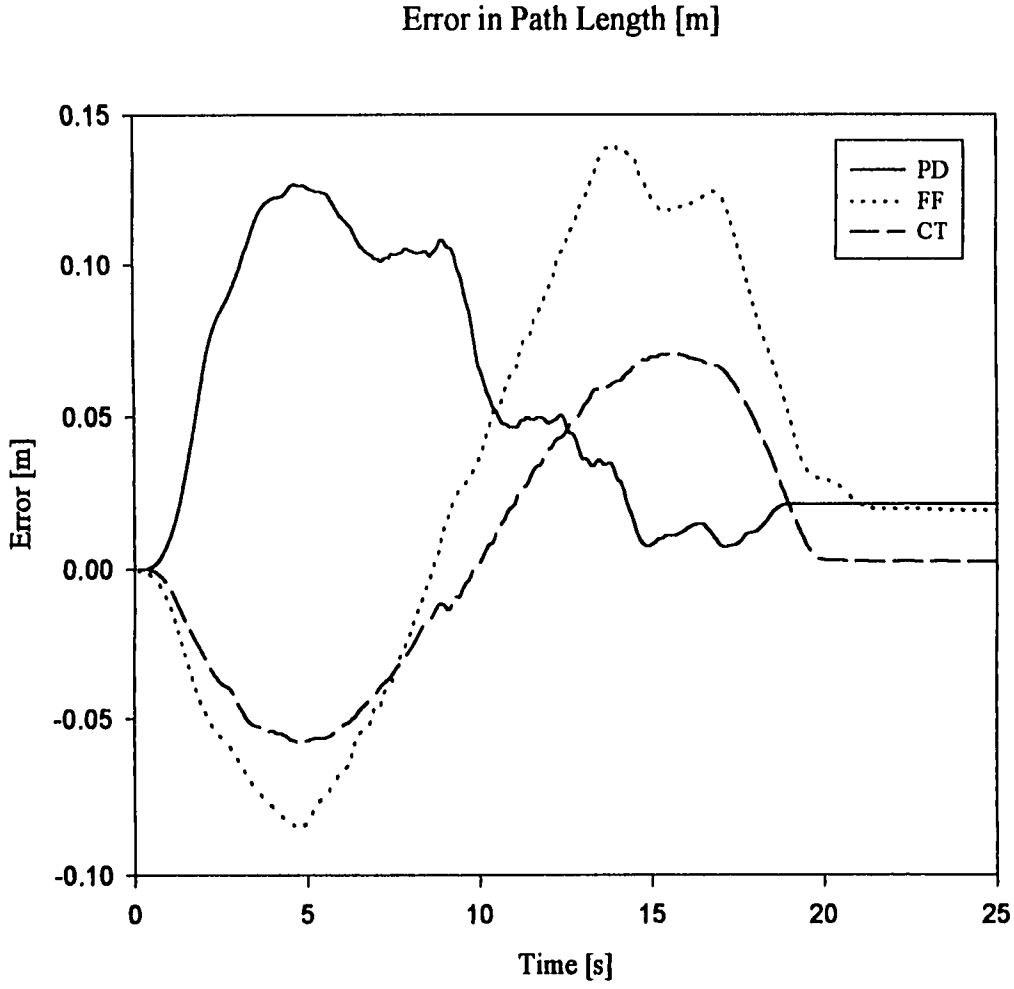

Figure 8.7 Errors in the path length during the straight line trajectory, SL_2.

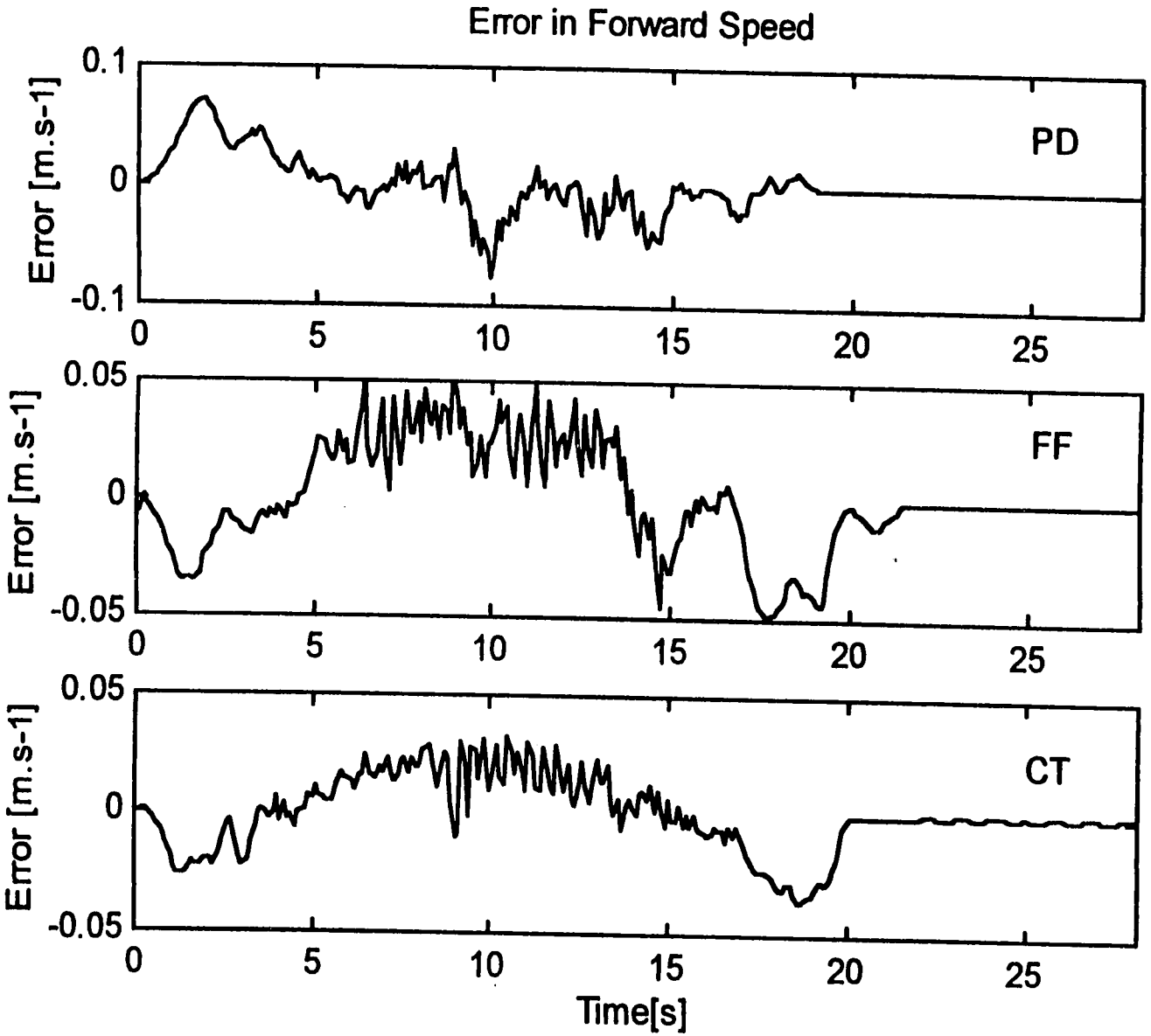

Figure 8.8 Errors in the forward speed during the straight line trajectory, SL_2.

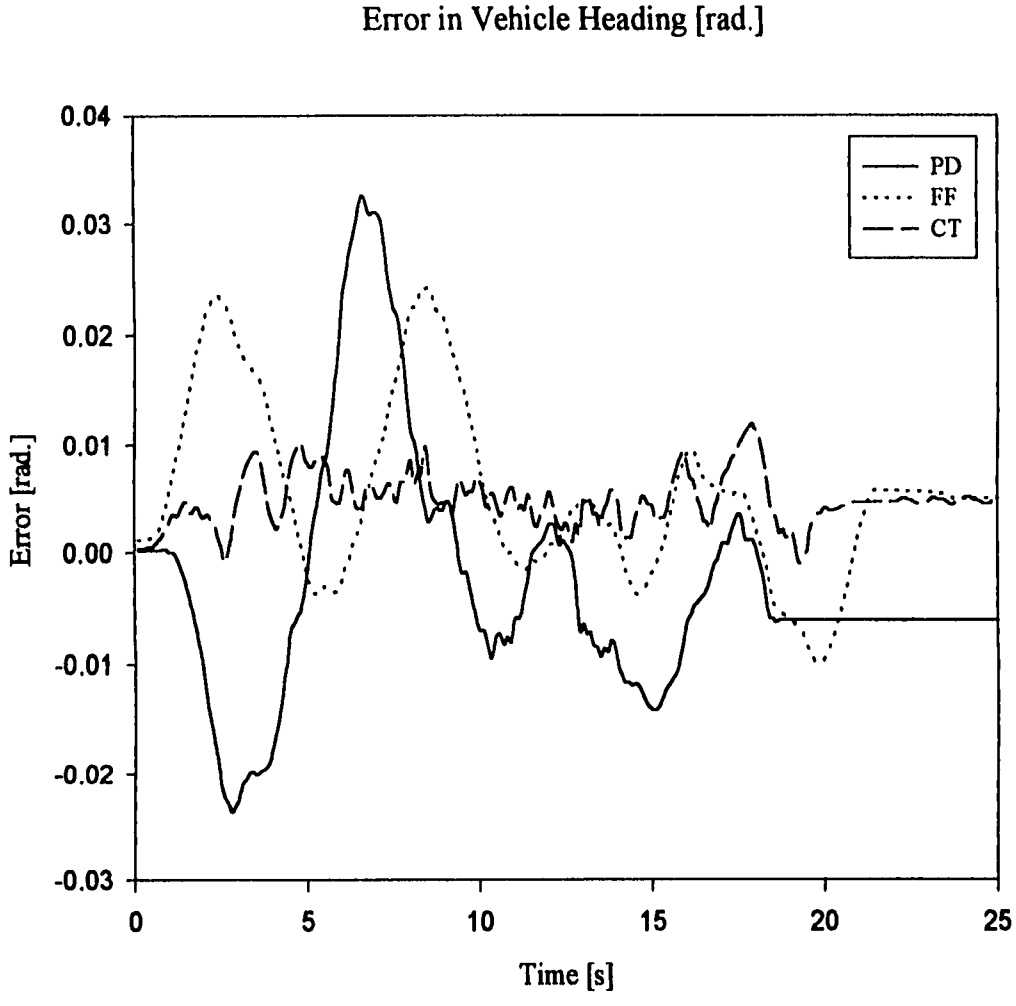

Figure 8.9 Errors in the heading during the straight line trajectory, SL_2.

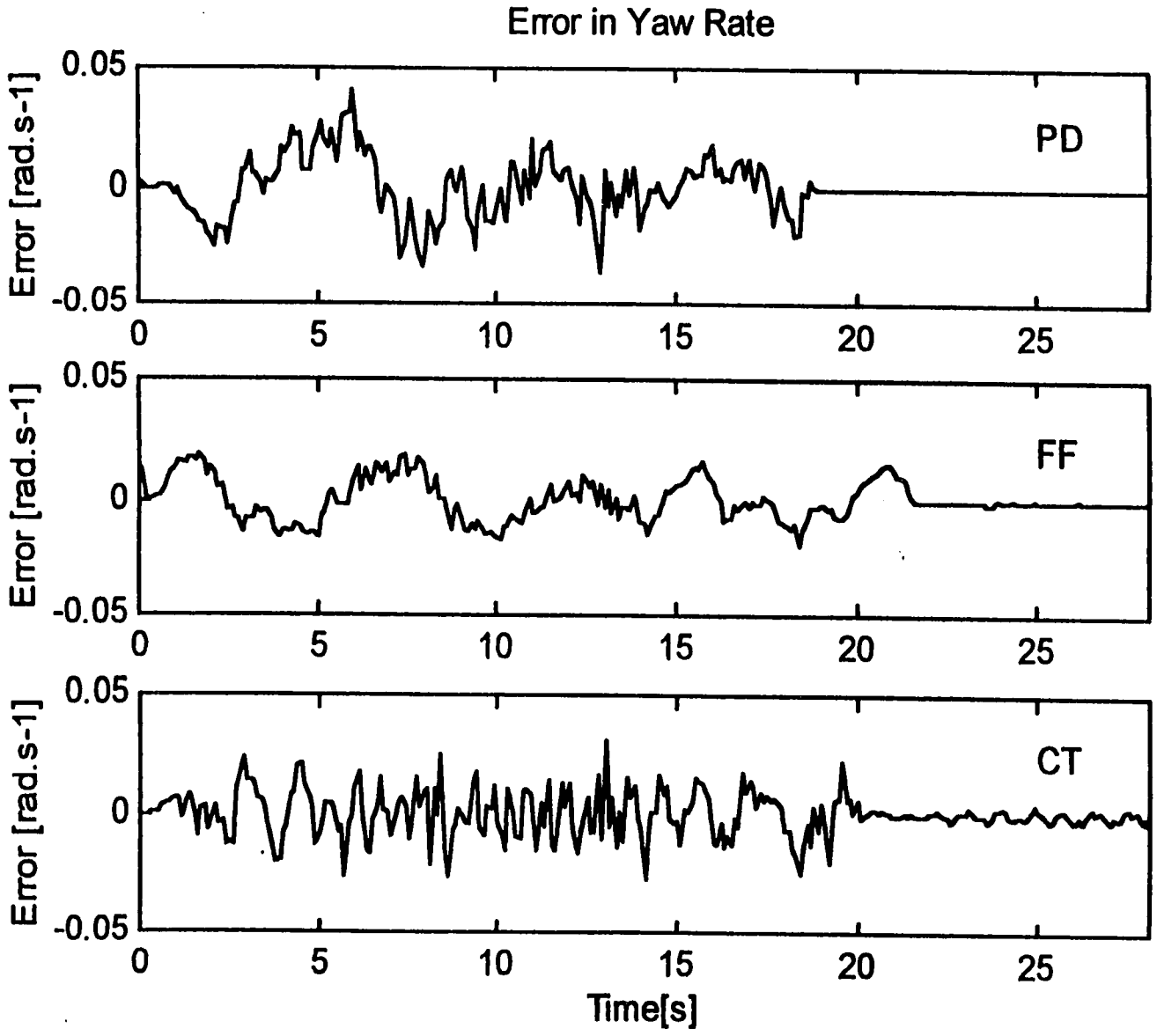

Figure 8.10 Errors in the yaw rate during the straight line trajectory, SL_2.

Table 8.2

Typical values of the performance indices for the straight line trajectory, SL_2.

Duration of trajectory 19 s

Maximum forward speed : 1.0 $m.s^{-1}$

Maximum Acceleration: 0.16 $m.s^{-2}$

Controller	Path Length Error RMS [m]	Path Length Error Max.[m]	Path Length Error SS.[m]	Forward Speed Error RMS [$m.s^{-1}$]	Heading Error RMS [rad.]	Heading Error Max.[rad.]	Heading Error SS.[rad.]	Yaw Rate Error RMS [$rad.s^{-1}$]
PD	0.0752	0.1273	0.0214	0.0258	0.0132	0.0326	-0.0061	0.0131
FF	0.0837	0.1402	0.0194	0.0264	0.0115	0.0242	0.005	0.01
CT	0.0457	0.0703	0.003	0.0175	0.0065	0.012	0.005	0.0108

(N.B: RMS = Root Mean Square value ; Max. = Maximum value ; SS. = Steady State value)

wheel speeds to provide the desired heading. The conventional PD controller, using only errors in the trajectory parameters of the individual wheels, effectively treats the non-holonomic system as two independent systems for control. Differences in the dynamic behaviour of the two drive wheels under the action of this independent control scheme are reflected as errors in the heading angle and the yaw rate. The higher speeds and accelerations required in this trajectory lead to greater differences between the two drive wheel units and large oscillations are seen in Fig.8.9 for the heading of the WMR under the action of the PD controller and the FF controller.

8.3.3 Lane Change Trajectory

During the lane change manoeuvers, the angular velocity and the angular acceleration of the vehicle influence the trajectory tracking performance of the dynamic controllers. In addition, in the tests carried out for this thesis work, a suspended load is used in these trials to provide additional disturbance to the vehicle. Two lane change trajectories are used to study the influence of increasing angular velocities and accelerations on the tracking performances of the controllers. As mentioned in Section 8.2, the trajectory generation scheme provides a 1-segment lane change trajectory with continously differentiable linear and acceleration accelerations.

The profiles of the desired trajectory parameters for the lane change trajectory (LC_1), are shown in Fig. 8.11. The WMR starts from rest and accelerates to reach a maximum forward speed of 1.0 $m.s^{-1}$ in a time of 15s. Simultaneously, the yaw rate increases to a maximum value of 0.04 $rad.s^{-1}$ with a maximum acceleration of 0.0081 $rad.s^{-2}$. The

maximum forward acceleration is 0.0963 $m.s^{-2}$. The trajectory is symmetric, and the WMR decelerates to a stop while simultaneously turning to regain the heading at the entry to the lane change. Simultaneous forward and angular accelerations are used to impose a greater disturbance on the trajectory tracking performance of the controllers. For illustration, two steel discs of a total mass of 20 Kg are used as the suspended load. The experimental setup allows the load to be a varible. The length of the swing arm is 0.4m. The load is free to swing along the transverse plane of the WMR due to angular accelerations experienced during the trajectory. Complete details of the suspended load system are provided in Appendix B.

The plots of typical performances of the controllers are shown in the set of figures, from Fig. 8.12 for errors in the path length, Fig. 8.13 for forward speeds, Fig. 8.14 for errors in heading and Fig. 8.15 for yaw rate. Table 8.3 lists the performance indices obtained during a typical test. The average value of swing angle for the load during trajectory execution is 0.03 radians ($\approx$ 2 deg.) and the rate of swing is 0.15 $rad.s^{-1}$ ($\approx$ 9 $deg.s^{-1}$).

The performances of the controllers in tracking the desired path length and forward speed resemble those observed during the high speed straight line trajectory, SL_2. In particular, the magnitude of the maximum path length error for the CT controller is reduced from 0.07m to 0.04m, a reduction of 60%. The maximum forward acceleration used in the lane change trajectory is 0.0963 $m.s^{-2}$ which is also very close to 60% of the maximum acceleration of 0.16 $m.s^{-2}$ used in SL_2. This further underlines the influence of the forward acceleration on the performance of the model based controller.

The CT controller in regards to the heading and the yaw rate shows better performance than both the PD and the FF controllers. The maximum error in heading for the

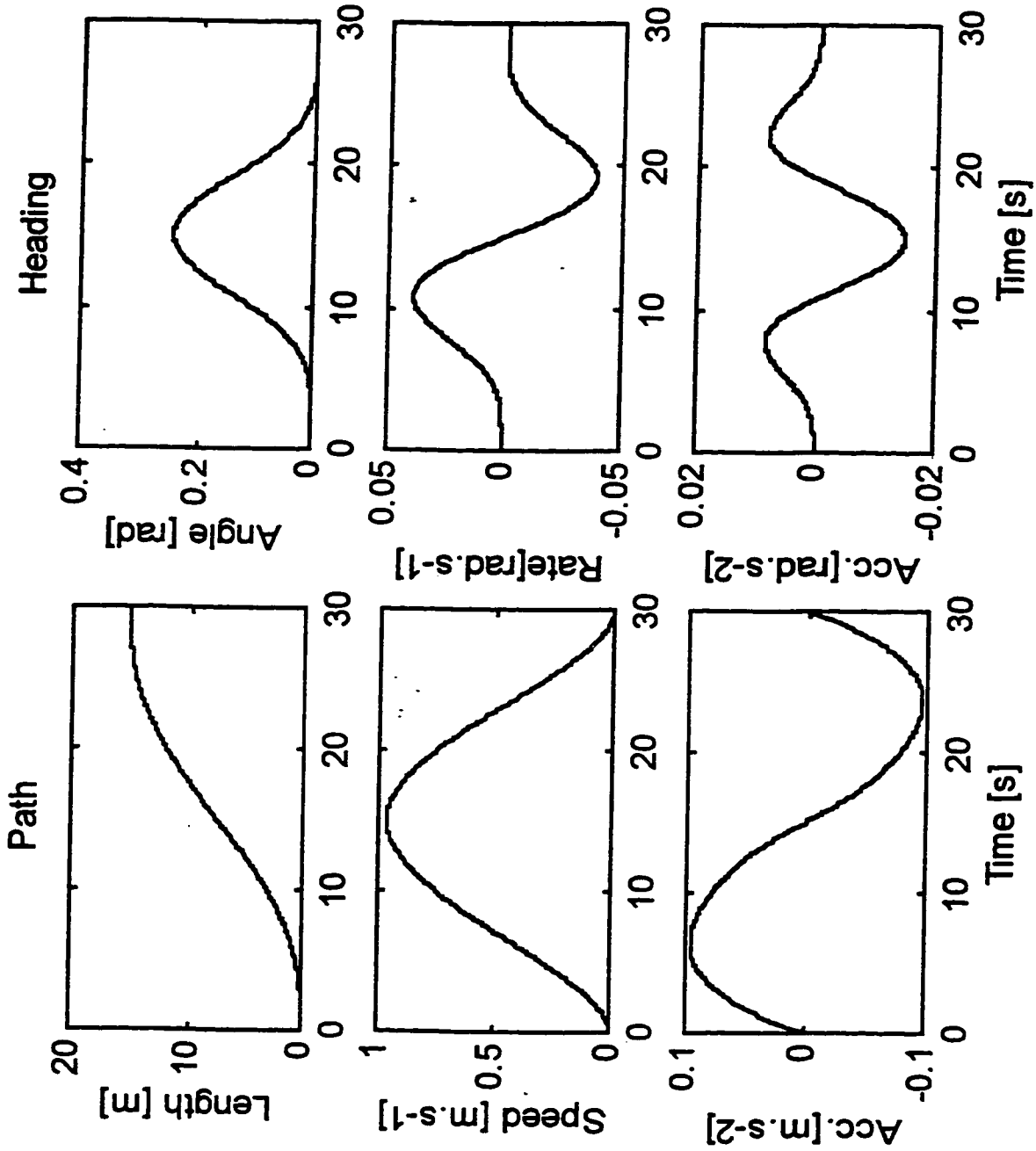

Figure 8.11 Desired path and heading parameters for the lane change trajectory, LC_1.

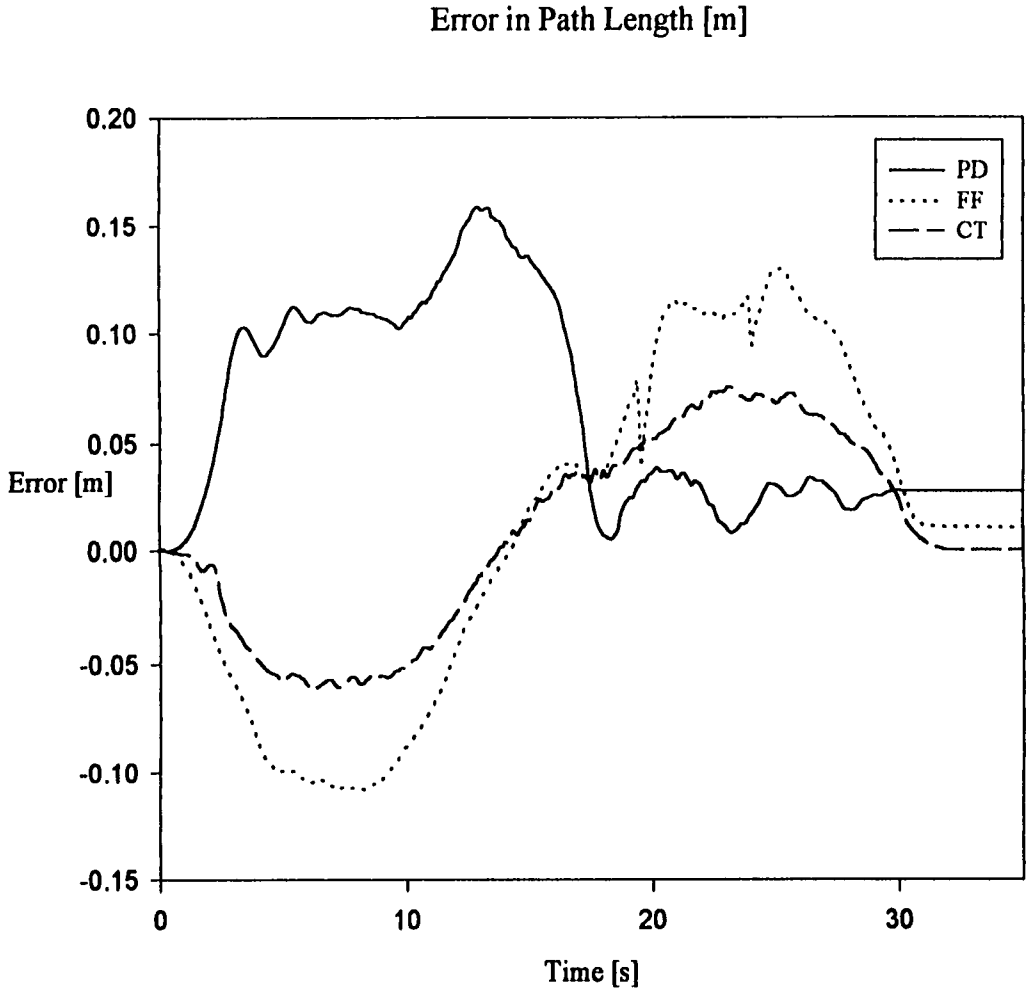

Figure 8.12 Errors in path length during the lane change trajectory, LC_1

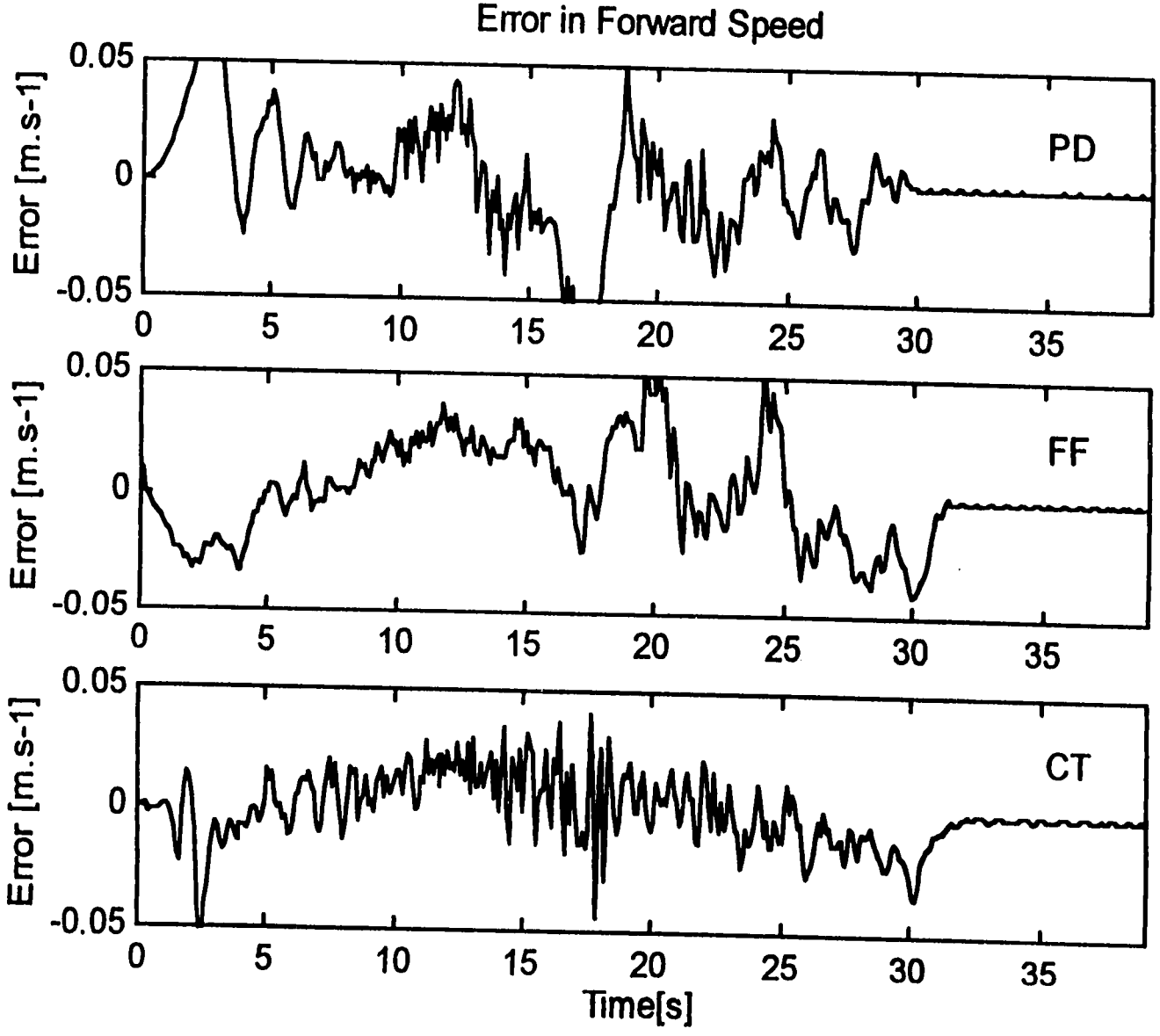

Figure 8.13 Error in the forward speed during the lane change trajectory, LC_1.

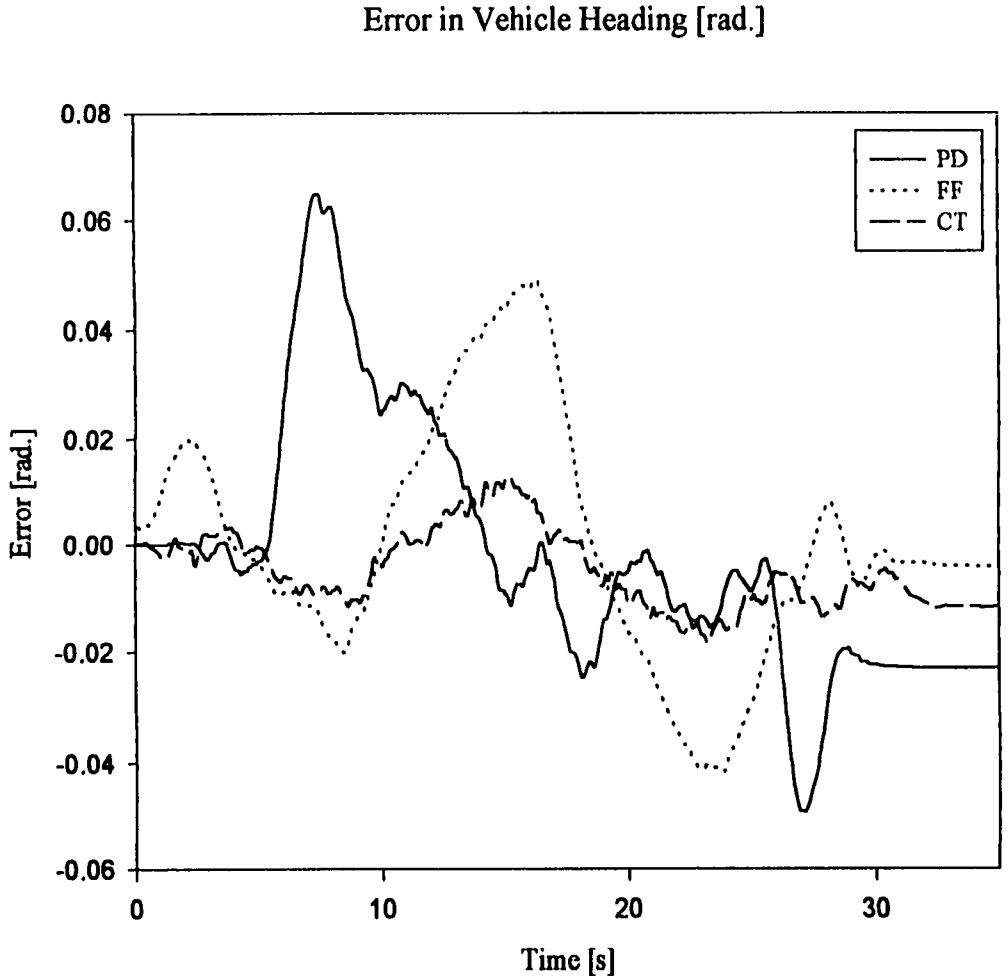

Figure 8.14 Errors in the heading angle during the lane change trajectory, LC_1.

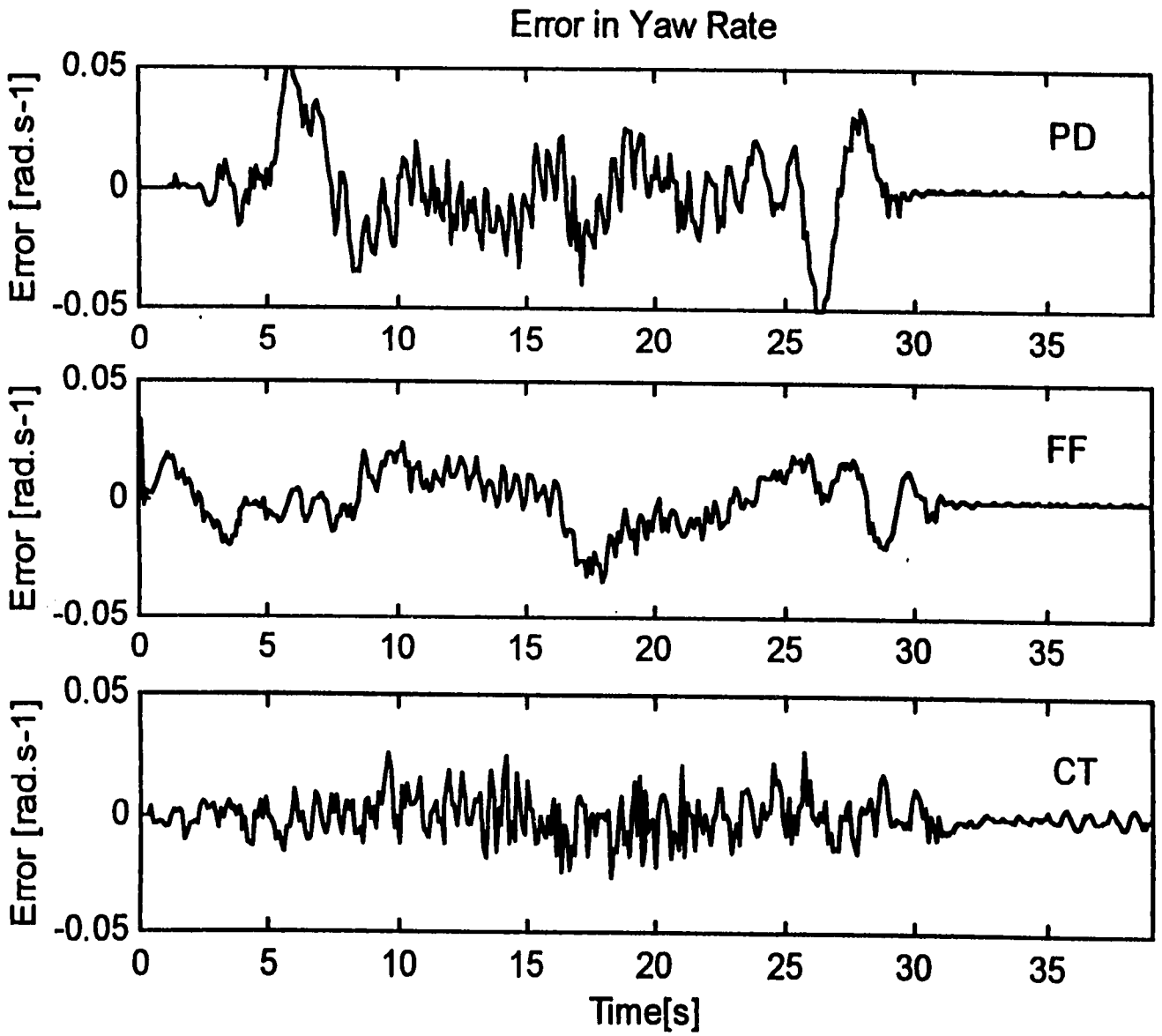

Figure 8.15 Errors in yaw rate during the lane change trajectory, LC_1.

Table 8.3

Typical values of the performance indices for the lane change trajectory, LC_1.

Duration of trajectory 30 s ; Suspended load of 20 kg on a 0.4m swing arm

Maximum forward speed : 1.0 $m.s^{-1}$; Maximum yaw rate: 0.039 $rad.s^{-1}$

Maximum forward Acceleration: 0.0963 $m.s^{-2}$; Maximum angular acceleration: 0.0081 $rad.s^{-2}$

Controller	Path Length Error RMS [m]	Path Length Error Max.[m]	Path Length Error SS.[m]	Forward Speed Error RMS [$m.s^{-1}$]	Heading Error RMS [rad.]	Heading Error Max.[rad.]	Heading Error SS.[rad.]	Yaw Rate Error RMS [$rad.s^{-1}$]
PD	0.0855	0.1594	0.0278	0.0257	0.027	0.0649	-0.023	0.0169
FF	0.0812	0.1819	0.015	0.0218	0.0238	0.0492	-0.0042	0.012
CT	0.0482	0.0425	0.0	0.015	0.0104	-0.0183	-0.0119	0.0091

(N.B: RMS = Root Mean Square value ; Max. = Maximum value ; SS. = Steady State value)

CT controller is 25% of that for the other two controllers. RMS values of the CT controller for both heading and yaw rate are 50% of those for the PD and the FF controller. However, it is also seen that the PD controller matches all the performance indices of the FF controller. The consistent performance of the CT controller validates the proposition that the inclusion of the dynamic model in the closed control loop results in improved tracking performance. Even though errors in the estimates of the model parameters increase the tracking errors, the absolute value of these error indices are only half those of the PD controller. It must be pointed out that PD controller gains were tuned for minimum error index values and the same numerical values of the gains were used for both the model based controllers. The FF controller uses feedforward drive torques, computed using the inverse dynamic model, only for open loop excitation during trajectory execution. Hence, inaccurate estimates in either or both the inertial parameters and frictional forces, results in feedforward drive torques that are proportionately different from the nominal values required by the WMR-load system. The magnitude of the errors in the FF torques act as disturbance signals of the same magnitude which, in addition to the disturbances from the environment during the trajectory, must be compensated by the PD controller. For large errors in both the model parameters, as is hypothesised in this thesis, the performance of the FF controller may degrade considerably.The model parameter values used in this thesis are mostly drawn from previous reported work or from calculations using simplifying assumptions.

8.3.4 Lane Change Trajectory

The forward and the angular accelerations during the lane change are increased in order to understand their combined influence on the performances of the dynamic controllers. In the generation of the desired trajectory parameters, the total duration of the trajectory was iteratively adjusted to give the maximum permissible acceleration values using the feedforward current values to test and to prevent actuator saturation. The maximum feedforward current value for this lane change trajectory (LC_2), is 11 amps, which is 90% of the continuous current value of 12.5amps. set for the power amplifiers.

The desired trajectory parameter plots are shown in Fig.8.16. In this one segment lane change trajectory, the WMR starts from rest and accelerates to a maximum forward speed of 1.0 $m.s^{-1}$ in a period of 10s. The maximum forward acceleration during this phase is 0.144 $m.s^{-2}$. The maximum yaw rate for the turn is 0.0442 $rad.s^{-1}$ and the angular acceleration is 0.0137 $rad.s^{-2}$. The forward acceleration for LC_2 is 1.5 times that used for LC_1 and ratio of the angular accelerations is 1.7.

Typical plots for the values of the errors obtained for the LC_2 trajectory with the suspended load of 20 Kg. are shown in Fig.8.16 for the path length error to Fig.8.20 for the errors in the yaw rate. The performance indices are listed in Table 8.4 for the three controllers. The increase in the forward acceleration increases the maximum values of the position error for the model based CT controller in the same proportion of 1.5. RMS values on the other hand are only 5% greater. The ratio of the maximum heading error for the two lane change trajectories is 1.3 and the RMS values are remain unchanged. This indicates that the values of the inertial parameters for rotation about the yaw axis used in the inverse

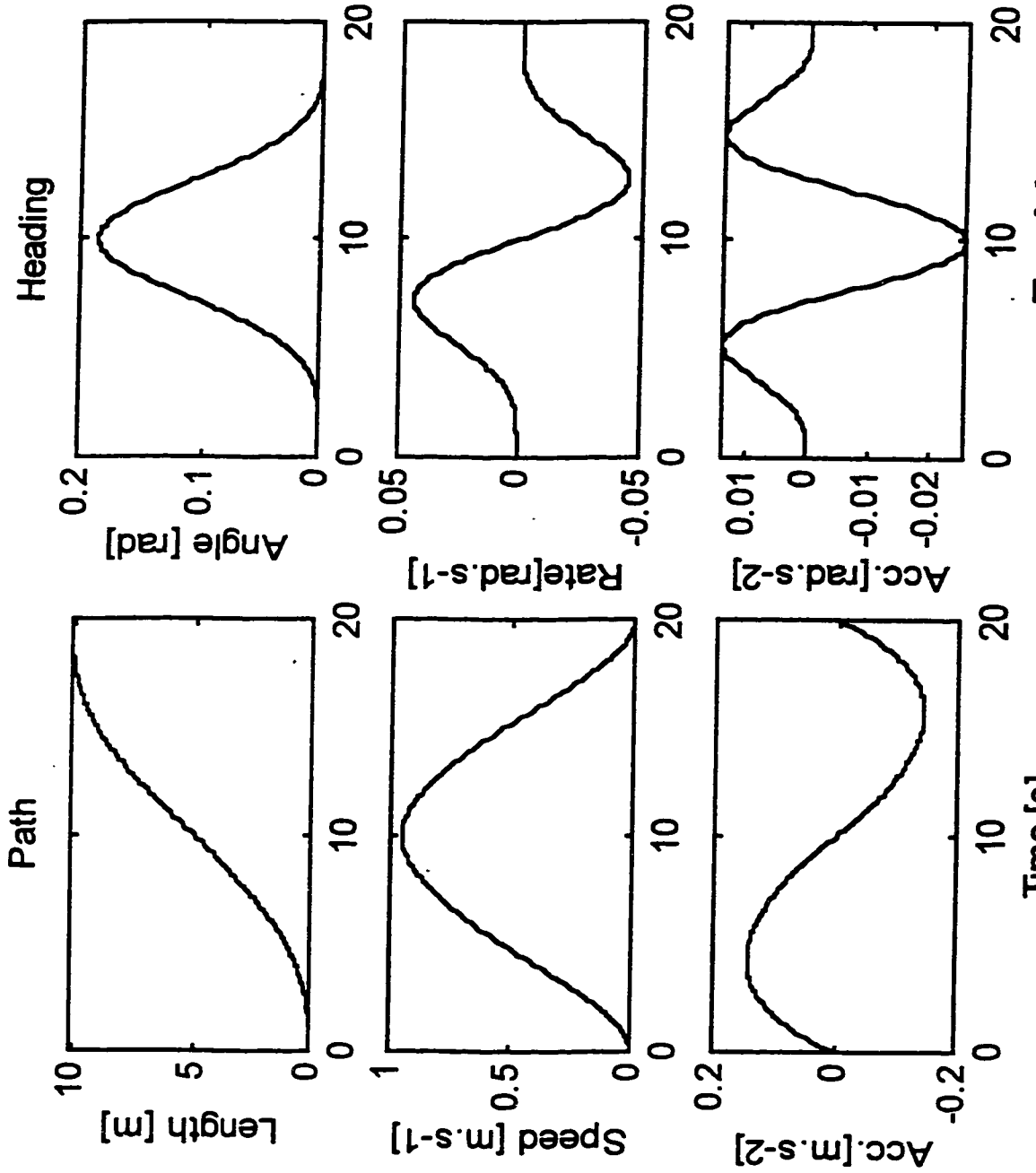

Figure 8.16 Desired path and heading parameters for the lane change trajectory, LC_2

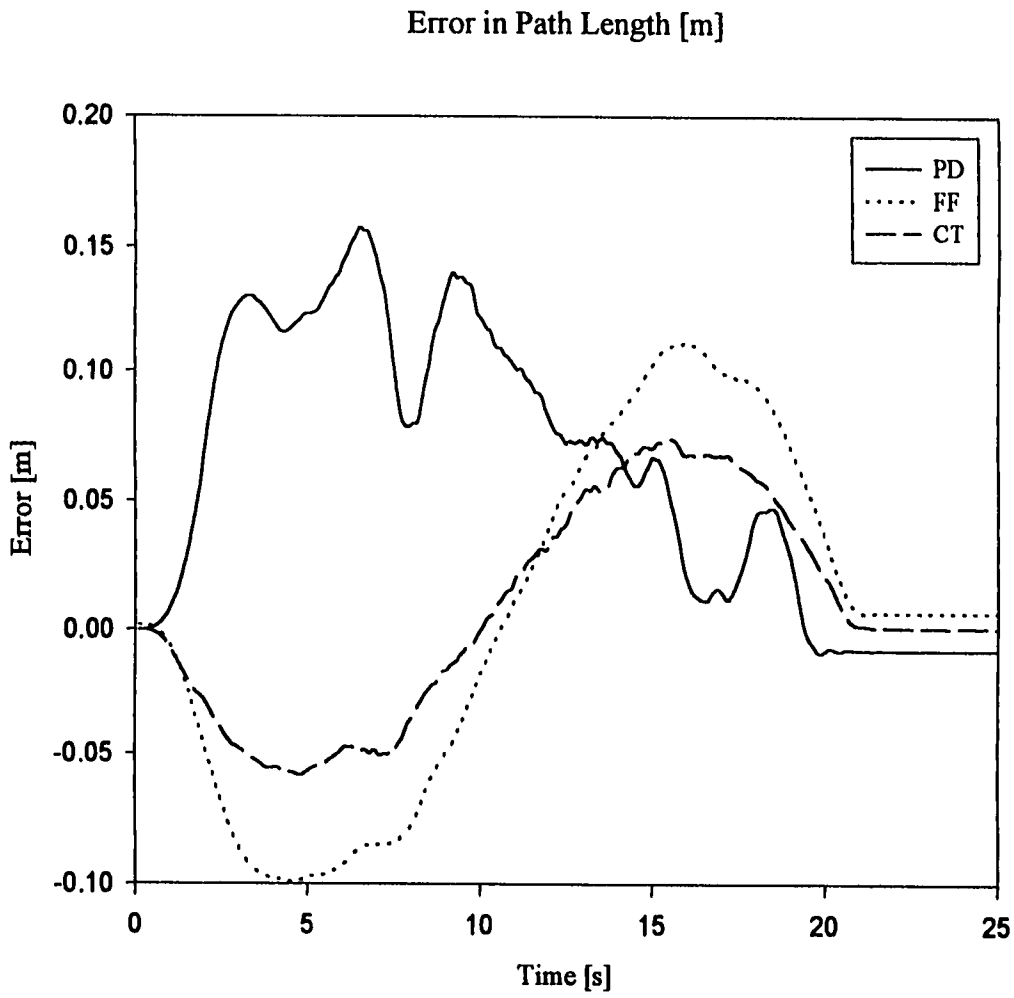

Figure 8.17 Errors in the path length during the lane change trajectory, LC_2

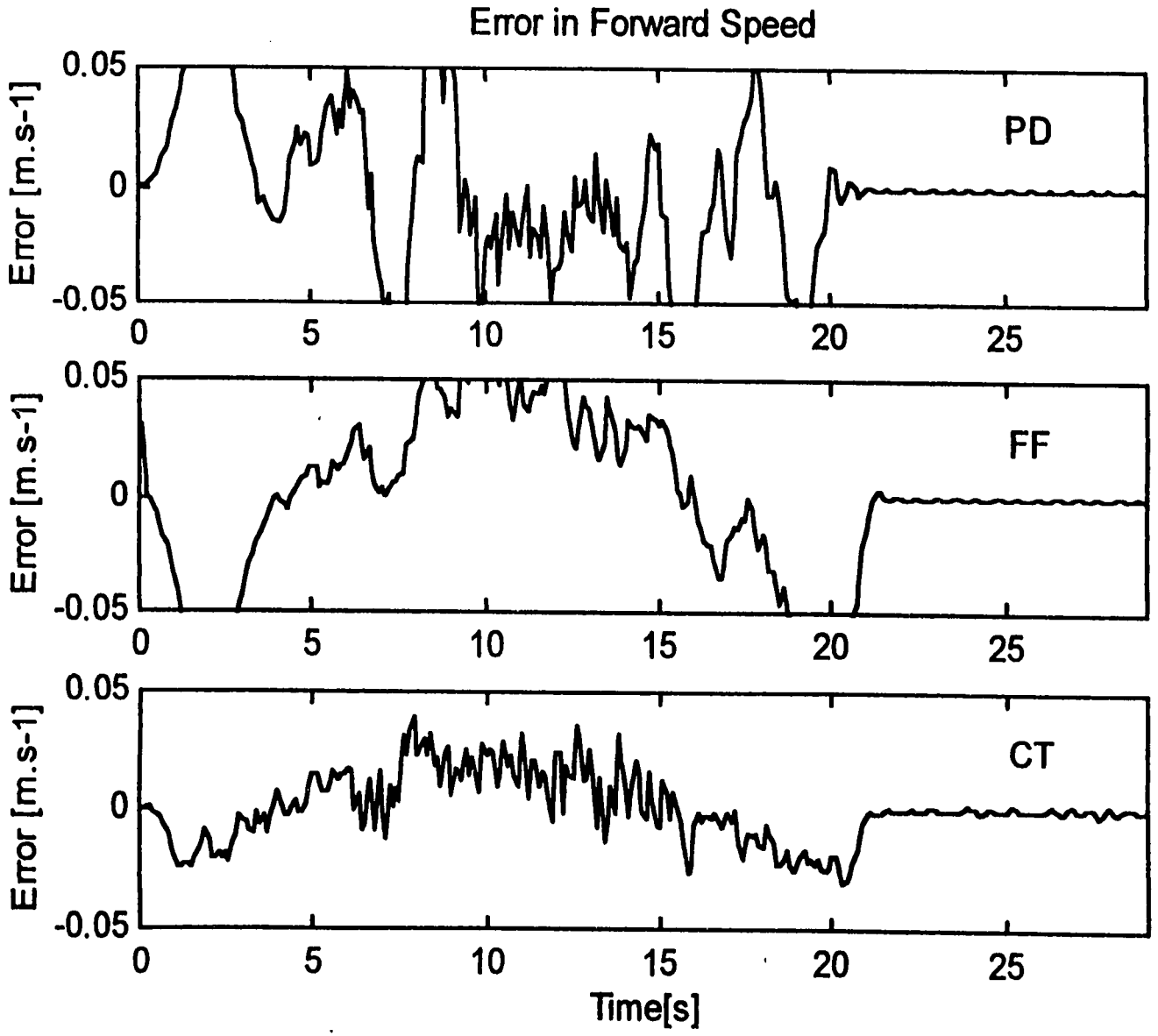

Figure 8.18 Errors in vehicle forward speed during the lane change trajectory, LC_2.

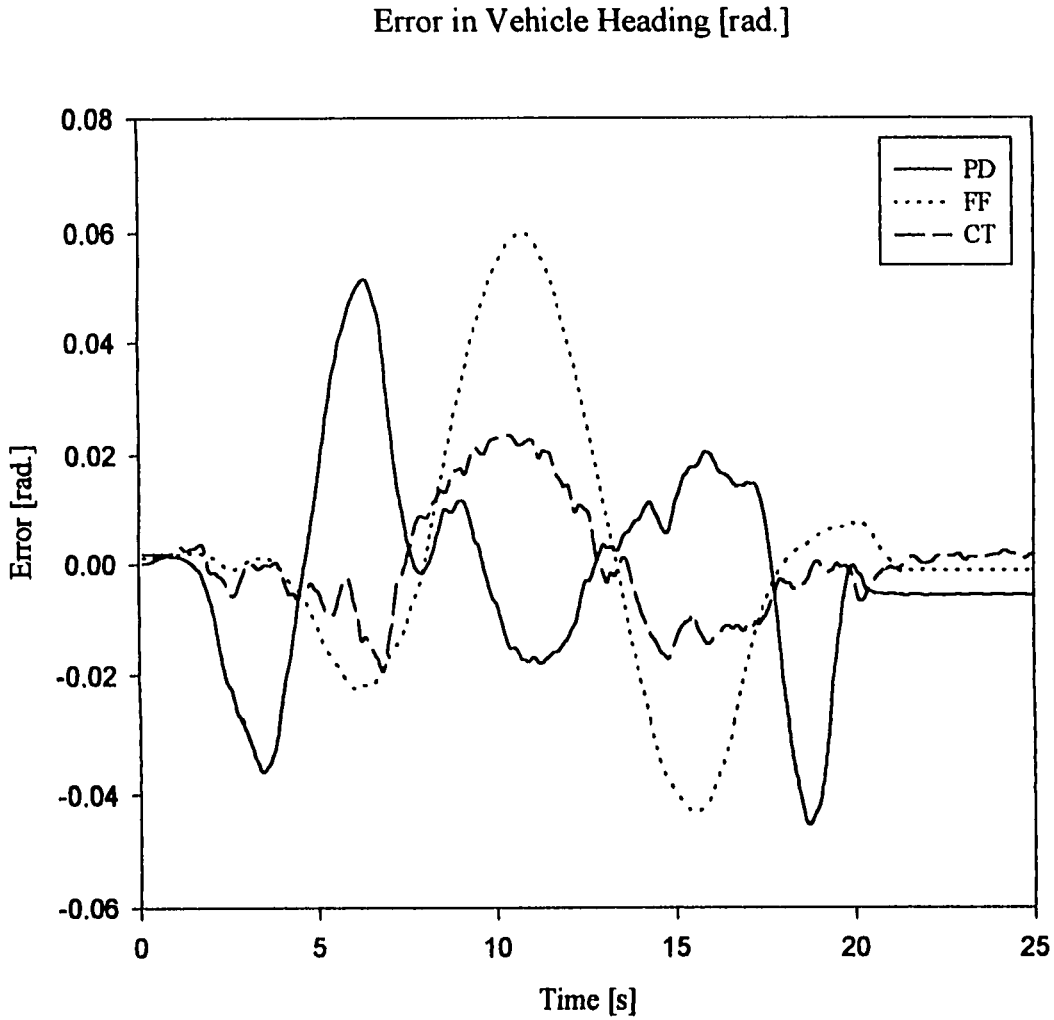

Figure 8.19 Errors in the heading angle during the lane change trajectory, LC_2.

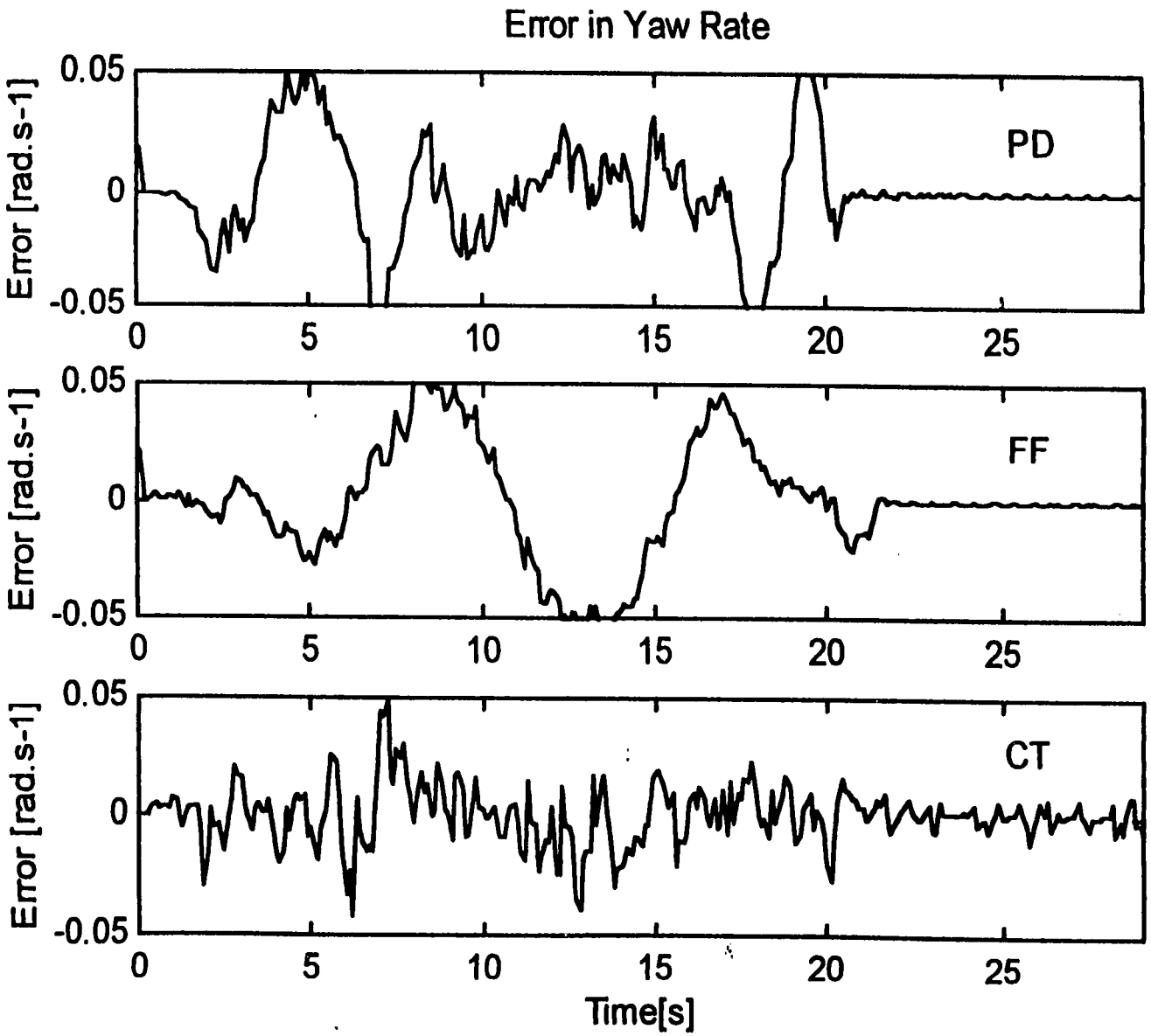

Figure 8.20 Errors in the yaw rate during the lane change trajectory, LC_2.

Table 8.4

Typical values of the performance indices for the lane change trajectory, LC_2.

Duration of trajectory 20 s ; Suspended load of 20 kg on a 0.4m swing arm

Maximum forward speed : 1.0 $m.s^{-1}$; Maximum yaw rate: 0.0442 $rad.s^{-1}$

Maximum forward Acceleration: 0.1444 $m.s^{-2}$; Maximum angular acceleration: 0.0137 $rad.s^{-2}$

Controller	Path Length Error RMS [m]	Path Length Error Max.[m]	Path Length Error SS.[m]	Forward Speed Error RMS [$m.s^{-1}$]	Heading Error RMS [rad.]	Heading Error Max.[rad.]	Heading Error SS.[rad.]	Yaw Rate Error RMS [$rad.s^{-1}$]
PD	0.0909	0.1578	-0.008	0.0407	0.0212	0.0517	-0.0056	0.0259
FF	0.0754	0.2604	0.0164	0.0403	0.0266	0.0998	-0.0017	0.0286
CT	0.0469	0.0661	0.0009	0.0166	0.0112	0.0236	0.0012	0.0143

(N.B: RMS = Root Mean Square value ; Max. = Maximum value ; SS. = Steady State value)

dynamic model of the controller are better estimates of the actual values. The RMS values of the errors in the yaw rate for both the PD and the FF controller performances indicate that the magnitude of the oscillation are increased in the proportion of 1.8 in keeping with the increase in the value of the angular acceleration.

8.4 Summary

A systematic experimental investigation has been conducted to evaluate the tracking performances of the model-based, FF controller and the CT controller, using a conventional PD controller to provide base line values for the comparison. In this thesis, the performances of the controllers are compared using instantaneous error plots, a RMS error index and also the maximum and steady state position and orientation errors during trajectory execution. Issues regarding the desired trajectory generation in the presence of dynamic constraints, the tuning of the gains used in the controllers and the frequency used for the digital control loop are presented.

Trajectory tracking performances of the controllers under linear acceleration are evaluated using two straight line trajectories, with the maximum forward speed and linear acceleration used in the second trajectory twice those used for the first. The results tabulated in this chapter, show that the RMS error indices in path length and forward speed for the CT controller are consistently only 50% of those for the PD controller. Lane change trajectories are used to introduce the effects of angular acceleration and yaw rate on the tracking performances of the controllers. Two trajectories of increasing values of angular speed and accelertion are used. The results indicate that the error indices for orientation for the CT

controller remain at 50% of those for the PD controller for both the trajectories.

The performances of the model-based controllers shown by the simulations presented in Chapter 6 are not borne out by the experimental results. The trends in the instantaneous path length errors and the vehicle heading errors for the FF and the CT controllers are an order of magnitude higher and show a consistent dependency on the desired linear and angular acceleration during the trajectory. Due to this dependency on the acceleration, the difference between the simulations and the experimental results is ascribed to overestimated values of the inertial parameters in the dynamic equation. In addition, the trends in the path length errors for the PD controller seen in the experimental results also indicate that values of the tire friction and actuator frictional forces provided by the friction model used in this work are underestimated. For the FF controller, the effects of these errors in the model parameter estimates and consequently in the feedforward drive torques, must be compensated by a PD feedback controller. The results indicate that, under these conditions of poorly estimated model parameters, the tracking performance of the FF controller degrades. However, the results also indicate that the CT controller which uses the inverse dynamic model with the same estimated values of the model parameters, is able to compensate and to maintain the RMS error indices at half the error values of both the FF and the PD controllers. The experimental results also indicate the need for a systematic estimation of the inertial parameters and of the coefficients in the model describing tire and actuator friction.

Chapter 9

Conclusions and Recommendations

9.1 Summary

In the study of mobile robots, this thesis has contributed to two main areas to enhance the trajectory tracking performance of WMRs, namely,

- development of a generic dynamic modelling scheme for WMRs
- model based control of WMRs.

The results obtained during the course of this work, though general in scope, is intended for the modelling and the control of WMRs used in the predominant industrial applications. With the evolution of the technology, the requirements imposed on the speed and the payload capability of mobile robots are also increasing. The dynamic modelling methodology incorporates several features which specifically address the drawbacks seen in the common methods in use. The model thus provides a better understanding of the dynamic behaviour under these operating and loading conditions. The simulations and the experimental studies on trajectory tracking control apply and extend this insight to evaluate the suitability and the performance of model-based controllers for WMRs under these conditions. The following discussions summarize the pertinent results and the contributions of this thesis.

9.2 Contributions to Dynamic Modelling of WMRs

The objective to develop a generalised dynamic modelling methodology for a WMR executing planar motion while carrying an active payload has been realised by applying the

Kane's approach to this non-holonomic multi-body system. A survey of the literature indicates that this is the first time the Kane's approach has been specifically applied for modelling WMRs, which form a general class of inter-connected rigid body systems with motion constraints. Earlier reported work in the literature using the Kane's approach has been confined to holonomic systems such as stationary robots or to non-holonomic space craft systems only. Even though the Kane's approach is applicable to the describe the dynamics of any physical system, the methodology presented here for WMR modelling highlights several advantages of this scheme over other methods seen in the mobile robotic literature.

The modelling methodology, described in Chapter 3, has been presented as a systematic 5-step procedure applicable to common wheel types and wheel configurations used for WMRs. The method starts with a derivation of the kinematic model of the WMR so that the non-holonomic constraint equations may be obtained. This also helps to identify the number of degrees of freedom present in the system and to define the generalised speeds which will represent them in the following steps of the derivation. Partial velocities and partial angular velocities of all the important points chosen by the user, usually the mass centres of the various dynamic components, are obtained on Step 2. The applied external forces and torques are then used to obtain the generalised external forces in Step 3. Step 4 involves derivation of generalised inertial forces from the inertial forces and torques obtained using the known inertial parameters of the WMR and the load and the linear and angular accelerations experienced by the constituent rigid bodies. The generalised external forces and generalised inertial forces for each degree of freedom are assembled in Step 5 to provide the complete set of dynamic equations.

The Kane's method incorporates the motion constraints of the WMR system into the derivation of the dynamic equations from the first step onwards. The succeeding steps relate only to the degrees of freedom of the system and this avoids the redundancy experienced in the other modelling methods. If the natural degrees of freedom are chosen on Step 3 to represent generalised speeds, all the intermediate terms in the derivation represent physical quantities which provide insight into the behaviour of the system. A variety of loads and motion conditions, such as climbing a ramp while carrying a suspended load, may be incorporated into the derived set of dynamic equations.

In addition, the methodology developed in this thesis offers a scheme to obtain the dynamic side forces and the vertical loads experienced by the wheels of the WMR during motion. These forces are obtained using a set of linear equations for the 'virtual' generalised speeds. The dynamic loads affect the frictional forces in the tires and the actuators.

The methodology has been applied to derive the equations of motion using a steer-drive wheel unit as the generic wheel type. For each other wheel type, the appropriate substitutions have been tabulated. The dynamic equations of a suspended load and the contributing terms to the dynamic equations of the WMR have been obtained. In all these derivations, the side forces and the vertical wheel loads have been taken into account so that the dynamic equations and the equations required to obtain the constraint forces are simultaneously obtained.

Thus the dynamic equations incorporate a variety of inertial forces such as the centrifugal and the coriolis forces and the wheel loads in addition to the dynamic applied forces due to payload dynamics. In the literature these forces are normally neglected under

the assumptions of low operating speed and acceleration and deadweight payload only.

In order to illustrate the proposed modelling scheme, three case studies have been presented. The WMR in each case utilises common wheel types and configurations commonly found in the literature and in practice. Using the 5-step procedure and the tabulated results for the various wheel types, the dynamic equations for each case have been derived. Each derivation also includes the set of equations for the wheel loads. The set of dynamic equations are in a form suitable for model based controller synthesis and implementation.

9.3 Contributions towards the Evaluation of Model Based Controller Performance

The objective to evaluate the performances of model based controllers for trajectory tracking in planar motion of a WMR under different loading conditions has been realised using both simulation studies and experimental trials carried out under realistic operating conditions. The experimental platform, CONCIC III, with wheels configured for differential drive was used for the experimental investigations.

Trajectory tracking performances of the controllers were first tested for simulated straight line trajectories. The results obtained indicate that the path length error values for the model based controllers are an order of magnitude smaller than those for the PD controller. Similar performance results for position as well as orientation are obtained from the simulated lane change trajectory where the WMR carried a suspended payload. However, the increase in the RMS error indices for both the path length and the forward speed, between the straight line and the lane change trajectories, for the FF controller is three fold. This indicates that the open loop nature of the feedforward signals makes this controller performance more

dependent on the trajectory parameters and the conditions of loading. For the CT controller the error indices in the simulations remain unchanged between the straight line and the lane change trajectories and for the active payload case.

The results of the simulations were verified by experimental investigations for different straight line and lane change trajectories. For the straight line trajectory, the performance of the CT controller, as indicated by the RMS error index, is seen to reduce instantaneous errors in path length and forward speed by 50% in comparison with the PD controller. The performance of the FF controller, on the other hand, is equal that of the PD controller though the trends in the errors during the trajectory are different.

The differences between the simulations and the experimental results for the FF controller in the straight line and the lane change trajectories are due to overestimates in the inertial parameter values. The errors in the estimates of these parameters affect the CT controller performance as well but the magnitudes of these changes are smaller due to the error compensation using the dynamic model. This proposition has been verified by simulations with varying values of inertial and frictional values. It is observed that an overestimate in the values of the inertial parameters and an underestimate in the frictional values produces patterns of errors similar to those observed in the experiments.

Simulations were also carried out for a high speed lane change trajectory at a maximum forward speed of 2 $m.s^{-1}$ and a maximum yaw rate of 0.1 $rad.s^{-1}$. In this trajectory, the PD controller exhibited large errors which induced an unstable motion and the simulated trajectory of the WMR diverged from the goal position. These results further underline the improved controller performance due to the presence of the dynamic model of the system in

the control loop.

Simulations were done to study the relation between the trajectory parameters and magnitudes of the side forces and the dynamic fluctuations in the vertical loads on the wheels during trajectory execution. Lane change trajectories with increasing speeds and accelerations were used. The results indicate that, for a given WMR, the magnitude of the side force, being directly related to the centrifugal force, increases with the square of the angular speed. The instantaneous vertical wheel load shows a 25% increase over the static load carried by the wheel under stationary conditions.

These observations prove that the dynamic nature of the wheel loads must be taken into account by model based controllers for improved performance. This information on the wheel loads is also useful for trajectory generation. The magnitudes of the wheel loads and the consequent frictional forces obtained through simulations may be used to check and to avoid wheel slippage due to the instantaneous drive torque exceeding the friction limit and the resultant loss of dynamic control of the WMR. Excessive frictional forces due to increased wheel loads may also lead to actuator saturation and consequent drop in trajectory tracking performance.

9.4 Recommendations for Future Work

The investigations carried out as part of this thesis work have met the objectives set forth at the beginning of the research. The generalised dynamic modelling methodology developed here provides a systematic approach to obtain the equations of motion of a WMR for different wheel types and configurations and different loading conditions. The simulation

and experimental results shed light on dynamic model based controller performances, both for Feed Forward compensation and for feedback Computed Torque error compensation. However, many areas that require further investigation surfaced during these investigations, as they do in any other such serious research undertaking. These topics and some proposed courses of action are given in the following short list in order to provide a way map for the future traveller along this path. The list of recommendations, not in any order of priority, is

- path planning and trajectory generation schemes taking dynamic constraints into account
- estimation methods for dynamic model parameters
- adaptive controllers and trajectory learning based control schemes

During the path planning and the trajectory generation stages, the lane change algorithms adopted from published literature for the trajectories used in the experimental work and the simulations were found to give rise to discontinuous jumps in angular accelerations. The reason for this limitation lies in the choice of the generalised coordinates and speeds used to describe the path being different from the generalised speeds representing the degrees of freedom of the WMR. For instance, in the differentially driven CONCIC III, the forward speed and the yaw rate represent the degrees of freedom of the WMR. The available path planning algorithms for WMRs, however, use cartesian coordinates with the y-coordinate expressed *solely* as a function of x. In other words, the path is planned for a point of reference and not for the rigid body system. The motion constraint that relates the position and the orientation of this wheel configuration is thus not incorporated in the algorithm. Hence, the trajectory exhibits discontinuous jumps in the angular accelerations. In

addition, the trajectories must be checked for actuator saturation and wheel slippage due to excessive drive torques and the parameters modified if either dynamic constraint condition exists. For mobile robots, thus, trajectory generation and dynamic simulation studies are interlinked but available schemes treat path planning as a geometric exercise. B-spline and other concepts from Computer Aided Graphic Design (CAGD) provide elegant methods of using generalised coordinates to generate $\mathbf{C}^n$ curves. These schemes permit modifying the generated curve locally in order to take into account kinematic or dynamic constraints without having to recalculate the complete path after each change. Combining the dynamic modelling methodology presented in this thesis with CAGD concepts for path planning would provide an useful tool for applications involving WMR systems.

The experimental results show the importance of obtaining and using estimates of the dynamic model parameters as close to the actual values as possible. Using the dynamic model, even with poor estimates of the parameters as in this thesis work, is seen to provide improvements in the trajectory tracking performance of the CT controller. Further gains in this direction have been indicated by the simulation results regarding the effects of the inertial and the frictional parameters. The physical structure of the WMR normally remains unchanged in industrial applications with only the inertial parameters of the payloads being different. Hence, the inertial parameters of the WMR may be estimated by techniques such as accurate weighing, CAD estimates and Tri-filar technique for obtaining rotational inertia.

Adaptive control algorithms that use on-line parameter estimations are a viable alternative to fixed model parameter estimates being used in the dynamic model. A vast amount of literature exists in the application of adaptive schemes for a variety of systems

including stationary robots. However, the application of such on-line identification and adaptive control schemes to WMRs is still in its early stages and no experimental work has been reported yet. Work is already afoot at the Centre in this direction using Fuzzy Modelling techniques. Mobile robots in industrial applications often execute the same trajectory repeatedly. This provides the opportunity to apply trajectory learning schemes to mobile robots in order to improve trajectory tracking behaviour. For stationary robots, learning techniques have been proven to provide a substantial improvement in controller performance and a large reduction in errors during successive executions of the trajectory. The mobile robot literature indicates that these learning techniques have not been tried yet for WMRs.

References

1. Lee, K., 1990, "Terminology", in "Concise International Encyclopedia of Robotics: Applications and Automation", Dorf, R.C., (editor), John Wiley & Sons, New York, pp. 999.

2. Cheng, R.M.H., Courbet, Y., Surpaceanu, M., Favreau, P. and Fahim, A., 1986, "Investigation of an automatic guided vehicle (AGV) driven by camera vision", Proc. of the International Conference on Intelligent Autonomous Systems, Amsterdam, The Netherlands, pp.162 - 167.

3. Rajagopalan, R., 1991, "Guidance control for automatic guided vehicles employing binary camera vision", (Ph.D Thesis), Concordia University, Dept. of Mechanical Engineering.

4. Rajagopalan, R., and Cheng, R.M.H., 1992, "Guidance and control of Automatic Guided Vehicles using binary camera vision", SME Transactions on Robotics Research, Vol.2, pp. 2.11 - 2.35.

5. Rajagopalan, R., Cheng, R.M.H., and Lequoc, S., 1992, "A guidance control scheme for accurate track folowing of AGVs", Proc. 1992 IEEE International Conference on Robotics and Automation, Nice, pp.188-193.

6. Mehrabi, M.G., 1993, "Path tracking control of automated vehicles: theory and experiment", (Ph.D. Thesis), Concordia University, Dept. of Mechanical Engineering.

7. Huang, M., 1991, "Dynamic modelling and simulation of an AGV (CONCIC II)", (M.A.Sc Thesis), Concordia University, Dept. of Mechanical Engineering.

8. Cheng, R.M.H., and Huang, M., 1990, "A study of guidance strategy for an AGV system using the simulation of the dynamic model", Proc. of the Thirteenth IASTED International Symposium, Robotics and Manufacturing, Santa Barbara, pp. 13 - 17.

9. Cheng, R.M.H., Huang, M., and Shankar, T.S., 1991, "Dynamic modelling and simulation of an AGV (The CONCIC II Vehicle)", Eighth World Congress on the Theory of Machines and Mechanisms, IFToMM Congress, Prague, Czechoslovakia, Aug.26 - 31, 1991.

10. Mehrabi, M.G., Cheng, R.M.H., and Hemami, A., 1993, "Dynamic modelling and control of wheeled mobile robots: theory and experiments", The 2nd. IEEE Conference on Control Applications, Vancouver, B.C.

11. Perelli, F., 1995, "Guidance control of an automated vehicle using CCD camera vision and parallel digital signal processing (DSP) controller", (M.A.Sc. Thesis), Concordia University, Dept. of Mechanical Engineering.

12. Rajagopalan, R., and Perelli, F., 1995, "Image processing performance of a digital signal processing system for guidance control of Automated Transit Vehicles using CCD vision", ROVA '95, International Conference, Bolton, England, pp. R.0201:1 - R.0201:10.

13. Rajagopalan, R., and Barakat, N., 1995, "Model based Computed Torque control of a differentially driven automated vehicle", Proc. of the 3rd International Conference on Robotics and Manufacturing, Cancun, Mexico.

14. Rajagopalan, R., and Barakat, N., 1997, "Velocity control of Wheeled Mobile Robots (WMRs) using Computed Torque Control and its performance for a differentially

driven robot", Special Issue on Mobile Robots - J. of Robotic Systems, April 1997.

15. Barakat, N., 1996, "Computed Torque Control of a differentially driven automated guided vehicle", (M.A.Sc. Thesis), Concordia University, Montreal, Dept. of Mechanical Engineering.

16. Thorpe, C., Herbert, M., Kanade, T., Shafer, S., 1988, "Vision and navigation for the Carnegie-Mellon Navlab", IEEE Trans. on Pattern Analysis and Machine Intelligence, Vol.10, No.3, pp.362 - 373.

17. Meystel, A., 1991, "Evolution of autonomous mobile robots", in "Autonomous mobile robots - Vehicles for cognitive control", World Scientific Publishing Co. Ltd., Singapore, pp. 30-74.

18. Amirouche, F.M.L., 1992, "Computational methods in multibody dynamics ", Prentice Hall Inc., New Jersey.

19. Krieg, W., 1989, "Future trends in production and distribution logistics", in Proc. of the 6th International Conference on Automated Guided Vehicle Systems, Hollier, R. H., (ed.), Brussels, Belgium, pp.3 -23.

20. Goldstein, H., 1980, "Classical Mechanics", 2nd edition, Addison-Wesley, Reading, Massachussetts.

21. Muir, P.F., Neuman, C.P., 1988, "Dynamic modelling of multibody robotic mechanisms: incorporating closed-chains, friction, higher-pair joints and unactuated and unsensed joints", Proc. of the 1988 IEEE International Conference on Robotics and Automation, Philadelphia, Pennsylvania, pp.1546 - 1551.

22. Muir, P.F., Neuman, C.P., 1987, "Kinematic modelling of wheeled mobile robots",

J. of Robotic Systems, Vol.4, No.2, pp. 281 - 340.

23. Saha, S.K., Angeles, J., 1989, "Kinematics and dynamics of a three-wheeled 2-DOF AGV", Proc. of the 1989 IEEE International Conference on Robotics and Automation, Scottsdale, Arizona, pp.1572 - 1577.

24. Cyril, X., Cheng, R.M.H., and Sankar, T.S., 1989, "On the dynamics of AGVs", Proceedings of the 4th. International Conference on CAD/CAM, Robotics and Factories of the future, India, pp. 264 - 273.

25. Kane, T.R., and Levinson, D.A., 1985, "Dynamics: theory and applications", McGraw-Hill, New York.

26. "Mechanical Design and Systems Handbook, 2 editon", 1985, Rothbart, H.A., Chief Editor, McGraw-Hill, New York, pp. 3.9

27. Wong, J.Y., 1993, "Theory of ground vehicles, 2ed., New York, John Wiley & Sons.

28. Chen, H., 1996, "Automated Modelling and simulation of automated vehicles" (M.A.Sc. Thesis), Concordia University, Montreal, Dept. of Mechanical Engineering.

29. Yu, S-H, and Moskwa, J.J., 1993, "A global approach to vehicle control: Coordination of four wheel steering and wheel torques", ASME J. of Dynamic Systems, Measurement and Control: Vol.116, pp 659-667 .

30. Dugoff, H., Brown, B.J., 1970, "An analysis of tire traction properties and their influence on vehicle dynamic performance", SAE 700377, SAE Transactions, pp.1219 - 1243.

31. Matsumoto, N., and Tomizuka, M., 1992, "Vehicle lateral velocity and yaw rate control with two independent control inputs", ASME Journal of Dynamic Systems,

Measurement and Control, Vol. 114, pp. 606-613.

32. Abe, M., 1985, "A study on vehicle turning behaviour in acceleration and in braking", SAE 852184.

33. d'Andrea-Novel, B., Bastin,G., Campion, G., 1991, Proc. of the 1991 IEEE International Conference on Robotics and Automation, Sacramento, California, pp.1130 - 1135.

34. Canudas de Wit, C., Roskam, R., 1991, "Path following of a 2-DOF wheeled mobile robot under path and input torque constraints", Proc. of the 1991 IEEE International Conference on Robotics and Automation, Sacrameto, California, pp. 1142 - 1147.

35. Zhao, Y., and BeMent, S.L., 1992, "Kinematics, dynamics and control of wheeled robots", Proc. 1992 IEEE International Conference on Robotics and Automation, Nice, France, pp.91-96.

36. Sarkar, N., Xiaoping, Y. and Kumar, V., 1994, "Control of mechanical systems with rolling constraints: Application to dynamic control of mobile robots", The International Journal of Robotics Research, Vol.13, No.1, pp 55-59.

37. Iyengar, S.S., and Elfes, A., (eds.), 1991, "Systems and Applications" in "Autonomous mobile robots - control, planning and architecture", IEEE Computer Society Press Tutorial, IEEE Computer Society Press, Los Alamitos, California, Vol.2, Chapter 4, pp.2-4, 231 - 466.

38. Zhao, F., 1995, "The development of a model-based robotic controller using the transputer technology", (M.A.Sc. Thesis), Concordia University, Montreal, Dept. of Mechanical Engineering.

39. An, C.H., Atkeson, C.G., and Hollerbach, J.M., 1988, "Model-based control of a robot manipulator", The MIT Press, Cambridge, MA.

40. Luh, J.Y.S, Walker, M.W., and Paul, R.P.C., 1980, " Resolved-acceleration control of mechanical manipulators", IEEE Transactions on Automatic Control, Vol. AC-25, No. 3, pp. 468 - 474.

41. Whitney, D.E., 1969, "Resolved motion rate control of manipulators and human prosthesis", IEEE Transactions on Man-Machine Systems, Vol. MMS-10, No.2, pp. 47 - 53.

42. Leahy Jr., M.B., Valavanis, K.P., and Saridis, G.N., 1986, "The effects of dynamic models on robot control", Proc. of the 1986 IEEE International Conference on Robotics and Automation, San Francisco, California, pp. 49 - 54.

43. Leahy Jr., M.B., and Saridis, G.N., 1987, "Compensation of unmodelled PUMA manipulator dynamics", Proc. of the International Conference on Robotics and Automation, Rayleigh, North Carolina, pp. 151 - 156.

44. Khosla, P.K., Kanade, T., 1986, "Real-time implementation and evaluation of model-based controls on CMU DD Arm II", Proc. of the 1986 IEEE International Conference on Robotics and Automation, San Francisco, California, pp. 1546 - 1555.

45. Goldberg, A.A., Apkarian, J.A., and Smith, H.W., 1989, "An approach to adaptive control of robot manipulators using the Computed Torque technique", J. of Dynamic Systems, Measurement and Control, Vol. 111, No. 11, pp. 1 - 8.

46. Uebel, M., Minis, I., and Cleary, K., 1992, "Improved Computed Torque control for industrial robots", Proc. of the 1992 IEEE International Conference on Robotics and

Automation, Nice, France, pp. 528 - 533.

47. Rajagopalan, R., and Cheng, R.M.H., 1994, "Computed Torque control of autonomous transit vehicles", Proc. of the 27th International Symposium on Advanced Transportation Applications (ATT and IVHS), ISATA, Germany.

48. Reister, D.B., 1992, "A new wheel control system for the omnidirectional HERMES - III robot", Robotica, Vol. 10, pp. 351-360.

49. Weisbin, C.R., et al, 1990, "HERMES III: A step toward autonomous mobility, manipulation and perception", Robotica 8, Part 1, pp. 7 - 12.

50. Bétouré, A. and Campion, G., 1996, "Dynamic modelling and control design of a class of omnidirectional mobile robots", Proc. 1996 IEEE International Conference on Robotics and Automation, Minneapolis, U.S.A., pp. 2810 - 2815.

51. d'Andréa-Novel, B., Campion, G and Bastin, G., 1995, "Control of nonholonomic wheeled mobile robots by state feed back linearization", The International J. of Robotics Research, Vol.14, No.6, pp. 543-559.

52. Campion, G., Bastin, G. and d'Andréa-Novel, B., 1993, "Structural properties and classification of dynamical models of wheeled mobile robots", IEEE Trans. on Robotics and Automation,

53. Sørdalen, O.J., and Canudas de Wit, C., 1993, "Exponential control law for a mobile robot: extension to path following", IEEE Transactions on Robotics and Automation, Vol.9, No.6, pp 837-842.

54. Samson, C., and Ait-Abderrahim, K., 1991, "Feedback control of a nonholonomic wheeled cart in cartesian space", Proc. 1991 IEEE International Conference on

Robotics and Automation, Sacramento, U.S.A., pp. 1136-1141.

55. Wiens, G.J., and Jang, W.M., 1994, "Passive joint control of dynamic coupling in mobile robots", The International Journal of Robotics Research, Vol.13, No.3, pp 209-220.

56. Joshi, J., and Desrochers, A.A., "Modelling and control of a mobile robot subject to disturbances", Proc. 1986 IEEE International Conference on Robotics and Automation, pp. 1508 - 1513.

57. Gat, E., Slack, M.G., Miller, D.P., and Firby, R.J., 1990, "Path Planning and executing for a planetary rover", Proc. 1990 IEEE International Conference on Robotics and Automation, pp.20-25.

58. Kanayama, Y., and Miyake, N., 1985, "Trajectory generation for mobile robots", Proc. Third International Symposium on Robotics Research, Faugeras, O.D., and Giralt, G., (eds.), Gouvieux, France, pp. 333 - 340.

59. Yates, R.C., 1974, "Curves and their properties", Classics in Mathematics Education, Vol.4, The National Council of Teachers of Mathematics, Karnes, H.T., (ed.), Louisiana State University, Louisiana.

60. Gaber, M., 1987, on path planning using klothoid pairs, Unpublished research papers, Centre for Industrial Control, Dept. of Mechanical Engineering, Concordia University, Montreal.

61. Mukherjee, R., and Anderson, D.P., "A surface integral approach to the motion planning of nonholonomic systems", ASME Journal of Dynamic Systems, Measurement and Control, Vol. 116, pp.315 - 325.

62. Reister, D.B., and Pin, F.G., 1994, "Time-optimal trajectories for mobile robots with two independently driven wheels", The International Journal of Robotics Research, Vol.13, No.1, pp. 38 - 54.

63. Wang, Y., Linnett, Roberts, J.W., 1994, "Motion feasibility of a wheeled vehicle with a steering angle limit", Robotica, Vol.12, No.3, pp.217 - 226.

64. Wang, Y., Linnett, Roberts, J.W., 1994, "Kinematics, kinematic constraints and path planning for wheeled mobile robots", Robotica, Vol.12, No.5, pp.391 - 400.

65. Kane, T.R., 1961, "Dynamics of nonholonomic systems", ASME J. of Applied Mechanics: Vol. 28, pp. 574-578.

66. Kane, T.R., 1968, "Dynamics", Holt, Rinehart and Winston, New York.

67. Huston, R.L., and Passerello, C.E., 1973, "On Lagrange's form of d'Alembert's principle", The Matrix and Tensor Quarterly: Vol.23, pp 109-112.

68. Huston, R.L., Passerello, C.E., and Harlow, M.W., 1978, "Dynamics of multirigid-body systems", ASME J. of Applied Mechanics: Vol.45, pp.889-894.

69. Kane, T.R., and Levinson, D.A., 1983, "The use of Kane's dynamical equations in robotics", International J. Robotics Research: Vol.2, No.3, pp. 3-21.

70. Kane, T.R., and Levinson, D.A., 1980, "Formulation of equations of motion for complex spacecraft", J. Guidance Control: Vol.3, No.2, pp.99-112.

71. Kane, T.R., Likins, P.W., and Levinson, D.A., 1983, "Spacecraft dynamics", New York, McGraw-Hill.

72. Thanjavur, K., and Rajagopalan, R., 1997, "Ease of dynamic modelling of Wheeled Mobile Robots (WMRs) using Kane's approach", 1997 IEEE International

Conference on Robotics and Automation, Albuquerque, New Mexico.

73. Thanjavur, K., and Rajagopalan, R., 1997, "Generalised dynamic modelling methodology for WMRs using Kane's approach", (in submission to) The International J. of Robotics Research.

74. Paul, R., 1981, "Robot manipulators: Mathematics, Programming and Control", MIT Press, Cambridge, Massachussetts.

75. Tzenov, P.I., and Cheng, R.M.H., 1996, "Traction control improvement in all-wheel drive", SAE Technical Paper Series 960956.

76. Cheng, R.M.H., and Rajagopalan, R., 1992, "Kinematics of automatic guided vehicles with an inclined steering column and an offset distance: Criterion for existence of inverse kinematic solution", J. of Robotic Systems: 9(8), pp. 1059-1081.

77. Fu, K.S., Gonzalez, R.C., and Lee, C.S.G., 1987, "Robotics: Control, Sensing, Vision and Intelligence", McGraw-Hill, St.Louis.

78. Nelson, W.L., 1989a, "Continuous steering-function control of robot carts", IEEE Transactions on Industrial Electronics, Vol.36, No.3, pp. 330 - 337.

79. Nelson, W.L., 1989b, "Continuous curvature paths for autonomous vehicles", Proc. 1989 IEEE International Conference on Robotics and Automation, Scottsdale, Arizona, pp. 330 - 337.

80. Farin, G., 1993, "Curves and surfaces for computer aided geometric design, A practical guide", Academic Press Inc., San Diego, Califronia.

81. MathWorks, 1992, "MATLAB®, High performance numeric computation and visualization software: Reference Guide", The MathWorks Inc., Natick, MA.

82. National Instruments, 1994, "NIDAQ® Users Manual, Function Reference Manual, Version 4.6.1", National Instruments Corporation, Austin, TX.

83. National Semiconductor, 1988, "LM 628/LM 629 Motion Controller Chip Data Sheets", The National Semiconductor Industries, U.S.A.

84. Intel Literature Department, 1987, "Microprocessor and peripheral handbook, Volume 1", Intel Corporation, Santa Clara, CA.

85. Ziegler, J.G., and Nichols, N.B., 1942, "Optimum settings for automatic controls", ASME Transactions, Vol. 64, No. 8, pp 759-762.

86. Jamsa, K., 1988, "Turbo C Programmer's Library", Programming Series, Borland-Osborne/ McGraw-Hill, Berkeley, CA, pp.84-87.

87. Traister, R.J., 1990, "Mastering C Pointers, Tools for Programming Power", Academic Press Inc., San Diego, CA, pp. 77 - 98.

88. Hollier, R.H., (ed.), 1987, "International trends in manufacturing technology - Automated guided vehicle systems", IFS Publications / Springer-Verlag, London.

89. Hollier, R.H., and Gelders, L.F.,(eds.), 1988, "Automated guided vehicle systems", Proc. of the 6th International Conference, Brussels, Belgium, IFS Publications/ Springer-Verlag, Oxford, U.K.

90. Spong, M.W., and Vidyasagar, M., 1989, "Robot dynamics and control", John Wiley and Sons, New York, pp.ix.

91. Groover, M.P., 1988, "Automation", in "International Encyclopedia of Robotics: Applications and Automation", Vol.1, Dorf, R.C., (ed.), John Wiley & Sons, New York, pp.136-137.

92. Nilsson, N.J., 1969, "A mobile automaton: an application of artificial intelligence techniques", Proc. of the International Joint Conference on Artificial Intelligence, Reprinted in "Autonomous Mobile Robots- control, planning and architecture ", 1991, Iyengar, S.S., and Elfes, A., (eds), IEEE Computer Society Press, Los Alamitos, California.

93. Thompson, A.M., 1977, "The navigation system of the JPL robot", Proc. of the International Joint Conference on Artificial Intelligence, Reprinted in "Autonomous Mobile Robots- control, planning and architecture ", 1991, Iyengar, S.S., and Elfes, A., (eds), IEEE Computer Society Press, Los Alamitos, California.

94. Moravec, H.P., 1983, "The Stanford Cart and the CMU Rover", Technical Report Robotic Institute, Carnegie-Mellon University, Pittsburg, Extracts reprinted in Meystel, A., 1991,"Evolution of autonomous mobile robots ", in "Autonomous mobile robots", World Scientific Publishing Co. Ltd., Singapore.

95. Giralt, G., Chatila, R., and Vaisset, M., "An integrated navigation and motion control system for autonomous multisensory mobile robots", International Symposium on Robotics Research, Reprinted in "Autonomous Mobile Robots- control, planning and architecture", 1991, Iyengar, S.S., and Elfes, A., (eds), IEEE Computer Society Press, Los Alamitos, California.

96. Belenkov, Y.O., Gusev, S.Y., Zotov, S.Y., Ruzhanskiy, Y.I., Timofeyev, A.Y., Frolov, Y.M., and Yakubovich, Y.A., 1978, "Adaptive system for control of autonomous mobile robot", Engineering Cybernetics, No. 6, Extracts reprinted in Meystel, A., 1991,"Evolution of autonomous mobile robots", in "Autonomous mobile

robots", World Scientific Publishing Co. Ltd., Singapore.

97. Tachi, S., Tanie, K., Komoziya, K., Hosoda, Y. and Abe, M., 1981, "Guide dog robot - Its basic plan and some experiments with MELDOG Mark I", Mechanisms and Machine Theory, Vol.16, reprinted in Meystel, A., 1991, "Evolution of autonomous mobile robots", in "Autonomous mobile robots", World Scientific Publishing Co. Ltd., Singapore.

98. Madarasz, R.L., Heiny, L.C., Cromp, R.F., and Mazur, N.M., 1986, "The design of an autonomous vehicle for the disabled ", IEEE J. of Robotics and Automation, Vol. RA-2, No. 3, pp. 117 - 126.

99. Cheng, R.M.H., and Mehrabi, M., 1992, "Dynamic modelling of wheeled mobile robots and automated transit vehicles using dimensionless 'Roll Number' ", The 1st. IEEE Conference on Control Applications, Dayton, Ohio, pp.160 - 167.

100. Advanced Motion Controls, 1992, "PWM Servo Amplifiers, Catalog", Advanced Motion Controls, Camarillo, CA.

Appendix A

A Brief History of Mobile Robotics

A.1 Introduction

Mobile robots made their first appearance on the industrial shop floor in the post II World War industrial boom of the '50s. In the short span of a few years and in ever increasing numbers, WMRs are finding application world wide for material handling and automated transportation, for example, in industrial and ware house applications. This growth has been fostered by an increasing amount of research and development both in universities and research establishments. The material presented attempts to trace the early history of experimental wheeled mobile robots. It has been collected from the extensive information on the subject in [17, 37, 88, 89]. The pioneering theoretical and experimental work done at the Centre for Industrial Control, Dept. of Mechanical Engineering, Concordia University since 1982 is also summarised.

A.2 Automation and Autonomy in Mobile Robots

The utility and the adaptability required by a reprogrammable multi-functional robot differentiates it from a simple automated system using mechanical contacts, relays and other hardwired circuits. The computer which acts as the brain of the robot is what gives the robot this versatility. In fact, according to Spong and Vidyasagar [90], the robotics revolution is part of the larger computer revolution. The exponential growth in computational power and the ever increasing integration and miniaturisation in sensors and actuators have greatly

contributed to this growth, in particular, in micro-manipulators for medical applications. These research advances have attracted increasing interest from the industries willing to invest in the robotic technology in order to stay competitive in the automated flexible manufacturing world of today.

The word *automation* is a short form for *automatic motivation* first introduced at the Ford Motor Company to describe a collective operation of many interconnected machines [91]. Unfortunately, in everyday parlance, the word has been connoted to mean the trend in the industries to replace human workers with machines. It has often been massaged by vested interests to evoke fear and mistrust. It is true that automation has been used to replace certain classes of jobs - welding, painting, machining and assembly line work to name a few. However, it must be emphasised that the primary targets for replacement are jobs which are hazardous, monotonous and repetitive, physically demanding and uncomfortable. The objective is to improve the quality of the products, assure consistency and last but not least improve the working environment for the blue collar workers. At these jobs, the evolving technology has produced machines that are able to operate with increased precision and speed with a declining trend in break downs and consequent down time. As with any new technology, there has to be a parallel development in the ethics on the usage of the double edged sword.

However, in regard to autonomous robots, today we still remain very far from the truly *autonomous* mobile robots of the early visionaries. The property of *autonomy* is understood as the ability to independently make intelligent decisions as the situation changes [17]. Such an ability is possible if intelligence allows a certain level of independence, i.e., if

the general goal of motion is formulated by a human operator but the specifics of the particular motion are taken care of by the robot with no direct human involvement. At the same time, some of the operations can be planned, controlled and executed with no human participation and are left wholly to the discretion of the robot. The ultimate robot would be the one that could see, hear, feel, speak, move about, manipulate objects and even think. Although our present level of technology is not able to produce such a machine, this is one of the ultimate goal of some areas of robotics research.

A.3 Early Experimental Mobile Robotics

One of the first mobile robots, Shakey, was developed at the Stanford Research Institute, Stanford University, California, as part of a project lasting from 1966 to 1972 [92]. Shakey had a TV camera, an optical range finder and several touch sensors. The purpose of the research project was to study processes for the real-time control of a robot system that interacts with a complex environment. The vehicle had to move about in its environment and perform various tasks. In the case of Shakey, the tasks were to rearrange large wooden blocks that were placed around it. The project led to significant developments in logic-based planning and problem-solving techniques bur did not focus on sensing or real-world modelling issues, thereby producing a system with extremely limited performance.

In the early 1970's, the Jet Propulsion Laboratory (JPL), Pasedena, California, constructed the Mars-Rover, a programme initiated by NASA to reduce ground support requirements and provide real-time control in the hostile environments of space exploration. The Rover, [93], was equipped with a robotic manipulator and a variety of sensors including

laser range finding systems, stereo camera systems and proximity sensors. It had an on-board minicomputer for the control of its actuators but was tethered to an off-board computer which did the planning and the decision making.

The Stanford Cart [94] developed and tested at the Stanford University Artificial Intelligence Laboratory in the period from 1973 to 1981 was a mobile robot equipped with a camera guidance system. Stereo imaging was used to locate objects, in which sets of points on the objects was tracked over several steps. The camera images were transmitted to a remote computer which did all the image processing. The mobile robot moved in steps of about 1 meter, took a sequence of images of its surroundings, analyzed them and then moved for another metre. Though slow, the project adequately demonstrated low-level vision and operation of mobile robots in real-world situations.

In France, the Institut National des Sciences Appliques developed the Hilare, [95], a semi-autonomous remote controlled mobile robot in 1978. The WMR was modelled after the Stanford Cart but was also equipped with a 3D vision system together with a video camera. For proximity sensing, Hilare was equipped with ultrasonic devices and infra red beacons, mounted in the corners of the room where the robot operated, provided absolute position information. The robot was designed to move in a straight line at a given speed or for a given distance and to turn about its own vertical axis through a commanded angle. The focus of the research was on multi-sensory perception, planning and navigation in an environment represented as graphs. The Vesa mobile robot developed later at the Institut was equipped with bumper skirts, sonar ranging systems and an on-board manipulator. The topics of research were mapping, path planning and navigation using information from several sensors.

In the USSR, at the Department of Bioengineering of the Academy of Sciences, the first generation of mobile robots was developed in the period from 1970 to 1978 [96]. A hierarchial control structure was used in which there were three levels of intelligence: decision of the manoeuvre, analyzing and breaking down the manoeuvre into elementary actions and finally executing the elementary actions. The first walking multi-legged robot was designed, simulated and then built at the Academy in collaboration with the Ohio State University in 1977.

In Japan, at the Mechanical Engineering Laboratory of MITI in the early 1980's, MELDOG, an autonomous mobile robot equipped with an ultrasonic vision system was developed as a guide dog for visually impaired people [97]. The ultrasonic vision system provided the mobile robot with obstacle avoidance capability and the robot had a very accurate system of speed and direction control. The human-user communicated through commands from a hand held control switch over a wire link. At each street intersection along the route, MELDOG stopped as a safety precaution. In case of a dangerous situation, the robot gave the master a warning in the form of mild electrical shocks in the hand. The robot was also designed to plan an optimal path in a geographical area in which the master was not familiar. The MELDOG was refined from Mark I through Mark IV in the period from 1978 to 1983.

From the early 1980's onwards there have been a large number of mobile robots developed in universities and research institutes world wide. In the U.S.A., among these are the MRL robots at Carnegie Mellon University's Mobile Robot Lab, Pittsburgh, the Blanche Mobile Robot at AT&T Bell Labs, Princeton, the Hermes Robot at the Oak Ridge National

Laboratory, Oak Ridge and the widely different mobile robots including single legged hopping robots developed at MIT's Artificial Intelligence Laboratory, Cambridge, Massachussets.

A.4 WMR Research at the Centre for Industrial Control, Concordia University

The material presented here adds detail to the descriptions given in Section 1.3 of the four generations of WMRs that have been designed and developed at the CIC.

Preliminary investigations from 1982 to 1985 led to the development of the first experimental platform, CONCIC I, a 3-wheeled WMR with tricycle wheel configuration. The WMR was designed to follow a guide path laid on the floor using camera vision with on-board image processing and path planning. With the tricycle wheel configuration, the front wheel acted both as the drive wheel and the steer wheel. A D.C. motor with a belt and chain drive was used as the main drive unit and a second D.C. motor connected to the steering axis through a chain reducing drive was used for steering. The two wheels on a single axis at the rear were castors free to rotate but fixed in the swivel axis. The vehicle controller adopted the parallel processing environment developed at the Centre. Three Zilog Z-80 processors were used in the main controller: the master processor for coordination and delegation of tasks and the two slaves, one for image processing and analysis and the other for low level motion control, both driving and steering. A modular structure was adopted for the controller to provide flexibility for future additions and expansions. The mobile robot could function as an automatic tractor pulling a trailer or as a unit load transporter. Cheng et al. [2] tested the CONCIC I on various types of paths. However, limitations in the turning radius due to the mechanical tri-cycle wheel configuration, limited vision capabilities, low computing power

and inflexibility in the overall design led to the development of the second generation of mobile robots.

The CONCIC II, the second experimental WMR designed and developed by Rajagopalan [3] and Rajagopalan and Cheng [5] at the CIC from 1988 to 1990 was designed with many new and practical features and also to address the shortcomings of the tri-cycle configuration used in CONCIC I. The mechanical and electronic control design used for CONCIC II, has since then been adopted as the standard for the next generations of mobile robots developed at the Centre. The development effort was steered by a strong support from a local manufacturer of mobile robots, the TOR group and later through a strategic research grant from the National Science and Engineering Research Council (NSERC), Canada, awarded to the centre for the development of a modular WMR. The design incorporated a modular mechanical design, with the frame composed of 9 similar box-sections. The drive wheel units and the castors could be located at any one of the 9 locations so that various wheel configurations could be tested. The mobile robot utilised a binary digitizing camera with DMA data transfer for the optical guidance system designed to follow an illuminated track laid on the ground. The digital controller was designed to recognize junctions and dead ends in the track and take appropriate action. For purposes of safety, as stipulated in all industrial applications, proximity sensing of obstacles in the path of the robot was provided by ultrasonic sensors. The main processor was programmed then to stop current motion and issue audible warning signals. A radio link was also implemented for remote control and wire less data transmission between the on-board master controller and a remote computer. The control software was designed with an open architecture and provided many options such as

keyboard mode, camera mode, turning mode, remote link, data acquisition and testing.

In the work reported by Rajagopalan [3], Rajagopalan and Cheng [4] and Rajagopalan, Cheng and Lequoc [5] a diamond wheel configuration was employed with two independently driven wheels located symmetrically along the transverse axis on either side of the geometric centre of the vehicle. Steering was achieved by differential drive, since the wheels were independently driven. Two free wheeling castors, located along the longitudinal axis, in the front and the rear of the geometric centre, provided stability ; since the castors were free to swivel about their pivot pins, the WMR could literally turn on a dime. A permanent magnet D.C. motor-in-wheel unit with an integral sun and planetary speed reducer was used for each wheel. These high torque drive units were chosen to provide enough power to drive the mobile robot at speeds found in an industrial setting while carrying a substantial payload. The servo-control of each wheel was done independently using a LM628, a special purpose motion control chip. A Intel 286-12 MHZ based master processor was used for image processing and path planning.

Three different approaches for the guidance control of CONCIC II were employed. In the first method, a single camera provided instantaneous position and orientation of the longitudinal axis of the vehicle with respect to the track. In the second method, a second camera at the rear was employed to provide position and orientation offsets of the WMR at both the front and the rear ends. In addition, this configuration used control laws that were synthesised to account for curvature in the track. A feed forward controller was added in the third approach in which the steering command was computed based on a predicted track profile ahead of the robot and a pre-defined driving criterion.

The modular mechanical construction of CONCIC II was adopted by Mehrabi [6] and by Mehrabi, Cheng and Hemami [10] in CONCIC III as well. The drive wheels in this case, however, were placed in the fore-aft axis. The wheels could be steered using a coordinated steering function. Two and three degree of freedom non-linear dynamic models were studied. Using parametric studies, Cheng and Mehrabi [98] and proved that a 3-degree of freedom could be simplified to a 2-dof model using a dimensionless Roll number. The experimental WMR used a dead reckoning guidance scheme in which the desired path that the mobile robot is to follow is stored in a look up table in the memory of the digital controller. The actual position and orientation are computed from wheel speeds using a kinematic model of the WMR. Using feed back linearization, an optimal dynamic controller was synthesised and implemented for CONCIC III.

The first Automated Transit Vehicle (ATV), the CONCIC IV, was designed and built at the Centre from 1994 to 1996 by M.Pharand and completed later by Perelli [11]. The WMR was much bigger in dimensions than its predecessors but the same modular mechanical design was adopted. Rajagopalan and Perelli [12] used a Charge Coupled Device (CCD) camera on the ATV for road following. A hierarchial control system was used with an Intel 486-66 MHZ processor, a C-40 transputer network and four LM628 servo motion control chips. For high speed image processing the Texas Instruments C-40 DSP network was used. This parallel processing network digitised the image from the CCD camera, filtered out noise in the image data and identified the centre of the road. Using a set of control laws, it then sent the drive commands to the servo-control, LM628 chips which took care of the low level driving and steering functions. The primary processor was used to provide user interface

through the keyboard, display on the monitor and also hard drive access. Several hardware and software safety features were implemented. The hardware included an RF remote control motor stopper and two emergency switches. The software safety features include detection of motion controllers malfunctioning, stopping of vehicle when no road is detected and stopping of the vehicle using any one of several keys on the keyboard. The software was also developed in a modular form for ease of modification and further development. The WMR was successfully tested at speeds upto 2 $m.s^{-1}$ while following standard road manoeuvres such as turns and lane changes.

Appendix B

Amplifiers and Wheel Units Calibration Data

B.1 Introduction

In this Appendix, the data and the regression curve fits obtained from the calibration of each power amplifier and DAC set is given. In addition, a no-load calibration of actuator friction for the motor-in-wheel drive units is also provided. Procedures adopted for the calibration of the amplifiers and the wheel units are also presented.

B.2 Power Amplifier - DAC calibration

In the experimental work, a power amplifier, model 50A8R , manufactured by Advanced Motion Controls, Camarillo, CA is used for each of the two drive motor-in-wheel sets. Complete details of the construction and the configuration of the power amplifier may be found in the manufacturer's catalog [100]. For this application, the amplifier is configured to operate in the current mode in which the current supplied to the motor is proportional to the reference voltage signal applied to the amplifier. The reference signal corresponds to the control signal from the digital controller and is sent to the amplifier through the 12-bit DAC on the NIDAQ Interface card [82].

In this hardware configuration, each amplifier-DAC system was individually calibrated using a Resistive-Inductive Load. The amplifiers were set to provide a peak current of 25 amps and a continuous current of 12.5 amps. These values were chosen using data reported by Barakat [15] from model-based control investigations done at the CIC using the CONCIC

III with a differential drive wheel configuration and the same drive wheel units.

As part of the calibration, the Offset Potentiometer, referred as Pot 2 in the manufacturer's catalog [100], and the Gain Potentiometer, Pot 3, were adjusted to provide the chosen values of the peak and the continuous current values. The values of the potentiometers have been measured and are given in Table A.1 for reference. The values of Pot 1 and Pot 4 are also given for the sake of completeness. *The calibration data given in this Appendix applies to these potentiometer settings only.* The applicability of these calibration data for other settings of the potentiometers must be verified. The value of the resistive load chosen was 1.9Ω with a power dissipation limit of 150W. A cooling fan was used to improve heat dissipation from the resistors. The inductive load of 0.1H was used to mimic the inductance of the D.C motor.

The static calibration was performed by sending a chosen set of voltages from the DAC to the power amplifier. The DAC output voltage, V, the actual current, I, the reference signal read back from the amplifier, Pin_9, and the actual current read back from the amplifier, Pin_8 were measured using sensitive multimeters. The sensitivity of the multimeters in the D.C voltage mode was ± 0.001V and in the D.C amp mode was ±0.01 amps. These values of sensitivity were chosen to be acceptable for the calibrations. The DAC voltage and the corresponding amplifier output amperage were recorded under steady state conditions. The tests were carried out ramping up and ramping down both in the positive and the negative ranges to test for linearity and hysteresis. The linear regression fits for each amplifier, identified by serial number, are given in Fig.B.1 to Fig.B.6 .

Table B.1 Potentiometer settings for the DAC-Amplifier sets.

Amplifier (serial number)	NIDAQ DAC Channel	Pot 1 [Ω]	**Pot 2** [Ω]	**Pot 3** [Ω]	Pot 4 [Ω]
AMP_A (9413-55986)	0	11.59	23.43	5.42	20.51
AMP_B (9413-55987)	1	10.01	23.98	3.216	19.95

The linear regression coefficients for the DAC-Amplifier sets are

AMP_A: $I = 1.2675V - 0.0094$

AMP_B: $I = 1.2695V - 0.0584$

where V is in DC volts and I is measured in DC amps.

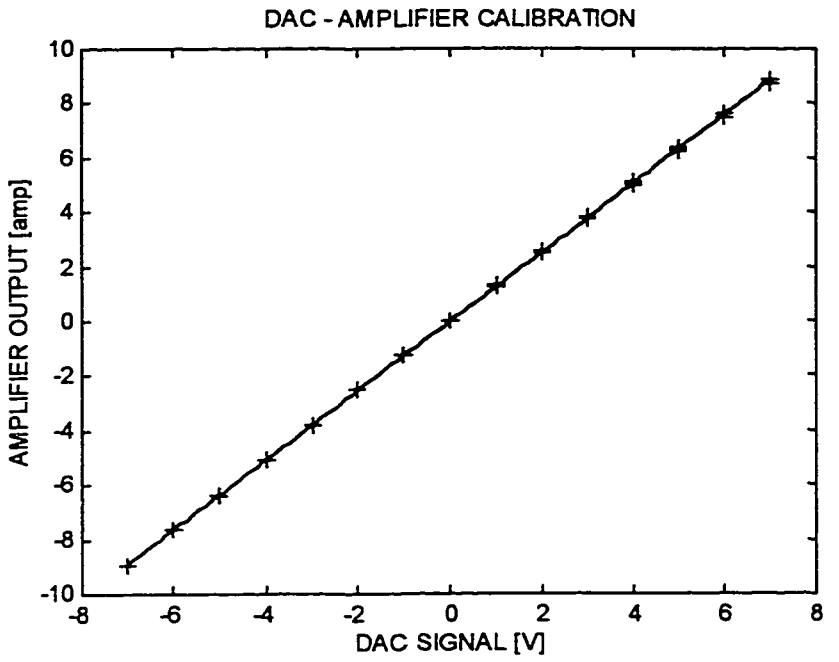

Figure B.1 Calibration curve of DAC - Power Amplifier, AMP_A.

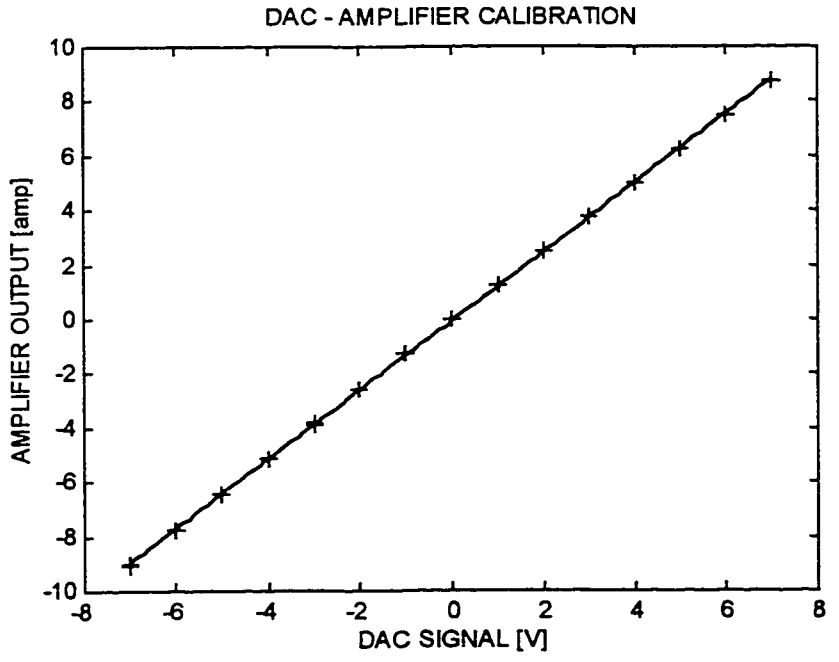

Figure B.2 Calibration curve of DAC - Power Amplifier, AMP_B.

B.3 Actuator No-load Friction Calibration

The mechanical friction present in the bearings of the drive motors, in the bearings of the reduction gear and the wheel and the friction in the gear train contribute towards the actuator friction. Due to the 9.9:1 gear ratio employed in the Schabmuller Motor-in-Wheel Drive Units (for further details, refer to Appendix C in Rajagopalan [3]), actuator friction can make a large contribution towards the total amount of mechanical friction in the WMR system. Hence, a no-load calibration was performed to obtain an estimate of the power dissipated in the actuator due to friction.

The actuator friction has been modelled as viscous friction which is dependent on the rotational speed. Hence, the calibration was done for different wheel speeds, both in the forward and the reverse directions. *The term no-load is specifically used since the calibration was performed with the drive wheel off the ground so that the vertical load on the wheel and bearings was absent.* Hence the calibration data provide only an estimate of the frictional losses in the actuators under a loaded condition of the WMR. Windage losses due to the rotation of the wheel in air were neglected due to the slow rate of rotation. Resistive losses in the power amplifiers have also been considered negligible.

For the calibration, the power amplifiers were used in the voltage mode so that the applied voltage on the drive motor was directly proportional to the reference signal. The value of the applied voltage, V, and the actual current, I, drawn by the motor were measured under steady operating conditions using sensitive multimeters. The wheel speed was measured using a hand held tachometer. The amplifier calibration in voltage mode was not needed since the applied motor voltage was directly measured. The armature resistance, R_a , of the drive

motors [3] is 0.602Ω. Hence the power dissipated by mechanical friction, P_f, is

$$P_f = VI - I^2R_a \qquad \textbf{(B.1)}$$

The motor sets have been identified as Set_A and Set_B in keeping with the amplifier sets connected to them. However, the manufacturer's serial numbers are also provided for reference. The regression fits for mechanical friction, measured as no load motor current versus wheel speeds for the motor set, Set_A are given in Fig.A.3 for forward WMR speeds and in Fig.B.4 for reverse speeds. The corresponding curves for the motor set Set_B are given in Fig. B.5 and in Fig. B.6. The least square fits between the motor no-load current, I, and the wheel rotational speed, ω, for each set of data for each wheel are given below. Both I [amp] and ω [rad.s^{-1}] are signed quantities.

Drive Motor Set_A:

Forward Speed: $I = 0.6232 + 0.0737\omega - 0.0021\omega^2$

Reverse Speed: $I = -0.5951 + 0.0599\omega + 0.0015\omega^2$

Drive Motor Set_B

Forward Speed: $I = 0.5476 + 0.0561\omega - 0.0014\omega^2$

Reverse Speed: $I = -0.4798 + 0.0547\omega + 0.0013\omega^2$

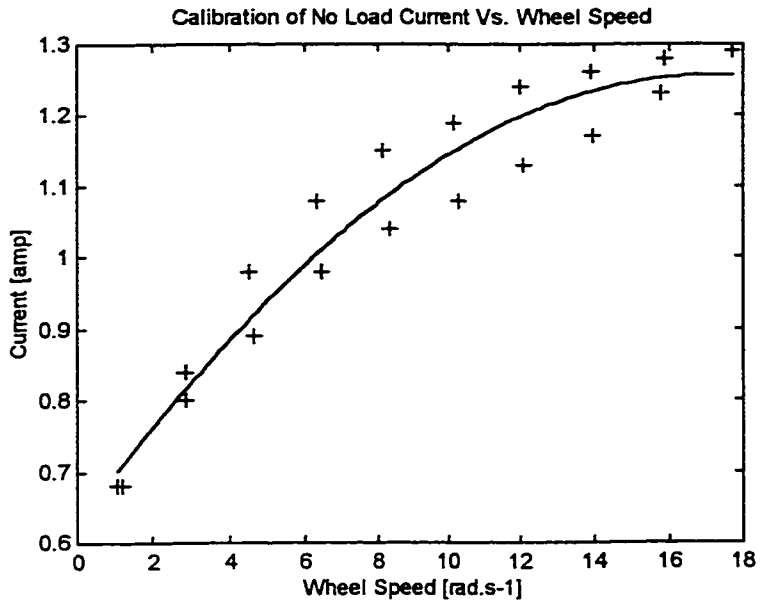

Figure B.3 Calibration curve of no-load (friction) current versus (forward) wheel speed for Drive Wheel Set_A.

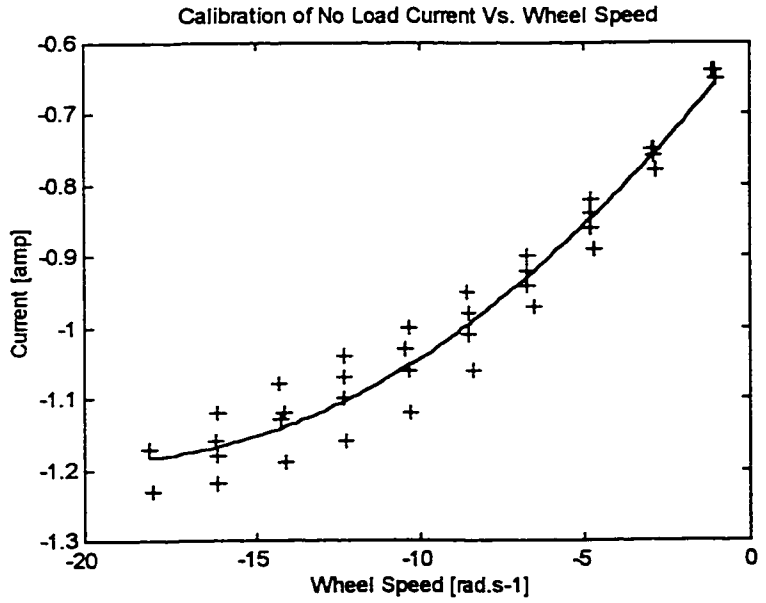

Figure B.4 Calibration curve of no-load (friction) current versus (reverse) wheel speed for Drive Wheel Set_A.

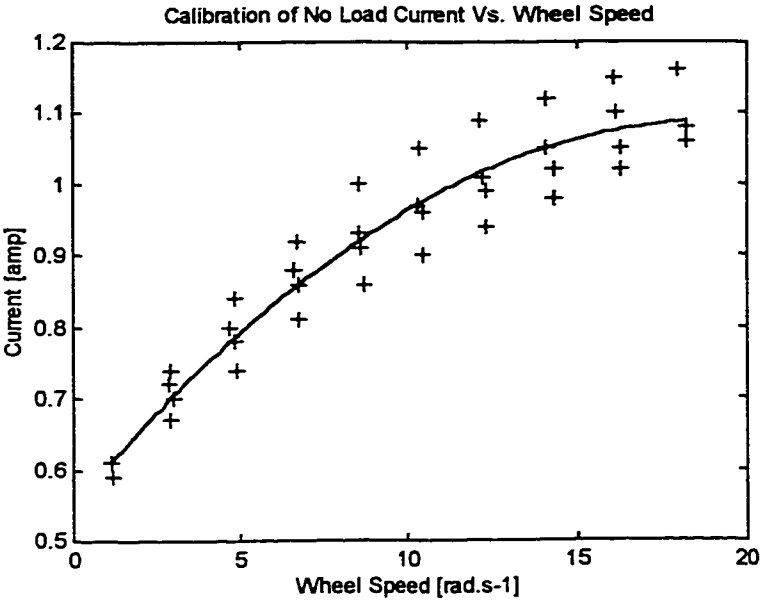

Figure B.5 Calibration curve of no-load (friction) current versus (forward) wheel speed for Drive Wheel Set_B.

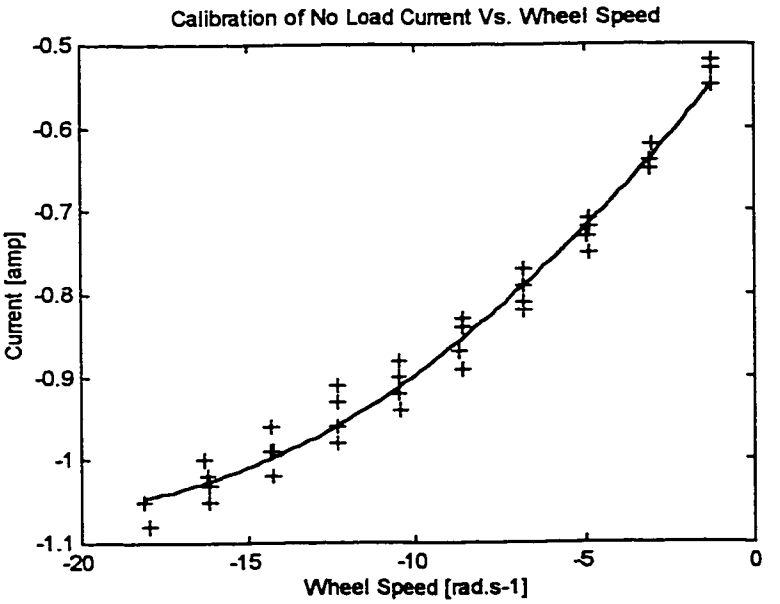

Figure B.6 Calibration curve of no-load (friction) current versus (reverse) wheel speed for Drive Wheel Set_B.

Appendix C

Physical Parameters of CONCIC III

The WMR, CONCIC III has been designed and built by Mehrabi [6] at the CIC for experimental work on WMRs. The design and the dimensions of the principal components used on the CONCIC III are identical to those of CONCIC II, designed and built by Rajagopalan [3] for research on camera guidance of WMRs for path following.The values of the inertial parameters of CONCIC III for the configuration used in this experimental investigation are given in this Appendix. The principal geometric and inertial values of the WMR were obtained from cited references [3, 6, 7,15]. Values related to the suspended load were obtained by direct measurement.

The layout of the principal components in the configuration used for CONCIC III for the experimental work is shown in Fig. C.1. The mass of each component and the distance between the centre of mass of the component and the geometric centre, G, of the WMR are given in Table C.1. These values are used to compute the location of the centre of mass of the WMR. The computation of the principal moment of inertia about the vertical axis, $^{1}n_{3}$, in the coordiante system fixed to the centre of mass, C, of CONCIC III is given in Table C.2. Each component has been assumed to be uniformly distributed and the average density computed using the mass of the component and its physical dimensions.The mass and the inertial properties of the two wheel sets are listed in Table C.3. The principal dimensions and the location of the load frame and the mechanical assembly used for the suspended load are shown in Fig. C.2.

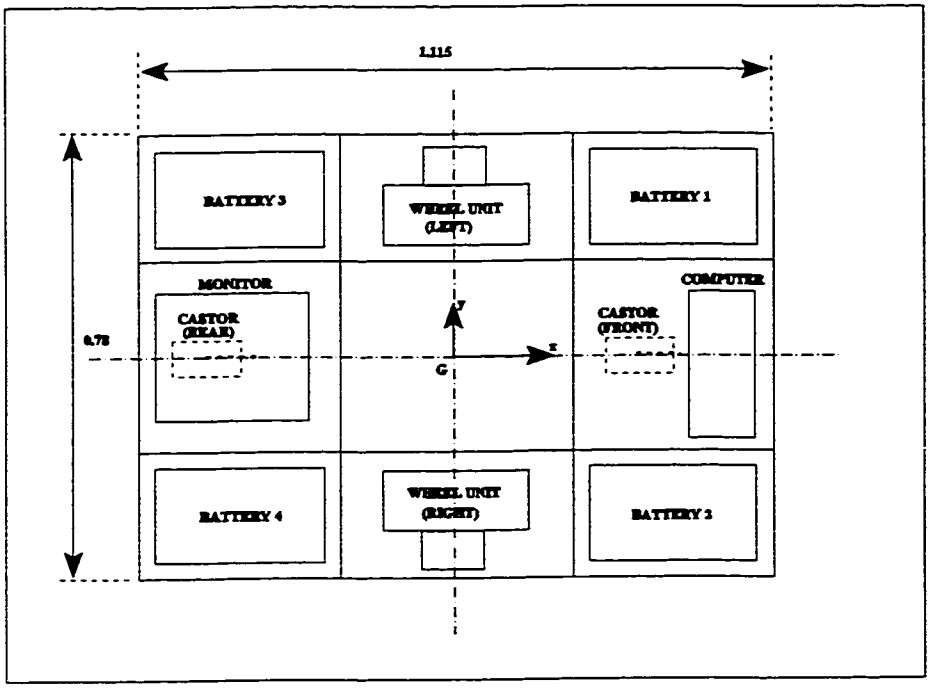

Figure C.1 Layout of the principal components on CONCIC III.

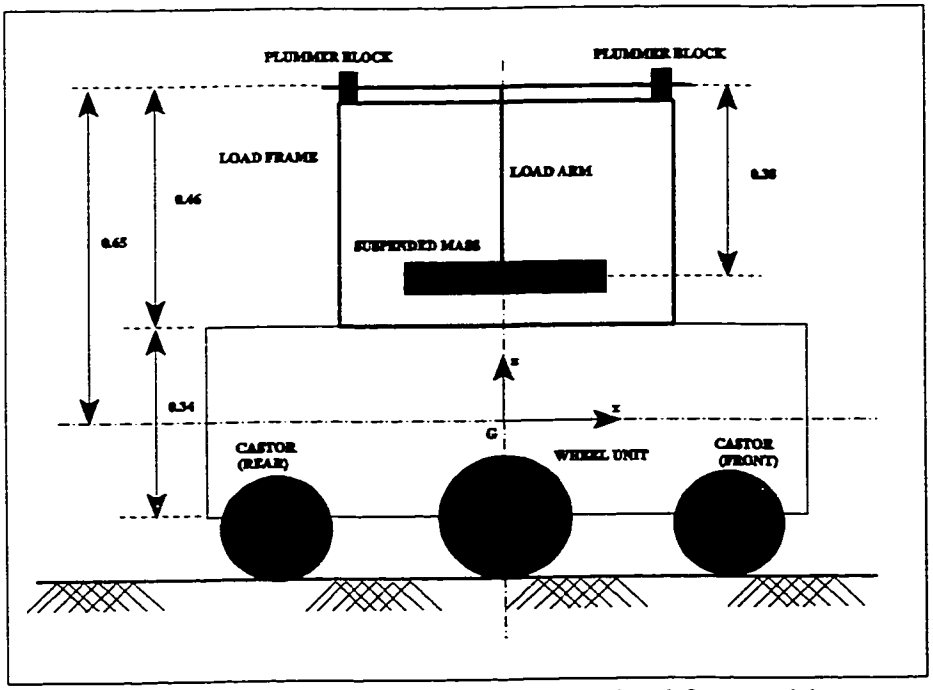

Figure C.2 Location of suspended load and load frame with respect to the geometric centre, G, on CONCIC III.

The mass of each wheel unit is 17.5 Kg and the location of the centre of mass with respect to the geometric centre, G, is (0.0, 0.25).

The location of the mass centre, D, of CONCIC III is calculated by taking moments of the weight of each component about the coordinate frame fixed to the geometric centre, G, of the WMR.

The total mass of CONCIC III is

$$m_D = \sum_{i=1}^{8} m_i = 148.5 \text{ Kg} \qquad \textbf{(C.1)}$$

where i denotes the eight components listed in Table C.1. Taking moments about the axis, ${}^1n_2$, fixed to G, the x location of D is

$$a = \left(\frac{1}{m_D} \right) \sum_{i=1}^{8} m_i x_i = -0.019 \text{ m} \qquad \textbf{(C.2)}$$

The y and z locations of D are obtained as

$$\begin{aligned} \bar{y} &= 0.0 \text{ m} \\ \bar{z} &= -0.02 \text{ m} \end{aligned} \qquad \textbf{(C.3)}$$

The moment of inertia, I_3^D , of the WMR about the yaw axis is required by the dynamic model. This is obtained by evaluating the principal moment of inertia of each component about the vertical axis through the mass centre of the component parallel to the ${}^1n_3$ axis of the coordinate frame fixed to G. Using the parallel axis theorem, these values of the inertia are then transformed to the ${}^1n_3$ axis. The computations are listed in Table C.2. Each component listed in Table C.1 is modelled as a rectangular parallelepiped whose mass is

assumed to be evenly distributed throughout its volume. The dimensions of the components given in Table C.1 are the dimensions of the parallelepiped used as the model.

The moment of inertia of the WMR is

$$I_3^D = \sum_{i=1}^{8} \bar{I}_{i33} = 29.41 \text{ N.m} \qquad \textbf{(C.4)}$$

Two steel discs stacked atop each other are used as the suspended load in the experiments. The mass of each disc is 10 Kg. The radius of each disc is 0.14m and the height is 0.025m. The moment of inertia of each disc about the vertical axis of the WMR is 0.098 $N.m^2$ and the moment of inertia about the (horizontal) axis of the swing arm is 1.7011 $N.m^2$.

Table C.1 Mass, physical dimensions and directed distances from geometric centre of the principal components of CONCIC III.

COMPONENT	MASS m_i (Kg)	LENGTH l_i (m)	WIDTH b_i (m)	HEIGHT h_i (m)	x_i (m)	y_i (m)	z_i (m)
Frame	15.0	1.115	0.78	0.34	0.0	0.0	0.0
Battery 1	29.0	0.3	0.15	0.2	0.3575	0.26	-0.07
Battery 2	29.0	0.3	0.15	0.2	0.3575	-0.26	-0.07
Battery 3	29.0	0.3	0.15	0.2	-0.3575	0.26	-0.07
Battery 4	29.0	0.3	0.15	0.2	-0.3575	-0.26	-0.07
Computer	5.0	0.4	0.2	0.35	0.4075	0.0	0.345
Monitor	11.0	0.4	0.35	0.3	-0.4425	0.0	0.32
Power Supply	1.5	0.2	0.2	0.16	0.0	0.0	-0.09
Total	m_D = 148.5						

Table C.2 Moment of inertia of the principal components about the vertical axis through the geometric centre, G

	COMPONENT	$\bar{I}_{33} = \frac{1}{12} m_i (l_i^2 + b_i^2)$ (N.m^2)	m_i (kg)	$d_i^2 = (x_i^2 + y_i^2)$ (m^2)	$\bar{I}'_{33} = \bar{I}_{33} + m_i d_i^2$ (N.m^2)
1	Frame	2.3145	15	0	2.3145
2	Battery 1	0.2719	29	0.1954	5.9387
3	Battery 2	0.2719	29	0.1954	5.9387
4	Battery 3	0.2719	29	0.1954	5.9387
5	Battery 4	0.2719	29	0.1954	5.9387
6	Computer	0.0833	5	0.1661	0.9136
7	Monitor	0.259	11	0.1958	2.4129
8	Power Supply	0.01	1.5	0.0	0.01

Table C.3 Mass and inertial properties of drive wheel sets.

	COMPONENT	MASS m_i (Kg.)	I.D (m)	O.D (m)	LENGTH (m)	$\bar{J}$ (N.m^2)	$\bar{I}_{33}$ (N.m^2)	$\bar{I}'_{33}$ (N.m^2)
1	Rotor	1.437	N.A.	0.053	0.076	5.046E-4	refer note 2	refer note 2
2	Wheel+Casing	3.378	0.09	0.112	0.121	7.507E-3	refer note 2	refer note 2
3	Spur Gear	0.937	0.132	0.17	0.013	N.A.	5.3788E-3	6.875E-2
4	Boss	2.737	N.A.	0.132	0.025	N.A.	0.0238	0.2089
5	Stator + Hub	3.947	N.A.	0.085	0.2025	N.A.	0.2034	0.7958
	Total	12.437						1.0734

I.D = Inner Diameter ; O.D = Outer Diameter ; $\bar{J}$ = Polar Moment of Inertia ; $\bar{I}_{33}$ = Principal Moment of Inertia about centroidal axis ; $\bar{I}'_{33}$ = Moment of Inertia about centroidal axis of CONCIC III.

Note 1: The distance, d, between the mass centre of the wheel unit and the mass centre of CONCIC III is 0.26 m.

Note 2: The moment of inertia of the components indicated have been added to that of the stator and hub. The mass indicated in the Table C.3, Item # 5 is the combined mass of the stator and hub only. In the calculation of $\bar{I}_{33}$ of Item # 5 (stator and hub), the masses of the rotational components, viz., the rotor, the wheel and the casing have been added to that of the stator and the hub.